JCU ePrints

This file is part of the following reference:

Mantovanelli, Alessandra (2005) *A new approach for measuring in situ the concentration and settling velocity of suspended cohesive sediment.* **PhD thesis, James Cook University.**

Access to this file is available from:

JCU
JAMES COOK UNIVERSITY

A New Approach for Measuring *in situ* the Concentration and Settling Velocity of Suspended Cohesive Sediment

Thesis submitted by

Alessandra Mantovanelli (MSc) UFPR-Brazil

in March 2005

for the Degree of Philosophy

in the School of Mathematical and Physical Sciences

James Cook University

Statement of access

I, Alessandra Mantovanelli, the author of this thesis, understand that James Cook University will make it available for use within the University Library and allow access to user in approved libraries. All users consulting this thesis must sign the following statement.

In consulting this thesis I agree not to copy or closely paraphrase it in whole or in part without the consent of the author; and to make proper written acknowledgment for any assistance that I have obtained from it.

Beyond this, I do not wish to place any restrictions on access to the thesis.

<div style="display:flex; justify-content:space-between;">

Alessandra Mantovanelli   data

</div>

Statement of sources

I declare that this thesis is my own work and has been submitted in any form for another degree or diploma at any university or other institution of tertiary education. Information derived from published or unpublished work of others has been acknowledged in the text and a list of references provided.

_____   _____

Alessandra Mantovanelli   data

Acknowledgements

I will always be grateful to the Ridd's families for their support and friendship during these years in Australia. Peter, Cheryl, Emma, James, Michael, Sue, Sarah and John, I thank you very much. Severine Thomas and Thomas Stieglitz thank you for your help, friendship and all pleasant moments we spent together. Sara, Leonardo, Laura and Paulo Busilacchi your friendship meant a lot.

Special thank for my family Lucia, Ricardo, Anaryá for their encouragement and love.

Very special thank to Eduardo for giving many insights for solving countless problems found during the instrument development and for his support throughout this work. Eduardo, Giovanni and Bruno thank you for your love, you have brought lots of inspiration and happiness to my life.

Abstract

The settling velocity of suspended particulate matter (SPM) is a key parameter controlling deposition processes and its accurate determination has been regarded as a top priority in improving numerical models of cohesive sediment transport. Because SPM occurs predominantly as aggregates of organic and inorganic particles in cohesive coastal systems, an *in situ* quantification of settling velocity is essential. The available techniques to measure the settling velocity of aggregates in the field include: Owen tubes and similar, settling columns equipped with optical sensors, laser systems or video cameras as well as acoustics and holographic systems. None of these techniques is able to directly measure the mass-concentration of SPM or its settling velocity mass distribution *in situ*.

In this work, a new instrument (SEDVEL – Sedimentation Velocity) was developed to directly and automatically measure SPM mass of cohesive sediments *in situ*, from which the mass/concentration distribution of settling velocities can be determined. This instrument consists of an underwater balance (resolution of 0.01 g) placed inside a settling tube, which directly measures the variation in time of the immersed weight of particulate matter (*PM*) as it settles on a plate located at the tube bottom under quiescent conditions. SEDVEL operates underwater and automatically withdraws water samples — deployment periods of a few days. The design of SEDVEL and its components are described as well as the procedure adopted in its calibration and data analysis. Results of the assessment of the instrument performance in the laboratory and in the field are analysed.

SEDVEL presented consistent and reproducible results when tested in the laboratory. It was able to reproduce the initial particles concentrations ranging from 7 to 200 mg l^{-1} ($r^2 = 0.9$, *p* < 0.01) in 13 laboratory experiments. Results also suggested that some particle reflocculation induced by the settling column can take place for concentrations higher than 50 mg l^{-1}. Field trials, carried out in Cleveland Bay at Berth 11 (Townsville Harbour, Australia) and at the Pier (Strand Beach, Townsville, Australia), showed that SEDVEL reproduced the general tendency of the measured SPM concentrations in 42 cycles of measurement ($r^2 = 0.65$, *p* < 0.01).

At the Pier, settling velocities presented a main mode of relatively slow-settling particles/flocs within $0.09 \leq W_s < 0.5$ mm s^{-1}, and usually a second mode of $1.5 \leq W_s < 3.0$ mm s^{-1}. The settling dynamics at this location were mainly determined by erosion and deposition of sediment particles from and to the bottom close to the headland as well as by advection of offshore floc populations during the rising tide. At Berth 11, aggregates were composed mainly of microflocs of low-density and slow settling velocities ($0.09 \leq W_s < 0.12$ mm s^{-1}). The estimated mean density of flocs, 40% smaller than the density of inorganic particles, represented better the settling mode measured at this site.

SEDVEL constituted a novel idea for measuring settling velocities *in situ*, and therefore, a considerable amount of development, prototyping and testing was required. Compared with other automated instruments for measuring settling velocities *in situ*, SEDVEL has a relatively simple working principle, calibration and data analysis procedure. It is also unique in furnishing direct and automated *in situ* measurements of immersed mass and mass-concentration of SPM. The main problems associated with the current SEDVEL version are: zero position drifting among the different cycles of the measurement and from its initial set-up, possible floc break-up due to the pumping system used in the water replacement, errors associated with a non-homogeneous distribution of particles on the balance plate and with the definition of the zero position. A general assessment of SEDVEL potential limitations, and improvements to be achieved in future versions of the instrument, are described.

Contents

List of Tables

List of Figures

1. General introduction

1.1. Cohesive sediments in coastal systems

Sediment present in coastal areas originates from runoff through catchment areas, river discharge and from bottom and shore erosion and remobilization. As fine sediment particles can be transported in suspension, new or remobilised sediments can be deposited at sites distant from their origin by the action of near-coastal currents generated by wind and tides. However, sediment particles are denser than seawater and thus they are not passive tracers. They can settle through the water column and deposit under calm conditions. The maximum speed at which particles settle in quiescent waters is called the particle settling (or fall) velocity. Nominal fall velocities depend upon a particle's size, density and concentration, and whether there is an individual particle or an aggregate of particles.

Suspended fine sediments including silts and especially clays are cohesive (Mehta, 1994), and consequently they form flocs and aggregates. This characteristic of cohesive sediments results in extremely complex transport, settling and erodibility behaviours, which are largely different from those of non-cohesive sediments, because of the overriding importance of cohesive forces that hydrodynamic forces have difficulty in overcoming (Mehta, 1994; Hamm and Migniot, 1994; Van Leussen, 1988). In fact, the suspended particulate matter (SPM) present in coastal and estuarine cohesive systems occurs predominantly as aggregates of organic and inorganic particles. They are bound by microbiological activity and electrochemical forces when particles are brought together by turbulence, differential settling, and to a less extent Brownian motion (Eisma, 1986; Eisma et al., 1991; Kim and Stolzenbach, 2004).

In coastal environments, the SPM experiences a continuous cycle of erosion, resuspension, vertical mixing, transport in suspension (advection), settling and deposition, with subsequent re-erosion or consolidation controlled by the hydrodynamical forces (Nichols, 1986; Odd, 1988) (Figure 1.1). Therefore, temporal and spatial changes of the turbulence level within these systems promote a continuous process of aggregation and disaggregation of flocs (Van

Leussen, 1988; Milligan and Hill, 1998). Further, temporal changes in organic particulate matter and local turbulence alter floc density spectra, flocculation efficiency and resistance to break-up, and influence the settling behaviour (Fennessy et al., 1997).
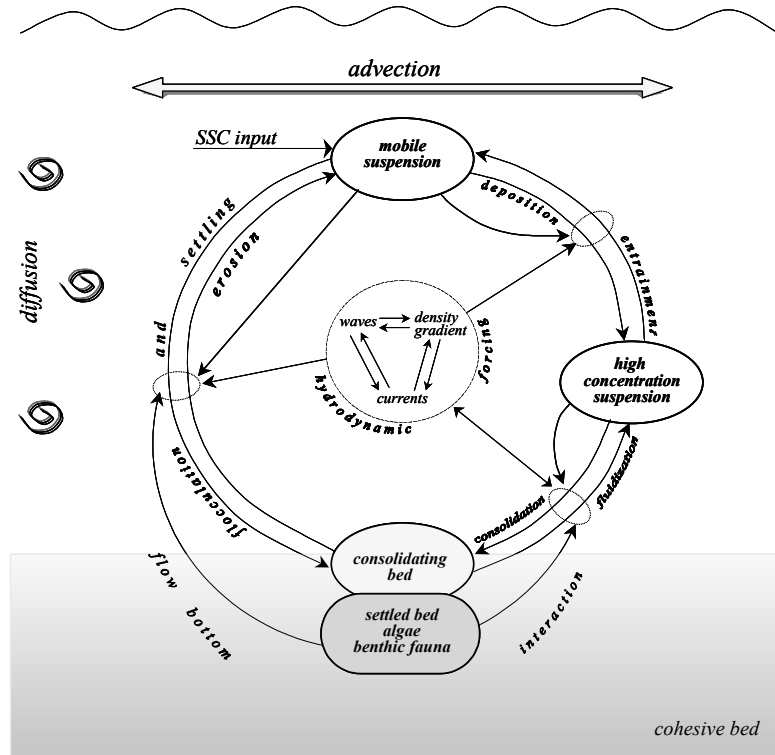
Figure 1.1. Cyclical cohesive sediment transport (modified from Hamm and Migniot, 1994).

Aggregates have shape, size, densities, optical properties and settling velocities quite distinct from those estimated on the basis of theoretical calculations for spherical inorganic particles. Flocs are often less dense, more spherical and a few orders of magnitude larger than primary particles, and therefore, they experience reduced drag compared to their constituent particles; as the last two factors are usually more significant than the decrease in density, they generally have settling velocity substantially higher than their constituent particles (Mehta, 1994; Van der Lee, 2000). Another important point to consider is that although aggregates can be stable in water, even under strong currents where their internal cohesion is roughly in equilibrium with the environmental shear, they prove to be very fragile when subjected to increased turbulence and shock waves as result of handling and sampling (Eisma et al., 1996).

Studies over the past few decades have shown that aggregate sizes and settling velocities measured in the laboratory can be one to two orders of magnitude smaller than values

obtained by *in situ* techniques, because the particle aggregates easily break up when sampled (e.g. by conventional sampling bottles or pumping) and manipulated (e.g. by dispensing suspensions), making it impossible to reproduce environmental conditions in the laboratory (Owen, 1971; Burt, 1986; Mehta et al., 1989; Kineke and Sternberg, 1989; McCave and Gross, 1991; Milligan, 1996). Therefore, an empirical quantification of the settling velocities of aggregates in the field is essential. As a consequence of this, a great effort has been made in estuarine and coastal research in order to quantify the settling velocities *in situ*, thus permitting the general behaviour of aggregate sedimentation to be better delineated (Dyer et al., 1996).

Determination of SPM concentrations and settling velocities are very important for studying sedimentation in coastal and riverine environments, such as wetlands, estuaries, reefs, seagrass beds and waterways. Settling velocity quantification has important applications to ecological studies, coastal engineering, navigation planning, water quality (particle-bound pollutants) and prediction of short-and long-term sedimentation in coastal environments, among others (Van Leussen and Dronkers, 1988). Furthermore, sedimentation regulates the light availability, as well as nutrient level and food supply to coral and seagrass bed communities. In addition, the presence of large settling particles, such as organic macroscopic aggregates (composed of plankton, detritus and fine inorganic particles) and fecal pellets has been claimed as an important mechanism for sediment removal from the water column (Van Leussen, 1988; Ayukai and Wolanski, 1997).

Settling velocity is a key parameter in the advection-diffusion models applied to describe the transport of SPM. The general form of this equation is classically written:

$$\frac{\partial \bar{C}}{\partial t} + \bar{U}_i \frac{\partial \bar{C}}{\partial x_i} + \frac{\partial W_S \bar{C}}{\partial z} = -\frac{\partial}{\partial x_i}(\overline{u_i' c'}) + S(x, y, z) \qquad (1.1)$$

where $\bar{C}$ and $\bar{U}_i$ are the mean concentration of sediment in suspension and the mean flow velocity, which instantaneous values "U_i" and "C" are given by the sum of the mean and turbulent components of the flow and sediment concentration respectively, i.e. $U_i = \bar{U}_i + u_i'$ and $C = \bar{C} + c'$. Also, "t" represents the instant of time and the three vector components of x_i and U_i are given by: $x_i = x, y, z$ and $U_i = U, V, W$, respectively. The settling velocity of

particles is given by W_S, and $S(x,y,z)$ is the source of sediment within the domain (Teisson, 1997). In addition, for the layer close to the bottom, the net flux of sediment corresponds to the sum of the fluxes due to deposition or erosion (Teisson, 1997).

Erosion and deposition fluxes and settling velocity are crucial inputs to the cohesive sediment models (Equation 1.1). Due to the impossibility of describing deposition and erosion process deterministically for cohesive beds, a hybrid approach (empirical and deterministic) has been adopted in mud transport models (Odd, 1988; Hamm and Migniot, 1994; Mehta, 1994). Numerical models that simulate estuarine and marine fluxes are dependent on reliable field data (Fennessy et al., 1997). The mass frequency distribution of settling velocities is needed for numerical modelling of SPM mass transport (Puls and Küls, 1996). Model sensitivity analysis has shown that settling velocity has a crucial influence in determining, for instance, the strength of the turbidity maximum in estuaries (Markofsky et al., 1986). Many simulations have made use of simple relationships between settling velocity and SPM concentrations; such terms are limited in their ability to reflect spectral changes that operate over tidal and seasonal scales (Fennessy et al., 1997). Therefore, the accurate determination of settling velocities and deposition fluxes are regarded as a top priority in improving cohesive sediment models for estuarine and coastal regions (Mcanally and Mehta, 2001). Improving the empirical method of measurement of cohesive sediment settling velocities in the field can increase the reliability and prediction capability of cohesive models for supporting management.

Settling velocities and concentrations of SPM can vary hourly in coastal systems. Therefore, their monitoring in the field is seldom simple, demanding automated measurement systems with high temporal resolution (Wren et al., 2000). A broad range of instruments has been used to measure settling velocities *in situ*, varying from simple, manually operated devices (e.g. Owen-kind settling tubes) to sophisticated and expensive equipment (e.g. laser diffraction and holographic methods). These can involve either direct measurements for determination of the settling velocity or indirect techniques that demand complex algorithms to translate the signal of instruments into SPM concentrations and particle settling velocities.

The different techniques used to measure settling velocities and SPM concentrations *in situ* are not directly comparable, since each one applies a different principle of measurement.

Further, none of the available instrumentation is completely free from any kind of error or limitation, and they are usually suitable for a particular application. At the moment, direct measurements of SPM mass concentration are only possible by using bottle sampling or settling tubes. Both these techniques require further laboratory analysis for gravimetric quantification of SPM mass concentration. At present, there is no instrument available to directly and automatically measure the mass concentration of SPM in the field.

1.2. This work

In this thesis, a new instrument (SEDVEL – Sedimentation Velocity) was developed to directly and automatically measure SPM mass concentrations of cohesive sediments *in situ*. This instrument consists of an underwater balance placed inside a settling tube, which directly measures the variation in time of the immersed weight of particulate matter (*PM*) as it settles on a plate located at the tube bottom under quiescent conditions. This instrument works submerged and it is fully automatic in terms of sampling, measurement and data storage. This instrument constituted a novel idea for its field of application, and therefore a considerable amount of development, prototyping and testing was required. It was designed, built, calibrated in the laboratory, and tested in the field.

Based on the temporal variation of the mass of SPM measured with SEDVEL during an experimental cycle, a methodology is proposed to estimate the mass distribution of settling velocity and to convert the effective immersed mass concentration into dry-mass concentration of SPM. Calculations of dry masses were needed to compare SEDVEL results with the traditional gravimetric analysis usually used as the standard against which other instruments are validated. Settling velocity and SPM concentrations obtained from several deployments of SEDVEL in Cleveland Bay (Townsville, Australia) are presented and analysed in order to test the instrument performance in the field. Results of settling experiments performed in the laboratory with known SPM concentrations and sizes are also described.

Thesis outline

This thesis starts (Chapter 2) with a review of the available instruments to measure the settling velocities and (mass or volume) concentrations of cohesive sediments *in situ*. Instruments are broadly classified as manual or automatic, using either direct or indirect techniques to quantify SPM concentrations and settling velocities. They are also divided into flow-intrusive and flow non-intrusive devices. In each case, the instrument description, working principle, potentialities and limitations are summarized. A general assessment is made by analysing the main issues associated with each kind of measurement, and identifying gaps in either information or instrumentation need to be filled.

Chapter 3 describes the chronological progression of prototypes of SEDVEL that lead eventually to the final design. Subsequently, general and detailed descriptions of the SEDVEL components are depicted. The calibration procedure and its controls are also described. A few examples of SEDVEL measurements carried out in the field are shown, and issues associated with the *in situ* operation of the instrument are explained.

Further, the methodology proposed for calculating deposition rates and settling velocities using SEDVEL is described. Results from experiments undertaken in the laboratory and from the deployments carried out in the field to test SEDVEL performance are presented and the respective settling velocity dynamics of the aggregates analysed (Chapter 4).

The thesis ends with a general assessment of the strengths, limitations and applications of SEDVEL, along with a discussion of suggested improvements to improve its quality and performance (Chapter 5).

The research in this dissertation has been presented for publication in peer-reviewed journals. The manuscript "Devices to measure settling velocities of cohesive sediment aggregates: a review of the *in situ* technology" by A. Mantovanelli and P.V. Ridd, encompasses the review presented in Chapter 2 has been submitted to *Journal of Sea Research*. A second manuscript "An underwater balance: a new approach for measuring *in situ* settling velocities and concentrations of suspended cohesive sediments" by A. Mantovanelli and P.V. Ridd to be submitted to *Marine Geology*. A third manuscript is currently being prepared for publication: "Settling velocity dynamics of suspended particulate matter close to a headland at the Strand

Beach" by A. Mantovanelli, P.V. Ridd and L. Bode to be submitted to *Continental Shelf Research*. This manuscript contains research from Chapter 4.

2. Devices to measure settling velocities of cohesive sediment: a review of the *in situ* technology

2.1. Introduction

Devices for measuring settling velocities *in situ* can be broadly divided into *manual* and automated devices, which apply direct or indirect techniques for settling velocity quantification. These devices can also be classified as flow-intrusive or non-intrusive. The device is classified as manual when most of the water collection and analysis is hand-operated. In contrast, automated devices have water sampling mechanism, data acquisition system and storage, controlled by a built-in controller and data logger. These devices are significantly less labour-intensive in terms of sampling and water analysis, although they may require a considerable effort in post-processing the data and calculating settling velocity and size spectra. Devices are classified as direct when they do not need calibration to obtain SPM concentrations (or mass) and settling velocities or when the calibration is straightforward. Conversely, indirect devices require *in situ* calibration to translate the instrument's signal into SPM concentrations and the use of often complex algorithms to calculate fall velocities.

Direct and manually operated devices include Owen tubes and similar instruments (e.g. Owen, 1971; Allersma, 1980; Van Rijn and Nienhuis, 1985; Cornelisse, 1996; Pejrup and Edelvang, 1996; Van Leussen, 1996; Jones and Jago, 1996). Alternatively, the settling velocity can be directly measured by using automated settling columns equipped with *in situ* video cameras (e.g. Dearnaley, 1996; Eisma and Kalf, 1996; Milligan, 1996; Sternberg et al., 1996). On the other hand, indirect techniques include automated settling columns equipped with optical sensors (e.g. Murray et al., 1996) or laser beams (e.g. Bale, 1996; Agrawal and Pottsmith, 2000). These devices are usually flow-intrusive since measurements are performed inside a closed settling column or in a confined volume of water, while the non-intrusive instruments take measurements in a sampling field of several centimetres (e.g. direct

holographic techniques) or a few metres (e.g. indirect acoustic backscatter) away from the sensors.

The most popular apparatus for measuring settling velocities of SPM *in situ* is the Owen tube − developed in the late sixties at the Hydraulics Research in the United Kingdom (Owen, 1971; Owen, 1976). Subsequently, many different kinds of hand-operated settling tubes have been developed or improved (e.g. Van Rijn and Nienhuis, 1985; Van Leussen, 1988). Within such an apparatus, a water sample is taken in the environment by using a sampling tube that acts as a sedimentation column, from which subsamples are withdrawn at progressive time intervals to quantify their mass concentrations by gravimetry in the laboratory. Although settling tubes are considered *in situ* devices for measuring settling velocities, most of their analytical procedures happen in the laboratory or on the ship deck.

Alternatively, autonomous devices can be used to determine settling velocities in the field, for instance settling columns equipped with optical sensors (e.g. Murray et al., 1996) or laser beams (e.g. Agrawal and Pottsmith, 2000). Although optical/laser devices present high sampling autonomy (long-term deployments), they suffer from calibration issues, since the translation of an instrument's signal into SPM concentrations depends on many particle characteristics and on the adopted optical coefficients (Renagi, 1999; Agrawal and Pottsmith, 2000; Hatcher et al., 2000; Sutherland et al., 2000).

In the last decade, video image systems have became very common, due to their direct and comparatively less disruptive system of simultaneously measuring settling velocities and size by imaging particles/flocs trajectory in successive time frames (e.g. Syvitski and Hutton, 1996; Van Leussen and Cornelisse, 1993a, 1993b; Fennessy et al., 1994). However, video image techniques sample only a very small portion of the mass flux (of the order of a few millimetres) and require complementary SPM mass quantification to obtain the total SPM concentration (Dearnaley, 1996). Overcoming the limitation of small sampling volume, holographic techniques are nowadays the state of the art in imaging and recording large volumes (up to 10^5 cm^3) of marine organisms and particles in a non-intrusive and non-destructive way, providing information on particle 3-D morphology, distribution and motion over a large depth of field and with high-resolution (Watson et al., 1999; Owen and Zozulya, 2000). Alternatively, multiple frequency acoustic sensors allow an indirect and non-intrusive

quantification of floc sizes and settling velocities. Nevertheless, these sensors still require improvements to work accurately for cohesive suspensions (Thorne and Hanes, 2002).

This chapter reviews the main devices used to date to measure *in situ* settling velocities of cohesive sediments in coastal systems. A brief description of different types of apparatus and theier measurement principles are presented. This chapter addresses the principal issues and advantages of each technique, compares their characteristics, and assesses which factors should be taken into account when designing/building new devices for settling velocity measurements in the environment. It concludes with a discussion of the areas in which further instrumentation development is needed to fill the key information gap for understanding the dynamics of suspended cohesive transport.

In the text below, dimensions for diameter, width, length, height and thickness are indicated by D, W, L, H, T, respectively, and are given in centimetres. A (cm^2) and V (l) refer to area and volume, respectively. Generic units of mass and volume are indicated by M and L, respectively.

2.2. Direct measurements

2.2.1. Settling tubes manually operated (Owen-kind tubes) and their working principle

The basic operation of the in situ settling tubes is to take a water sample at a given depth, bring it to the surface as quickly as possible, and keep it still in a vertical position, allowing particles to settle. Subsamples with volumes ranging from 10 to 550 ml, depending on the tube design, are manually taken close to the tube base at regular (or logarithmic) time intervals until the settling column is emptied, where therefore, the last sample contains any residual sediment trapped within the tube. Subsequently, SPM mass concentrations (M L^{-3}) of each subsample are gravimetrically quantified in the laboratory (Owen, 1976; Pejurup, 1988; Cornelisse, 1996; Jones and Jago, 1996; Pejrup and Edelvang, 1996). Usually there is a lag of 20 to 50 seconds between sampling and the beginning of analysis (when the tube is in its vertical position), with the first withdrawal occurring within 1–1.5 minutes after trapping the water sample; the total settling period lasts from 50 to 180 minutes (Dyer et al., 1996).

Settling tubes are usually cylindrical in shape, but their dimensions, sampling volumes, withdrawal and closure systems differ from one to the other. Subsamples can be withdrawn from the tube bottom (bottom withdrawal) (e.g. Owen, 1976) or through the sidewall close to the tube base by using a pipette (pipette withdrawal system) (e.g. Van Rijn and Nienhuis, 1985). Most devices are positioned horizontally at the sampling depth to take the water sample (i.e. horizontal tubes). Then, they can either be immediately brought to the vertical position after trapping a water sample, or be raised in the horizontal position and rotated to the vertical position at the surface. Some operators also rotate the tube (through its horizontal axis) before holding it in the vertical position in order to resuspend any particles that had settled onto the tube wall (e.g. Jones and Jago, 1996). Some tubes enclose the water volume already in the vertical position, but this procedure is not appropriate if SPM concentrations change over a distance of the water column equivalent to the tube height (Puls and Kühl, 1996). Whatever the case, the sedimentation process starts when the tube is in a vertical position, and it is assumed that the SPM within the tube forms a homogeneously distributed suspension (Dyer et al., 1996; Eisma et al., 1997). Table 2.1 summarizes the principal characteristics of the *in situ* settling tubes. A detailed description of these apparatuses can be found in Eisma et al. (1997).

Volumes and weights of the SPM subsamples are applied to compute the settling velocity distribution and median settling velocity. When computing settling velocities, corrections are applied to the weight and time to take into account the fact that: (*i*) successive samples come from a progressively smaller volume of the whole suspension; and (*ii*) the later the sample the shorter the distance settled (Owen, 1976; Bartz et al., 1985; Van Leussen, 1996). The median settling velocity (W_{50}) is obtained by dividing the column height by the clearance time of half of the initial suspension concentration (Cornelisse, 1996; Van Leussen, 1996). Results obtained from settling tubes produce a curve relating the quantity of material settled out in discrete time intervals (the "Odén curve", Figure 2.1a), which can be also expressed in terms of the material left in suspension as time progresses (Figure 2.1b). Settling velocities are generally calculated by dividing the fall height (that varies after each sample extraction) by the elapsed time since the beginning of the experiment (Cornelisse, 1996). More elaborate methods for computing the mass frequency distribution of settling velocities, based on the Odén's theory of sedimentation of polydisperse systems using graphic analysis of Odén curves as well as its mathematical validation can be found in Fisher and Odén (1923-24), Kumbein and Pettijohn (1938) and Subcommittee on Sedimentation (1953).
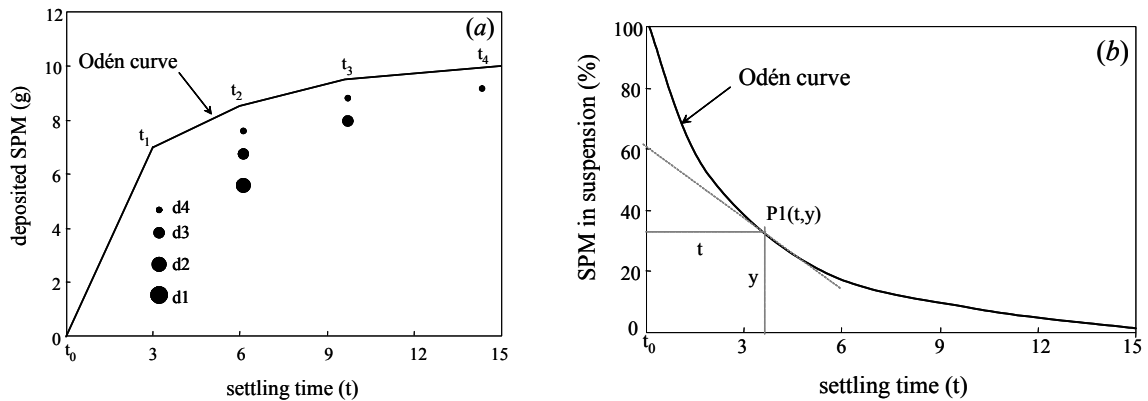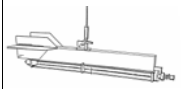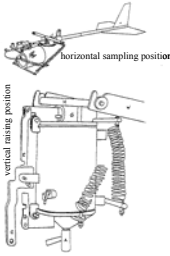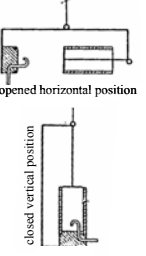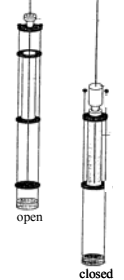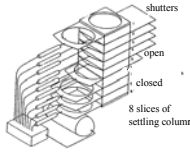
Figure 2.1: (*a*) Odén curve showing the temporal mass accumulation on the bottom of the settling tube for a SPM sample composed of 4 hypothetic discrete particles sizes (d1 > d2 > d3 > d4). All particles are in suspension at t = t_0, when t = t_1 all particles d1 plus some d2 and d3 particles have settled out the suspension, and then successively as indicated by the circumferences on the picture (*b*) Representation of the Odén curve in terms of percentage of material left in suspension. Figures adapted from Subcommittee on Sedimentation (1953).

2.2.1.1. Advantages and constraints of the settling tubes

Owen-kind settling tubes have the advantage of being able to directly quantify the SPM mass concentration (M L^{-3}), and do not require further calibration. Such hand-operated devices are relatively simple and inexpensive, since they basically consist of a water sampler, with no further instrumentation. They are also the unique devices that allow the user to determine the settling velocity distributions, not only of the entire SPM mass but also of each of its constituents (e.g. organic matter, POC, particulate nitrogen or bound lead) provided their masses are measured in each subsample (Puls and Kühl, 1996). They work over a wide range of concentrations, e.g., 2–50 to over 1000 mg l^{-1} (McCave and Gross, 1991).

Some matters associated with the original version of the Owen tube have been improved in later versions. One issue concerned the so-called 'wall effect', which is experienced for large flocs that settle across the horizontal tube before it is set upright and then cascade down the wall instead of settling through the fluid when the tube is placed in the vertical position (Jones and Jago, 1996; Wolfstein, 1996). Some workers have minimized this effect by rotating the tube 180 degrees after recovery and before placing it in the vertical position (Puls and Kühl, 1996), or by using vertical sampling tubes. The wall effect is bigger for small tube diameters.

Table 2.1: Summary of the main characteristics of the in situ settling tubes. First row brings the tubes picture. Pictures of the tubes were extracted from: [1] Fig. 5 of Owen (1976), [2] Fig. 3 of Eisma et al. (1997), [3] Fig. 1 of Jones and Jago (1996), [4] Fig. 14 of Allersma (1980), [5] Fig. 1 of Cornelisse (1996), [6] Fig. 1 of Van Leussen (1996), [7] Fig. 1 of Puls and Kühl (1996) and [8] Fig. 11 of Bartz et al. (1985). The subsequent row are numbered and their contents are as follow: 0 – Tube developer, 1 – Tube dimensions for diameter and height (D × H, cm), 2 – settling period (min), 3 – range of measurable SPM concentrations (mg l^{-1}), 4 – range of measurable settling velocities (mm s^{-1}), 5 – thermal insulation system when present, 6 – sampling position, 7 – sampling set-up, 8 – withdrawal system and sample volume (ml, unless otherwise specified), 9 – closure system, 10 –particularities of each tube and 11 – some references to obtain more information about tube description and field applications.

	Owen tube[1]	Baystoke 110 tube[2]	Quisset tube[3] (Quasi in situ settling velocity)	Allersma tube[4]	FIPIWITU[5] (Field pipette withdraw tube)	RWS tube[6]	Bigdan tube[7]	BEAST[8] (Benthic autonomous settling tube)
0	M. W. Owen Hydraulics Research, UK	Owen tube commercial version, Valeport Ltd.	I.N. McCave, Cambridge University and University of Wales	NEDECO (1965), The Netherlands	Van Rijn and Nienhuis (1985a), Delft Hydraulics	Van Geldermalsen, Rijkswatertaat, The Netherlands	GKSS, Germany	Bartz et al. (1985)
1	5 x 100	5 x 100	9.5 x 100	8 x 32	12.5 x 30	10.4 x 21.1	19 x 100	30 x 82 (8 slices H =10)
2	60 to 180	64	180	30 to 10 days	60	60	120	750
3	50 to 3000	> 40	1 - 50 to 1123	na	20 to 2000	5 to 2000	2 to 6	0.1 to 100
4	0.02 to 8.0	0.03 to 4.9	0.0003 to 0.3-0.8	na	0.05-0.5 to 3.5	0.005-0.15 to 3.5	0.01 to 2.0	0.005
5	no	no	water jacket	no	double-insulated wall	double-insulated wall	gold-coated envelope	it works on the seabed
6	horizontal	horizontal	horizontal	horizontal	horizontal	horizontal	vertical	vertical
7	It is balanced to lie horizontally in water and to hang vertically in air.	It has a tail fin to line it up in the current direction.	It is mounted in a 2 m long frame and held opened at one end by stretched elastic cords.	The tube slides along a frame to which a plunger and a cork are attached.	It has a large tail fin to keep it horizontal. It is put in a vertical position as soon as it closes.	It immediately rotates to vertical position after sampling.	Both ends of the tube are opened; the lifted tube and its metal bottom are 1 m apart.	It sinks to the bed and it isolates 8 samples in a timed sequence from the bottom upwards while SPM is settling.
8	bottom (200 - 250)	bottom (200-250)	bottom (550)	pipette (10)	pipette (200)	pipette (200)	pipette (1000-3000)	closing 8 chambers (5000)
9	The inner tube rotates ¾ of a turn relative to the outer and socks at both ends are twisted to seal.	It is closed by releasing a messenger that seals both ends at same time.	It traps a volume of water by moving the tube horizontally past a piston.	It has valves at both ends connected to a spring system that are closed by releasing a messenger.	It is lowered in the horizontal position and the sample is taken by pulling a rope that causes the body and pipe to slide towards the cork, closing the tube in the vertical position.	It is pulled down by an extra weight connecting to the tube bottom.	It cuts downward and encloses a volume of water when triggered by a messenger.	Chambers are closed by sliding flat sheets drove by hydraulically powered shutters.
10	Operable for currents greater than 0.4 m s^{-1}.		It can be automatically triggered 1 m above the bed.	It has exchangeable tubes.		It has exchangeable tubes.	Pipette is connected to a peristaltic pump with controlled flow intensity. Operable current range 0.1 to 0.5 m s^{-1}. Markdan is a smaller (5 l) version of Bigdan.	It is semi-automatic. After the settling period it sheds ballast and returns to the surface. Shutter relies on high deep sea pressures. Contamination among chambers occurred.
11	Owen (1971, 1976) Eisma et al. (1997)	Pejrup (1988) Pejrup and Edelvang (1996) Mikkelsen and Pejrup (1998)	Jones and Jago (1996) Jago and Jones (1998) Jones et al. (1998)	Allersma (1980) Van Leussen (1988) Eisma et al. (1997)	Van Rijn and Nienhuis (1985b) Cornelisse (1996)	Van Leussen (1988, 1996) Van Leussen and Cornelisse (1993a,b)	Puls and Kühl (1996)	Bartz et al. (1985)

In addition, settling tubes are outside the water during subsample withdrawal (settling periods ranging from 1 to 3 h), and hence they can be subjected to rapid temperature variations that can generate convection currents inside the tube and hence alter the settling velocities of aggregates. It has been shown in laboratory tests that temperature changes of 10ºC lead to statistically different median settling velocities (Puls and Kühl, 1996), and therefore these authors recommended that all Owen-kind settling tubes be equipped with thermal insulation.

There are also two issues related to the subsamples extraction: (*i*) contamination of one subsample by the previous one can take place if particles from the previous sample withdrawal were not completely removed; and (*ii*) the break-up and change of the settling velocity of aggregates generated by turbulent-like currents within the tube during its closure and retrieval, as well as during subsample withdrawal (Pejrup, 1988; Dearnaley, 1996; Puls and Kühl, 1996). Fluid motion in the range 20–30 mm s^{-1} was observed within an Owen tube during subsample withdrawal (Dearnaley, 1997).

Improvements in earlier versions of the Owen tube have included: (*i*) the use of a steeper cone angle and rapid sample withdrawal to minimize the settlement of SPM onto the cone sides during analysis (as in the QUISSET tube, Tab. 1), although some contamination can still occur at high sediment concentrations (Jones and Jago, 1996); and (*ii*) the use of the pipette-withdrawal system that suppresses turbulent water movements inside the tube (Puls and Kühl, 1996). By comparing an old version of the Braystoke tube (with sealing cap ends) with the improved pipette withdrawal system, it was observed that the sealing cap version leads to a 30% reduction in the median settling velocity (Puls and Kühl, 1996). Other authors have also claimed that sampling tubes destroy large flocs, since much higher settling velocities are obtained by video systems than those measured with settling tubes (Van Leussen, 1988; Van Leussen and Cornelisse, 1993b; Dearnaley, 1996; Fennessy and Dyer, 1996).

Settling tubes entail a time-consuming procedure, since they require people to collect and analyze the water samples. They also have a low temporal resolution (one sample is taken in each time interval). According to Pejrup and Edelvang (1996), a major weakness of the method is its sensitivity to the individual operator carrying out the analysis. This is because large differences in median settling velocities may occur as a result of inaccuracies related to how fast the subsamples are withdrawn and how precisely their volumes are extracted. Also,

the precision of the method is limited at low SPM concentrations (< 50 mg l^{-1}) due to the small amount of material available for each subsample. Furthermore, the collection of water samples occurs over discrete time intervals and usually takes 20 to 30 s, while the sedimentation process, however, is continuous. They neither measure size nor aggregate structure; they estimate the net settling velocity of material within the settling column.

2.2.2. Settling columns equipped with automated in situ video cameras

In situ devices equipped with video cameras use sequential images to directly follow the displacement of particles/aggregates in order to obtain their settling velocities between successive frames (e.g. Syvitski and Hutton, 1996). A grid or a millimeter scale is often used as a focusing target for image calibration (Van Leussen and Cornelisse, 1996; Sternberg et al., 1996). Most video systems apply a silhouette technique where particles appear dark on a light background or vice-versa (Fennessy et al., 1994; Milligan, 1996; Manning and Dyer, 2002a). Within video systems, the small effects of water circulation observed inside the settling columns are corrected by assuming that the motions of the smallest visible suspended particle are equivalent to water movements; hence the settling velocities of larger flocs are derived by calculating the difference in the vertical movements of the finest particles and the larger flocs (Van Leussen and Cornelisse, 1993a, 1996; Sanford et al., 2004).

Data analysis can be done on a manual basis by taking measurements from a video monitor (e.g. Fennessy et al., 1994; Manning and Dyer, 2002a) or by applying computer-based image processing techniques to the digitised images (e.g. Knowles and Wells, 1996). As well, particle track computational methods have been developed to follow the particles over some time and distance in order to derive the settling velocity distribution (Van Leussen and Cornelisse, 1996). Sophisticated commercial software is also available for data analysis, which provides a large number of other parameters related to the aggregate dynamics (e.g. excess density, porosity, mass flux, mass concentration, number concentration) (Syvitski and Hutton, 1996; Sternberg et al., 1999). For instance, the excess density ($\rho_e = \rho_f - \rho_w$) is derived from the well-known Stokes's Law or based on the drag coefficient (C$_D$), i.e. $\rho_e = C_D \rho W_s^2 /(4/3\,gd)$, using the observed floc settling velocity and diameter; while the floc mass (M) is determined by multiplying the floc excess density (ρ_e) by its volume V_f ($M = \rho_e V_f$), which is usually obtained by assuming a spherical or ellipsoidal shape and

introducing the measured floc diameter (Syvitski and Hutton, 1996; Manning and Dyer, 1999; Van der Lee, 2000). Similarly, the dry mass is obtained by $M = V_f \rho_e \rho_s / (\rho_s - \rho_w)$, where ρ_s is the mean dry density of the primary particles often estimated by making assumptions about the mineral (2600 kg m^{-3}) and organic (1030 kg m^{-3}) densities and applying generic inorganic to organic mass and volume ratios (Manning and Dyer, 1999). These parameters are combined to estimate the volumetric concentration, mass flux and others, as described by Syvitski and Hutton (1996). A few examples of underwater video systems, which measure both size and settling velocities of individual flocs are presented next.

2.2.2.1. Examples of the available video systems for settling velocity measurement

INSSEV (*In situ* Settling Velocity Instrument, Plymouth University) is a high-resolution monochrome video camera with a ship-borne control system that allows the determination of both floc size (from 20 μm) and settling velocities (Fennessy et al., 1994; Fennessy and Dyer, 1996; Fennessy et al., 1997; Manning and Dyer, 2002a). This apparatus has two-chambers separated by a slide door: (*i*) a decelerator chamber ($D \times H = 10 \times 40$ cm) that allows residual turbulence to decay after capturing a water sample; and (*ii*) a still settling column ($D \times H = 10 \times 18$ cm) filled with filtered water of known density. The amount of particles introduced in this column is set by an operator by controlling the time that the slide door is kept opened, based on the independently assessed SPM concentrations (Fennessy et al., 1994). Moreover, the decelerator chamber flap doors open and close at a speed proportional to the ambient current velocity (independently measured by current meter). Operation of INSSEV requires the current direction to be less than 5–15º away from the decelerator axis to avoid sidewall turbulence. This is achieved by using a heavy tripod (180 kg) sat on the bed, which has a fin that aligns the device with the main flow. Photos of low-density macroflocs (a few millimetres long) interlinked by fine strands suggested that the instrument has a low disruption effect on flocs (Fennessy et al., 1994; Manning and Dyer, 2002a, 2002b).

VIS (Video *in situ* of Rijkswaterstaat and Delft Hydraulics, Netherlands) is composed of a funnel-shaped capture/stilling chamber ($D \times H = 10 \times 15$ cm) connected to a vertical settling tube ($D = 3$ cm) with two light sheet windows and a CCD video camera (HTH-MX-C) (Van Leussen and Cornelisse, 1996; Figure 2.2a). Both the capture/stilling chamber and the

settling tube have their water replaced by very cautious pumping. The device is placed in a stainless steel housing ($D \times H = 30 \times 60$ cm) with a float, independently drifting during image recording. Therefore, this device is robust even in very high currents and wind speeds (up to 2 m s^{-1}), and under SPM concentrations up to 600 mg l^{-1}. The floating system also reduces the effect of horizontal advection on the measurement and the shear around VIS that could cause floc break-up. The system is connected to a monitor and the settling process can be directly observed on board (Van Leussen and Cornelisse, 1993a, 1993b; Van Leussen and Cornelisse, 1996; Van der Lee, 2000). The video system has resolution of 10×15 μm^2, total image size of 9×6 mm^2 and a time step of 0.01 s. The error in settling velocity and size is within 10–20% for VIS measurements (Van der Lee, 2000). Figure 2.2a shows settling velocities computed from VIS measurements during a tidal cycle; other examples of VIS applications are found in Van der Lee (1998, 2000).

Unlike the previous devices, a compact benthic video system (Sternberg et al., 1996) was designed to work moored on a tripod for 4 months, logging for 7s (30 frames per second) every 6 h, with the maximum record time limited to one hour. This video system is composed of a miniaturized sediment trap ($L \times W \times H = 9.7 \times 3.4 \times 25.5$ cm), a video camera (Sony TR600-Hi8) with controller board and an underwater light (Sternberg et al., 1996, 1999; Figure 2.2b). It provides remote operation, independent control capability, low power consumption and a controller/data logger. The system size resolution ranges from 100 to 1000 μm, and it can operate at high concentrations (values not specified). The sediment trap has two particular features: a honeycomb baffle ($W \times H = 0.3 \times 0.8$ cm) at its top, and a double funnel shape (the top funnel collects water and the bottom one the settled sediment) divided by an constricted section 3 mm wide in front of a video camera viewing field that places all particles in focus (Figure 2.2b).

The Floc Camera Assembly (FCA, Heffler et al., 1991) is composed of two stereo 50 mm lens cameras, one 200 mm lens camera, and a collimated plane of light ($W = 2.5$ cm, focal distance). For settling velocity measurements, the FCA is mounted on a frame with a stilling tank that lies on the seafloor. Photographs are taken through acrylic walls of the tank giving the position of sinking particles every 10 s. Usually a large number (concentration dependent) of particles is analysed (hundreds to a few thousand) (Syvitski and Hutton, 1996; Hill et al., 1998). Accuracies for size, shape factor and settling speed are, respectively, within ±20 μm,

±0.05 and ± 0.02 mm s^{-1} range, and its minimum size resolution is 50 μm. FCA can be used as a profiler for sampling floc sizes through the water column or moored at the bottom to take sequential images for settling velocity determination (Syvitski and Hutton, 1996).
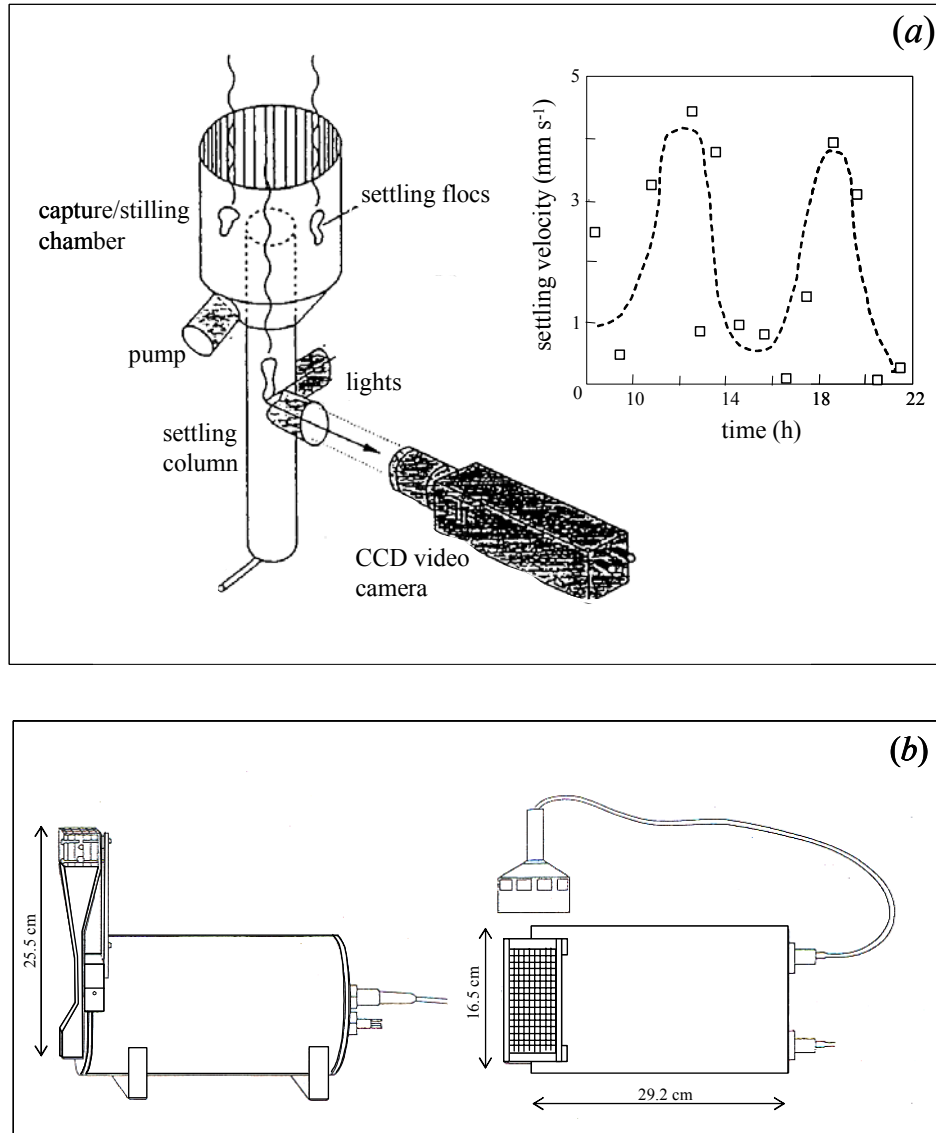
Figure 2.2: Examples of underwater *in situ* video camera devices (*a*) schematic representation of VIS (Video *in situ*) (right) and an example of floating measurements of settling velocity in the EMS estuary during a tidal cycle (left) (modified from Fig. 1 and Fig. 3e of Van Leussen and Cornelisse, 1996) (*b*) Side (left) and top (right) views of a compact benthic video system with a honeycomb baffle (as presented in Fig. 1 of Sternberg et al., 1996).

Sanford et al. (2004) applied the VISTA system (Video *in situ* Settling Tube Apparatus) composed of a settling tube and an underwater video camera (PULNIX CCD, field of view 8.3 × 11.2 mm; resolution of 30 μm), to perform *in situ* measurements of settling velocity and size. In this system, water is pumped to flush the tube, and then valves at the top and the

bottom of the vertical section are triggered to trap a water sample and create a settling chamber. Due to a 90 degree turn at the tube's intake and rapid closure of the valves, some turbulence is generated inside the tube.

2.2.2.2. Advantages and constraints of the in situ video cameras

Video camera devices have the advantage of giving detailed information on the nature of sediment particles (shape and size), often ranging from 20−200 μm to up to a few millimetres, although a size resolution as fine as 4 μm can be achieved (Eisma et al., 1990). These image systems are also able to provide size and settling velocity spectra simultaneously though direct observation of particle tracks in time, from which the effective density can be calculated (Fennessy et al., 1994; Manning and Dyer, 2002a). Size and distance calibrations are straightforward using only a grid or a millimetre scale. They are generally less disruptive than other flow-intrusive devices in terms of sampling, preserving the large aggregates. Some video systems can work in relatively energetic environments (currents of 0.4 to 1−2.0 m s^{-1}) (e.g. Van Leussen and Cornelisse, 1996).

Video measurements do not depend on any particle or medium characteristic except for light quality requirements (Eisma and Kalf, 1996), although some video systems can operate well even at high-suspended loads. For example, the INSSEV video system was found to be very effective at measuring floc characteristics even within concentrations up to 8 g l^{-1} (Manning and Dyer, 2002a). In addition, high-quality video image analysis provides a comprehensive information about floc size, structure and characteristic and allow infer details about floc formation and temporal dynamics (Manning and Dyer, 2002a; 2002b).

However, as the focal distance of video systems is usually restricted to a distance of a few millimetres, they sample only a small number of flocs and a small portion of the settling flux. Hence, a large number of particles must be counted for appropriate statistical estimation and they also require a separate method to furnish the total SPM concentration (Dearnaley, 1996; Traykovski et al, 1999). Jackson et al. (1997), compared five different techniques for measuring particle sizes, and indicated that the sample volume was the most important factor in determining the maximum particle size. Therefore, the upper size limit is set by the rarity of large particles in the small sampling volumes of the image systems, thus compromising their full particle size capabilities.

Only a few comparisons are available between the SPM concentrations estimated from the video image analysis and those independently measured in the field in order to access the capability of the video techniques in representing the settling flux. For instance, Manning and Dyer (2002b) found a good agreement (around 100%) between the SPM concentration computed from the floc population measured by INSSEV and the SPM concentration measured from a filtered gravimetric sample, excepting at high SPM loads when video method underestimated the actual concentration by 20−30%.

Further, mass or volume concentration calculations derived from settling velocity and size measurements require assumptions on the 3D nature of particles based on a 'sphere equivalent diameter' or fractal analysis. This imposes uncertainties to the analysis, since particles are seldom regular in the environment and an irregular particle can have different 'diameters' (e.g. projected area diameter, Feret's diameter, sedimentation diameter) depending on the position in which the cross-section chord is drawn and on the adopted measurement technique (Skinner, 2000). Therefore, the projected particle cross-sections can change, depending on their orientation relative to the photographed angle of view. This again leads to the adoption of a statistical geometric diameter and recourse to a large number of measurements (Syvitski and Hutton, 1996).

Restrictions on the lower detection limit of video cameras (usually 20-100 μm) leaves a certain amount of small particles undetected, and this can lead to an overestimation of the size of flocs. Also, if flocs are partially illuminated, out of focus or overexposed, their boundaries are not sharp and they may be digitized bigger or smaller than the actual size (Van der Lee, 2000). Corrections to the settling velocity, due to water movement inside the settling columns, can be complicated if the smallest observable floc set by the instrument resolution is already large (e.g. 85 μm) (Van der Lee, 2000).

The post-processing image analysis is time-consuming, but with the advent of high speed computers and the development of sophisticated computer techniques, the time required to process an image has been drastically reduced. However, care must be taken to control the amount of pre-processing of images and to reduce the subjectivity of the analyses (Milligan, 1996). The analysis is not automated to the same extent as optical or laser diffraction techniques, as a result of the limitation in the maximum recording time. Some shear can be

expected with the narrow camera sampling volume and mechanisms have been adopted to minimize the fluid flow relative to the measurement path (e.g. floating devices, fins to align instruments to the flow).

2.3. Indirect measurements

2.3.1. Settling columns equipped with optical instruments

The basic working principle of settling columns equipped with optical instruments (optical backscatter (OBS) sensors and transmissometers) is to indirectly monitor the depletion of SPM in time by measuring the rate of clearance (transmissometers) or decrease in the backscatter signal (nephelometers). Transmissometers measure the summed attenuation (due to the water, SPM and dissolved material) of a transmitted light beam along a fixed path length, while OBS sensors work by emitting a light beam (infrared or visible) and registering the amount scattered back to a light sensor (receiver) mounted adjacent to the transmitter (Fugate and Friedrichs, 2002; Ridd et al., 2001). Both sensors quantify turbidity by measuring total grain cross-sectional area per unit area (A) rather than mass concentration; the backscatter is proportional to A and transmission to $1-A$, and A is directly proportional to the particle volume concentration (C_V) and inversely proportional to the particle diameter (d) integrated over n size classes, i.e. $A \sim \sum_n C_{Vn}/d_n$ (Fugate and Friedrichs, 2002).

2.3.1.1. Examples of in situ settling columns equipped with optical instruments

Kineke at al. (1989) proposed an *in situ* spring-loaded cylinder ($D \times L = 13 \times 28.5$ cm) which traps a parcel of fluid between two end plates, and is equipped with a vertical array of five miniature nephelometers used to monitor the decaying backscatter signal with time. This cylinder is mounted on a tripod that sits on the bed, and it is closed by an electrical signal sent from the ship through a cable. Records show a period of 10 to 50 s of high, rapid sensor output fluctuations due to turbulence inside the cylinder, and the swing of the ship limits the length of time that the tripod can remain on the bottom to 3−15 minutes (Kineke et al., 1989; Kineke and Sternberg, 1989). Maximum settling velocity resolutions are 13.3 and 66.7 mm s^{-1} for the top and lower sensors, respectively. Problems associated with the settling cylinder include: (*i*) a large mass of particles remained in suspension by the end of monitoring time;

(*ii*) errors were introduced by calibration and cross-calibration of the optical sensors; (*iii*) residual turbulence during/after the cylinder closure may disrupt the flocs; and (*iv*) the particles may continue to aggregate after sampling (Kineke et al., 1989).

ROST (Remote Optical Settling Tube) (Zaneveld et al., 1982; Bartz et al., 1985) is a rectangular box ($W \times H = 10 \times 25$ cm) equipped with a trasmissometer (light beam 25 cm long, detection volume of 8.8 cm^3). The top and bottom of the box close at the same time, enclosing a volume of water for 22 h before opening again to allow a 2 h flushing period. It was designed to work in water depths of up to 5000 m for several months and to obtain particle settling velocity data with a resolution of 10 μg l^{-1} and 0.1% accuracy, at sampling rates varying from 10 s to 5 min. Within this device measurements can be taken 10 min after the closure of the lids, the time required for the residual turbulence to cease (Zaneveld et al., 1982; Bartz et al., 1985; McCave and Gross, 1991).

A successor of ROST was built, which consists of a rectangular settling box ($W \times L \times H = 25 \times 13 \times 100$ cm) equipped with a transmissometer (Sea Tech, 25 cm of path length and sampling rate of 1 Hz), which is opened and closed with end plates that pivot into position (Hill et al., 1994) (Figure 2.3a). Two problems were found with this box system: (*i*) imperfect sealing which promoted mixing and penetration of sediment-laden fluid within the box; and (*ii*) a relatively high interval of time (i.e. 10 min) required for the damping of turbulence after closure (Hill et al., 1994).

An autonomous apparatus for long-term deployment (2 months) has been developed at Cambridge University. It consists of a cylindrical settling *box* ($D \times L = 25 \times 30$ cm) that traps water parcels (at specified time intervals) between two end lids and measures the decaying backscatter signal of four miniature sensors (MOBS, 3.5×1.7 cm, sample rate 1 Hz, infrared 850 nm) positioned at different heights inside the box (Murray et al., 1996). The settling box has an automatic system that slowly opens and closes the lids in order to minimize turbulence. When opened, the lids form a 45° angle in relation to each other, so that the flushing is maximized (Figure 2.3b). Turbulence induced by door closure takes typically three minutes to damp, and measurements during this period are discarded. Attempts to suspend the settling box (plus a lead weight) in the water column under high currents (1.5 m

s^{-1}) did not succeed, and measurements were restricted to calm periods (Murray et al., 1996). Some data obtained with this device is presented in Figure 2.3b.
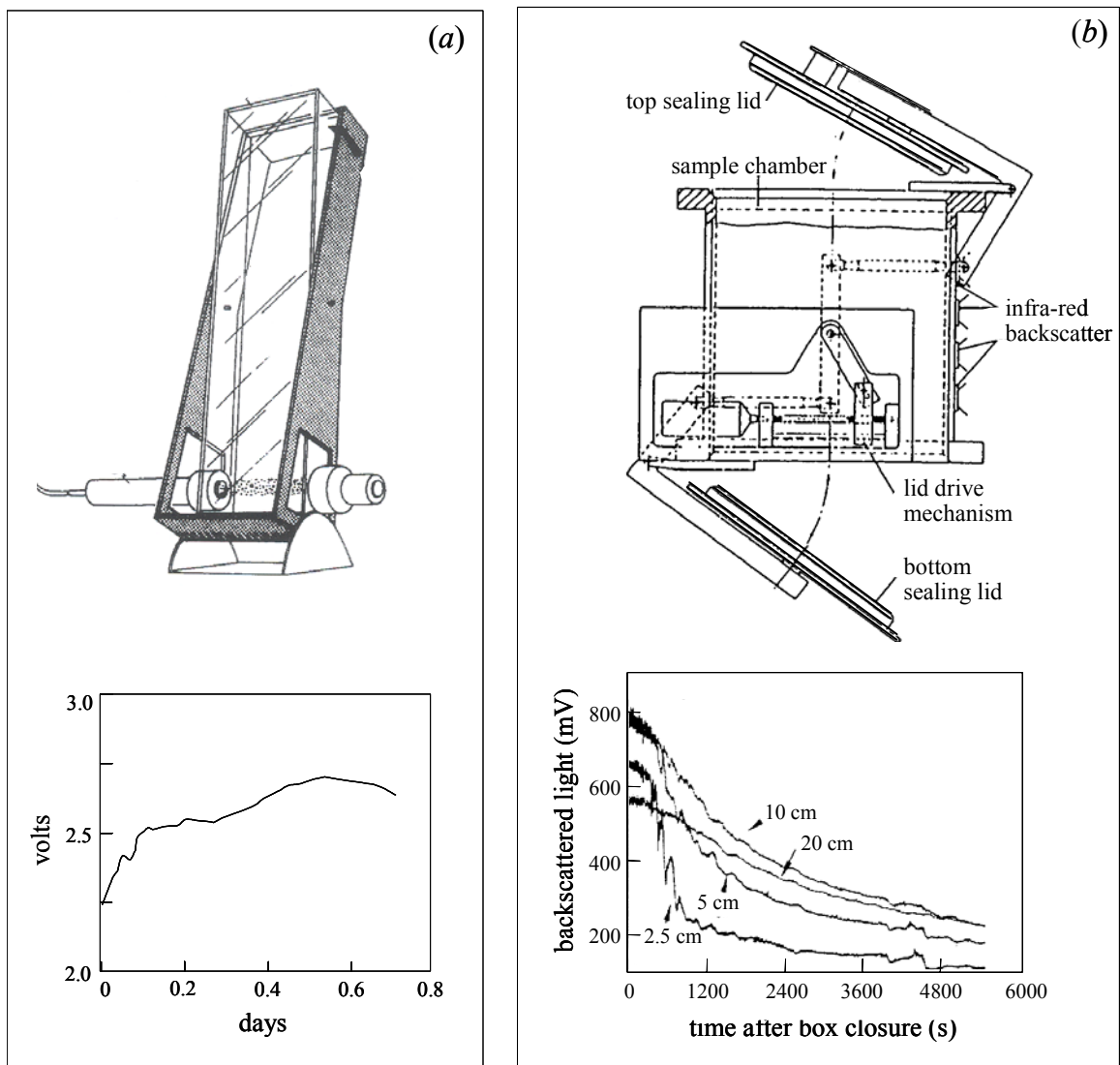
Figure 2.3: (*a*) Remote optical settling box with pivoting doors and a sketch of a typical transmissometer output showing an increase in the transmissivity with time (modified from Fig. 2 and Fig. 3 of Hill et al., 1994), (*b*) schematic diagram of the *in situ* settling velocity box equipped with four miniature OBS sensors (MOBS) and example of the raw data showing the decaying of the backscatter signal with time at the four MOBS located at 2.5, 5.0, 10.0 and 20.0 cm below the top lid (modified from Fig. 1a and Fig. 4 of Murray et al., 1996).

2.3.1.2. Advantages and constraints of settling columns equipped with optical instruments

Settling columns equipped with optical instruments are automatic in terms of sampling, data recording and storage, and they often have a great sampling autonomy (weeks to a few months). Single-frequency optical backscattering and transmission sensors have become very popular for producing series of data with high temporal resolution over a wide range of

concentrations, i.e., between 0.1 to 200 g l^{-1} (Sutherland et al., 2000), although multiple scattering effects and absorption usually occur at high concentrations (Fugate and Friedrichs, 2002). However, they are likely the most suitable techniques to use in very high sediment concentrations (of a few grams) at which most of the other available methods have their measurement capabilities limited.

All one-parameter sensors (e.g. OBS, transmissometers and single frequency acoustic sensors) give a weighed sum of the concentrations of underlying size classes; no size quantification is possible (Agrawal and Pottsmith, 2000). Although OBS response is primarily sensitive to SPM concentration, calibration curve constants and the backscatter signal depend upon a large number of particle characteristics, such as: shape, roughness, refractive index, density, mineralogy, degree of flocculation, colour, and particularly, the particle size (Renagi, 1999; Hatcher et al., 2000; Sutherland et al., 2000). Their sensitivity to the SPM size distribution has been widely demonstrated, and it can result in poor calibration relationships between optical instruments outputs and the SPM mass concentrations, when size distribution varies over time or space, conditions that are common in estuaries (Fugate and Friedrichs, 2002; Murray et al., 1996; Mantovanelli et al., 1999; Agrawal and Pottsmith, 2000). Therefore, despite their sampling autonomy, they require traditional bottle sampling to be extensively taken *in situ* and filtered in the laboratory for SPM mass concentration (M L^{-3}) quantification in order to obtain calibration curves. In addition, Murray et al. (1996) demonstrated the importance of adopting time-variable calibration curves to compute the effects of an increasing backscatter signal with decreasing particle size during the settling inside a settling column, and also the need to use site representative material to convert OBS response into SPM mass concentration.

Similarly, transmissomiter attenuation coefficients for the particles are dependent on many factors, such as: floc diameter, spectral shape, density and organic content, number of particles per unit volume and the scattering efficiency factor. In addition, the calculation of these parameters involves several steps and the use of many conversion factors and assumptions regarding particle 3D fractal dimension, mass distribution and density, which are usually derived from relations between settling velocity and diameter (indirectly obtained by the Stokes Law) (Boss et al., 2001; Zaneveld et al., 1982; McCave and Gross, 1991; Hill et al., 1994). Uncertainty regarding the ratio of particle mass to particle diameter degrades the transmissometers results; if particles are treated as uniform-density quartz spheres with

constant scattering efficiency, the conversion from attenuation to mass scales linearly with particle diameter; if particle bulk density is a decreasing function of particle size, the conversion scales as diameter to a power less than unity. Therefore, the sensitivity of the results of the assumed geometry makes it imperative to better understand the fractal geometry of marine aggregates (Hill et al., 1994).

2.3.2. Settling columns equipped with laser diffraction equipment

The working principle of laser diffraction instruments consists of emitting a laser beam (usually $\lambda \approx 670$ nm) into a suspension of particles, creating a multi-angle scattering pattern that is detected by a series of concentric ring detectors of progressive diameters (Sequoia Scientific, application note L002; Wren et al., 2000; Figure 2.4a). The recorded data is mathematically inverted to obtain the area distribution of particles, and the volume distribution is obtained by multiplying the area in any class by the median diameter in that class and using an empirically determined volume calibration constant. All classes are added to furnish the total particle volume concentration (L^3 L^{-3}) that is independent of particle density or size distribution (Agrawal and Pottsmith, 2000; Wren et al., 2000; Fugate and Friedrichs, 2002). The median diameter within each size class is calculated from knowledge of the scattering angle by applying Mie Theory for spheres and generally assuming a constant refractive index (Traykovski et al., 1999; Wren et al., 2000).
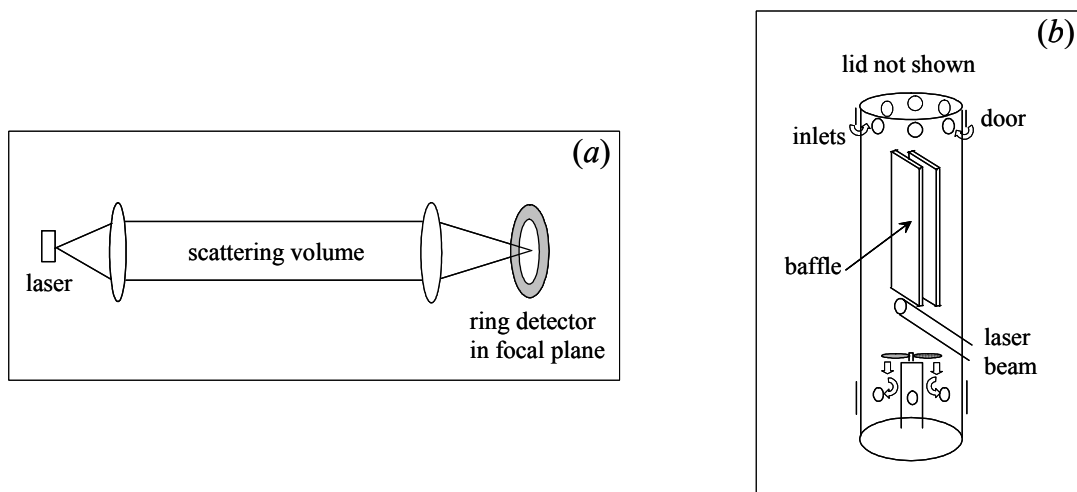
Figure 2.4: (*a*) Configuration of the laser particle sizer instrument (LISST-100) (*b*) and the LISST-ST settling column (Sequoia Scientific, Inc., Application note L002, Application note L007, www.sequoiasci.com).

Laser diffraction techniques are primarily used to obtain particle size distributions. An automated *in situ* laser device (LISST100, Laser *in situ* Scattering and Transmissometry), manufactured by Sequoia Scientific Inc., has been extensively applied for measuring volume concentrations (L^3 L^{-3}) and size spectra (5 to 500 μm) using laser diffraction plus a beam transmission (Agrawal and Pottsmith, 2000; Mikkelsen and Pejrup, 2001; Fugate and Friedrichs, 2002; Serra et al., 2002; Ellis et al., 2004) as well as a similar laser diffraction sizer (Cilas 9250) (e.g. Van der Lee, 1998). An alternative laser technique that uses a focused beam reflectance is described elsewhere, and encompasses the commercially available laser reflectance particle-sizing instrument (Par-tec 100, Lasentec, Inc., Redmond, WA 98052) (Bale, 1996; Law et al., 1997; Law and Bale, 1998). In contrast with the laser diffraction method, the focused-beam reflectance devices are based only on the period of the backscattered pulse when the irradiated laser beam intersects a particle and not on pulse intensity (independent of nature of particles). Therefore, they are able to measure broader particle size spectra (2 to 1000 μm) and concentrations (0.01 to 50 g l^{-1}) at high sampling rate (seconds to few minutes) and with minimal floc breakage (Law et al., 1997: Law and Bale, 1998). Both of these laser devices give volume concentrations (L^3 L^{-3}) of the size spectra, not mass concentration (M L^{-3}).

When using laser particle sizers to quantify particles size spectra, the settling velocity distribution can be indirectly obtained by using the well-known Stokes Law and an estimated excess density of flocs (ρ_e) based on relationships between the floc density and diameter (Krishnappan, 2000) or alternatively, derived from a division between the total SPM mass concentration (independently measured by taken water samples) and the total floc volume concentration obtained from LISST-100 (Mikkelsen and Pejrup, 2000, 2001).

Further, an *in situ* Laser Settling Tube (LISST-ST, Sequoia Scientific Inc.) was developed to obtain settling velocities of 8 size classes in the 5−500 μm range, with sampling autonomy of 83 scans per day in long-term deployments (up to 21 days) (Agrawal and Pottsmith, 2000). The LISST-ST is composed of a settling tube ($D \times H = 5 \times 30$ cm) with an enclosed settling column ($W \times L \times H = 1 \times 5 \times 30$ cm) and a laser beam near its bottom (identical to LISST-100). Samples enter at the top of the tube (through 1.3 cm holes) and a propeller at the bottom is used both to clean the tube and optics and to draw a new sample (Figure 2.4b). A

few seconds after the propeller has been turned off, the top and bottom doors are rapidly closed (Agrawal and Pottsmith, 2000).

With the LISST-ST, the settling velocity of any class-size of particles settling through a column is obtained by dividing the column length by the time needed for the particles to reach the sensor. A particular feature of the LISST-ST is its self event-trigger that uses its built-in pressure and temperature sensors to program the logging schedule based on tides, waves, storms (pressure variance) or fronts (temperature gradients) (Agrawal and Pottsmith, 2000). Noise can be generated inside the settling column due to: (*i*) incomplete mixing of the initial sample at the start; (*ii*) measurement noise; (*iii*) presence of particles of different densities; and (*iv*) the errors of inversion employed in estimating size distribution from the multi-angle scattering. These errors are minimized by estimating the settling times, using a fitting procedure that matches an ideal concentration history to the measured history in a least squares sense (Sequoia Scientific, Inc., application note L007).

2.3.2.1. Advantages and constraints of settling columns equipped with a laser beam

Laser devices can collect and process data quickly and they allow accurate particle sizing because particle composition does not determine its scattering characteristics, but they rely on the assumption that: (*i*) flocs are spheres; (*ii*) the laser beam scatters mainly from the cross-sectional area of a floc, rather than the primary particles that compose porous flocs; and (*iii*) the refractive index of natural flocs is uniform and they can be approximated to those of uniform spheres (Lynch et al., 1994; Mikkelsen and Pejrup, 2001; Agrawal and Pottsmith, 2000). Results of several laboratory and field measurements have suggested that the second assumption is valid and that *in situ* laser instruments are able to measure flocs. They also indicate that the spherical approximation has only a limit effect on size spectra at least for elliptical flocs, as reviewed by Mikkelsen and Pejrup (2001). However, errors become significant when the refractive index of natural particles is vastly different from that used in the computation of the scattering matrix (Agrawal and Pottsmith, 2000; Lynch et al., 1994). Although laser diffraction methods measure without contacting the sample, they require short optical paths (2.5-5.0 cm) that may cause shear-induced flocs breakage (Law et al., 1997; Wren et al., 2000, Wren and Kuhnle, 2002).

Laser diffraction devices are also technologically complicated and expensive. Their use is limited at low concentrations (if there are not enough particles to measure the diffracted signal), as well as at high concentrations (200-500 mg l^{-1}) by light obscuration and multiple scattering effects. They also operate within a limited size range between 5 and 560 µm (Bale, 1996; Agrawal and Pottsmith, 2000). However, Taykovski et al. (1999) showed through laboratory experiments that this upper size limit of 560 µm is restricted to 250 µm when measuring natural sediments. This is because the finite size of the detector limits the range of observable particles (Lynch et al., 1994). Furthermore, the presence of particles finer and coarser than the measured size range affects the estimated size distributions. Also, it is very complicated to estimate volume calibration constants for estuarine/coastal particles because of their size-density dependence and fragility (Fugate and Friedrichs, 2002). Finally, Fugate and Friedrichs (2002) pointed out that the inversion approach used to find particle diameter from the laser diffraction method is "an inherently underdetermined problem and the resulting size distribution is approximate", especially when considering multimodal distributions. In the case of LISST-100, the resolution of 32 size classes is only possible for a noise-free data set, because the inverse matrix amplifies any noise in the measurement and distorts the resulting estimate size spectra. In practice, only about 10-12 sizes can be resolved within the 200:1 observable size range (Sequoia Scientific, Inc., application note L008).

On the other hand, regardless of their broad concentration and size resolution, focused-beam devices work poorly for amorphous particles high in organic matter, which have little or no reflectance, and in situations when particles shapes vary drastically from spheres (Wren et al. 2000). The calibration procedure for multimodal size distributions is also complicated, and the reflectance method is less effective (Law et al., 1997). In addition, the laser beam only focuses on a very small area (< 2 µm^2) (Wren and Kuhnle, 2002).

2.4. Miscellaneous techniques

Different designs of sediment traps can be used for measuring particle sedimentation fluxes in the ocean, although the use of trapping mechanisms present three main concerns: hydrodynamic bias; sample contamination; and particles degradation as discussed elsewhere (Asper, 1996; Thomas and Ridd, 2004). For instance, commercial versions of sediment traps (Model PPS4/3, Technicap, France) have been used in 36–48 h deployments to monitor *in*

situ settling velocities of particles in wind-disturbed lakes. This trap ($D \times H = 25 \times 100$ cm) consists of a 12-bottle carousel with a programmable settling period interval (e.g. 3–4 h). The sediment collected in each bottle is gravimetrically quantified on retrieval, and the sediment flux corresponds to the mass collected divided by the collecting area and sampling time (Douglas et al., 2003). This method gives an estimate of the total settling velocity integrated over the sampling period. More sophisticated free-floating sediment traps equipped with holographic cameras have also been used for measuring particle 3-D size and settling velocities (Carder et al., 1982; Costello et al., 1989) as described in section 2.5.1.

A very complete device called INSSECT (*In situ* size and Settling Column Tripod) has been developed for simultaneously measuring ambient floc size, settling floc size, settling velocity and Reynolds stress (turbulence) *in situ* (Mikkelsen et al., 2004). It is composed of several instruments including: a digital silhouette floc camera (DFC, resolution of 45 μm, minimum measurable size 135 μm); a digital silhouette video camera (DVC, with resolution of 66 μm, clips of 1 min) plus a settling column; a unique sediment trap; a laser sizer (LISST-100); an optical backscatter sensor (OBS); a compass and tilt meter; and a modular acoustic velocity sensor that measures turbulence (Mikkelsen et al., 2004). This instrument also includes a programmable sediment trap carousel (with 24 cups). The equipment is attached to a rotating frame mounted on a tripod base, which has a fin to align it to the flow direction. This rotating frame ensures that the instruments, which have flow-through sensing zones (e.g. DFC and LISST-100), are kept perpendicular to the flow to minimize floc break-up. A critical point about INSSECT is its recovery, which has to be very careful to prevent loss of particles accumulated in the cups. It can be deployed for up to 2 weeks from smalls vessels, operating in shallow waters, and be recovered, turned around and redeployed quickly (Mikkelsen et al., 2004).

Another technique under development (MOPAR, Moored Optical Particle, Dynamics Technology, California) includes: (*i*) a multi-aperture detector composed of several photodiodes; (*ii*) a dual-purpose imager that includes both a shadowgraph technique and laser diffraction instrument; and (*iii*) a sending device. This instrument will simultaneously be able to provide three-dimensional trajectories of multiple particle and size-specific particle abundances. It is designed to be moored and to gently withdraw the water sample, aiming to minimize floc break-up (Asper, 1996).

2.5. Non-intrusive measurements of settling velocity in a turbulent field

Some methods allow a non-intrusive *in situ* determination of floc settling velocities without confining a water volume, and therefore they do not influence the ambient turbulence or the flocculation dynamics. Two examples are explained in more detail – direct holographic techniques, and indirect acoustical sensors. Alternatively, *in situ* non-intrusive settling velocity evaluations can also be performed by: estimating the clearance rates of sediment from a plume (e.g. Hill et al., 2000); analysing the decaying of SPM concentrations in consecutive profiles measured before and after a dredger (Wolanski and Gibbs, 1992); or monitoring over the time the disappearance from the water column of fluorescent tracers to quantify the rate of paint/dye deposition (Adams et al., 1998).

2.5.1. Direct holographic technique

In the last few years underwater optical holography has gained both increasing feasibility and the range of applications for which it is used in oceanographic measurements, including for instance: *in situ* observation of living, motile, marine organisms (e.g. Chalvidan et al., 1998; Watson et al., 1999; Katz et al., 1999; Malkiel et al., 1999); inter-particle relationships; turbulence; local shear and relative motion (Katz et al., 1999), and a particle velocimeter (e.g. Carder et al., 1982; Costello et al., 1989). A few examples of holographic systems that have been directly applied to measure particle settling velocity in marine devices are described here. The hologram measurement principle consists of emitting a collimated and spatially filtered laser beam which traverses the ambient water between the two windows. This light is diffracted by the particles in the sample volume and their interference pattern can be recorded on a high-resolution film (Malkiel et al., 1999) or a charge-coupled device (CCD camera) (Owen and Zozulya, 2000) (Figure 2.5).

They can work in one of two geometrical configurations, "in-line" or "off-axis", with the second method usually presenting a smaller size resolution but a larger sampling volume, i.e. a concentration of particles more than an order of magnitude larger (Malkiel et al., 1999).
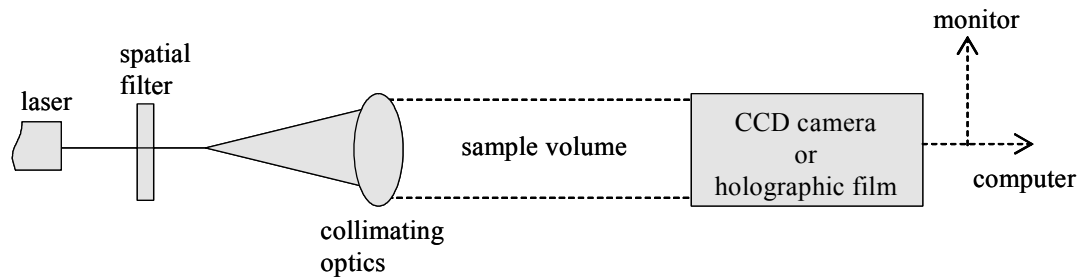
Figure 2.5: Diagram of the holographic array composed of a laser light that is spatially filtered and collimated, a remote sample volume and a CCD camera or holographic film connected to a computer and video monitor (modified from Owen and Zozulya, 2000; Costello et al., 1989).

One of the first contributions to *in situ* holography was due to Carder et al. (1982) who developed a free-floating sediment trap equipped with a submersible holographic particle velocimeter (HPV) for recording *in situ* sizes, shapes, orientations and settling rates of microscopic particles. The HPV uses an in-line hologram to record the interference between the far field diffraction patterns scattered by the particles and the collinear background in the HeNe (2 mW) laser-illuminated sample volume (3.27 ml) (Carder et al., 1982). Measurements are taken in a settling chamber ($W \times L = 4.5$ x 50 cm) opened only at the top and fitted with two sets of flow dampers ($L = 5$ and 10 cm) to minimize water motion in the sampling path. The HPV is controlled by a digital timer and programmed to trigger exposures at 7, 7.5, 9 and 13.5 s after starting the laser, with the system able to collect a total of 250 exposures (Carder et al., 1982). At that stage data reduction was manually performed by reconstructing the holographic images onto a white screen (200× magnification) and measuring 30 particles dimensions and displacement between frames with a micrometer (Carder et al., 1982).

A similar sediment trap system was used in 28 deployments in the North Pacific Ocean (depths of 37 to 907 m) that produced 4000 holograms with 10^8 observable data planes. This system integrates a free-drifting sediment trap with two independent holographic imaging systems, with HeNe laser illumination to record sequential particle movements through the collection cup from two orthogonal perspectives (Costello et al., 1989). The trap ($H = 300$ cm, 350 kg in air) has six conical cups ending in a small sampling volume ($V = 7$ cm^3), where mass accumulation is monitored by an upward-looking holographic system. Six sequential samples of SPM can be collected over periods ranging from 3 h to 6 days, at a sampling rate varying from 15 s to 29 min. The maximum measurable fall velocity corresponds to that of a quartz sphere with a diameter of 76 μm. The sampling cups are filled either with a high

viscous fluid to observe the settling and shape of mineral particles, or high-salinity water to allow observations of the light organic material and organisms (Costello et al., 1989).

The previous devices, although using holography, are flow intrusive since they measure the particles settling inside small chambers. Devices developed more recently are flow non-intrusive and utilize a bigger sample volume. For instance, a submersible holographic camera that records single or multiple exposure holograms (300 exposures per deployment) for measuring particle sizes (from 10 μm) and motion in the ocean. This is a battery powered, modular, self-contained system remotely operated by a PC through fibre optic links. It also contains a buoyancy control system that allows deployment as a neutrally buoyant drifter or in a slow profiling mode. It consists of a pulsed ruby laser (694.3 nm light, power of 30 mJ and pulse of 30 ns) and two independent dual flash lamps. It can be configured both for in-line and off-axis holography of a sampling volume ranging from 732 to 1964 cm^3, in which typically 5000 to 20000 identifiable particles are recorded (Katz et al., 1999; Malkiel et al., 1999).

Most recently, a commercial version of a digital in-line holographic sensor (DHS) has been developed (Owen and Zozulya, 2000). This device has two laser diodes (680 and 780 nm), with a 25-cm depth of field and uses a CCD array to record the diffraction patterns formed by the particles. Over 200 sequential holograms can be recorded at a 30 Hz sampling rate and with a size resolution of 5 μm. Sophisticated software module (Holomaker) numerically reconstructs the particle images in two-dimensional slices taken through the 3D sample volume (Owen and Zozulya, 2000).

Modern holographic techniques provide a non-intrusive measurement of size and settling velocities of a large number of particles since they sample a much larger volume compared with video systems. Data processing of hologram information is time consuming, but it has been facilitated by the use of advanced software for image reconstruction.

2.5.2. Indirect acoustic methods

Multiple-frequency acoustic backscatter can be used for measuring particle concentrations, size and current velocity by emitting very short pulses (≈ 10 μs) of sound of high frequency (≈ 1−10 MHz) through the water column, which are scattered back by the suspended particles

and registered by a pressure sensor. Then, inversion methods are applied to convert the backscatter pressure profiles as a function of z, the height above the bed, to particle diameter (62−2000 μm) and SPM concentration profiles (up to 30 g l^{-1}) (e.g. Kawanisi and Yokosi, 1997; Thorne et al., 1991; Rose and Thorne, 2001; Wren and Kuhnle, 2002). The acoustic backscatter signal can be empirically calibrated to mass concentration of SPM by collecting and analysing water samples taken *in situ* (e.g. Holdaway et al., 1999; Fugate and Friedrichs, 2003; Voulgaris and Meyers, 2004). Alternatively, the calibration can be performed in the laboratory using bottom sediment from the sampling site (e.g. Thorne et al., 1991; Kawanisi and Yokosi, 1997; Willians et al., 1999).

The equation used to compute the concentration profiles of suspended particles based on the backscatter pressure profiles depends on the backscatter pressure, density of sediment, the sediment backscattering form factor, attenuation coefficients due to water and suspended sediments as well as on other sensor specific parameters (e.g. acoustic power, gain, beam strength) (as described in Vincent and Downing, 1994, Eq. 1). In addition, temperature and to a lesser extent salinity can influence the total acoustic attenuation coefficient in seawater containing suspended particles (Richards, 1998). The intensity of the backscattered pressure due to suspended particles (I) is proportional to the particles concentration (C) multiplied by a form factor (f) and divided by the diameter of particles (d) integrated over the n size classes, i.e. $I \sim \sum_n C_n f_n^2 / d_n$; where the form factor is a complex function of grain size, shape, elasticity and density (Lynch et al., 1994; Fugate and Friedrichs, 2002). The form factor (or f_n^2 / d_n) is generally inferred by calibration in the laboratory by analysing the acoustic scattering properties of disaggregated sediments from the area of interest (e.g. Sheng and Hay, 1988; Lynch et al., 1994).

Through the acoustic method, settling velocities of near-bed suspended particles may be indirectly estimated by assuming a lowest-order sediment concentration balance between gravitational settling and upward turbulent diffusion, i.e. $-W_{sn} C_n = K \, dC_n / dz = -\langle w' C'_n \rangle$, where W_{sn}, C_n are, respectively, the settling velocity and concentration of particle type n, K is the eddy diffusivity and the turbulent fluctuations in both vertical velocity (w') and backscatter (C') can be measured directly with the acoustic Doppler velocimeter (ADV) (e.g. Vincent and Downing, 1994; Fugate and Friedrichs, 2002, 2003). The above equation can be

integrated under steady state conditions to produce the Rouse equation (Rouse, 1937), from which *in situ* settling velocity can be computed based on vertical SPM concentrations and bed shear stresses (Dyer, 1986). Again, the wave-current bed shear stresses and SPM concentrations applied to the Rouse equation can be measured by acoustic backscatter sensors (e.g. Williams et al., 1999; Rose and Thorne, 2001; Williams et al., 2002). Alternatively, Kawanisi and Yokosi (1997) estimated temporal variations of SPM settling velocities using the non-steady form of the transport equation of suspended sediment and applying ADV data to estimate turbulent fluctuations of SPM concentration and velocity.

Acoustic backscatter offers a very high temporal (≈ 0.1 s) and spatial (≈ 1 cm) resolution and, additionally, the ability to measure SPM concentrations non-intrusively and to observe the behaviour of turbulent processes very close to the bed. The method also provides a temporal location of the bed and samples of a large stratum (few metres) of the water column (Thorne et al., 1991; Rose and Thorne, 2001). The acoustic method also allows estimating *in situ* settling velocities without affecting the ambient turbulence (Fugate and Friedrichs, 2002).

However, acoustical techniques require the use of complicated interactive-algorithms to translate the sensor response into SPM concentration and size distribution, which need to take into account several compensations for variations in water properties (e.g. temperature, salinity), instrument characteristics (e.g. power, frequency) and the dependency of the calibration to the size of sediment in suspension (e.g. Thorne et al., 1991; Vincent and Downing, 1994; Thorne and Hanes, 2002). Therefore, in order to calibrate the acoustic instruments is necessary to know the size of material in suspension and; changes in the in situ size distribution in relation to sediment sizes used to calibrate the sensor will increase uncertainty in the estimation of concentration values (Thorne et al., 1991). This fact is particularly critical when working with cohesive sediments, since the behaviour of the form factor (f_n^2/d_n) as a function of particle size is unknown for naturally aggregated silts and clays (Fugate and Friedrichs, 2002). The acoustic backscattering characteristics of porous aggregates are still unexplored due to the difficulty in retrieving undamaged, unaltered samples of aggregates from the field (Lynch et al., 1994) and due to the inexistence of well-defined inversion algorithms for use with cohesive sediments, especially in high concentration environments, when attenuation is substantial (Thorne and Hanes, 2002). Further, Fugate and

Friedrichs (2002) suggested that the acoustic form function depends mostly on the size and shape of the constituent grains rather then the size or shape of the aggregate as a whole.

In a review of acoustic methods, Thorne and Hanes (2002) pointed out that the use of sound to measure SPM concentration and particle size has been successful in non-cohesive environments; and therefore, there is a need to understand acoustic properties of more complex suspensions of combined cohesive and non-cohesive sediments, if the development of such instruments is to progress. However, the much larger sensitivity of acoustic sensors to sand-sized particles (tens to hundreds of microns) (Osborne et al., 1994; Gartner, 2002; Voulgaris and Meyers, 2004) complicates the interpretation of the acoustic signal in mixed non-cohesive/cohesive environments.

In addition, the translation of acoustic backscatter signal strength into SPM concentrations and size is very complicated due to the difficulty in creating apparatus in the laboratory that can maintain uniform sediment concentrations suitable for calibrating instruments; furthermore these laboratory facilities (e.g. large-scale flumes) may not be always available (Wren et al., 2000; Thorne and Hanes, 2002). Ultimately, the presence of biological material and bubbles can contaminate the acoustic backscatter signal (Thorne and Hanes, 2002).

2.6. General assessment

The devices available to quantify settling velocities of cohesive sediments have demonstrated both the feasibility and the importance of *in situ* measurements. These *in situ* measurements have been performed by applying different devices and measurement principles over the last four decades. Even though many improvements and much technological sophistication have been achieved, there remain some issues to be resolved, mainly associated with difficulties in quantifying and predicting the complex properties of particles aggregates and in finding mechanisms to perform an undisruptive sampling. Although there is no ideal instrument, since each device was designed to meet a specific scientific purpose and a particular research application; it is valuable to put into perspective the different options available and the factors that should be taken into account when analysing results obtained with a particular device or comparing results between them. Moreover, some concerns are common to all or

most of the instruments and they need to be considered when improving or building new devices.

Most methods of measuring the settling of aggregates involve their capture in settling tubes or stilling chambers by trapping or withdrawing a water volume *in situ* through different sampling mechanisms, such as: pumping, lids or valves closure systems; vertical/horizontal tube displacement; flow decelerators (e.g. baffles); and so on. These methods are all flow intrusive and can themselves alter the flow and aggregate characteristics. Although most authors agree that different devices can disturb to more or less extent fragile aggregates, the absolute quantification of the amount of disruption is very difficult because of the dissimilarity of the measurement principles and design among devices, or the lack of well-controlled protocols for operating similar devices (such as the settling tubes). This makes comparisons of the results among them debatable.

As an example, Dearnaley (1996) observed an order of magnitude reduction in the settling velocities obtained with an Owen-tube (not thermally insulated) compared with those derived from image analysis. By contrast, Sanford et al. (2004) found reasonable agreement between the settling velocities obtained with a Valeport settling tube and those measured by an *in situ* video system. They attributed this to (*i*) their sampling of break-up resistant resuspended flocs; (*ii*) sampling low enough SPM concentrations so that interactions between particles were negligible; and (*iii*) careful insulation of the tube from external temperature fluctuations. An inter-comparison investigation for testing ten devices (i.e. seven different settling tubes and three video image systems) used to quantify *in situ* the settling velocity of aggregates in the turbidity maximum of the Elbe estuary found differences of an order of magnitude between the results. These discrepancies were partially attributed to small-scale spatial and temporal SPM patchiness in the turbidity field, and also to differences in the setup/design/measurement principle of the devices, the experimental procedure and methods used to calculate median settling velocities, and the use of distinct starting times for computing settling velocities (Dyer et al., 1996).

Another issue common to all settling columns is the turbulence induced by the closure of the apparatus. The turbulence usually takes a few minutes to cease and prevents the settling behaviour from being reliably measured during this period. All settling tubes exhibit this phenomenon to an extent that is dependent on the column dimensions and closure system. If

the influence of trapped turbulence is ignored there will be an underestimation of the settling velocities (Murray et al., 1996), since the settling velocities of the faster larger aggregates are not well represented. This can be the case, not only for the Owen tubes, but also other devices. Although it would be difficult to idealize a completely non-disruptive device in terms of water sample capture system and settling column closure, some design solutions can help minimize this influence. For instance, the feedback system used in the INSSEV instrument for closing the chamber flap door at a rate proportional to the ambient current speed potentially reduces the induced turbulence inside the tube (Fennessy et al., 1994). In addition, the rotating frame proposed by Mikkelsen et al. (2004), which orients itself with the flow, largely solves the problem for those instruments that need to be aligned to the flow, and diminishes the current shear on the devices under high currents.

In addition, generating still conditions within the settling columns can interfere with the particle-fluid interactions. When particles settle in a confined settling tube through a fluid of finite extent the drag on particles is increased because when the fluid streamlines around the particle impinge on the tube walls, they are reflected back on the particles; and because as the fluid is stationary at a finite distance from the particle there is a distortion of the flow pattern, which reacts back on the particle (Allen, 1981). Interactions among particles in a polydisperse suspension can also change their terminal settling velocity compared to that of a single particle. For example, the entrapment of slower particles within the wakes and vortex rings of faster particles ("hydrodynamic wake capture") increase the settling velocity of the clustered particles (Lovell and Rose, 1991a,b). Therefore, settling columns dimensions and flocs-fluid interactions can affect the measured settling velocities. A minimum internal tube diameter of 4.5 cm has been recommended to avoid wall and wake capture effects (Lovell and Rose, 1991b). Conversely, in a large tube diameter, large flocs are formed and settling is more rapid than in a small tube, where large flocs cannot develop (Eisma, 1986).

Another source of error is inherent to all instruments and methods that apply the Stokes' Law to indirectly estimate settling velocities from size measurements (or vice versa). In either case the estimate is very crude because of the unknown density (Fennessy et al., 1994). The density is extremely important to determine the settling velocity of the flocs, and to a lesser extent the flow through and around a porous floc can also affect its fall speed (Lick and Huang, 1993). Van der Lee (2000) found a large scatter when plotting floc settling velocities as a function of their size and attributed this to differences in floc densities. Therefore, a more

accurate prediction of the floc effective density (or excess density) is obtained when the Stokes' Law is inputted with both size and settling velocities, directly and simultaneously measured. Also, more robust mass flux estimates can be achieved by including assumptions about flocs' mean dry density based on their organic content (Manning and Dyer, 1999). Furthermore, it has been demonstrated in laboratory experiments that fractal permeable aggregates produced settling velocities 4 to 8.3 times higher than those predicted by using either an impermeable sphere model (Stokes' law) or a permeable sphere model that specified aggregate permeability for a homogeneous distribution of particles within an aggregate (Johnson et al., 1996). Therefore, the Stokes' Law underestimates floc settling velocities because porous, permeable aggregates have different drag relationships from those of spherical particles (Mikkelsen et al., 2004).

Estimates of aggregates density are still more demanding, since density depends not only on the floc sizes, but also on their organic content and structure (Van der Lee, 2000). The aggregate density and effective density are required to calculate vertical settling fluxes, when measurements of aggregate mass are not available. Particularly, even a small number of macroflocs can account for a large portion of the vertical settling flux (Van Leussen and Cornelisse, 1993b). Even if the aggregates could be properly preserved after their collection in the field, the direct determination of the floc density in the laboratory is difficult. For instance, when measuring the density by settling flocs in sucrose solutions, the pore water of flocs is quickly replaced with the sucrose solution, thus altering the floc density (Gibbs, 1985). At present, there is no instrument available to directly measure the density of flocs *in situ*.

In addition, none of the existing instrumentation can simultaneously measure the settling velocity, size and density of aggregates, all of which are crucial parameters for describing the dynamics of the aggregates. These parameters change over time in coastal systems, as a function of variations in the balance between the forces of aggregation and disruption (Fennessy et al., 1994), mainly driven by the turbulence level within the water column. Therefore, researchers have become more aware over time of the need to combine diverse kinds of instruments to be able to measure the different aspects of cohesive sediment dynamics, and to join the various pieces of information together to delineate the whole picture. This approach has been adopted in recent studies where compound instrumentation for simultaneous measurement of floc sizes and settling velocities (through multiple methods) as well as flow monitoring (3D velocity and water density) has been applied using

an instrumented platform (e.g. Mikkelsen et al., 2004) or simultaneous deployments (e.g. Sanford et al., 2004).

The use of multiple instruments in simultaneous deployments that follows a consistent sampling protocol to facilitate data comparison seems a more appropriate approach to investigate the cohesive aggregate dynamics. In addition, measurements of the physical characteristics of the settling medium (e.g. current speed, Reynolds regime, salinity and temperature) are very important as are comparisons between the aggregates' sizes and settling velocities measured inside (maximum settling velocity) and outside (turbulent-dependent) the settling columns. In order to perform these measurements, both flow intrusive and non-intrusive techniques need to be applied.

One of the most challenging tasks is the design of non-intrusive sampling devices and settling chambers, since some turbulence is inevitably generated during sampling or water sample replacement. Most of the optical, laser and video techniques require a short scan path and focal window dimensions, and they usually use small sampling chambers that can promote some instrumental shear-induced floc breakage. Although there is some speculation about the potential floc disruption during sampling, there are a few systematic attempts to quantify this effect. Some effort should be directed to designing and testing different settling columns dimensions and shapes, as well as less disruptive ways to confine the water samples. Moreover, a few devices can successfully work as profilers and be deployed on the bottom. Higher flexibility in this direction could be sought by designing more robust devices to work while suspended in the water column under high current velocities. Increasing the portability of instruments (by reducing their weight and size) would also broaden their application to different environments (both shallow and deep coastal systems) and reduce the logistic and personal requirements for operating them.

2.7. Conclusions

A better understanding of the dynamics of aggregates could be achieved if their settling velocity, size and density could be measured at the same time in a non-disruptive way. Despite the large number of devices available to measure settling velocity in the field, there is a lack of autonomous instrumentation to quantify, *in situ*, the settling velocity mass distribution and particulate matter density. Simultaneous measurements of these two

parameters, together with the determination of the particle size distribution, would considerably improve the knowledge of cohesive sediment dynamics, filling an information gap that would clarify uncertainties associated with some of the theoretical assumptions (e.g. uniform floc density, spherical shape) inherent to most of the techniques. Additionally, the determination of the mass frequency distribution of settling velocity would improve the numerical modelling of SPM mass transport.

Indirect mass estimates of *PM* based on simultaneous measurements of size and settling velocities are still just approximations, considering the large number of assumptions involved in these calculations. Direct devices used for this purpose have the advantage of reducing the build-up of errors that occur during data calibration and in the use of various mathematical procedures for data analysis. In summary, further instrumentation development is needed to measure *in situ PM* mass and settling velocity distribution as well as *PM* density. In addition, further development is required for new mechanisms to enclose and replace water samples inside settling columns in order to reduce the break-up of fragile flocs.

3. SEDVEL: an underwater balance for measuring *in situ* settling velocities and suspended sediment concentrations

3.1. Introduction

As explained in Chapter 2, direct measurements of mass-concentrations and settling velocities of suspended particulate matter (SPM) can only be done by using bottle sampling or settling tubes. Both techniques require further laboratory analysis for gravimetric quantification of dry particulate matter (*PM*) mass per unit volume of suspension. As there was no instrument available to directly measure mass concentration of SPM in the field, the work in this thesis was aimed at developing an automated mass balance that could work under water.

Gravimetric analytical balances have been used in the laboratory for temporal monitoring of sand grains and silica particles settling inside a tall sedimentation tower ($D \times H = 20 \times 200$ cm). In the laboratory set-up, an electronic mass balance is placed at the top of a cylindrical tower, while the weighing scale plate is located at its bottom, held by an under-hook suspension system. This balance is connected to a computer that allows continuous readings to be taken. These balances usually have a high accuracy and reproducibility (Rigler et al., 1981; Renagi, 1999; Ridd et al., 2001). Using a similar set-up, various commercial computerized sedimentation analysers are available for measuring size and settling velocity distributions of sand-sized material in the laboratory (e.g. MacroGranometer).

Restrictions on the employment of gravimetric quantifications for *in situ* applications include the difficulty of sealing electronic balances for underwater use, as well as their high power consumption. An alternative design of a mass balance has been proposed in this thesis, which can work underwater and requires low power consumption.

In this work, a new instrument (SEDVEL–Sedimentation Velocity) was developed to measure *in situ* SPM mass concentrations and settling velocities of particles and aggregates.

SEDVEL directly measures the variation in time of the immersed weight of particulate matter (*PM*) as it settles on a plate located at the bottom of a settling tube, which is filled with a water sample taken in the environment and kept under quiescent conditions. It basically consists of a mass balance, which uses a magnetic spring system and a distance sensor that detects micrometric variations in the balance plate equilibrium position as particles/flocs settle on it. This instrument works under water and is fully automatic in terms of sampling, measurement, and data storage.

SEDVEL has the advantage of being able to directly measure the *PM* mass, and therefore it does not require multiple parameter calibrations and indirect mass estimation. Its calibration is straightforward, even though as the balance plate works immersed, buoyancy effects can alter its equilibrium position, and therefore the density of the medium can alter the balance sensitivity.

This chapter describes the first SEDVEL prototypes and how the instrument evolved to its final design. Further, a detailed description of the SEDVEL components and its calibration procedure are given as well as a discussion of some measurements carried out in the field. The SEDVEL is presented in the following order:

- issues associated with the different versions of the balance and SEDVEL prototypes and the adopted solutions
- SEDVEL general description
- detailed description of SEDVEL parts and working principle
- calibration procedure and factors that influence the balance calibration and sensitivity
- examples of SEDVEL data series in the field
- SEDVEL applications and limitations

3.2. First ideas and prototypes

The very first idea for the underwater balance involved having a set-up similar to the sedimentation towers used in laboratory, but one that could work submerged. A balance plate would be placed at the bottom of a settling column and an analytical balance would be located inside a waterproof container. This idea was discarded, due to the difficulty in finding

an efficient system for sealing an analytical balance to make it waterproof. Even if the electronic parts were immersed in silicon oil, sediment could accumulate at the interface between the oil and the saline water after a few cycles of measurement and could prevent a proper balance plate movement. Even if a proper sealing system was found, the commercially available precision weighing balances do not work well when exposed to vibrations, high humidity environments and temperature changes. In addition, the high power consumption is another drawback. These characteristics make them unsuitable for *in situ* applications.

At this stage an extensive search was done on the working principles of existing analytical balances to determine if they could be adapted to an underwater use. Most of the analytical balances work mechanically as a simple lever and fulcrum system: one end of the lever holds the weighing pan where the unknown weight is placed, while the opposite end is a force coil suspended in a magnetic field (Figure 3.1). Then, a displacement sensor detects changes in the position of the force coil when it is pulled up by the leverage exerted from a mass on the weighting pan. The displacement sensor and a power amplifier produce an appropriate current to hold the lever balanced in the null position for any weight placed on the pan. The amount of current required to do this is proportional to the weight on the pan. As temperature affects the magnet and weight data, these balances also include a temperature sensor, which allow the use of a temperature coefficient to correct the measurements (www.balances.com). However, these balances are not suitable for an underwater operation.
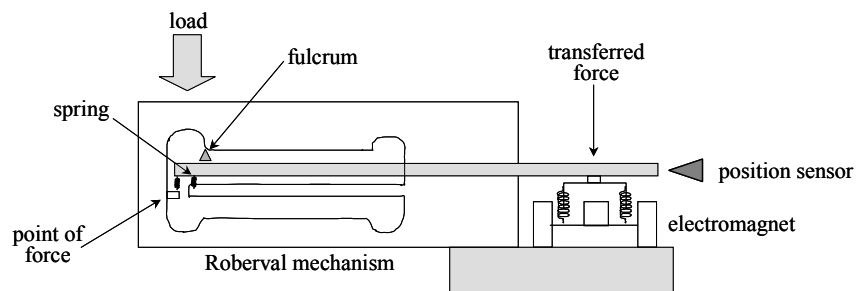
Figure 3.1: A basic measurement principle of a SHS balance (www.balances.com).

As an alternative, the company Rubotherm (www.rubotherm.de) has developed a magnetic suspension balance in the late 1980s, that is able to weigh samples in a non-contact manner under nearly all environments (e.g. corrosive gases or fluids, pressures up 2000 bar, temperatures up to $250 - 2000^{\circ}$C) with high resolution (up to 1 μg). This suspension balance consists of a free-floating permanent magnet located inside the measuring cell to which the

sample is connected, a sensor core, a device for decoupling the measuring load (sample) and an electromagnet hanging at the underfloor weighing hook of a microbalance located outside the chamber, which works at atmospheric conditions (Figure 3.2). Using this magnetic suspension coupling, the measuring force is transmitted without physical contact from the measuring chamber to the microbalance. The electromagnet voltage is modulated by a controlling unit (PID controller and position transducer) in such a way that the suspension magnet and the connected sample achieve a constant vertical position in the measuring cell; they are freely suspended and their masses are transmitted to the microbalance through the wall of the glass (or metal) pressure vessel (Dreisbach and Lösch, 1999, 2000).
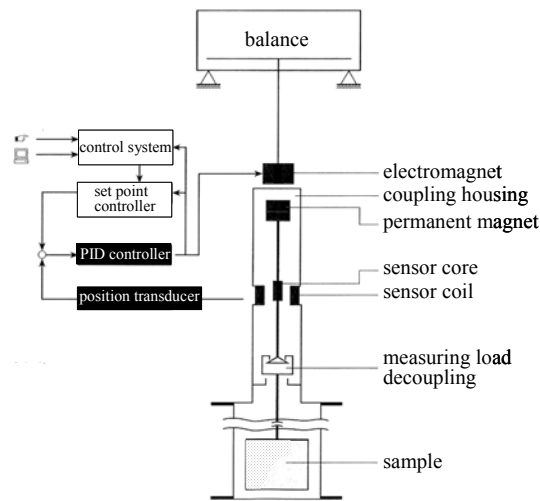
Figure 3.2: Operating principle of the magnetic suspension balance manufactured by Rubotherm (www.rubotherm.de).

The working principle of the suspension balances for measuring the weight of a sample without contact was applied in the development of the SEDVEL. Firstly, an electromagnet and a permanent magnet were employed, but this arrangement was later changed to a lower energy system that relies only on a permanent magnet and a position sensor, as presented below.

Prototype 1: The first idea was to have an almost neutrally buoyant balance pan that could freely float inside a vertical tube filled with water of a known density. Then, its slight negative immersed weight would be balanced by an electromagnet located underneath it, which also would be used to counteract any weight deposited on the balance plate (also referred to as the "pan"). This floating plate consisted of a PVC disc (D = 18.0 cm and T =

0.05 cm), a float (D = 6 cm), a rod (H = 22 cm) and a container ($D \times H$ = 2.0 × 3.0 cm) with two neodymium magnets (D = 2 cm) inside, ending in a titanium 'V'-shaped tip (Figure 3.3a).

The whole device consisted of a balance plate with a concave electrode at its base (top electrode), a bottom electrode with a convex tip, a transformer connected to an oscillator and a coil fed by a power supply (Figure 3.3a). The transformer generated alternating current which was transmitted to the bottom electrode. When the top electrode touched the bottom electrode, the circuit was closed and the current flowing through it could be measured with an ammeter. A big coil was placed around the bottom electrode to produce a magnet field and a magnetomotive force (see Appendix A), the intensity of which could be modulated by changing the current flowing through the coil. Regarding the coil characteristics, initially a single coil ($D_{external}$ = 11 cm, $D_{internal}$ = 5.6 cm, H = 2.5 cm) with 300 turns (copper wire, D = 0.02 cm) was used. This was later replaced by two coils in parallel of 150 turns (copper wire, D = 0.02 cm) in order to reduce the supplied voltage by 50%.

The calibration of prototype 1 was performed by placing small discs of known mass (weights) on the top of the balance plate and measuring the amount of current that should be supplied to the coil to balance these weights. Initially, while the top and bottom electrodes were in contact, a constant electrode current was measured. Then, the current supplied to the coil was slowly increased until it was just enough to lift the balance plate off the contact. At this stage the electrode current should drop to a value close to zero (opened circuit). The repulsive force upwards balances the immersed weight (gravity force less the buoyancy) put on the top of the balance plate.

Figures 3.3b and 3.3c show several calibration curves for prototype 1, which relate the electrode current measured by ammeter to the current supplied to the coil for different testing discs. Although there was a general tendency of an increase in the total coil current necessary to open the circuit contact as the weight placed on the pan became heavier, results were neither consistent nor reproducible. Moreover, once the balance plate was lifted off the bottom contact, the pan was subject to considerable up/down oscillations, which caused the bottom electrode to touch the top concave electrode not only at its centre, but also on its lateral walls, thereby producing a noisy reading (Figure 3.3b, c). It was very difficult to produce a clear on/off contact and control the slight increments of the coil current required to

"just" lift off the plate. In addition, the stabilization period after each measurement was too long.
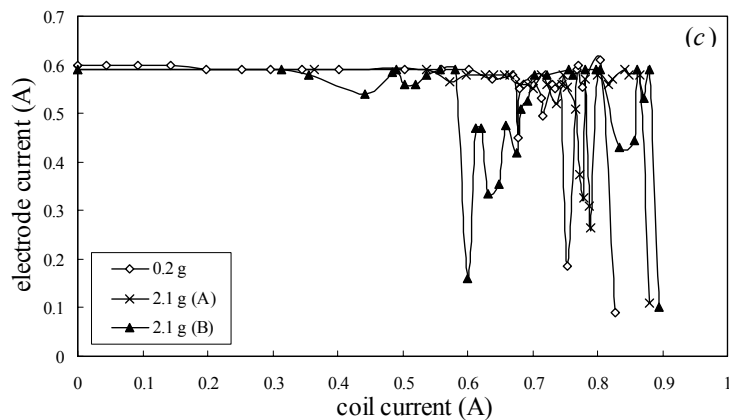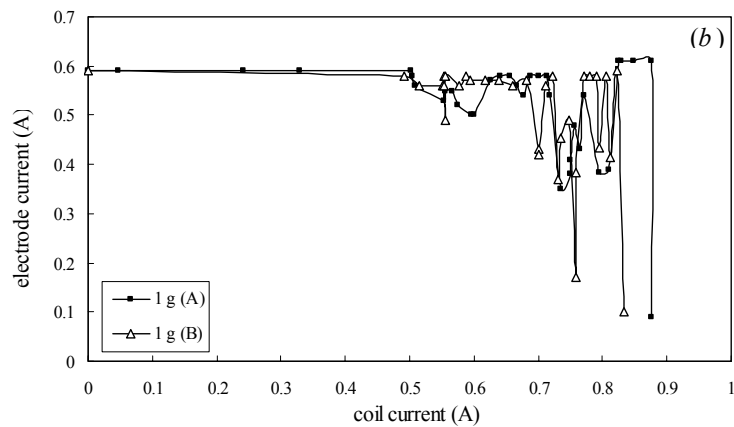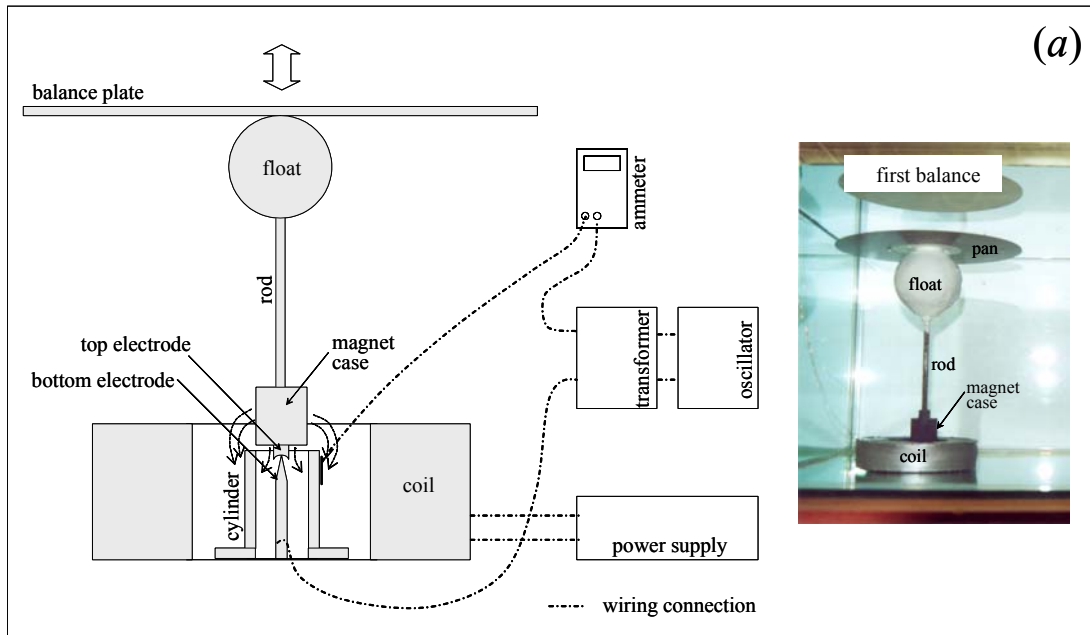
Figure 3.3: (*a*) Schematic representation of the first prototype components (right) and a photograph of the balance plate (left). When the top and bottom electrodes are in contact, current flows through the water and closes the circuit with the external cylinder; (*b*) and (*c*) calibration curves of the first balance performed in a freshwater tank; the masses of the discs placed on the top of the pan, varying from 0.2 to 2.1 g, are indicated on the legend.

Further, a big balance plate ($A = 140$ cm^2) and float were required to counteract the magnet weight and make the system neutrally buoyant. Importantly, it would also be very difficult to control and relocate the balance plate on its contact position after finishing one measurement, prior starting a new one.

Prototype 2: The floating pan idea was abandoned and a small pan ($A = 36$ cm^2) held by a support was used instead. This pan had a small magnet ($D = 1.0$ cm, $H = 0.15$ cm) fixed close to the outside end of its inferior surface. The contact region for the bottom electrode was placed on the lower side of the pan, where one end of the electrode wire was attached with conductive paint (top electrode). A large magnet ($D = 2.4$ cm, $H = 1$ cm), located underneath, was used to repel the small magnet placed on the pan and balance its weight. Two coils in parallel (3.5 cm below the pan) were used simply to balance the calibration weights placed on the balance plate (Figure 3.4a).
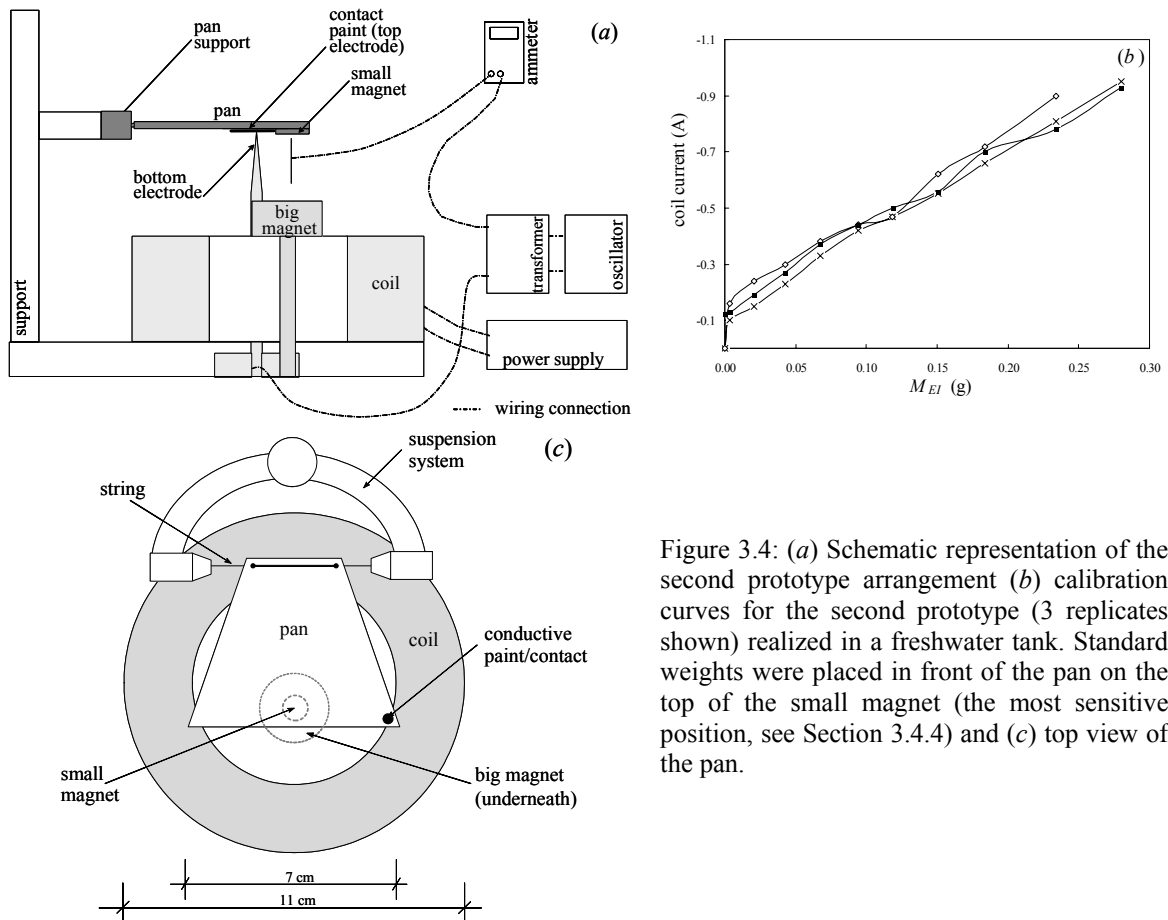
Figure 3.4: (*a*) Schematic representation of the second prototype arrangement (*b*) calibration curves for the second prototype (3 replicates shown) realized in a freshwater tank. Standard weights were placed in front of the pan on the top of the small magnet (the most sensitive position, see Section 3.4.4) and (*c*) top view of the pan.

Calibration of this second prototype was performed by placing the standard weights on the pan and registering the amount of current necessary to lift the pan off the contact, after the pan oscillation had stopped. The calibration curves produced much more stable and reproducible measurements (Figure 3.4b). However, the stabilization time required to stop pan vibration after losing the electrode contact was still relatively high, and a faster self-adjustable system to increase the current flowing in the coil was necessary. Further, the coil heated up, producing bubbles and convective currents that could alter the balance calibration, especially if the bubbles adhered to the pan.

The adopted coil configuration in the second prototype (two coils of 150 turns in parallel) was able to measure about 0.3 g of effective immersed mass, which corresponded to a dry SPM concentration of 200–250 mg l^{-1} for a fall tower height of 30 cm and diameter of 15 cm, assuming SPM densities of 1.5–2.0 g cm^{-3}. In order to increase the measurement range, allowing larger masses to be quantified, a stronger magnetic field from the coil on permanent magnet would be required. A total dry SPM concentration of 1000 mg l^{-1} could be measured by using a bigger coil. Several theoretical calculations and empirical tests were conducted to determine the optimum coil parameters, and minimize power consumption for the necessary magnetomotive force. It was found that two coils ($D_{external}$ = 12.1 cm, $D_{internal}$ = 10.6 cm, H = 7.9 cm) with 800 and 890 turns made of copper wire (D = 0.05 cm) would suit the desired measurement range. Both the serial and parallel configuration would produce comparable flux densities at a distance of 1.5 cm from the coil top for a similar current range (Figure 3.5a). The parallel configuration was preferred, because currents 2.3 times higher could be applied using 60% less maximum supplied voltage, compared with the serial set-up (Figure 3.5b).
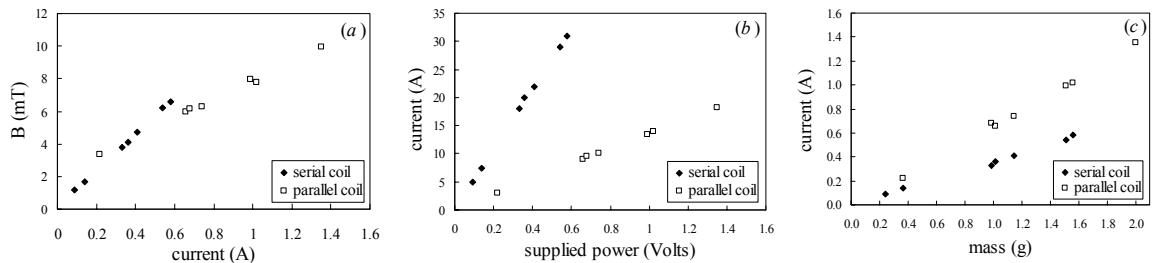
Figure 3.5: (*a*) Flux densities (mT) measured 1.5 cm above the top of two coils of 800 and 890 turns for the serial and parallel connections; (*b*) relationship between the current and the supplied voltage for the serial and parallel configurations of the two coils; and (*c*) input current to these two coils and the respective mass lifted.

Therefore, a large and heavy ($\approx$ 2 kg) parallel coil was required to lift a 2 g (Figure 3.5c). In addition, even with the optimised power consumption (maximum of $\approx$18 V) of the parallel coil configuration, the required voltage and current were still excessively high for a long-term deployment of the instrument in the field. Moreover, the time necessary to adjust the supplied current to the coil and to stabilise the pan in a constant horizontal position for each weight increment was still high, considering that the sedimentation of *PM* on the pan would be a continuous process. Therefore, this coil arrangement was replaced by a new system where only the permanent magnet was used to balance the balance plate weight and the standard calibration weights placed on it. This solution had the advantage of requiring less power consumption and resulted in a simpler set-up.

Prototype 3: With this new set-up, a small pan with a small magnet attached to its under side was held by a suspension system on the top of a big magnet. The pair of magnets was set up to repel each other. The big magnet (D = 2 cm, H = 1 cm) was fixed to a micrometer connected to a small motor, which allowed very small vertical movement of the magnet (Figure 3.6a). For this third prototype, calibrations were performed in air, by placing standard discs on the balance plate and measuring the change in the magnet position needed to balance each new weight. All measurements were done by measuring the amount of magnet displacement (mm) needed to return the plate, after each new weight increment, to its zero position, i.e. the initial distance measured between the balance plate kept in a horizontal position and the magnet when there was no weight on it. The magnet displacement distance was related to the accumulated weight (Figure 3.6b).

This set-up produced consistent results and good reproducibility. However, difficulties still remained, related to the amount of time needed to adjust the magnet position to a given weight increment. For the *in situ* configuration of the instrument, where the balance plate would work immersed, moving the plate every time step of measurement could cause undesirable pan oscillations that could take a few seconds to stabilise. Aiming for simplicity, a new configuration was tested, in which the balance plate immersed weight was supported by a large permanent magnet underneath. Then, the plate was allowed to move downwards as a function of accumulated masses placed on its top. The balance plate and the magnet spring system worked inside a tank filled with fresh water.
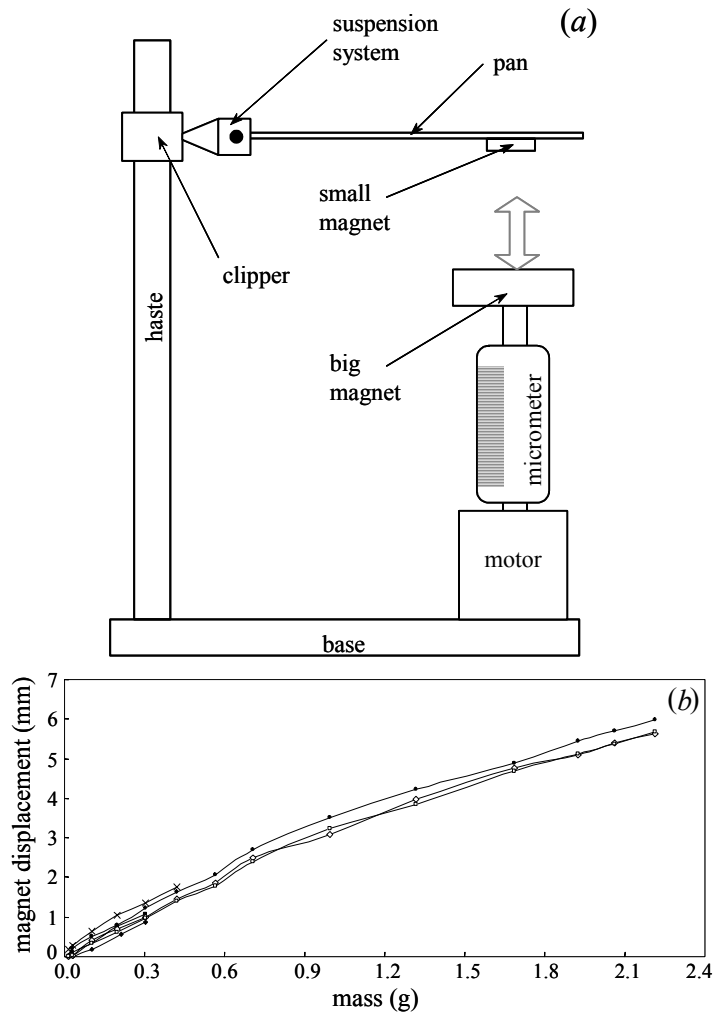
Figure 3.6: (*a*) Third prototype schematic representation (lateral view); and (*b*) calibration curves made in air with the third prototype, relating the magnet displacement (mm) to the accumulated dry-mass (g).

At first, the pan displacement was visually marked and measured after each increment of weight in order to estimate the possible balance resolution (Figure 3.7). According to these measurements, a displacement of 0.1 mm (best visual accuracy) corresponded to a resolution of better than 0.01 g (Figure 3.7). These measurements confirmed that the pan displacement could be used for estimating the effective immersed mass (defined in Section 4.3.1) with a good balance resolution. This was the basis for the first "SEDVEL" prototype.

Prototype 4: The fourth prototype, i.e. first SEDVEL version was composed of an acrylic pan with a small magnet and an aluminium target attached to it, and a suspension system consisting of a fastening screw and a nylon string, which worked immersed inside a vertical settling tube. In addition, a displacement sensor (DVRT, Microstrain, Inc.; Arms, 2004) protruding outside the sensor case was located underneath the pan target. This sensor

measured micrometric changes of the pan position as a function of the mass placed on its top. A big magnet was placed inside a sealed sensor case and this was used to balance the pan weight and set up the zero position of the balance (Figure 3.8a, b). Typical calibration curves of the SEDVEL version are given in Figure 3.8c for two different instrumental sensitivities (i.e. pan zero positions) (see Section 3.5.2.1).
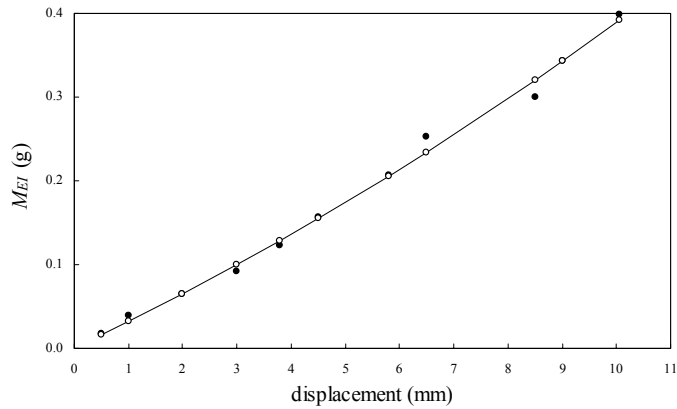
Figure 3.7: Calibration curve relating the balance plate displacement (mm) as a function of the accumulated effective immersed mass (M_{EI}, g) in a freshwater tank. The balance plate position was visually marked and measured with a millimetre scale; the standard weights were placed in front of the pan (the most sensitive position, see Section 3.4.4).

A few improvements were made in this first version, including: (*i*) changing the pan material from plastic to aluminium in order to increase the measurement range while keeping a good balance resolution; (*ii*) development of the balance plate suspension system to make it more reliable; (*iii*) improvement of the fixation system of the settling tube to the main instrument body, because the initial system caused water infiltration and some small turbulence inside the tube that increased the reading noise; and (*iv*) adding a new system for water replacement and balance plate cleaning. After these alterations, this prototype is referred in the text as "the second SEDVEL version" or "SEDVEL". A general and detailed description of the second SEDVEL version is subsequently presented. Additionally, some illustrations of the impact of these improvements on the instrument results are depicted in Section 3.6.
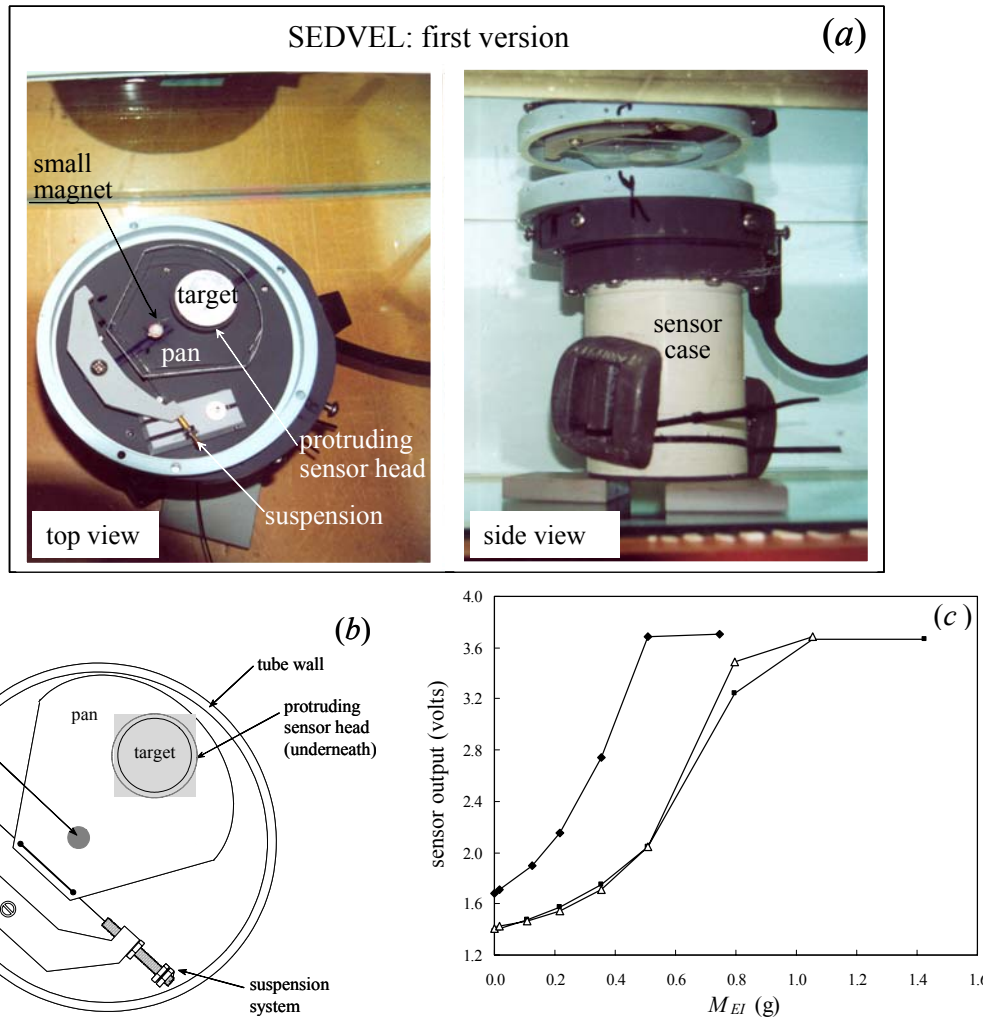
Figure 3.8: (*a*) First SEDVEL version: photography of the balance plate (top view, left) and sensor case (side view, right); (*b*) schematic representation of the balance plate (top view); and (*c*) examples of calibration curves for the first SEDVEL version considering two starting zero positions (1.4 and 1.7 Volts).

3.3. SEDVEL

3.3.1. General description and working principle

The main body of SEDVEL is composed of a balance, a sensor case, a vertical settling tube (D = 14.5 cm, H = 32.1 cm) and a set of submersible pumps (total weight of about 20 kg). The main body of the instrument is connected to a battery case and a data logger/controller unit, which are arranged on a tripod frame to be moored on the seabed (Figure 3.9a). SEDVEL's balance consists basically of a pair of magnets, a displacement sensor and a plate. The plate is made of conductive material, which serves as a target for the displacement sensor located beneath it. A thin string holds the balance plate on its smallest side (Figure 3.9b).
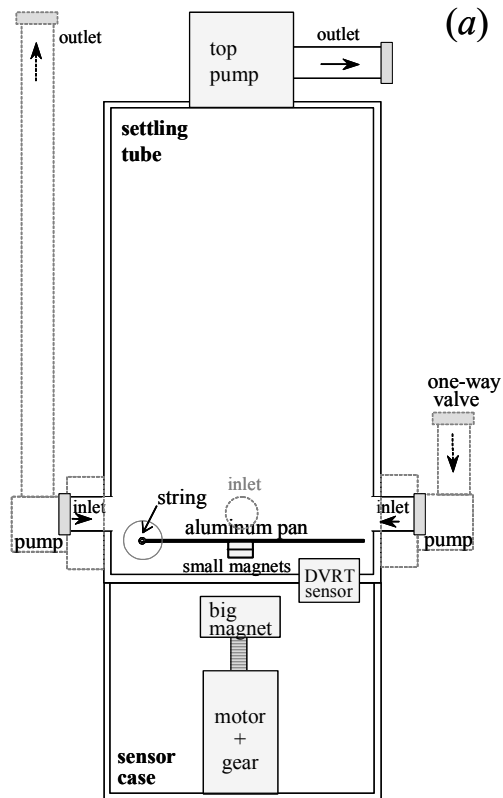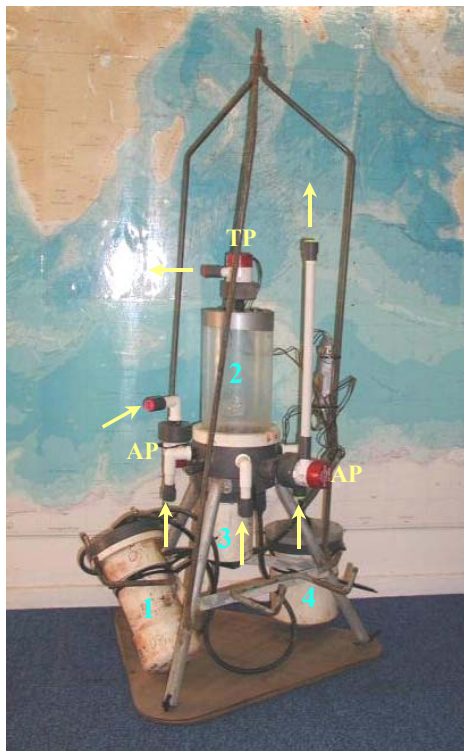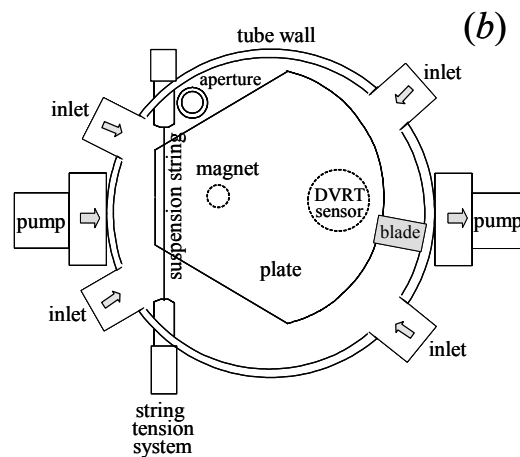
Figure 3.9: Schematic representation of the main body of SEDVEL (*a*) side view and (*b*) top view (right) and a photograph of the whole instrument (left top) and the balance plate (left bottom). Data logger/controller and battery case are not shown in the drawings. Arrows in the top photograph indicate the water flow direction during water replacement and the numbers the main parts of SEDVEL, namely: (1) data logger, (2) settling tube, (3) sensor case and (4) battery case.

The basic working principle of SEDVEL is a magnetic spring system driven by a pair of magnets, one located below the balance plate and the other placed inside a sealed sensor case (Figure 3.9a). The balance plate works immersed, and is located at the bottom of the settling tube. The plate moves downwards as the particulate matter (*PM*) deposits on it, and a high-

resolution displacement sensor detects its micrometric changes (in relation to its equilibrium position). These changes are proportional to the immersed weight of the sediment, and the actual sediment mass can be obtained by calibration with known masses.

The balance zero position corresponds to the initial distance between the balance plate (held in a horizontal position) and the head of the DVRT sensor, which is set up by changing the relative distance between the pair of magnets (i.e. changing the repulsive force). This instrument is fully automatic in terms of water sampling, measurement and data storage. It can operate in concentrations ranging from 5 to about 500–800 mg l^{-1}, with a resolution better than 0.01 g and a sampling autonomy of 3 to 5 days. The total settling period can be set as required from a few minutes to many hours, with a minimum sampling interval of 20 s.

3.4. SEDVEL components

3.4.1. Displacement sensor

The displacement sensor (DVRT−differential variable reluctance transducer, manufactured by MicroStrain, Inc.) is a key part of SEDVEL, since it infers the variations of plate position as sediment particles settle on it. This is a non-contacting sensor: it measures the micrometric distance between the sensor head and a conductive target without physical contact between them. The DVRT ($D = 1.9$ cm, $L = 3.0$ cm) has a resolution of 2 μm, repeatability of $\pm$ 2 μm, a measurement range of 5 mm, and it can operate in temperatures ranging from −55 to 105°C. It requires 8 to 12 V as an input voltage, has a current consumption of 10 milliamps, and its output ranges from 0.2 to 4.8 V (specifications as furnished by MicroStrain, Inc., USA) (Figure 3.10a).

The DVRT working principle is described below. Some theoretical concepts and terms used in the explanation are referred to in Appendix A. The DVRT sensor is a transducer composed of a sense coil and a compensation coil used as a reference. If a nonmagnetic conductive target is introduced into the coil field, eddy currents are induced in the target surface. These currents act to reduce the apparent permeability of the magnetic circuit (μ), resulting in a decrease of inductance (L) of the sensing coil in the DVRT. Hence, when the face of the transducer is brought in close proximity to a highly conductive material, the reluctance ($\Re$)

of the sense coil is changed while the compensation coil acts as reference (Arms, 2004). This relies on the fact that when two coils are over a test material of flaw-free area, no differential signal is developed between the coils, but when one a coil is over a target and the other is over a reference material, a differential signal is produced (NDT, 2004). The two DVRT coils are driven by a high frequency sine wave excitation, and their differential reluctance is measured using a sensitive demodulator. Differencing the two coil outputs provides a sensitive measure of the position signal, while cancelling out variations caused by temperature. An important characteristic of this kind of sensor is that measurements are unaffected by interposed non-metallic or non-conductive materials, such as polymers and biomaterials (Arms, 2004). In addition, the space between the target and the sensor head is filled with seawater during measurements; however the conductivity of seawater is much less than the conductivity of the conductive target and its influence is minor.
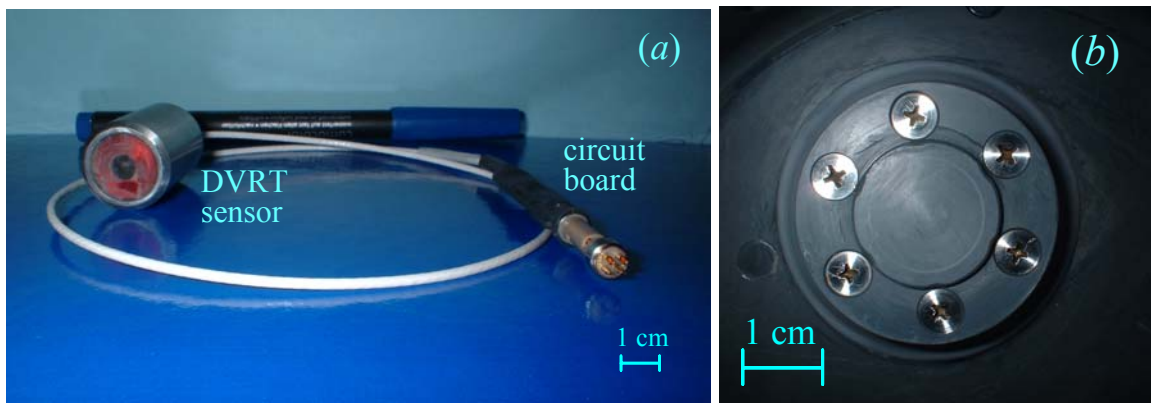
Figure 3.10: (a) Photograph of the DVRT sensor manufactured by MicroStrain Inc., showing the sensor coil encapsulated in a stainless steel case (on the right) and the circuit board (on the left), and (b) a detail of the PVC membrane covering DVRT sensor head.

Eddy current transducer performance is basically dependent on the impedance, coupling between the electromagnetic field in the sensor coil and the eddy currents in the conductive target. This coupling depends on the inductive and resistive components of the mutual inductance between the coil and the target material (Figure 3.11). The sensor performance is evaluated by measuring variations in the effective impedance (Z_{eff}) of the sensor coil as its distance to the conductive target changes. The effective impedance depends upon the complex interaction among several variables (e.g. coil inductance, angular frequency and eddy current path) (Welsby and Hitz, 1997).
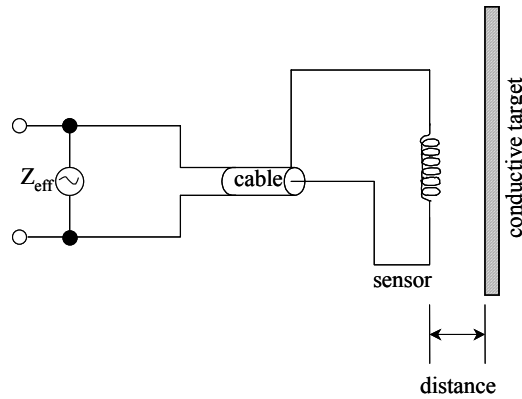
Figure 3.11: Schematic representation of the eddy current transducer sensor, which detects changes in the measuring system's coil impedance caused by varying the distance between the sensor (coil) and the surface of a conductive material (target). Z_{eff} is the effective impedance (extracted from Welsby and Hitz, 1997).

In the SEDVEL application, a balance plate made of aluminium works as the conductive target. Aluminium was chosen as a target because it is a corrosion resistant, light weight, non-magnetic conductive material with low resistivity and a magnetic permeability of 1. Such characteristics provide high output sensitivity in terms of impedance change per unit of target displacement. Besides, an optimal aluminium target should be at least 0.3 mm thick and have a diameter 2.5–3.0 times the sensor diameter (Welsby and Hitz, 1997). These particularities make the calibration of the sensor dependent on the target characteristics (e.g. permeability, resistivity, size, thickness), and therefore this kind of sensor must be calibrated with the exact target as in the actual application (Welsby and Hitz, 1997). The SEDVEL balance plate (pan) had a thickness of around 0.7–0.8 mm, and a second version of the instrument uses the whole pan as a target, fulfilling the recommendations.

Although the DVRT sensor comes with an epoxy packaging for submersion in aqueous environments, extra protection was added to prevent the sensor getting wet after long-term immersion in saline water. This protection consisted of a very thin PVC membrane (thickness of 0.4 mm) that covers the sensor head. The sensor head protrudes (1.4 cm) outside the sensor case where the DVRT sensor is sheltered (Figure 3.10b). Calibration curves of the sensor (plus the PVC membrane) response as a function of its distance to a conductive aluminium target furnished an output ranging from 1.2 to 3.1 V for supplied input voltages of 7–8 V; this is equivalent to the raw data logger output ranging from ≈ 3100 (when the target is firmly touching to the sensor head) to ≈ 1200 when the plate is 5 mm away from it (Figure 3.12; see section 3.4.6). A 12-bit logger system was adopted for recording values of the DVRT sensor output. A stable DVRT sensor output was produced when a fixed distance was

56

kept between the target and the sensor head, during its calibration in air. Differences in the sensor readings between two replicate calibration curves were less than 3%.
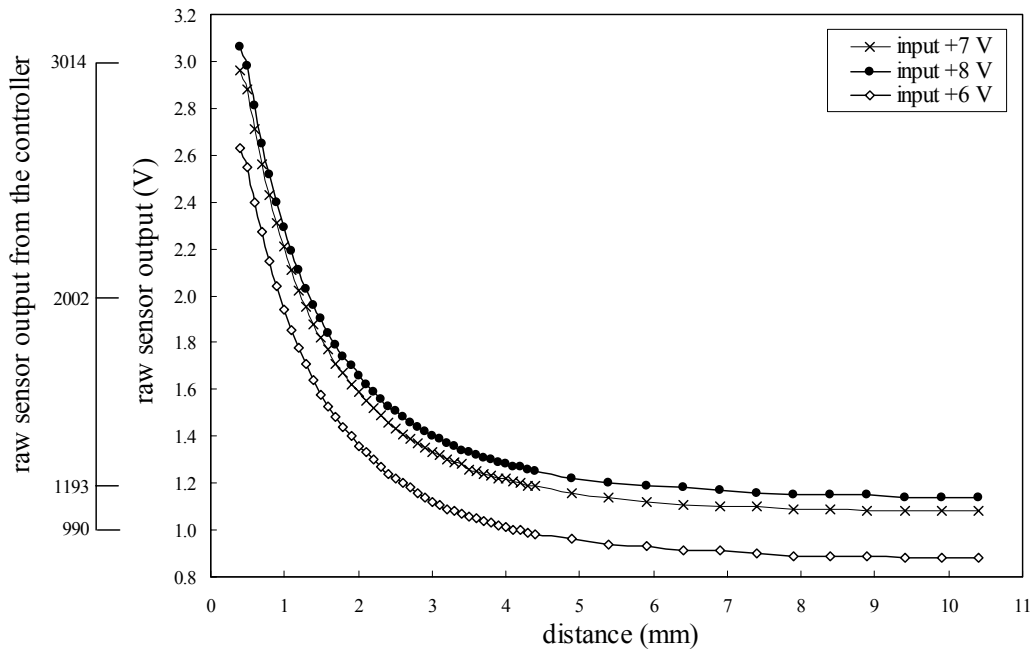
Figure 3.12: Response of the DVRT sensor (SR) plus a 0.4 mm PVC membrane (**Volts**) as a function of the distance (mm) between the conductive target and the sensor head. The raw sensor output from the controller and data logger is shown for comparison. A relationship between the raw sensor output of DVRT furnished by the data logger/ controller unit and its response in volts is presented in Appendix B.

The DVRT sensor has a sigmoidal response, being highly sensitive when the target is very close to the DVRT sensor head. In particular, a small variation in distance promotes a large change in the sensor output for distances below 2 mm. The DVRT sensor detects the target within the first 4 mm of distance; when the target is beyond this limit the sensor output becomes approximately constant. Therefore, a high change in the reluctance per unit of displacement occurs in the proximity of the target, and a low variation farthest from the target. In addition, varying the supplied input voltage to the DVRT sensor also promotes different sensor responses (Figure 3.12). The relationship between the raw sensor output in volts and in arbitrary units produced by the data logger/controller is given in Appendix B.

A high sensitivity of the instrument refers to its ability to measure very small changes, i.e. small variations in the parameter to be measured cause a large variation in the output of the sensor or instrument. In order to illustrate changes in the sensitivity of the DVRT sensor as a function of its distance to the target, the ratio between the DVRT response and the distance (first derivative) was calculated. A plot of the slope (first derivative) of the DVRT response

as a function of the distance (dS_R/dx), and the ratio between the first derivative estimated at the distance "i" and the maximum slope ($(dy_i/dx_i)/(dy/dx)_{max}$) are presented in Figure 3.13. Higher DVRT sensitivities were obtained at small distances from the target, being 50% of the maximum sensitivity reached at a distance of 1.7 mm. Less than 10% of the maximum sensor sensitivity occurred at distances greater than 3 mm.
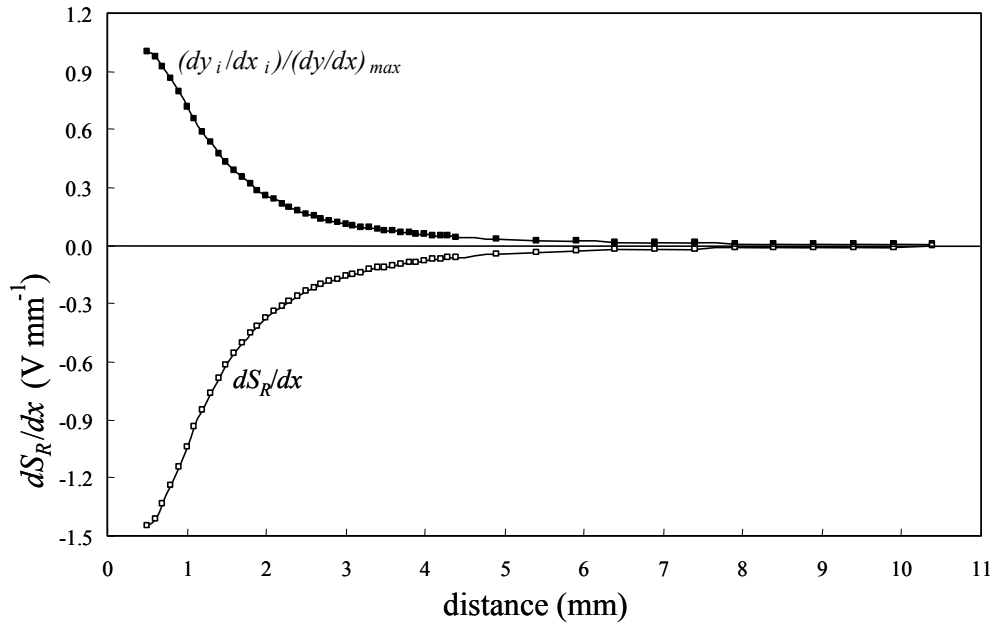
Figure 3.13: Plot of the slope (first derivative) of the DVRT raw sensor output (S_R) as a function of the distance (x) (dS_R/dx, white squares), and the ratio between the first derivative at the distance "i" and the maximum slope (black squares): $(dy_i/dx_i)/(dy/dx)_{max}$. The last ratio ranges between 0 and 1. These derivatives were calculated based on the values presented in Figure 3.12 for the calibration curve of a +8V input of the DVRT sensor. Derivation was performed in Curve Expert 1.38, which uses a central difference scheme with Richardson extrapolation to compute the derivatives (Hyams, 2001).

3.4.2. Magnetic spring balance

The magnetic spring balance forms the core of the SEDVEL instrument. It consists of two permanent magnets that repel each other: one located under the balance plate and the other inside the sealed sensor case. Changing the relative distance between the two magnets alters the intensity of their repulsive force and allows an equilibrium balance position to be achieved under different water densities (starting zero position). A brief description about theory of magnetism is following presented as well as a detailed explanation of the magnetic spring balance set-up.

3.4.2.1. Magnet field and induction

When analysing permanent magnet materials, most of the magnetic behaviour can be described by three interrelated vector quantities: (*i*) magnetic field, (*ii*) magnetic induction (or flux density) and (*iii*) magnetization (Trout, 2003). A magnetic field is produced in a volume of space whenever there is electrical charge in motion. Then, there is an energy gradient which produces a force that can be detected by the acceleration of an electric charge moving in the field, by the force on a current-carrying conductor, by the torque on a magnetic dipole (such as a bar magnet), or even by the reorientation of spins on electrons within certain types of atoms (Jiles, 1991). The magnetic field (*H*) is perpendicular to the current direction, and it is expressed in Oersted (Oe) in CGS or Ampere-turn/meter (A/m) in SI.

When a magnetic field *H* has been generated in a medium by a current, the response of the medium is its magnetic induction *B* (or flux density). The magnetic flux passing through a unit area of magnetic field in a direction at right angle to the magnetic force is the magnetic induction (*B*) (Jiles, 1991). It is expressed in terms of flux lines per unit of cross-sectional area, which units are Gauss in CGS and Tesla in SI. The third vector corresponds to the magnetization (*M*) that is a quantity describing the magnetic state of the material, representing the sum vector of individual atomic magnetic moments (*m*) per unit of volume (*V*), i.e. $M = \sum m/V$. It is expressed in emu/cm^3 (emu = electromagnetic unit) in CGS and A/m in SI (Dobbs, 1984; Trout, 2003). Inside the magnet, the magnetic field strength (*H*) is a combination of magnetization (*M*) and magnetic induction (*B*) described by $H = B/\mu_0 - M$ in the SI system of unit. Outside the magnet, the magnetic field is given by $H = B/\mu_0$, where the constant $\mu_0 = 4\pi 10^{-7}$ Tesla-m/A (in SI) is the permeability of free space (Lorrain and Corson, 1970; Trout, 2003). Figure 3.14a shows the lines of *M*, *B* and *H* for an ideal permanent bar magnet.

Permanent magnets are designed to provide a definite magnetic flux in an air gap (Smith, 1960). The basis of magnet design is the B-H curve, or hysteresis loop, which characterizes each magnet material, since different materials exhibit different flux densities when

subjected to the same magnetization levels. This curve describes the cycling of a magnet in a closed circuit as it is brought to saturation, demagnetized, saturated in the opposite direction, and then demagnetized again under the influence of an external magnetic field (Design Guide, 2000). A typical B-H curve (or hysteresis loop) and its main characteristics are represented in Figure 3.14b. The second quadrant of the B-H curve, referred to as the "Demagnetization Curve", is commonly used to display the properties of permanent magnets, i.e. the conditions under which they are used in practice (Design Guide, 2000; Group Arnold, 2000).
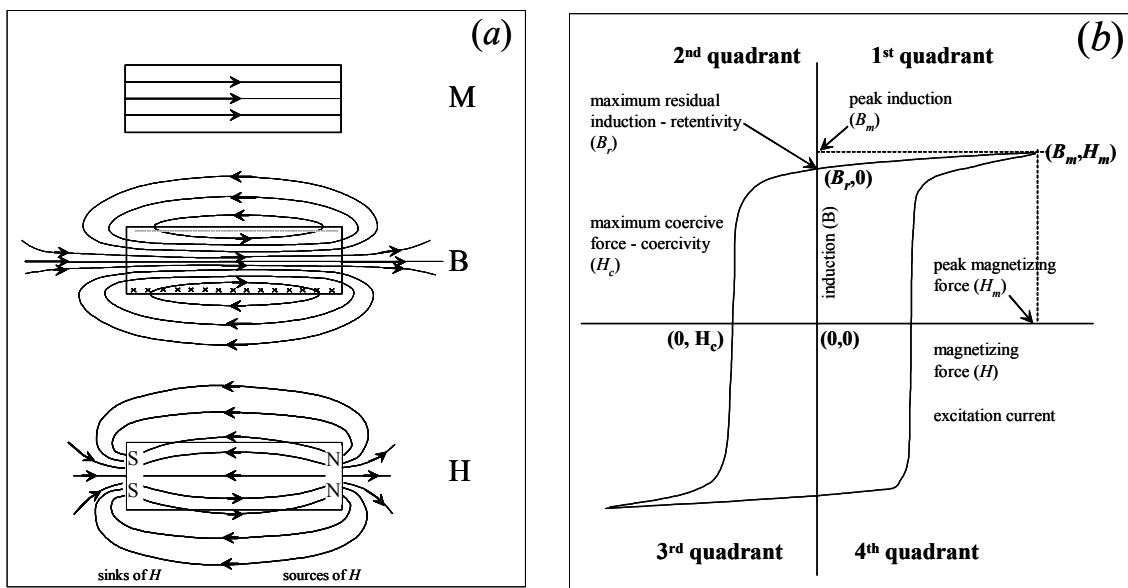
Figure 3.14: (*a*) Lines of magnetization (*M*), flux induction (*B*) and magnetic field (*H*) for an ideal bar magnet (as presented in Duffin, 1980, Fig. 12.14) and (*b*) a typical *B-H* curve and its main characteristics represented by the points at which it intersects the *B* and *H* axes, where B_r is the residual induction correspondent to the maximum flux that the magnet produces under closed circuit conditions; H_c is the coercive force that corresponds to the point at which the magnet becomes demagnetized under the influence of an externally applied magnetic field; and $+B_m$ is the maximum flux density and $+H_m$ is the maximum m.m.f applied, i.e. the maximum energy product (Design Guide, 2000: Group Arnold, 2000).

For cylindrical magnets with straight-line normal demagnetization curves, such as Rare Earths and Ceramics, the flux density (B_x, in Gauss) at a distance x from the pole surface (where $x > 0$) on the magnet's centerline is given by: $B_x = \dfrac{B_r}{2} \left(\dfrac{(l+x)}{\sqrt{r^2 + (l+x)^2}} - \dfrac{x}{\sqrt{r^2 + x^2}} \right)$,

where B_r is the residual induction (as pointed in Figure 3.14b), l is the magnet height, r is the magnet radius and x the distance from the pole surface (Design Guide, 2000).

The force that produces a magnetic field is called magnetomotive force or magnetomotance, measured in ampere-turn (At). The magnetomotance (m.m.f. or F_m) is defined in vacuo as the line integral around a closed path (s) of B/μ_0, being equivalent to the total conduction current (I_c) linking the path, i.e. $F_m = \oint_C H\,ds = I_C$ (Duffin, 1980).

The magnetic field allows the magnet to exert a force (attract or repel) on other magnetic materials. The repulsive force exerted by a pair of magnets depends on many different factors, such as: size, shape, magnetization, orientation, separation and magnetic field strength of the magnets (Wikipedia, 2002). Therefore, calculating the attractive or repulsive force between two magnets is, in the general case, an extremely complex operation, although the simple case of the force ($\vec{F}$) between two magnetic poles (m_1, m_2) can be described by the Coulomb's Law, i.e. $\vec{F} = m_1 m_2 / \mu r_p^2$, where m_1 and m_2 are pole strengths (+ or -), μ is the permeability of the medium between poles and r_p is the distance between poles (Wikipedia, 2002). This relationship shows that the force is inversely proportional to the distance that the magnets are apart.

3.4.2.2. Magnetic spring balance set-up

The magnetic spring system consists of two small magnets ($D = 1$ cm, $H = 0.3$ cm, referred to as "small magnets") glued to the aluminium plate of the balance and a big magnet ($D = 2.4$ cm, $H = 0.9$ cm) firmly attached to a support inside the sealed sensor case. Neodymium NdFeB (Rare earth) magnets were used. Permanent NdFeB magnets have the advantage of presenting a relatively high maximum energy product (BHmax up to 25-39 MGOe) and intrinsic coercive force (11-25 kOe) at temperatures up to 200 ºC. However, they have lower resistance to corrosion than SmCo magnets and they are usually covered by a thin plating of zinc or nickel, used as a protective layer (TDK, 2003). Despite the protective coating, the prolonged immersion of the NdFeB magnet in saltwater caused considerable corrosion. Therefore, the two small, immersed magnets were covered with an additional layer of epoxy resin.

During the zeroing of the balance, the big magnet repels the small magnet, supporting the balance plate and keeping it in the horizontal position, within the zero position range adopted.

The zero position is set before deploying the instrument under water in the field, or before each calibration or experiment performed in the laboratory. The zero position setup occurs once every time the instrument is started and lasts the same amount of time chosen for the experimental cycle duration. Therefore, the zero position is adjusted only in the first cycle of measurement after the instrument has started; the big magnet does not move during the subsequent cycles of measurements. The desirable zero position range is adjusted by moving the big magnet up (if the plate is too low) or down (if the plate is too high) until the fixed zero position range is reached. This range is chosen according to the required instrument sensitivity (see Section 3.5.2.1).

A motor plus gearbox controls the big magnet movement. This motor (RC-260, Tamiya, Appendix C) has its speed of rotation reduced by a set of 7 epicyclic gears (a total of 40,000: 1 reduction; Figure 3.15a). A logical test within the data logger plus a circuit board built to control the magnet movement was used to turn the motor on/off and switch its direction of rotation if needed (see Appendix C). The motor stays on for 5 s every time that it starts, then it stops and the logical test is evaluated again, and so on until the end of cycle of measurement, which usually ranges from 60 to 90 minutes. The correct rotation speed was adjusted by testing the amount of time necessary to bring up the big magnet, until the balance plate returned to its original zero position, after putting a standard weight on it. If a reduction of 8,000:1 was applied, the speed of rotation was very fast, and the pan came back to its zero position within about 3 to 9 seconds for standard weights of 0.7 and 1.7 g (Figure 3.15b). This could augment the pan vibrations and also cause the magnet to overshoot the sought zero position range, making it difficult to keep the pan within the narrow zero position range usually adopted (see Section 3.4.6). Therefore, a higher reduction was used (40,000:1) which resulted in an adjustment time about 10 times slower and a very low speed rotation for the output shaft of the gear box. This was more suitable since variations in the position of the pan due to changes in water density were usually smaller than the standard weights applied in these tests, and a fine adjustment was thereby necessary.

The repulsive force (F_R) between two attached small magnets ($D = 1$ cm, $L = 0.6$ cm) and a big magnet ($D = 2.4$ cm, $H = 0.9$ cm) as a function of the distance (d_a) apart was measured in the laboratory (Figure 3.16a). Within the experimental setup, the big magnet was placed on the top of a 0.5 cm thick PVC blade and attached to a device that allowed its proximity to the two small magnets glued to an analytical balance (resolution of 0.1 g) to be measured. Then,

the increase in weight due to an increasing repulsive force when reducing the distance between the pair of magnets was recorded. Magnets used in the experiment were the same as those used in the SEDVEL. Measurements could not be taken for distances below 1.8 cm, due to the very high coercive force experienced by the magnets.
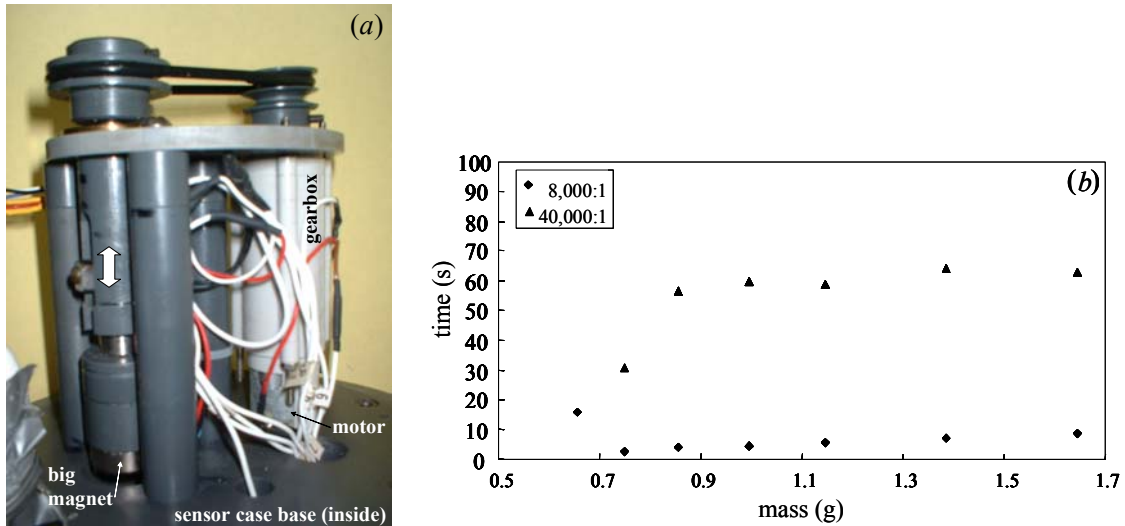
Figure 3.15: (*a*) Photograph of the magnet motor and gear box located inside the sensor case and (*b*) test to choose the gear set reduction for the slow rotation motor, showing the time needed for to the pan come back to its initial position (without load) after adding standard accumulative masses. This time is dependent on the gearbox ratio that moves the magnet up to counteract the weight placed on the pan. See legend for the adopted reductions of the motor speed.

An inverse exponential function was found between the distance (d_a) and the repulsive force (F_R) between the magnets (Figure 3.16a). The repulsive force decays quickly (from 1.2 to 0.4 N) with distance within the first few centimetres ($d_a < 3$ cm), and exhibits a slower decrease when the magnets are set between 3 and 7 cm apart. In the actual SEDVEL configuration, the minimum and maximum distances that the magnets are brought into close proximity correspond approximately to 3 and 5 cm.

Figure 3.16b shows the first derivative of the curve presented in Figure 3.16a. A relatively much bigger variation of the distance with force is seen for distances greater than 5 cm. For high sensitivity we require $d(d_a)/d(F_R)$ to be large, i.e. a large variation in distance (pan displacement) occurs for a small increment in force. This requires the distance between the two magnets to be large ($d_a > 3-4$ cm).
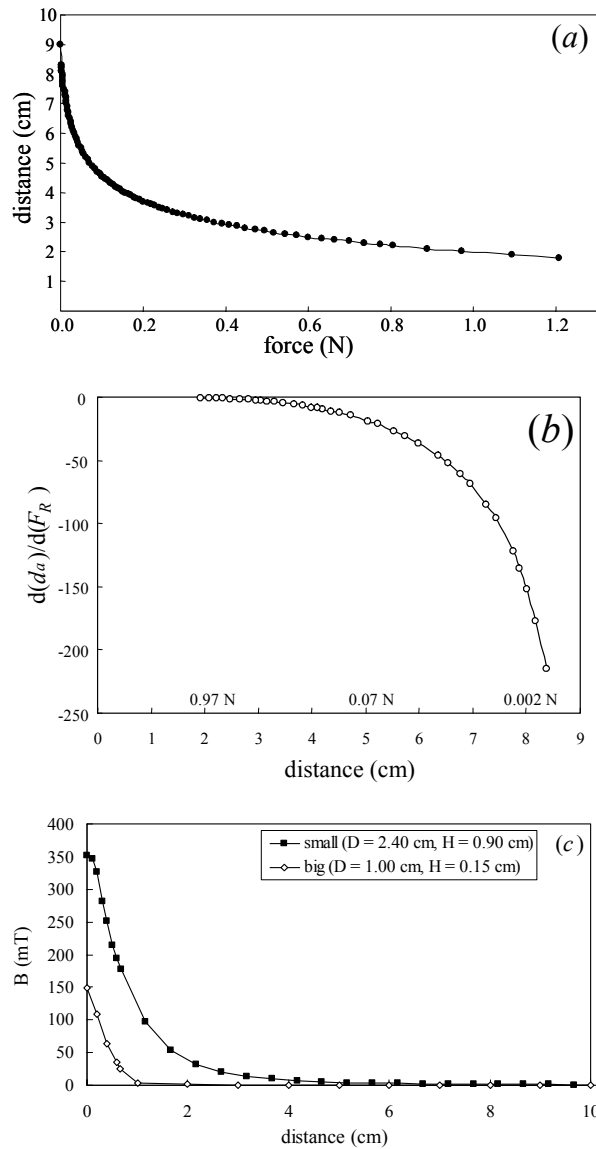
Figure 3.16: (*a*) Relationship between the repulsive force (F_R, N) between the two attached small magnets ($D = 1$ cm, $L = 0.6$ cm) and a big magnet ($D = 2.4$ cm, $H = 0.9$ cm) as a function of the distance (d_a, cm) they were set up apart, described by $d_a = (9.10 \cdot 0.20 + 0.64 \cdot F_R^{0.64})/(0.20 + F_R^{0.64})$, with r^2 =0.99; (*b*) a plot of the slope (first derivative, $d(d_a)/d(F_R)$, N cm^{-1}) of the curve shown in Figure 3.16a, relating the variation in distance (d_a, cm) with the variation in the repulsive force between two attached small magnets ($D = 1$ cm, $L = 0.6$ cm) and a big magnet ($D = 2.4$ cm, $H = 0.9$ cm). This derivation was performed in Curve Expert 1.38, which uses a central difference scheme with Richardson extrapolation to compute the derivatives (Hyams, 2001) and (*c*) variation of the flux density (*B*, mT) with distance (cm) for a big ($D = 2.40$ cm, $H = 0.90$ cm) and a small ($D = 1.00$ cm, $H = 0.15$ cm) neodymium magnets.

Figure 3.16c shows the variation of the flux density (*B*) with the distance from the pole surface of a big ($D = 2.4$ cm, $H = 0.9$ cm) and a small ($D = 1.0$ cm, $H = 0.15$ cm) neodymium magnets, similar to those used in the SEDVEL instrument. Measurements were made with a Gaussmeter at fixed positions along the magnet axis (centreline).

3.4.3. Suspension system

The suspension system consists of a thin Dyneema string (diameter of 0.14 mm) that holds the balance plate on its smallest side and a spring tensioning system that maintains a constant tension on the string. The Dyneema string (Berkley Fireline, 14lb) is a uni-filament line made

from an unique gel-spun polyethylene fibre. It can hold 6.3 kg with minimum stretching and zero memory (i.e. reduced friction and hysteresis) (http://www.cabelas.com).

The Dyneema string crosses the pan and two PVC cases (at both ends), which passes through the tube wall (Figure 3.17a,b). These PVC cases are tightly fitted to the oblique hole made in the tube wall, so that there is no water seepage and they are protected on their outside end by a lid. A small O-ring between the PVC cases and the lids prevents water leakage (Figure 3.17c).
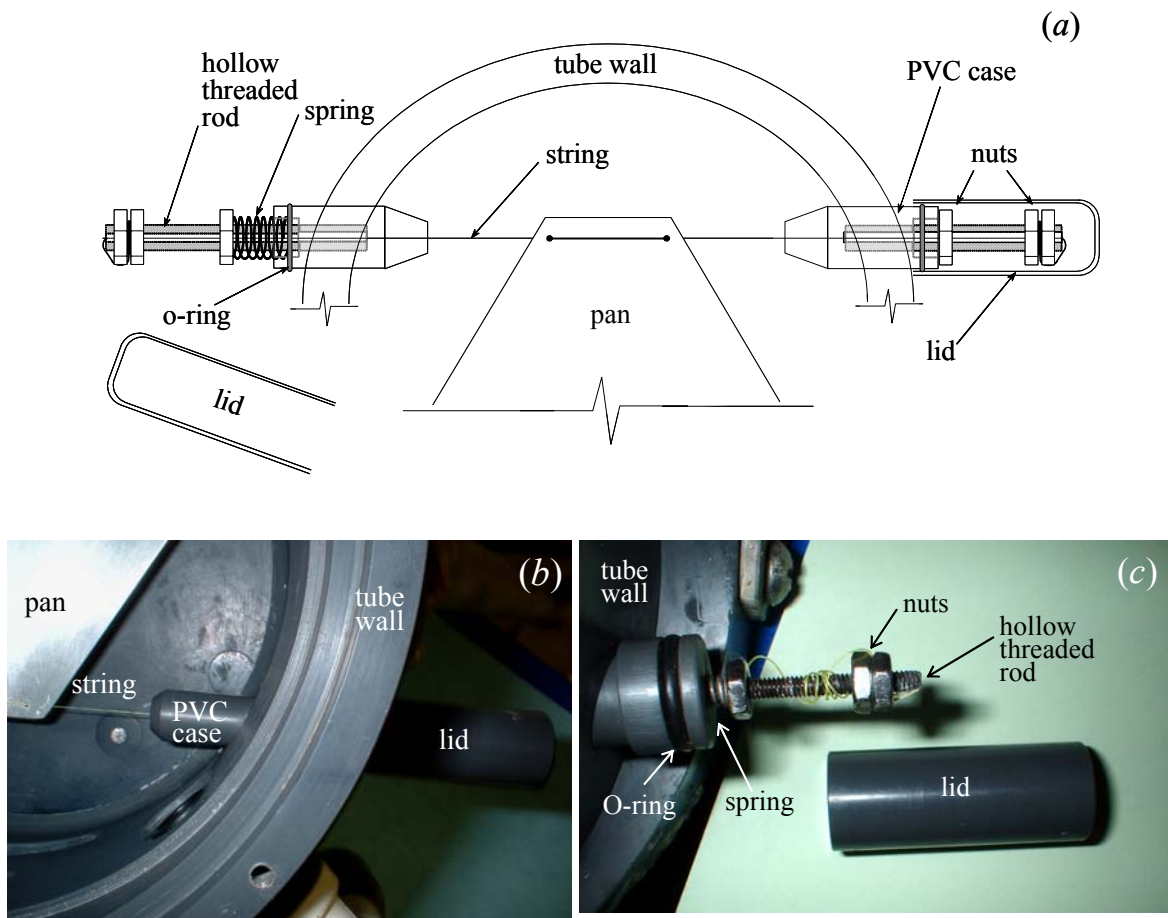
Figure 3.17: (*a*) Schematic drawing showing the components of the suspension system used to hold the balance plate (*b*) Photograph showing the suspension system fitting to the tube wall and (*c*) a detail of the spring system.

Inside the PVC cases there is a hollow threaded rod that allows the string to pass through its central hole. A pair of nuts fixes the string at both ends. One end also has a small stainless steel spring that can be compressed in order to fasten the string until it is tight (Figure 3.17c). The spring was used to ensure that the same tension on the string could be achieved every

time the string had to be replaced. Further, the spring also keeps a constant tension on the string, producing stable readings of the zero position with time (Figure 3.18).
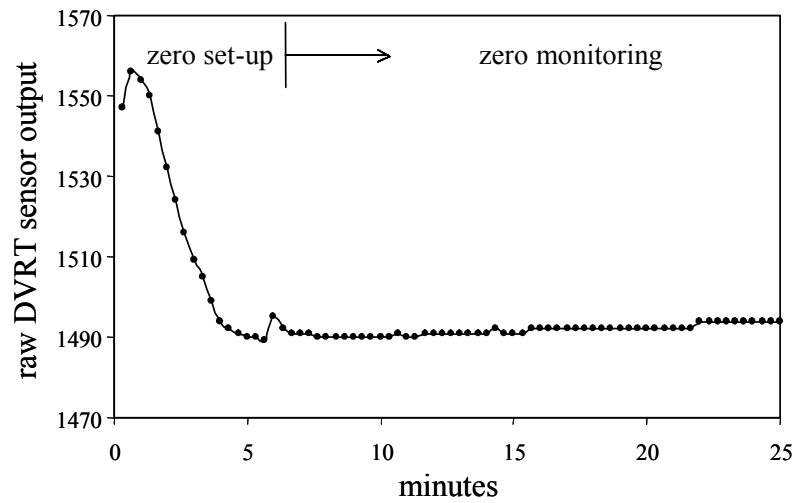
Figure 3.18: Zero position set-up (first 6 minutes) and monitoring during 20 minutes.

Different kinds of string were tested until a material was found that allowed the pan to freely pivot on its suspension axis, and which does not deform or become loose with time. Nylon string suffered deformation with time, while a thin stainless steel wire produced too much torque on the pan. Other kinds of string were also tested, such as monofilament-braided lines, but these experience a larger stretch (about 20%) compared with the micro Dyneema line that stretches less than 5%. Therefore, an ultra-low stretch, very thin Dyneema string was more appropriate, since it produced a more stable zero position and constant tension on the string over the time period required.

3.4.4. Balance plate

The balance plate (also referred to in the text as "the pan") serves as a base to collect the settled sediment and also as a target for the DVRT sensor. The balance plate is located about 1.7 cm above the bottom of the settling tube (Figure 3.9a,b). It is made of aluminium ($A = 71$ cm^2, $T = 0.1$ cm) and has two small neodymium magnets ($D = 1$ cm, $L = 0.3$ cm) attached with epoxy resin to its lower side (Figure 3.19). The magnets lie on the same axis as the pan's centre of mass (*CM*), but their centre is shifted about 2 cm away (closer to the support) of the pan's *CM*. The pan is covered by two thin layers of nail polish to avoid corrosion.

As the plate works submerged, its immersed weight (P_I) is the difference between the force of gravity acting downwards and the buoyancy force acting upwards. An example of the calculation of the immersed weight and effective immersed mass (defined in Section 4.3.1) of the balance plate is presented in Appendix D. The repulsive force exerted by the big magnet on the small magnets attached to the pan counteracts its immersed weight (P_I), as measured in the first cycle of measurement. The actual immersed weight of the pan can change as a function of differences in water density observed at distinct cycles of measurement, which can alter its buoyancy.
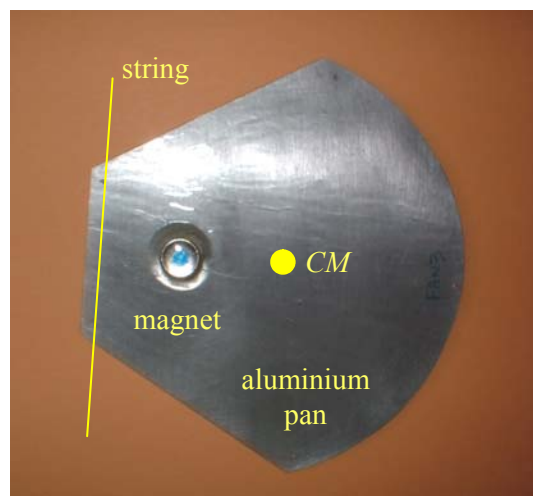
Figure 3.19: Photograph of the lower side of the aluminium pan with the two small magnets glued to it by a layer of epoxy resin. The position of the centre of mass (*CM*) is also shown.

Furthermore, as the balance plate is held by one of its sides, it is important to guarantee a homogeneous distribution of sediment on the plate. Because of this, if a particle (with mass equal to M_1) falls on the plate in different positions, different sensor readings are obtained. The further the particle is from the plate support (suspension system), the larger is the sensor output. However, when a homogenous distribution of particles is achieved, the situation is the same as if all particles were deposited on the centre of mass of the balance. Hence, applying a force on the plate's centre of mass is equivalent to having a force uniformly distributed over the whole pan, i.e. a homogeneous mass distribution of sediment on the top of the balance plate.

Also, a practical test was applied where a weight (aluminium disc) was placed on the pan at different test positions (P1 to P5) as illustrated in Figure 3.20a, and at the pan's centre of mass (*CM*). Then, the sensor output was registered for 2 minutes for each position at a time,

and an averaged value adopted. Tests were repeated 8 times with different zero positions (Figure 3.20b). The lowest sensor readings are obtained at P1 and P2, close to the pan suspension string, intermediate values at P3 and P5, and the highest output occurs when the disc was sited at P4, the position farthest from the pan support with highest torque. Note that mirror positions, i.e. P1–P2 and P3–P5, produced similar readings (Figure 3.20b). Differences between the averaged reading for P1 to P5 and the output obtained when the weight is located at the centre of mass were less than 0.2–1.3%.

Figure 3.20c shows the variation in percentage of the raw sensor readings at different axial positions along the balance plate in relation to those registered at the *CM* for an equal weight increment. Larger variations were found for higher values of the zero position (*ZP*, greater balance sensitivity). Average values were considered for P1 and P2 located close to the pan suspension support and mirrored positions P3 and P5 located slightly underneath the *CM* axis. Readings at P3 and P5 were at most 4% higher than those registered at the *CM* for the same weight increment. A maximum increase of 20.6% in the sensor output, relative to that of the *CM*, occurred at P4 for *ZP* = 1557, the position most distant from the pan support string. By contrast, the maximum decrease of 13.5% (at *ZP* = 1557) in the sensor output was obtained at positions P1 and P2, adjacent to the pan support.

Figure 3.20: (*a*) Schematic drawing of the balance plate showing the six test positions (P1 to P5) and the centre of mass (*CM*), (*b*) graphic showing the raw sensor output when an aluminium disc is placed at the different test positions (one position at each time) and also the value for the centre of mass position (*CM*) and the averaged value for positions P1 to P5 ($\bar{x}$) and (*c*) percentage of the raw sensor response increase or decrease in relation to the centre of mass output (*CM*), considering an averaged output for P1 and P2, P3 and P5 and the output registered at P4.

3.4.5. Pan cleaning system and water replacement

In the first SEDVEL version, the instrument base was attached to an acrylic settling tube fitted with an outlet pump on its top. There were two inlets located close to the base of the tube used for water replacement and cleaning. These inlets were fitted with a pair of hoses, which terminated a little higher than the top pump and were kept open. The hoses were later replaced by rigid pipes, and then by rigid pipes ending in "U" tubes pointing downwards. This arrangement with two inlets generated a vortex in the middle of the tube, promoting a spiral pattern of particle deposition on the pan when the water movement stopped. This caused an uneven deposition of material on the plate, which could interfere with the balance calibration. In summary, the water replacement system of the first SEDVEL version had three main problems: (*i*) it did not guarantee a homogeneous distribution of sediment on the pan after the pump had stopped; (*ii*) it did not properly avoid water percolation to the settling tube when settling was occurring; and (*ii*) it did not properly clean the balance plate under high sediment concentrations (see Section 3.6).

The first issue was solved by increasing the number of opening inlets to four: the adoption of four inlets created a turbulent motion inside the tube, without rotation, and ensured a homogeneous distribution of particles on the balance plate. It was visually observed that using only two opening inlets generated a vortex in the middle of tube, which disappeared when adopting four opening inlets. Also, when only two inlets were used, the sediment deposited on the balance plate formed a spiral pattern, which was replaced by a homogeneous layer of settled material when four opening inlets were fitted to the tube. The second matter was resolved by fitting one-way valves to the tube inlets and outlets. Further water percolation was also prevented by building a more robust system to fix the tube to its base. Finally, an upgrade of the balance plate cleaning system was performed by adding two auxiliary pumps close to the tube base.

In the second SEDVEL version, the function of the two auxiliary pumps is to clean the pan, while the pump on the tube top serves for the water replacement (Figure 3.21). Bilge pumps (12 V, 2.5 A, 0.53 l s^{-1}, Rule) were used. The two auxiliary pumps (AP) suck water in and out, creating a jet that flushes the sediment accumulated on the pan out after each

measurement (Figure 3.21a). These pumps are then stopped and the top pump (replacement pump) is turned on to renew the water inside the tube (Figure 3.21b). Arrows in Figure 3.21 indicate the movement of water in and out of the tube. The amount of the time that the pumps stay on is defined in the instrument software configuration. The applied values varied from 1 minute, in environments with low sediment concentrations, to 2.5 minutes, at high SPM concentrations. A longer cleaning period was needed at high concentrations because a thicker layer of sediment accumulates on the pan and tube base (see Section 3.6).
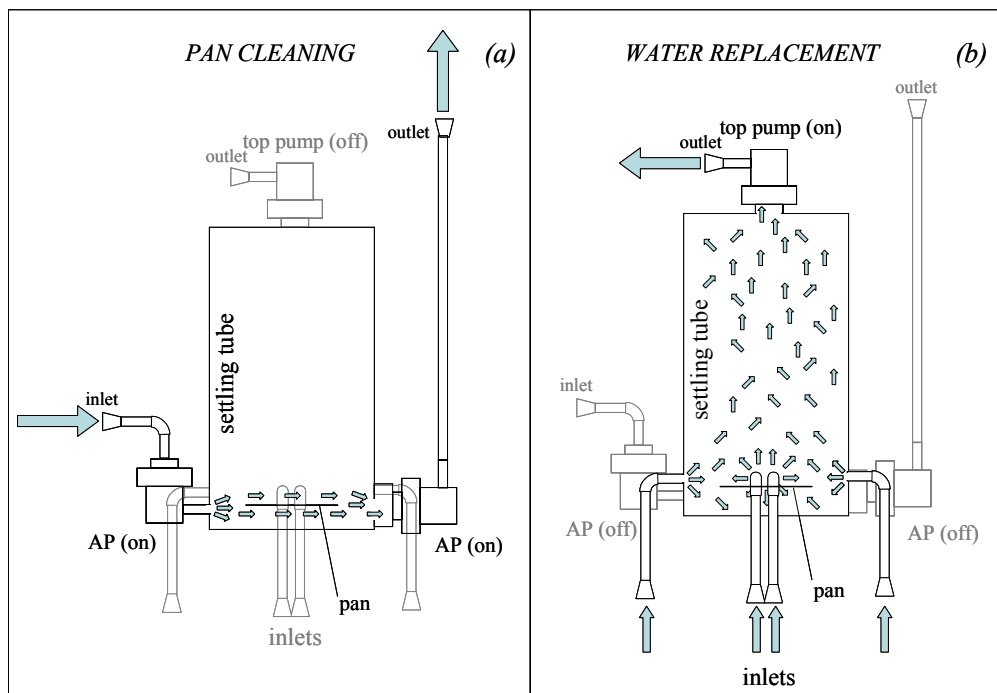
Figure 3.21: (*a*) Schematic drawing of the system to clean the balance plate; the two auxiliary pumps are turned on and the top pump stays off; (*b*) schematic drawing of the system for water replacement; the top pump is turned on and the water enters through the four opening inlets. The arrows indicate if the pipe works as an inlet or outlet to the settling tube.

When the replacement pump sucks water out of the tube top, a new water sample enters close to the tube base through four inlet doors (see arrows in Figure 3.21b). These inlet doors and all pump exits are fitted with one-way valves to ensure unidirectional flow and to avoid water percolation to the tube during the experiment, as well as after the pump has stopped and quiescent conditions have been achieved inside the tube. When water is sucked out the tube on the top, the silicone membranes of the one-way valves fold, opening the inlet doors (Figure 3.22a) and new water gently enters through the bottom of the tube. When the pump stops, the membranes return to their closed flat positions (Figure 3.22b). During deployment in environments with high SPM concentrations and also detritus, two one-way valves were fitted in sequence to each tube inlet in order to guarantee that the tube would be properly

sealed. This gave good sealing even when large plant fragments were present (see Section 3.6).
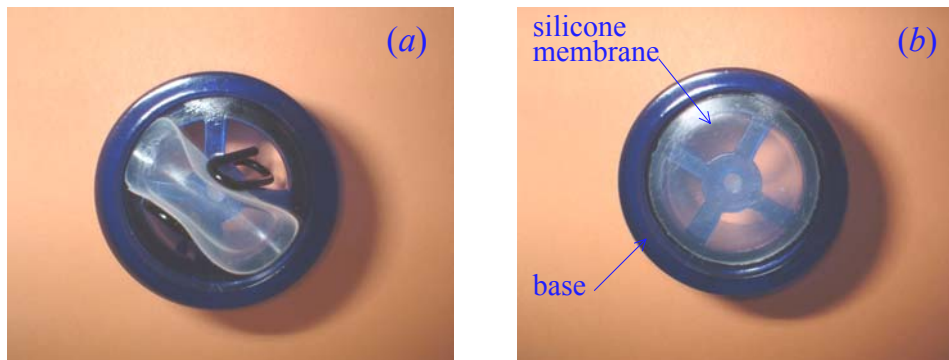
Figure 3.22: Detail of the one-way silicone valve in its opened (*a*) and closed (*b*) positions.

In addition, a small blade located on the top of the pan (Figure 3.9b) restricts its movement to a couple of centimetres while the pumps are working and helps the plate to return to a horizontal position soon after the pumps are deactivated. This caused the horizontal oscillations of the pan to be damped more quickly after the pumps stopped, and the equilibrium position to be achieved faster, than would have been the case if the pan had been allowed to move freely.

3.4.6. Housing, data logger and controller circuits

All SEDVEL parts are made of non-corrosive material, including the acrylic settling tube, PVC and stainless steel bolts and screws. The sensor, data logger/controller and battery cases are waterproof shelters fitted with O-ring bands for sealing, which can withstand a maximum pressure of 5 kg cm^{-2} when submerged. Waterproof 4 pin and 9 pin cables (Subconn, 20AWG, 300V) were used to connect the main body of the instrument to the battery and data logger/controller unit.

The data logger/controller unit (LC) functions include: (*i*) supplying power to the DVRT sensor and magnet motor, (*ii*) controlling logical circuits to switch the magnet slow-rotation motor on/off and up/down (zero position set up, motor circuit) (*iii*) to turn the main and auxiliary pumps on/off (pumps circuit) at the beginning of each cycle of measurement and (*iv*) data storage.

The logger/controller (LC) of SEDVEL was taken from a standard James Cook University (JCU) nephelometer (OBS) (Ridd and Larcombe, 1994) (see technical information in Appendix E) and modified to host additional channels for DVRT connection, magnet motor and pump controls. A 12-bit Analogue to Digital Converter (ADC, 4096 point scale) was adopted for recording values of the DVRT sensor output. This 12-bit device is centred on +2.5 V and ranges between 0 and +5 V. The main data logger battery (9 V) supplies power for the DVRT sensor and the magnet motor and an additional battery (12 V) is used to drive the three submersible pumps. In addition, two circuit boards were connected to the LC for controlling the magnet motor (motor circuit) and the three pumps (pump circuit).

A power converter (NML0509S, single output DC/DC) was used to convert the input voltage furnished by the LC unit of +5 V to a +9 V power supply required by the DVRT sensor. The DVRT output voltage (0.2–4.8 V) is within the range of the ADC (i.e. 0–5 V) of the LC unit. In addition, a voltage regulator (MAX667, CPA0023) was used to supply a regulated output voltage (+ 5 V) to the magnet slow-rotation motor.

The main data logger/controller sends a +5V logical signal to the two attached circuits, which triggers the mechanisms that switches the motor up and down (motor circuit) and the pumps on and off (pumps circuit). The activation/deactivation of the +5V logical signal is controlled by a software command, which depends on the set-up configuration. Drawings of the electronic circuits used for the magnet motor and pump controls are summarised in Appendices C and F, respectively.

A software program 'XTALK' is used for communicating with the LC to perform activities, such as: inputting the sampling set-up, logging and downloading the data at a speed of transmission automatically adjusted by software (default baud: 19200). Regarding its sampling set-up configuration the following parameters can be altered within the measurement range: (*i*) time between logs equivalent to the sampling rate (20 s), (*ii*) the motor up and down values, which corresponds to the minimum and maximum values of raw sensor output chosen for the zero position (*ZP*) range (e.g. $1400 < ZP < 1410$), (*iii*) pump on time is the amount of time in seconds that the two auxiliaries and the main pump will be kept on (e.g. 60–150 s), (*iv*) settling time that corresponds to the duration of the cycle of measurements (e.g. 60-180 minutes), (*vi*) the number of scans averaged within the log

interval (5000) and (*vii*) the starting time is used to define the day and hour when the instrument will start logging. Data is downloaded in ASCII format.

3.4.7. SEDVEL operational procedure in the field

During SEDVEL field operations, the whole instrument works attached to a tripod fixed to a triangular wood base (Figure 3.9). This triangular base helps to keep the instrument level with the seabed. Inlets for sampling were located about 40 cm above the bottom. Three sequential operations are performed in the field: (*i*) instrument calibration (zero position set-up), (*ii*) tube filling and (*iii*) deployment. The instrument zero position set-up is made at the beginning of each deployment while the instrument is still outside the water. A pre-filtered water sample (mesh 0.45 μm) taken *in situ* is used for zero position adjustment at "zero SPM concentration" and at environmental density. This procedure guarantees that the instrument starting position is set-up with water at environmental density, reducing calibration drift. This pre-filtered water sample is gradually introduced through the tube base (see aperture hole, Figure 3.9b) until the entire pan is covered by a few centimetres of water. The water introduction through the tube has to be very slow with the aim of preventing bubbles sticking to the balance plate. In addition, the filling aperture was built a few millimetres higher than the balance plate level. As a result, if air bubbles enter through the pipes, they will be released above the plate. This reduces the probability of them attaching to the pan.

After calibration, the settling tube is carefully filled with water taken from the environment through an aperture located at its base (Figure 3.9b). Then, a tap fixed to the tube opening is gently closed in order to seal the tube without allowing bubbles to be introduced inside the tube. Subsequently, the whole device is cautiously lowered in the water column and deployed to lie on the seabed. The instrument deployment has to be done very carefully to avoid gross shaking or tilting, which can result in a dislocation of the balance plate initial position and thus compromise the whole set of measurements.

After each cycle of measurement, the balance plate is cleaned and the water sample trapped inside the tube is automatically renewed, i.e. the old water sample is pumped out and a new water sample is pumped in. To do this, pumps are activated for 1.5 to 2.5 minutes at intervals of 60 to 90 minutes (cycle of measurement). This generates a turbulent flow inside the tube that maintains particles in suspension. It is assumed that turbulence ceases within the first

minute or two after the pump has stopped, since after this period of time the balance plate stops oscillating and returns to its horizontal position.

3.5. Balance calibration and factors that affect its sensitivity

Two main factors interfere with the balance reading: the homogeneity of settled material on the balance plate and the adopted zero position (balance starting point). The first factor affects the balance accuracy and the second one its sensitivity (resolution) and its range of measurement. The zero position itself basically changes as a function of the density of the water (fluid medium) and presence of bubbles. Further, diverse balance sensitivities can be achieved by using balance plates with different densities. These factors are discussed below.

3.5.1. Verification of homogeneity of settled material

Experiments were performed to check if a homogeneous distribution of the settled sediment was achieved. An acrylic tube (with a diameter of 15 cm and height of 35 cm) was filled with a mixture of water and dry sediment through an aperture on its bottom. For each experiment, six to eight pre-weighed vials ($D = 3$ cm, $H = 5$ cm) were distributed on the tube bottom for collecting the settled sediment. After a day, the tube was carefully emptied and the excess of water in the vials removed with a syringe. Vials were weighed again and masses of sediment obtained by subtracting the masses of the clean vials. Three concentrations were tested 100, 350 and 550 mg l^{-1}, considering two grain size distributions: (*i*) 89% of silt plus clay and 11% of sand and (*ii*) 49% of silt plus clay and 51% of sand.

Differences among net weights of sediment inside of each vial in relation to the averaged value for each experiment were less than 6% for 83% of the replicates, and less than 15% for all the replicates. When applying a Dunkan test (95% confidence level), all replicates were included within the same sampling population, indicating a homogeneous particle distribution on the tube bottom.

3.5.2. Balance calibration procedure

Balance calibration was performed by pilling up standard weights of known masses and densities on the balance plate centre of mass (*CM*). Aluminium or PVC discs with effective immersed masses (as defined in Section 4.3.1) ranging from 0.02 to 0.20 g were used as standard weights. Increasing and accumulative increments of mass were applied until reaching the balance saturation, i.e. maximum DVRT sensor output observed when the pan touches the sensor head. After placing every new disc on the pan, the raw sensor output was recorded for about 1–2 minutes, and an averaged value within this period was considered as representative of the accumulative effective immersed mass on the pan. A stair like pattern is obtained for the calibration curve as shown in Figure 3.23a.
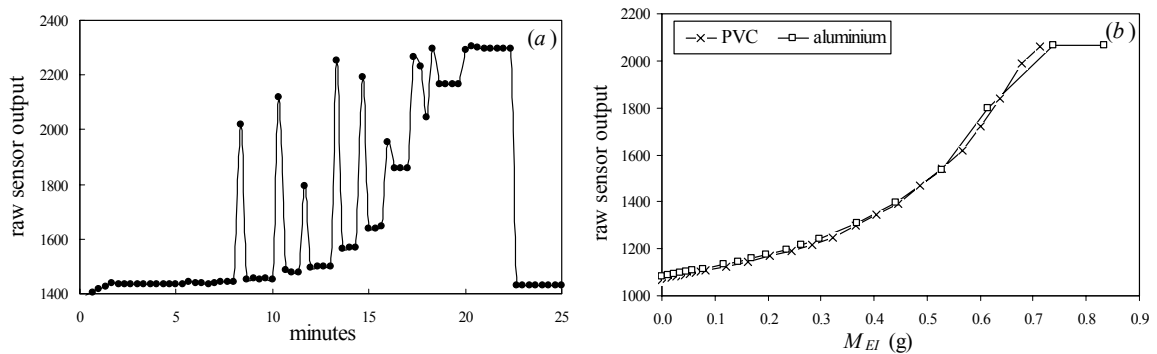
Figure 3.23: (*a*) Calibration curve showing the response of the DVRT sensor every time a new standard weight disc is added on the pan centre of mass. The first five minutes are used to set up the zero position, which is again monitored at the end of calibration when all discs are removed from the top of the pan. Every sensor output increment corresponds to the addition of a new disc on the top of the previous one. Spikes correspond to the instants of time when the weights have been manipulated; (*b*) Calibration curve relating the effective immersed mass (M_{EI}, g) to the raw sensor response, performed with PVC and aluminium discs (see legend on the Figure) for the same pan configuration. Experiment was realized with freshwater at temperatures between 18.9 and 19.2°C and similar starting zero positions.

Using aluminium or PVC discs with very distinct densities gives the same result providing the effective immersed mass is adopted for drawing the calibration curve, as shown in Figure 3.23b.

3.5.2.1. Calibration curves and balance sensitivity

Typical calibration curves of the second SEDVEL version relating the raw sensor output to effective immersed masses are presented in Figure 3.24. Different starting zero positions were adopted for comparison as indicated in the legend. All calibrations were performed in

similar water densities. These curves differ from the family of calibration curves obtained for the first SEDVEL version (Appendix G) because the distances between the pan and DVRT sensor and the pair of magnets were a little different in the second version, this led to a reduction of the measurement range and a slight increase in sensitivity.

The family of calibration curves presented in Figure 3.24 shows that the greater the value of the starting position (*ZP*, arbitrary units), the higher is the instrument sensitivity. However, as the sensitivity increases the measurement range narrows. For example, a zero position of 1440 allows a maximum effective immersed mass of about 0.35 g, with a reasonable sensitivity for the whole range. Conversely, a higher sensitivity is achieved (steeper curve slope) when starting at 1565, but the balance saturates with around 0.20 g of effective immersed mass because the DVRT reading goes off scale.
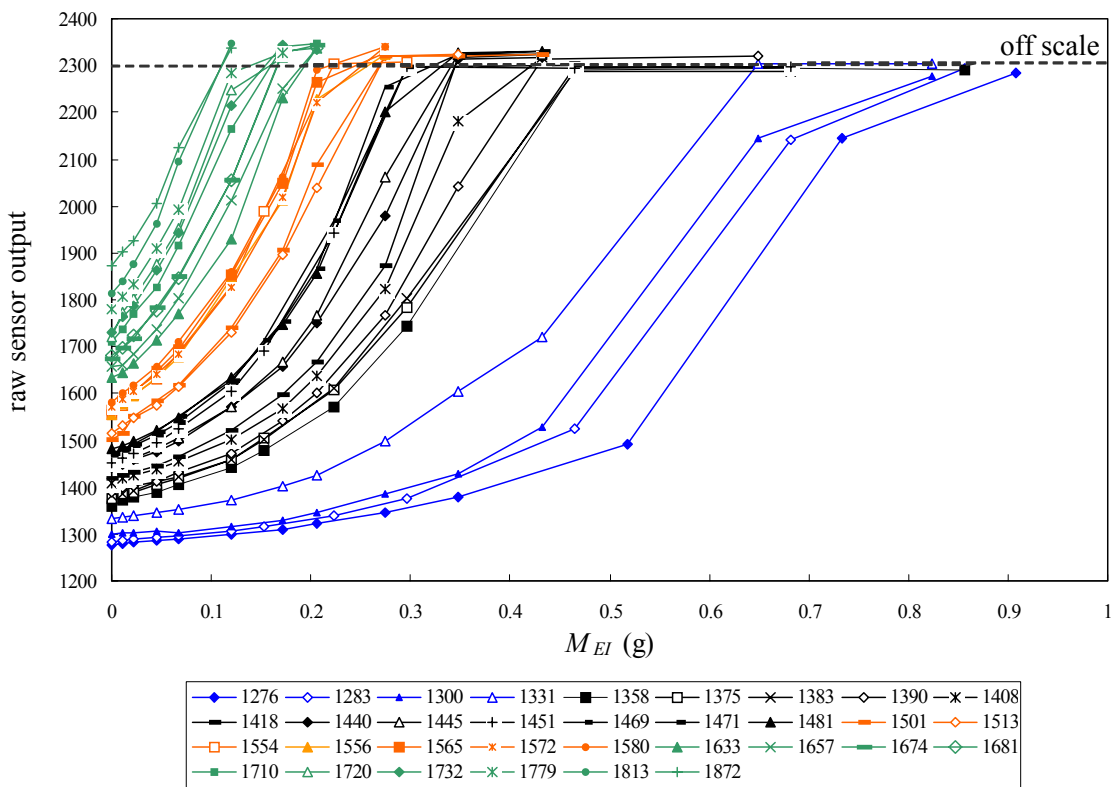
Figure 3.24: Set of calibration curves for the second SEDVEL version (aluminium Pan 4) relating the effective immersed mass (M_{EI}, g) to the raw sensor output (SR) for different starting positions. Calibrations were performed at salinities between 36 and 37 and temperatures between 24 and 25°C. The maximum sensor output is located around 2350 (off scale).

Very high sensitivity can be achieved for zero positions above 1600 (green curves in Figure 3.24), while low resolution occurred for zero positions below 1350 (blue curves in Figure

3.24), especially for effective immersed masses less than 0.4 g. An intermediary range of sensitivity (black and orange curves in Figure 3.24) was adopted for most measurements performed with SEDVEL in this work. These differences in sensitivity according with the zero position are related to the increasing sensitivity of the DVRT sensor, as the target gets closer to it when raising the zero position value. In conclusion, the instrument sensitivity can be increased or reduced by changing the starting zero position in order to meet the measurement range requirements.

This family of curves were used to estimate effective immersed masses of particulate matter measured in the laboratory or in the field. In order to do this, rational equations were formulated to relate the effective immersed mass (M_{EI}, dependent variable) to the raw sensor output (SR) for each distinct starting zero position and specific water density (as measured in laboratory or in the environment). Rational fittings were performed in Curve Expert 1.38 (Hyams, 2001), and all correlation coefficients (r^2) were above 0.98. An example of this calibration curve fitting is shown in Figure 3.25.

$$M_{EI} = (a + b \cdot S_R)/(1 + c \cdot S_R + d \cdot S_R^2)$$
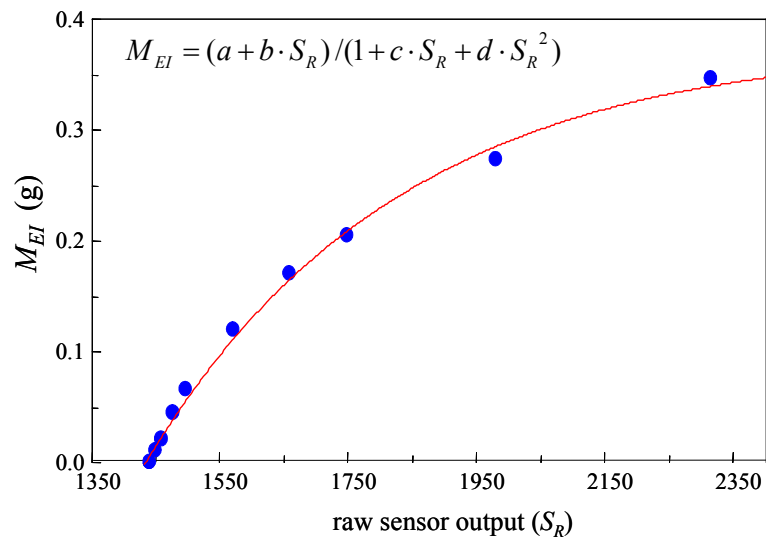
Figure 3.25: Calibration curve showing the effective immersed mass (M_{EI}, g) as a function of the raw sensor output (S_R, arbitrary units). The rational function adopted to relate these parameters is also shown.

Another point to consider is that the balance resolution increases as the accumulative weight on the pan increases, i.e. for the same mass increment the raw sensor output increases to a greater extent at the middle of the calibration curve (higher sensitivity) than at its origin (lower sensitivity) (Figure 3.24), especially at low zero positions (e.g. 1283 in Figure 3.24). In order to illustrate this effect the first derivative relating the variation in the effective

immersed mass (M_{EI}) as a function of the raw sensor output (S_R), i.e. dM_{EI}/dS_R, was plotted for eight different curves starting in different zero positions (Figure 3.26). Note that the original functions used in the derivative were rational equations in the form presented in Figure 3.25, where the *x* and *y* axes were swapped in relation to Figure 3.24. These curves show that the instrument sensitivity is not constant over the whole range of measurement. For example, the derivative curve starting at the zero position of 1283 shows that a bigger increment of mass represents only a small variation in the sensor response (i.e. bigger rates dM_{EI}/dS_R) at small values of S_R, while for S_R above 1500 the sensitivity is considerably increased. However, similar variations of sensitivity as a function of S_R is obtained for curves starting at zero positions above 1550. The instrument sensitivity varies to a lesser extent at the calibration region between 1550 and 1900 than at zero positions between 1200 and 1350, considering the whole range of measurement, because calibrations approached more to linear functions in the first region (Figure 3.26).
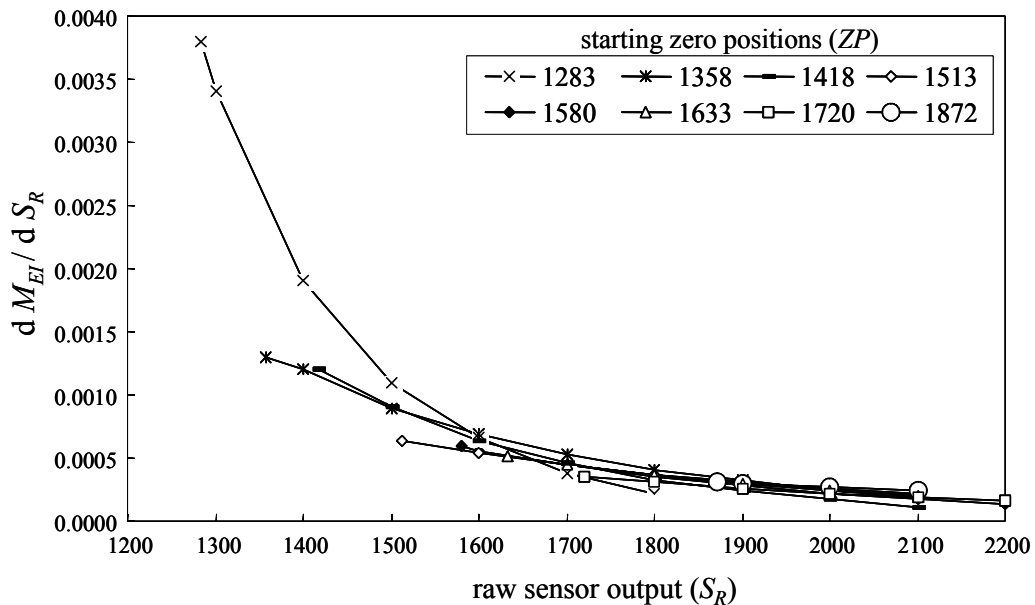
Figure 3.26: First derivative (dM_{EI}/dS_R) for calibration curves starting at the different zero positions showed in the inlet, relating the incremental variation in the effective immersed mass (M_{EI}) with the variation in the raw sensor output (S_R). Original functions were rational equations in the form presented in Figure 3.25. This derivation was performed in Curve Expert 1.38, which uses a central difference scheme with Richardson extrapolation to compute the derivatives (Hyams, 2001).

As mentioned before, during the measurements the big magnet stays at a fixed starting position as set-up at the beginning of the measurements (first cycle). At this starting position, the repulsive force exerted by the big magnet on the two small magnets attached to the pan is just enough to support the balance plate in a horizontal position. When an extra weight is

placed on the top of pan due to the falling sediment particles, it will drop slightly (proportional to the weight placed on its top) and approach the DVRT sensor. Thus, the small magnet will approach the big one, causing an increase in the repulsive force between the pair of magnets enough to balance the weight and reach a new equilibrium. The pan displacement is proportional to the sediment weight, but the total amount of pan sensitivity is dependent on both the distance between the pair of magnets and the distance between the pan and the DVRT sensor. The importance of the relative distance between the pair of magnets in determining the pan sensitivity is demonstrated below.

3.5.2.2. Balance sensitivity for balance plates with different masses

Distinct balance plates with different effective immersed masses were tested in order to analyse alterations in the instrument sensitivity promoted by changes in the pan buoyancy. Three plates were made of aluminium with different thickness and weights in air (PA1, PA2 and PA3), although PA1 and PA2 represented similar effective immersed masses. A fourth pan was made of PVC and had a large aluminium target attached to it (PP). The last pan had the highest buoyancy, and therefore, the smallest effective immersed mass (M_{EI}). Calibration curves were performed using these four different pans under the same testing conditions, i.e. similar water densities and starting zero positions. The pans with distinct effective immersed masses (e.g. PA3 and PP) produced different instrument sensitivities, while pans with similar effective immersed masses gave very close results, as illustrated in the Figure 3.27. The lighter the balance plate when submerged; the higher the instrument sensitivity and narrower the measurement range.

When the effective immersed masses of the different pans are input to the equation presented in Figure 3.15, relative distances between the pair of magnets of 4.4, 4.6 and 4.8 cm are obtained for PA1=PA2, PA3 and PP, respectively. These differences can be explained in terms of variations in the sensitivity of the magnetic spring system, since all calibrations were performed in similar environmental conditions and calibration curves for the different pans started at very close zero positions. As showed in Figure 3.16, the larger the distance the magnets are set apart, the wider is the variation in distance as a function of force. Therefore, with the lighter pan arrangement (PP) the magnets were 4.8 cm apart, at this region the repulsive force is weaker and a larger displacement will result from a given change in force

on the pan (see Figure 3.16). This resulted in a higher sensitivity and a narrower measurement range observed for this pan (i.e. PP).
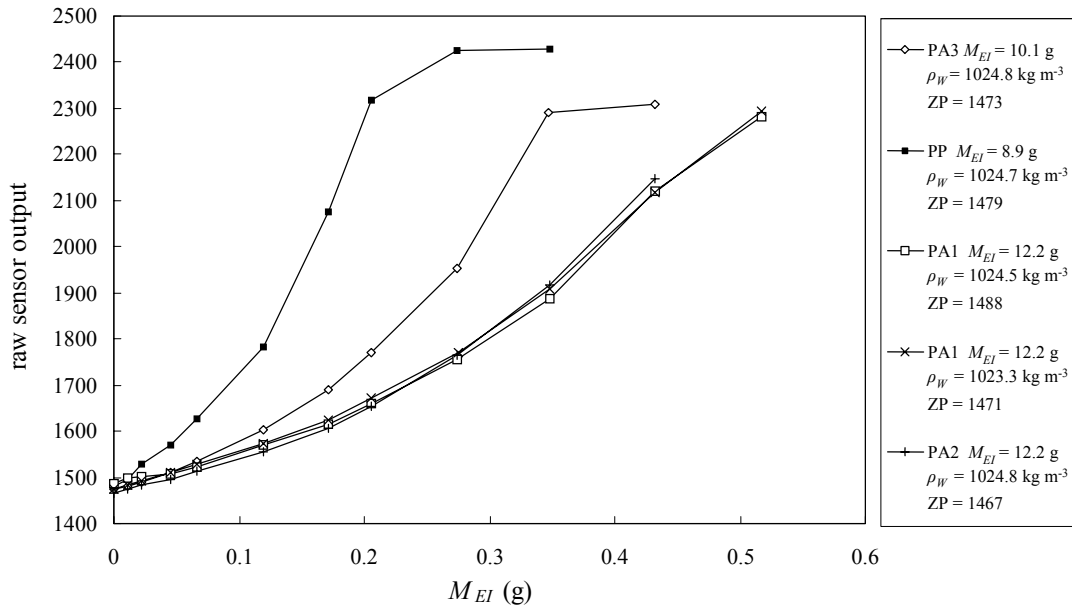
Figure 3.27: Different calibration curves produced by balance plates of different effective immersed masses. Where M_{EI}, ρ_W, ZP are the effective immersed mass of the pan, water density and the zero position, respectively for each one of the tested pans.

Further, environmental conditions can alter the instrument sensitivity due to changes in the set-up starting position mainly promoted by variations in water density among the cycles and contamination of the measurements by air bubbles, as discussed next.

3.5.3. Zero position changes

3.5.3.1. Influence of water density variations on the zero position

In the field, the balance zero position can also be altered in relation to its initial set-up (starting zero position) due to changes in water density between different cycles of measurement that cause variations in the balance plate buoyancy. The density of water can vary due to changes in water salinity and/or temperature. In the laboratory, although temperature and salinity were kept approximately steady, small oscillations of these parameters can also lead to shifting of the starting zero position. If the density of the water decreases, the buoyancy force acting on the balance plate reduces, and the plate becomes heavier and drops in relation to its initial equilibrium position. Therefore, it comes close to

the DVRT sensor and the instrument output increases. Contrarily, if the density increases, the sensor output decreases. As the magnet motor is not activated between the different cycles of measurement, these changes in the immersed weight of the balance plate are not compensated by increasing/decreasing the magnet force on it, and small differences in the starting zero position are expected among the distinct experimental cycles. In order to illustrate this effect, some laboratory tests were performed to measure the zero position changes as a function of salinity variations.

3.5.3.2. Salinity influence on the balance zero position

The selected zero position was first set-up at a salinity of about 35–35.5. Next, the water inside the tube was gradually diluted from a salinity of about 36 to zero. Sensor response was recorded for 5 minutes in each salinity, and an averaged value taken as representative of the respective salinity. Changes of the initial zero position as a function of the water salinity were tested for salinities ranging from 0 to 35–35.5 and starting zero positions varying from about 1290 to 1560 (n = 9) (Figure 3.28). The averaged temperature used at the different tests was 24.4 ±0.5 ° C, and the averaged temperature oscillation within each run was 0.3±0.1 ° C. The biggest change in water density was from freshwater ($\rho_W = 997.2$ kg m^{-3}) to salt water at 35.5 ($\rho_W = 1023.9$ kg m^{-3}).
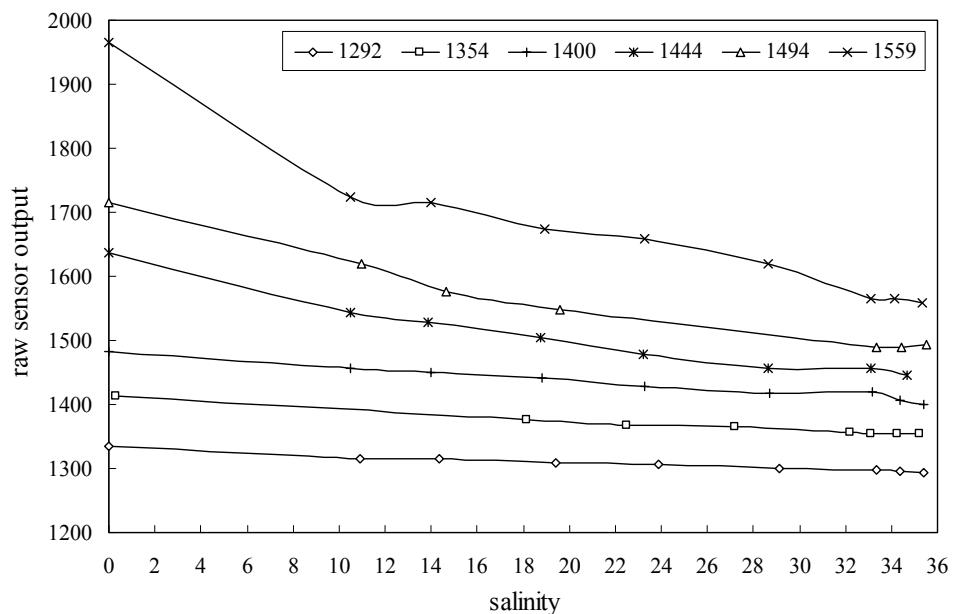
Figure 3.28: Change in SEDVEL raw output (S_R) as a function of salinity for the different starting zero positions indicated in the legend.

These tests showed that the higher instrument sensitivity (higher zero position), the larger is the change in the sensor output as a function of salinity (Figure 3.28). For salinities between 35–35.5 to 10.5–11, the zero position rises by less than 10.6% of its original position. Greater variations were found when changing from salt (35–35.5) to freshwater. Rises of 3.3, 4.3, 5.9, 13.4, 14.7 and 26.0 % were observed from initial zero positions of 1292, 1354, 1400, 1444, 1494 and 1559, respectively.

These experiments were also represented in terms of water density for reference (Figure 3.29).
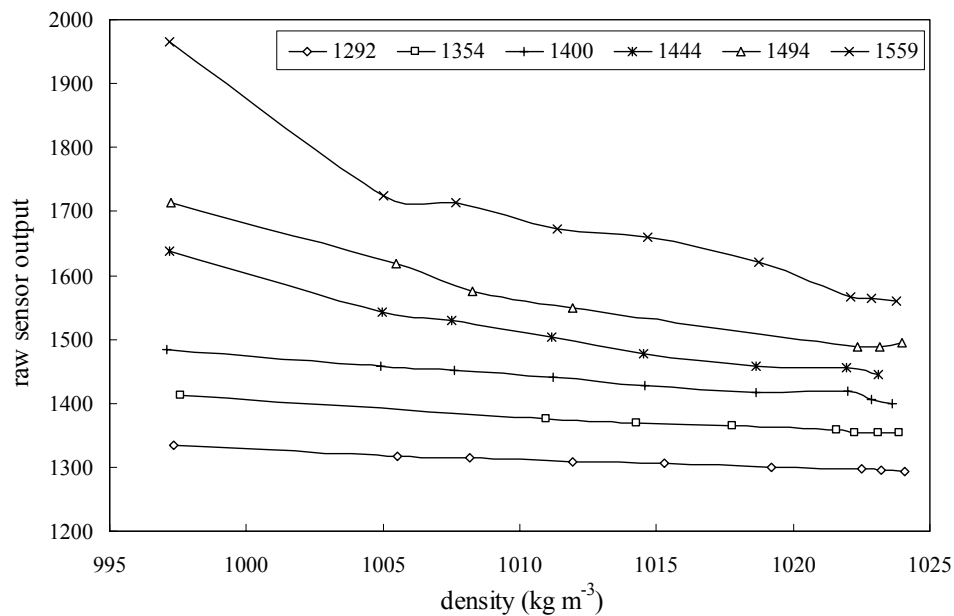
Figure 3.29: Changing of SEDVEL raw output (S_R) as a function of water density for the different starting zero positions indicated in the legend.

Even though these variations were generally small (< 15%), they can promote a large error in the weight estimation if the right calibration curve is not applied, especially at zero positions with high sensitivity. For example, if the calibration curve with zero position of 1445 is used to convert an arbitrary sensor output of 1570 to effective immersed mass (M_{EI}), a $M_{EI} = 0.11$ g is obtained. Now if an increase of 8% is considered in the starting zero position (i.e. $ZP = 1554$) the estimate mass for 1570 is 0.01 g, i.e. 11 times smaller.

If the density of the water changes during the field-monitoring period, the zero position will drift in relation to its initial settling. This was the case during the SEDVEL field trials, when the zero starting positions among the monitored cycles often differed. This does not prevent measurements being obtained, and this matter can be solved by applying the right calibration curve considering the zero position and water density when measurements were performed.

3.5.3.3. Bubbles

The zero position can also be altered in relation to its initial set-up due to the presence of bubbles, which can adhere to the balance plate altering the balance plate buoyancy. Bubbles were usually present during laboratory calibrations if tap water was used. Their formation was reduced by boiling the water used in the experiments or by manually removing them. In the field, bubbles could be accidentally introduced in the settling tube during filling (before deployment) even with a careful filling procedure. Therefore, the first few cycles of measurements were frequently discarded due to considerable changes in the zero position by the "bubble effect". However, after a few cycles of measurements bubbles were removed with the cleaning and water replacement processes. After the initial releasing of the bubbles, the introduction of new bubbles was not verified while the instrument was operating under water.

3.5.3.4. Magnetised sediment

After instrument deployment in the field, magnetised particles of sediment were generally found attached to the small magnet located under the balance plate. This could have led to variations of the zero position between consecutive cycles of measurement, since these particles are unlikely to be removed during water replacement.

In order to test the influence of magnetised sediment on the instrument output a simple test was done. This consisted of monitoring the instrument output at a fixed zero position with the magnetised particles adhered to the magnet and after removing these particles. The magnetised particles on the magnet represented the total amount attached after a few days of the deployment in the field (i.e. 17 cycles). The difference in the effective immersed masses between the two situations was around 0.01 g. Assuming that equivalent amounts of magnetised particles had been adhered to the magnet in the different cycles; this would result

in a small mass (i.e. 0.001 g per cycle) being attached to the magnet each cycle. The total change in the zero position is within 10 to 20 units (arbitrary units of the S_R) for the total amount of particles.

Therefore, it is expected the influence of magnetised particles on the measured weight to be small. If there were some contribution to the weight due to the attached particles, this would be computed together with the total *PM* mass. As the magnets are localised close to the pan centre of mass, bias expected due to a non-homogeneous distribution of the magnetised particles should also be small.

3.6. Examples of SEDVEL measurements in the field

The aim of this section is to give a few examples of the SEDVEL performance in the field and illustrate some problems detected during its deployment. SEDVEL field trials were carried out in Cleveland Bay (Townsville, Australia). These deployments took place in this shallow muddy embayment at two locations: the Strand beach (1 to 4 m deep) and the Townsville Harbour (8 to 10 m deep). Details about these locations are given in Section 4.5.1.

Figure 3.30a illustrates the temporal variation of SEDVEL sensor raw output during 57 consecutive cycles of measurement ($\approx$ 2.5 days) at the Townsville Harbour. Each cycle lasted 60 minutes. The spikes correspond to the time when the bottom and top pumps were activated. Zero positions varied less than 20 units (arbitrary units of the S_R) among the different cycles for this particular deployment (Figure 3.30a), although bigger variations were observed in other deployments. A detail of the first ten cycles is shown in Figure 3.30b. The observed pattern at each cycle was an increase of the sensor reading as the particulate matter (*PM*) settled on the balance plate, making it approach the DVRT sensor head, until most of the *PM* had been deposited and the sensor output became almost constant with time. After one cycle of measurement, the pumps were activated and material on the pan removed, resulting in a sensor output drop to a value close to the starting zero position of the previous cycle. A comparatively larger amount of *PM* was deposited in the seventh cycle, while the quantity of settled *PM* was reduced for the last three cycles (Figure 3.30b).

Not all SEDVEL deployments produced satisfactory results as shown above. Some problems that reduced instrument performance included: (*i*) changing of instrument sensitivity due to variations of its zero position *in situ* (*ii*) bubbles introduced before instrument deployment, (*iii*) improper pan cleaning after a cycle of measurement, (*iv*) water percolation during measurements and (*vi*) dislocation of the pan during instrument handling. These issues are discussed below.
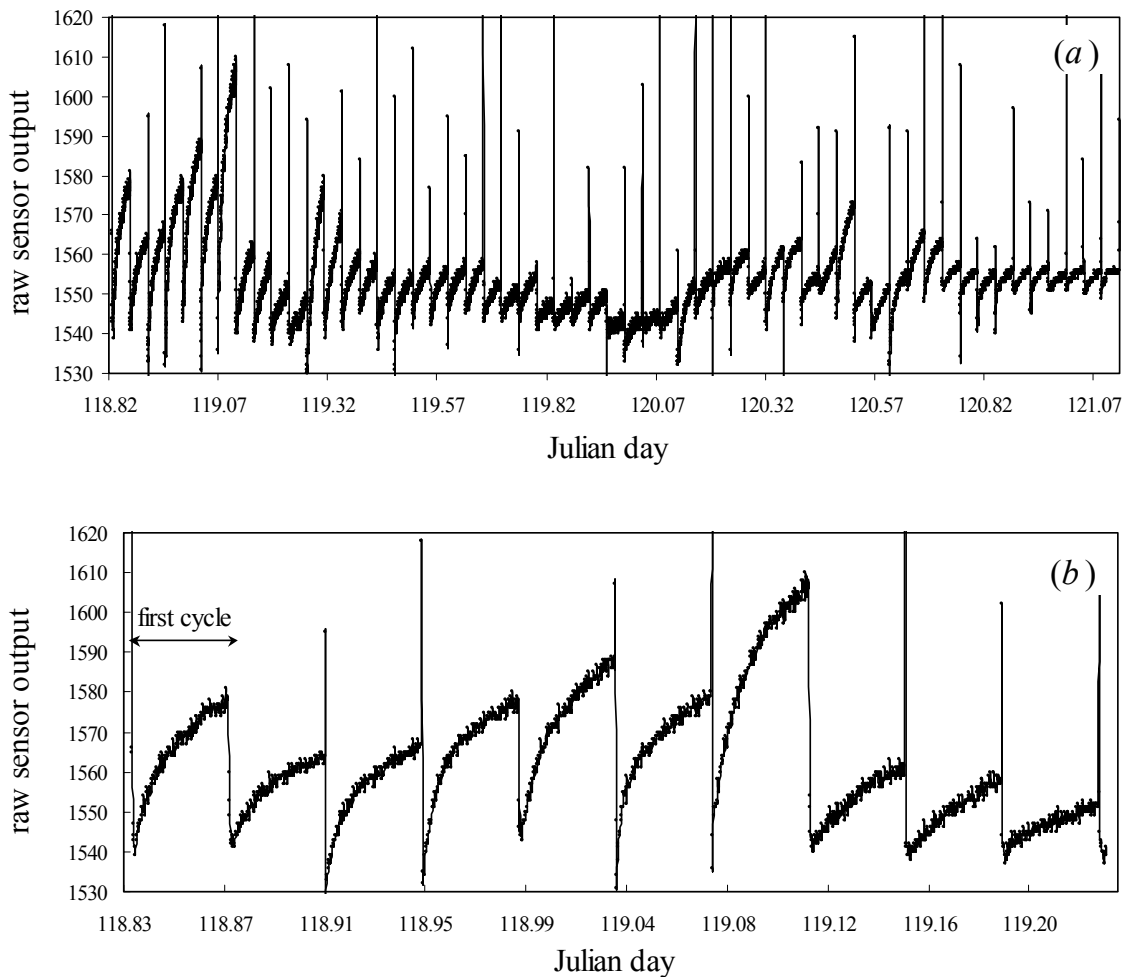
Figure 3.30: (*a*) Data series of 57 consecutive cycles of SEDVEL measurement at the Townsville Harbour, (*b*) a detail of the first ten cycles of measurement. Each cycle lasted one hour and pumps were on for 60 s.

Small variations of the zero position among the different cycles of measurements were observed at most of the deployments. More often data series showed a rise of the zero position from the beginning to the end of the deployment, indicating that the balance plate moved slightly closer to the target. On a few occasions, the zero position also decreased (i.e. the pan rose). Small variations of the zero position among the different cycles usually do not prevent measurements being done but they require a demanding calibration procedure. This means that when post-processing the data, several different calibration curves have to be

performed considering the zero position and environmental water density observed in each cycle of measurement in order to obtain more accurate results.

Factors that could have been responsible for variations of the zero position among the different cycles of measurement include: (*i*) water density variations (independently determined from water temperature and salinity measurements) among the different cycles of measurement which led to changes in the pan buoyancy (*ii*) a slight stretching of the suspension string (less than 5%) or small suspension system displacement due to the pan oscillations during the pumping, (*iii*) small amount of magnetized particles attached to the small magnet and (*iv*) a thin layer of *PM* sticking to the pan that was not properly removed.

Further, drastic variations of the zero position set up before the deployment of the instrument occurred if bubbles were introduced in the tube during filling. This effect is exemplified in Figure 3.31 where a drop of over 200 units was observed between the zero position set up outside the water and the zero position verified in the first cycle of measurement with the instrument moored on the bed, which considerably reduced the balance sensitivity. A few small bubbles can alter the balance plate buoyancy, and therefore, its position. As the displacement sensor has a very high resolution, even a slight variation of the pan position can lead to a considerable change of the sensor reading. As bubbles increase the pan buoyancy, they often cause a zero drift to the calibration region where the balance is less sensitive. Bubbles introduced in the tube during filling were minimized by adapting a tap to the aperture located at its base. The tap was carefully closed when the tube was full of water preventing the bubbles forming inside the tube. In addition, differences in temperature between the water used for calibration and the water temperature *in situ* could have contributed to a zero position drifting, since the tube did not have any thermal insulation. Therefore, the small volume of water used in the calibration could have suffered a significant temperature change, even during a short period of time used for the zero position setting up (i.e. 60 to 90 minutes).
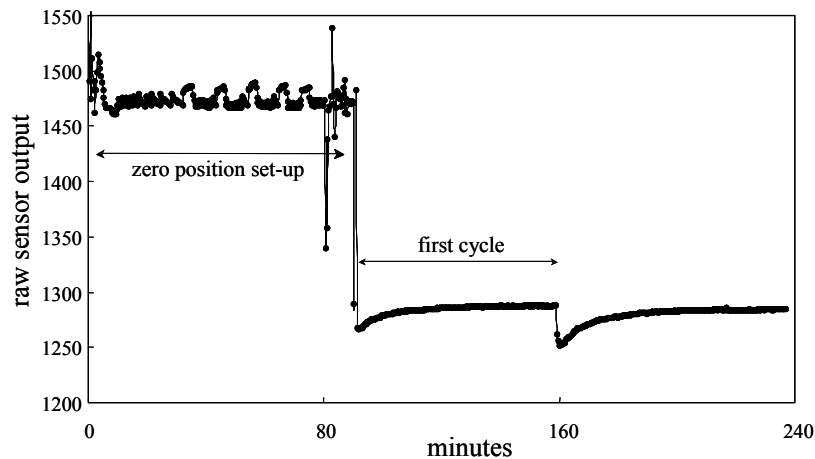
Figure 3.31: Displacement of the zero position calibration due to bubbles accidentally introduced in the tube during its filling before the deployment.

As mentioned before, some of the problems associated with the water replacement and cleaning of the balance plate present in the first SEDVEL version were solved in the second SEDVEL version. Figure 3.32a shows a few cycles of measurement of the first SEDVEL version where the four inlet pipes operated without the one-way valves. During this deployment, the sensor output continuously increased instead of reaching values approximately constant by the end of the experimental cycles when most of the *PM* should be settled. This indicated that there was a water percolation through the system during the measurements, causing a small input of SPM that continued to fall on the pan. Further, the readings presented a relatively high noise demonstrating that there was some water circulation inside tube.

Figure 3.32b depicts another deployment of the SEDVEL first version, in which one-way valves were fitted to all tube inlets and outlets, but there was only the top pump functioning for replacing water and cleaning the pan. Even though the sensor reading stabilized by the end of each cycle and the data noise had been reduced, the balance plate was not properly cleaned between cycles of measurement, as indicated by the continuous zero position rising from the beginning to the end of the monitoring period. During this deployment low SPM concentrations were measured (< 20 mg l^{-1}), and measurements could still be performed without the saturation of the balance, but samples probably suffered contamination from the previous samples.

Contrarily, balance saturation was observed at the end of another deployment undertaken with the second SEDVEL version equipped with the two auxiliary pumps and one-way

valves (Figure 3.32c). During this deployment the first cycle was performed at a low SPM concentration (< 20 mg l^{-1}), which increased in the subsequent cycles to values between 50 and 100 mg l^{-1}. In this case, two factors could have caused the balance saturation: (*i*) the pan was improperly cleaned at high sediment loads because the auxiliary pumps stayed on only for short period (i.e. 60 s) and (*ii*) some water percolation could have occurred because of inadequate shutting of the one-way valves.
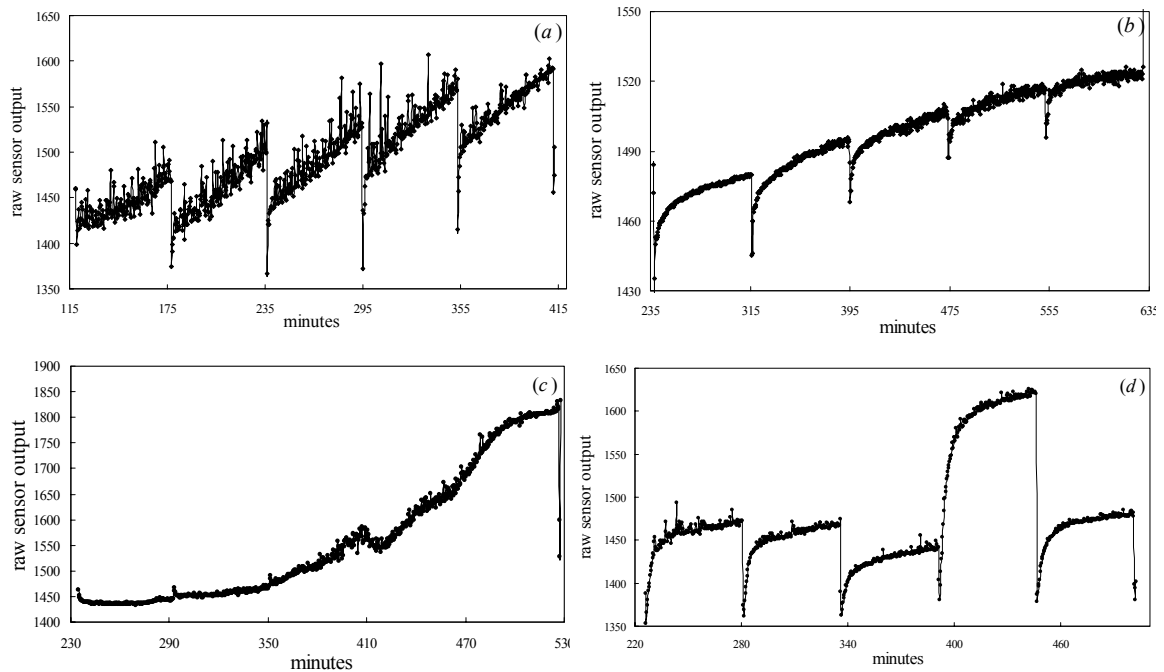
Figure 3.32: Deployments of the SEDVEL instrument at the Strand Beach (Townsville, Australia) (*a*) of the first SEDVEL version with opened inlets and outlets, showing the effect of the water percolation; (*b*) of the first SEDVEL version with inlets and outlets fitted with one-way valves and without the auxiliary pumps, showing the effect of improper pan cleaning; (*c*) of the second SEDVEL version using a short pumping period, showing the pan readings saturation, and (*d*) of the second SEDVEL version, showing a proper pan cleaning between the different cycles of measurement and reading stabilization at the end of each cycle.

These deployments took place in a muddy beach about 30 m distant from the shore and the presence of large seagrass detritus and algae filaments was observed at several occasions during the instrument deployment in the region. These filaments were also observed between the membrane of the one-way silicone valve and the valve base after the instrument retrieval on a few occasions. This is likely to have resulted in the valves inefficiently sealing and some water flow (and sediment input) to the tube. In order to fix these deficiencies, two changes were adopted (*i*) the period of time the auxiliary and top pumps stayed on was increased to 150 s and (*ii*) two one-way valves were fitted in sequence to the tube inlets, hence the second valve served as a backup in case some large filament was trapped in the first one.

The above modifications improved the SEDVEL performance at high sediment concentrations as shown in the Figure 3.32d. During this particular deployment, even under SPM concentrations ranging from 55 to 106 mg l^{-1}, a proper balance pan cleaning after each cycle of measurement occurred as well as a stabilization of the sensor output reading at the end of each cycle when most of the *PM* had already been deposited on the pan. Therefore, the jet used to clean the pan was able to remove the material previously deposited at high sediment loads if a higher pumping period was adopted. Also, the one-way valves closed adequately, since the sensor output stabilized at the end of each cycle. In addition, readings displayed a small noise level.

Deployments carried out with the second version of SEDVEL, after all the above improvements had been performed (e.g. efficient pan cleaning system, use of two valves in sequence, increasing the pump period), had a rate of success of about 62%. Three of eight deployments did not produce good results. One because of zero position changes induced by bubbles introduction, and in the other two the instrument recorded a maximum sensor output during the whole period of monitoring, except during its calibration. As this happened in the moment the device was being deployed, a possible explanation is that the pan got jammed (touching the sensor head) due to instrument tilting or shaking during its lowering to the water level. Also, an improper levelling of the instrument on the seafloor could cause the balance plate to lean, not allowing it to return to its horizontal position.

The main problem observed during the successful deployments was the variation of the zero position (*ZP*) among the different cycles of measurement, which required a demanding post-calibration of the instrument. Future SEDVEL modifications that allow the *ZP* to be set up at the beginning of each cycle of deployment would greatly improve the instrument reliability and facilitate the calibration procedure.

The SEDVEL output can be used to calculate two important parameters associated with the cohesive sediment transport in coastal areas: SPM mass concentrations and aggregates settling velocities. A detailed description of SEDVEL data analysis and results is presented in the Chapter 4 as well as a comparison between SPM mass concentrations estimated from SEDVEL measurements and those quantified from water samples collected simultaneously in the field.

3.7. Advantages and constraints of SEDVEL

Considering the devices available to quantify settling velocity and SPM concentration in the field (as exposed in the Chapter 2), SEDVEL is unique in furnishing direct and automated *in situ* measurements of the effective immersed mass of particulate matter (*PM*) and SPM mass concentration (M L^{-3}). SEDVEL operates in concentrations ranging from 5 to about 2\00−500 mg l^{-1}, with a resolution better than 0.01 g and a sampling autonomy of 3 to 5 days. It records almost continuously (every 20 s) the floc settling, and it is flexible regarding the monitored settling period. It does not require extraction of samples to obtain sediment mass and allows the measurements to be done in place, avoiding the floc break-up and settling velocity alterations observed, e.g. in the Owen-kind tubes due to the development of a little circulation inside the tube during the subsamples withdrawal and manoeuvring of the tube on its retrieval to the surface.

SEDVEL constitutes a novel approach and an alternative to automatically measure the mass-concentrations of suspended particulate matter (SPM) *in situ*. Direct devices used for this purpose have the advantage of reducing build-up errors that occur during data calibration and the mathematical procedures used for data analysis of the output of indirect instruments. Settling tubes (Owen-kind tubes) and SEDVEL are the only direct devices available for the quantification of the *PM* mass and mass distribution of settling velocity, SEDVEL being a unique autonomous device.

Compared with other automated instruments, SEDVEL has a relatively simple working principle and calibration. It does not require the use of complex calibration constants or inversion techniques to access the floc settling velocity, as it is the case of the indirect automated techniques, such as optical, laser and acoustical devices. Further, properties of particles/flocs, such as size, shape, roughness, colour, do not influence instrument calibration or response. Although calibration depends on the medium density (salinity and temperature changes), these are straightforward parameters to measure in order to apply the correct calibration curve.

SEDVEL can work both in freshwater and saltwater environments provided it has been calibrated at the environmental density and the appropriate calibration curve has been applied. In environments subject to large salinity variations, as usually occurs in estuaries, measurements could probably still be performed, but the instrument zero position (and sensitivity) would change considerably among the experimental cycles. For instance, if a zero position (ZP) around 1400 were used initially at a salinity of 35.5 (1024 kg m^{-3}), a subsequent salinity drop to 10 (1005 kg m^{-3}) would make the ZP rising to 1457 (as shown in Figures 3.28 and 3.29). Measurements could still be performed at this ZP range, with an increase in the sensitivity, in this particular case, as salinity reduces. Although the instrument has not been tested in an estuarine system, in theory, it would work properly; providing appropriate calibration curves were adopted for the different cycles of measurement according to the observed ZP and water densities. Preferably, the instrument should be re-calibrated at the beginning of each cycle of measurement at the instantaneous water density, in environments subjected to fast salinity changes. Practical restrictions to this procedure include the difficulty in obtaining a water sample at the *in situ* density and free of SPM to perform an underwater calibration. This would also require a fast calibration cycle, since if a long period of time is applied (e.g. 1 h), the density of water can vary again between the beginning of calibration (sample withdrawal) and the starting of the next cycle of measurement.

Contrarily, the instrument probably would not work efficiently in environments subjected to drastic variations in the SPM concentrations, ranging, for example, from a few milligrams per litre to a few grams per litre. This is because measurements at low SPM loads require high instrumental sensitivity, and consequently lead to a narrower measurement range; while a lower sensitivity and a wider measurement range is recommended for areas with high SPM concentrations. Therefore, a wide range of concentrations could not be measured in a set of consecutive measurements without sacrificing the instrument resolution. Both a high sensitivity and a broad range of measurements could be achieved by using two different balance plates (with distinct buoyancies) or set-up at different zero positions inside a bigger tube or two small tubes.

The instrument was tested in the field under slow current intensities (< 0.2 m s^{-1}) and calm to moderate wave regimes, i.e. heights varying from a few centimetres to 0.5–1.0 m. Under these environmental conditions, only minor oscillations (reading noise) were observed inside the tube (when properly sealed) possibility caused by the whole device vibration (high-

frequency oscillations) induced by the action of the waves and currents. SEDVEL application to more energetic environments would probably require a more robust frame and settling column in order to avoid tube vibration. A double-walled tube fitted with some insulating material could be used to both absorb and damp some high-frequency vibration and as thermal insulation. The thermal insulation is highly recommended for avoiding changes of the water temperature during calibration outside the water as well as during the underwater measurements.

The problem of circulation inside the tube when it did not seal properly was considerably improved by the adoption of a double one-way valve system. Most of the devices used to measure settling velocity *in situ* apply complex systems to close the settling column, such as lids, pivoting plates, sliding sheets, messenger activated valves/caps and vertical/horizontal tube displacement (see Chapter 2). Therefore, the use of one-way valves constituted a simple and efficient solution, especially if two sequential valves are employed (one for back-up). However, this system can eventually fail, especially in environments with high concentration of fragments of detritus and high SPM loads due to improper valve closure. It is advisable that all valves and settling tube are properly cleaned after each deployment to avoid the building up of a sediment crust at the tube entrances and exits doors. The use of bigger valves is also the recommended.

Another point to consider is that a turbulent condition is generated inside the tube as the pump sucks the water out through the top to replace the water sample, which keeps a homogeneous mixing inside the tube. This turbulent regime can cause some flocs' disruption. However, this effect if present is difficult to quantify. The use of one-way valves possibly helped minimizing floc/aggregate disruption during the sample withdrawal, since the water does not pass through the pump on its way in, only on its way out the tube (see Figure 3.21b). Therefore, the new water sample and particles "smoothly" enters the tube when the valves are opened (Figure 3.22a). Visual underwater observations revealed that the displacement of the one-way valves membranes from their opened to their closed position (Figure 3.22b), when the top pump stops (tube closing), is "gentle" and cause little turbulence. Nevertheless, turbulence generated in the settling columns due to the water movement in and out of the tube takes about 1–1.5 minutes to damp. After this interval of time, the balance plate returns to its horizontal position and the measurements can be properly done. This period is less than the amount of time needed to damp turbulence in other devices, for example: three minutes

for the cylindrical settling box after the doors' closure (Murray et al., 1996) and ten minutes after the closure of the lids for the ROST instrument (Zaneveld et al., 1982; Bartz et al., 1985).

Another source of error is related to a non-homogeneous distribution of sediment on the balance plate. Even though a homogeneous distribution of particles is achieved for sediment particles, if large detritus/floc settles on a location far away from the plate center of mass, it will cause an error in the overall sensor reading. It has been demonstrated in the section 3.4.4 that maximum errors are within ±20% interval for zero positions less than 1557 (arbitrary units). These errors could be minimized by using a less elongated pan. This is because the torque produced by a certain mass placed on the pan is proportional to the distance that it is from the pan support (suspension system). Therefore, a shorter pan would be subjected to a reduced torque. However, how a reduced torque and a smaller pan (with different immersed weight) would affect the balance sensitivity and the measurement range was not investigated. Changing the pan shape, while keeping the same pan weight, probably would not alter the balance sensitivity. Also, locating the small magnets attached to the pan right on its center of mass would eliminate some possible influence of a non-homogeneous distribution of the magnetized particles adhered to them.

One of the most critical problems associated with the actual SEDVEL configuration is the zero position (*ZP*) drifting among the different experimental cycles because this can lead to changing of the instrument sensitivity and involves a demanding calibration procedure. Reasons that cause the *ZP* to vary among experiments have been previously highlighted (Sections 3.5.3 and 3.6). As the balance plate works immersed, it would be very difficult to completely get rid of these variations. Reducing the balance plate volume, while keeping the same weight would reduce its buoyancy, and therefore, the balance would suffer less influence of medium density on its calibration. However, changing the balance plate buoyancy would also affect the balance sensitivity (see Section 3.5.2.2). In addition, a system that permitted the balance to be re-calibrated at the beginning of each cycle of measurement would considerable reduce the post-calibration effort and minimize the problem of the zero position drifting among the different cycles of measurement. The balance re-calibration could be done by using a feedback system within the controller (LC unit), which would move the big magnet a certain distance at the beginning of each cycle of measurement. This distance would correspond to the necessary increase/decrease in the repulsive force to balance the

immersed weight of the pan at the specific water density measured at the beginning of each cycle in order to keep the same *ZP* among the different cycles. In order to do this, relationships between (*i*) the distance between the two magnets and the immersed weight of the pan at different water densities for a particular zero position and (*ii*) the number of turns of the magnet motor and the total displacement of big magnet would need to be established in the laboratory. Therefore, if the water density was determined at the beginning of each experimental cycle *in situ* and automatically recorded, a feedback system within the LC could control the necessary number of turns of the magnet motor to bring it back to its original position, i.e. a constant *ZP* regardless the water density.

In addition, balance sensitivity varies with the adopted zero position (*ZP*); also balance resolution is higher for bigger masses until a saturation point is reached. This is because the DVRT resolution increases as the target gets closer to the sensor head (see Figure 3.13). The bigger the adopted sensitivity, the larger will be the measurement errors and the drift of the *ZP* associated with, for instance, a non-homogeneous distribution of particles on the pan and variations in water density. Even though a high balance resolution was achieved, a constant resolution should be sought for the whole range of measurement. This could be achieved if there was a distance sensor with the same resolution and characteristics of DVRT that presented a linear calibration. The displacement of the balance plate as a function of the accumulative mass can be approached to a linear equation as shown in Figure 3.7. The rational function fitted to the DVRT calibration represents a typical response of this kind of sensor. Alternatively, a balance calibration that related the number of turns of the magnet (or displacement distance) to the accumulative weight would also produce a calibration curve closer to linear (see Figure 3.6). However, within this instrument configuration the constant up and down movement of the pan could cause undesirable pan oscillations and the pan stabilization could take longer than required, considering that sedimentation is a continuous process. In this case, the challenge would be to find a motor speed rotation fast enough to balance the settled weight in a very small fraction of time, and slow enough avoid excessive pan oscillation and stabilization time. Also, as the balance sensitivity is not constant in the whole range of measurements, it is likely that the needed speed of rotation of the magnet would have to be changed as the weight on the pan increases.

The final balance sensitivity depends on a complex interaction of the following factors: (*i*) the relative force between the pair of magnets composing the balance magnetic spring

system, which is dependent on the distance they are set apart, (*ii*) the distance between the aluminium target (pan) and the DVRT sensor head, (*iii*) the balance plate mass (and buoyancy), and (*iv*) the torque exerted on the pan due to the suspension system. The effect of the torque (item *iv*) has not been investigated in the present work because it was assumed that its effect is small in relation to the other factors involved. A good reproducibility of measurements can be achieved if the instrument configuration (e.g. balance plate material and position, suspension system, zero starting position) is kept constant among the different cycles of measurement. Further research is needed to better understand the interactions among the factors listed above that can influence the balance resolution and calibration.

Bubbles introduced during the tube filling, before deployment, and improper instrument handling during lowering to the water level and lying down on the bottom are the two main reasons that renders unsuccessful deployments with the actual instrument configuration. However, if only a small amount of bubbles enters the settling column, they usually are eliminated after a few experimental cycles (2 to 3 cycles) and further measurements can still be performed. A careful procedure during tube filling and manoeuvring is highly recommended. A reduction of the whole apparatus weight would increase its portability and facilitate its displacement and adjustment at the moored position.

4. SEDVEL performance in the laboratory and *in situ*

4.1. Introduction

Settling velocity corresponds to the constant velocity at which a particle settles through a static fluid as soon as the resistance of the fluid exactly equals the downward force of gravity acting on the particle. The settling velocity depends on the particle density, shape, size, roundness and surface texture, and on the density and viscosity of the fluid (Krumbein and Pettijohn, 1938; Dietrich, 1982). For low concentration suspensions of cohesionless particles, not subjected to aggregation, the settling velocity of particles can be calculated by theoretically derived expressions, such as the well-known Stokes Law (Stokes, 1851). This equation describes the settling velocity (W_s, m s^{-1}) of small spheres (diameter < 0.1 mm) of uniform density settling in the viscous Reynolds number (Re) regime under constant temperature, i.e. $\text{Re} = W_s d / v < 1$ as:

$$W_s = \frac{\Delta g d^2}{18v},$$
(4.1)

where g is the gravitational field strength (m s^{-2}), d is the equivalent spherical diameter of particle (m), v is the kinematic viscosity of water (m^2 s^{-1}), $\Delta = \rho_e / \rho_w$ and $\rho_e = \rho_f - \rho_w$ is the effective density (excess density, differential density or density contrast), with ρ_f and ρ_w being, respectively, the bulk floc/sphere and fluid densities (kg m^{-3}) (Stokes, 1851; Krumbein and Pettijohn, 1938; Dyer, 1986).

Assumptions implicit within the Stokes Law are rarely met in nature, or even under laboratory conditions, since sediment particles and aggregates are seldom homogeneous in terms of grain size, shape and density. In addition, the flow field and fall speed are modified due to flow through porous flocs as well as around the flocs (Lick and Huang, 1993). Despite its limitations, the Stokes Law has been widely used to calculate W_s, d or ρ_e (e.g. Hill et al., 1998; Xia et al., 2004). Provided two of these parameters are known, the third can be

calculated, but rarely all these three parameters are measured on the same floc (Fennessy and Dyer, 1996).

The settling behavior of aggregates in coastal waters is very complex, depending on a large number of factors and on the interactions among them, such as: size, shape, roundness, texture, density and organic content of the flocs as well as the degree of aggregation (cohesiveness), inter-particle interactions, salinity, temperature, the properties of the ambient fluid (e.g. viscosity, density and shear), and especially the suspended particulate matter (SPM) concentration (Dietrich, 1982; Kranck, 1986; Hamm and Migniot, 1994; Syvitski and Hutton, 1996). Settling velocity of aggregates in coastal systems typically ranges from 10^{-4} to 10 mm s^{-1} for suspended particulate matter (SPM) concentrations of 10 to 1000 mg l^{-1} (Berlamont et al., 1993; Dyer et al., 1996).

A relationship between settling velocity (W_s) and concentration (C) of the form $W_s = kC^n$ has been established in *in situ* measurements for different estuaries and coastal systems. In this equation, k and n are empirical constants, and n usually ranges from 0.6 to 3.6 depending upon the particle/floc characteristics (Burt, 1986; Jones and Jago, 1996; Van Leussen 1996; Eisma et al., 1997; Agrawal and Pottsmith, 2000). The above equation applies to concentrations ranging from 10 to 10,000 mgl^{-1} (Van Leussen, 1988; Dyer et al., 1996; Eisma et al., 1997), although Mehta (1994) suggests that the inter-particle collision increases aggregation and leads to higher settling velocities at concentrations above 100−300 mg l^{-1}. At very low and very high concentrations, the above relationship does not work. For particles concentrations below 10 mg l^{-1}, Mikkelsen and Pejrup (2001) did not find a significant correlation between settling velocity and SPM concentration. At very high concentrations (i.e. 80–100 g l^{-1}), the settling velocity decreases with increasing concentration (hindered settling), because the flocs become so closely packed that they induce a flux of water upwards (dewatering process) (Mehta, 1994). In a such condition, settling velocity is described by $W_s = w_o[1 - k_2(C)]^\beta$, where k_2 is a coefficient that depends on sediment composition and $\beta = 5$ (Van Leussen, 1988).

Even though the relationship $W_s = kC^n$ applies to different environments in a broad range of concentrations, the absolute values of settling velocity for a given concentration can vary by an order of magnitude among them, since the k value changes as a function of SPM

characteristics (Burt, 1986). When W_s and concentrations are plotted in a logarithmic scale, straight lines are obtained, as shown in Figure 4.1.
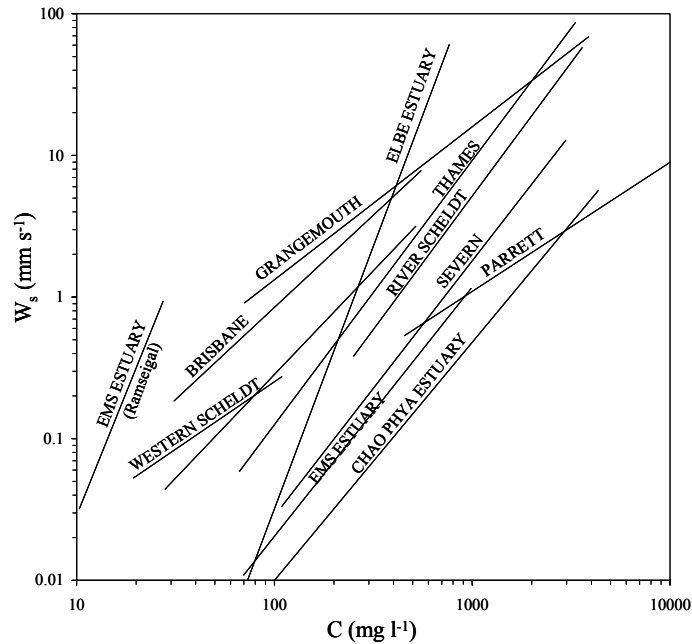
Figure 4.1: Relationship between the median settling velocity and concentration in different environments (extracted from Eisma et al., 1997, Figure 16, pg: 36).

However, there is a large variability in the slopes of these lines. This variability may result from variations in the density and organic content of flocs as well as differences in the turbulence regime during floc formation (Dyer, 1995). Moreover, this variability may partly result from differences in the instruments, field and analytical techniques used to compute settling velocities or disturbance of aggregates during sampling (Dyer at al., 1996; Pejrup and Edelvang, 1996; Ten Brinke, 1997).

The above demonstrated that suspended concentration is an important parameter conditioning settling velocities of the aggregates. For example, Pejrup and Edelvang (1996) have shown that the suspended concentration accounted for 82% of the variance in field settling velocities. Although SPM concentrations can explain a large amount of settling velocity variability, the relationship between these parameters is usually subjected to a great scatter (Burt, 1986; Pejrup, 1988; Dyer et al., 1996; Van Leussen, 1996). This shows that settling velocity behaviour cannot be described by single parameter relationships, since a large number of factors are involved.

Very often simultaneous measurements of settling velocity and aggregate size are performed, and these are used to estimate other aggregate properties, such as their excess density, volume and mass. While a positive relationship between settling velocity and aggregate size has been established in many studies (Fennessy et al., 1994; Fennessy and Dyer, 1996; Sternberg et al., 1996; Van Leuseen and Cornelisse, 1996; Mikkelsen and Pejrup, 2001; Voulgaris and Meyers, 2004), these data also exhibited a large scatter. Conversely, Van der Lee (2000) did not find a clear correlation between settling velocity and floc size due to the large scatter in the data, which was attributed to differences in the floc density for similar particle sizes. Most of the studies have demonstrated a reduction in the floc density (and excess density) as their size increases, even though large deviations in the data usually occurs (Gibbs, 1985; Fennessy et al., 1994; Mikkelsen and Pejrup, 2001).

In marine and estuarine systems aggregate size and settling velocitiy vary over short-term, tidal and seasonal time scales due to the continuous aggregation and disaggregation of particles, conditioned by changes in the turbulence level in the water column, deposition and resuspension intensities (Eisma and Li, 1993; Ten Brinke, 1994; Chen et al., 1994; Van Leussen and Cornelisse, 1993b; Mikkelsen and Pejrup, 2001). In addition, the presence of large settling particles, such as organic macroscopic aggregates (composed by plankton, detritus and fine inorganic particles) and fecal pellets produced by filter-feeders organisms (*e.g.* copepods, mussels, cockles) has been claimed as an important mechanism for sediment removal from water column (Van Leussen, 1988; Ayukai and Wolanski, 1997). For example, Widdows *et al.* (1998) established that biodeposition rates for sites with high density of cockle suspension-feeders (ca. 6.61 g m^{-2} h^{-1}) were an order of magnitude higher than the natural sedimentation (ca. 0.66 g m^{-2} h^{-1}). Furthermore, aggregates are formed by organic and inorganic matter glued together by organic polymers released by algae and bacteria. As a result of this process of aggregation, aggregate strength varies in time because the organic part of the suspended matter varies in time (Ten Brinke, 1997). Therefore, the role of organisms gluing particles together and changing the deposition process can be very large (Eisma, 1986). The importance of the biological component in the floc formation and deposition adds to other sources of variability in the settling velocity measurements.

In conclusion, the *in situ* fall velocity of cohesive particles cannot be calculated by using theoretical expressions, since the aggregation modifies the settling behaviour, and also because the interaction among particles/flocs at high concentrations alters the flow resistance.

Therefore, settling velocities of aggregates must be measured in field. Although great effort has been expended in finding simple relationships for describing settling velocity of aggregates, the settling behaviour is complex. It is usually explained by a combination of factors that change both spatially and temporally in coastal systems. Generalizations are also complicated because of the large range of instrumentation and methodologies applied, which demand careful comparisons between different studies. Simultaneous measurements of the characteristics of different aggregates (e.g., W_s, size, density, mass, organic content), and their reduction to inter-comparable quantities (despite methodological approaches), are still required in order to better understand the dynamics of cohesive aggregates. In addition, the density of settling flocs is usually indirectly calculated in order to obtain the settling mass flux, which demands the knowledge of the spectral distribution of floc mass (Fennessy and Dyer, 1996). Settling tubes represent the only apparatus able to directely measure the mass distribution of flocs with different settling velocities.

In this chapter, it is demonstrated that SEDVEL can measure automatically and *in situ* masses of suspended particulate matter (SPM). Based on these measurements, the mass distribution of aggregates settling velocities can be derived. In addition, techniques to transform the effective immersed mass obtained from SEDVEL measurements into estimates of dry-concentrations and settling velocities of SPM are presented. An alternative approach is proposed to obtain aggregate density based on its organic content. Further, the Odén theory of sedimentation, often used in the analysis of the results of settling tubes, was applied to convert the accumulative masses obtained from the SEDVEL measurements into a frequency distribution of concentrations in each settling class. Subsequently, the results from the test of SEDVEL performance in measuring SPM concentrations and settling velocities in the laboratory and *in situ* are presented and discussed.

4.2. Theory

4.2.1. Deposition of cohesive sediments

In the absence of continuing aggregation and under steady or quasi-steady turbulent flow, the rate of deposition per unit of area of cohesive sediments (*D*) is expressed as:

$$D = \frac{dC}{dt}h = \frac{dm}{A\,dt} = -pW_s\overline{C}, \tag{4.2}$$

where m is the mass, A is the area of deposition, t is time, $p[0,1]=1-\tau_b/\tau_{cd}$ is the probability of deposition, τ_b is the bed shear stress, τ_{cd} is the critical shear stress for deposition, W_s is the settling velocity and $\overline{C}$ is the uniform or depth-averaged SPM concentration over the water depth h through which the particles settle (Krone, 1993; Mehta, 1988, 1994).

The SPM is composed of distinctive sizes and kinds of sediment particles or aggregates and possesses a continuous distribution of settling velocities, being sorted during the deposition process (Van Leussen, 1996). Therefore, the total deposition rate corresponds to a sum of the depositions in each individual class i, given by:

$$D = \sum_{i=1}^{N} W_{si}C_i p_i , \tag{4.3}$$

where W_{si} is the settling velocity of the settling class i, N is the maximum number of classes considered, C_i is the concentration of class i near the bed, and p_i is the probability that once the particle of class i has reached the bed, it will remain there (Mehta, 1988).

4.2.2. Odén theory of sedimentation applied to the analysis of settling tubes results

The theory of sedimentation of polydisperse systems, i.e. various particles sizes, was established by Odén in 1915. This theory relies on several assumptions, namely: (*i*) that the particles are uniformly distributed through the liquid; (*ii*) the radii of successive groups of size differ by infinitesimal amounts; (*iii*) that particles do not interfere with each other during descent; and (*iv*) the temperature of the system remains constant (Krumbein and Pettijohn, 1938; Subcommittee on Sedimentation, 1953).

Now consider a settling tube filled up with a homogeneously dispersed mixture of water and particles of various size fractions (polydisperse suspension). After the sedimentation has begun, the accumulation of particles at the bottom of a column of height h at any time t consists of particles with settling velocities high enough to fall the entire column and also of

smaller particles, which had a shorter distance to fall. Therefore, the total amount of material (mass) settled on the bottom at each instant of time (M(t)) comprises of two fractions: (*i*) the size class fractions which have completely settled out the suspension with $W_s > h/t$, plus (*ii*) some part of the size fractions composed of smaller particles which have partially settled, which have $W_s < h/t$ (Subcommittee on Sedimentation, 1953; Krumbein and Pettijohn, 1938). A simple explanation of Odén's theory of sedimentation of polydisperse systems using graphic analysis of Odén curves as well as its mathematical validation can be found in Krumbein and Pettijohn (1938). The concepts of the graphic analysis of Odén curves and the computation of the frequency distribution of settling velocity, presented by these authors and in the Subcommittee on Sedimentation (1943, 1953), are summarized below.

A curve can be plotted relating the mass of material settled out to the bottom of the tube (M(t)) with time (t) (the Odén Curve) as shown in the Figure 4.2a. The derivative of the M(t) curve at any point corresponds to its slope at that point (i.e. tan α), and represents the rate of deposition during a time interval (i.e. *dM*/*dt*). Based on the schematic picture presented on Figure 4.2a, the tangent at the point A can be written as:

$$\tan\alpha = AC/BC ,\qquad\qquad(4.4)$$

where *AC* corresponds to the fraction partially settled in a particular time *t* and *BC* represents the time of sedimentation (*t*). Replacing $\tan\alpha$ by *dM* / *dt* in the Equation 4.4 and setting *BC* to *t* results in:

$$t\,\frac{dM(t)}{dt} = AC = BD .\qquad\qquad(4.5)$$

Therefore, as shown in Figure 4.2a, the total mass deposited in a particular time *t* (M(t)) corresponds to the distance *OD*. The portion of particles that has partially settled out (M$_{PS}$(t)) is equal to the distance *BD* = *AC*, and consequently, the portion that has completely settled out the suspension at the time *t* (M$_{CS}$(t)) is given by the distance *OB*. The value *OB* corresponds to the distance between the origin and the point where a particular tangent line intercepts the *y*-axis. Thus, if tangents are drawn to the curve at any two points corresponding to the times t_1 and t_2, the difference between the corresponding masses given by OB_2 and OB_1 represents the amount of material (i.e. mass) in settling velocity class with limits determined

by the settling times t_1 and t_2 (Figure 4.2b). If settling intervals are chosen corresponding to the settling velocities of a particular size range, the histogram of frequency for each size or settling velocity class can thereby be established, as represented by Figure 4.2b.
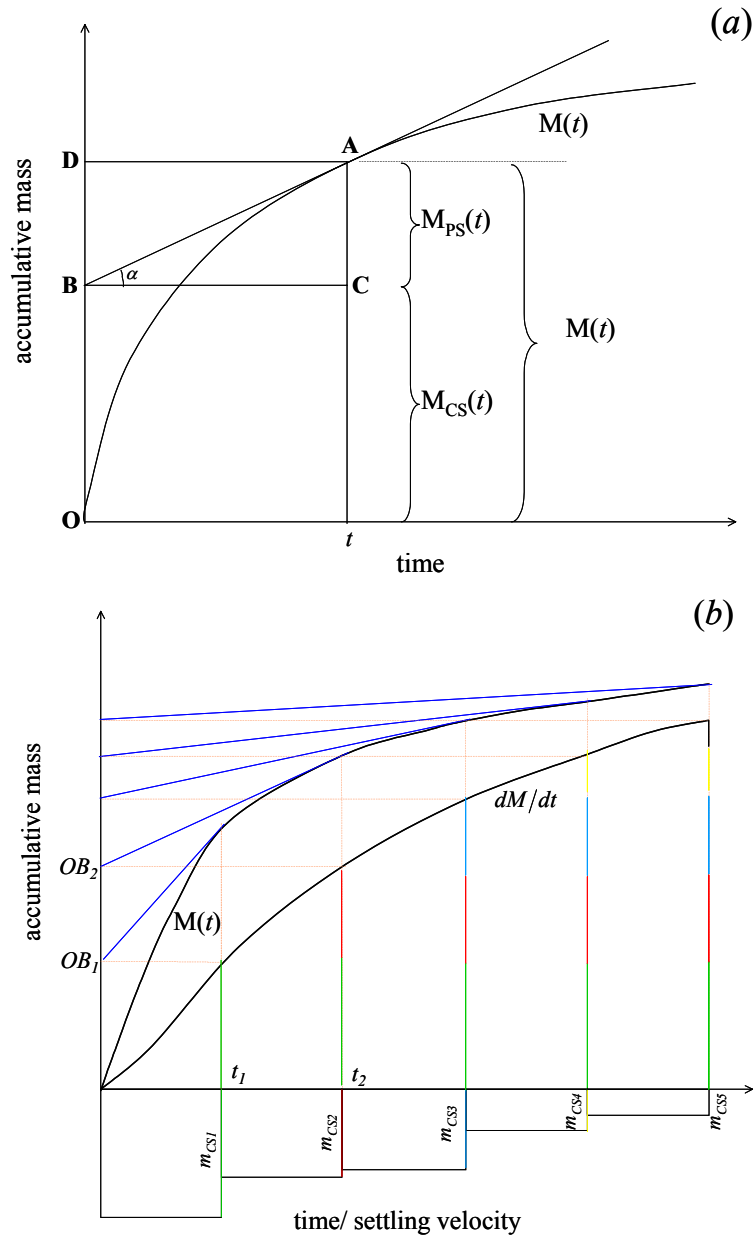
Figure 4.2: (*a*) Schematic representation of the Odén curve graphic method of obtaining the partially settled mass fraction ($M_{PS}(t)$) and the completely settled mass fraction ($M_{CS}(t)$), and (*b*) the method of obtaining the *OB* segments and the mass completely settled in each size or settling velocity fraction (i.e. m_{CS1}, m_{CS2}...m_{CS5}). Based on these masses, the frequency histogram can be established (as drawn under the graphic).

4.3. SEDVEL data analysis

Figure 4.3 shows a raw SEDVEL output for one cycle of measurement (60 minutes) that is used to exemplify the procedure used in the SEDVEL data analysis. Following the water replacement carried out at the beginning of each cycle of measurement, turbulent activity ceases around three to four readings (about 1 to 1.5 minutes) after the top pump has stopped. Then, sediment gradually accumulates on the plate, reaching approximately stable values at the end of each cycle of measurement (Figure 4.3).
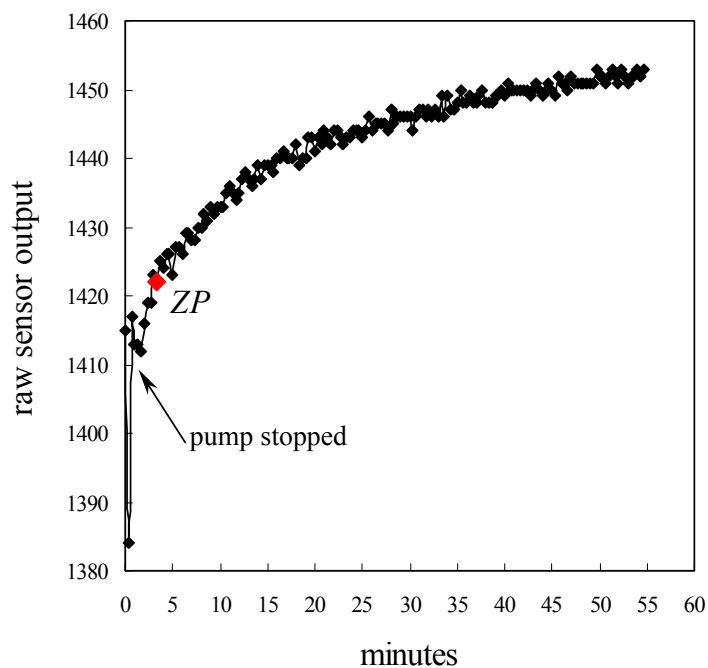
Figure 4.3: Variation of the raw sensor output with time during a cycle of measurement. The moment that the all pumps have stopped and the chosen zero position (*ZP*) are indicated in the graphic. Data collected at Strand Beach on 21/09/04.

The first step of the data analysis is to choose the zero starting position. This process is to some extent subjective, but usually the first three or four recorded values are discarded, when the balance plate is not completely still. The sensor reading registered after this period is assumed as the starting zero position (*ZP*) (as shown in Figure 4.3). The raw sensor output (S_R) is converted into effective immersed mass (M_{EI}), using one curve of the family of calibration curves (see Section 3.5.2.1). The calibration curve is selected based on the adopted zero position and on the water density measured at the beginning of the cycle of measurement.

If there was no calibration curve with the required ZP in the family of calibration curves, two closer curves with higher ZP_H and lower ZP_L zero positions than the sought ZP value were used. Considering equal intervals of mass, the outputs of the higher (ZP_{HO}) and lower (ZP_{LO}) curves were interpolated via a weighed average, with the weighing factor being given by $f_{ZP} = (ZP - ZP_L)/(ZP_H - ZP_L)$, with ZP, ZP_H, ZP_L being the sought, high and low zero position values, respectively. The calculated values of output were applied to the same mass interval and used to draw a new calibration curve starting at the sought zero position (ZP). These new values corresponded to $ZP_O = (1 - f_{ZP}) \cdot ZP_{LO} + f_{ZP} \cdot ZP_{HO}$, where ZP_O, ZP_{LO} and ZP_{HO} represents the outputs for the curves starting at sought, low and high zero positions. These values were used to fit a new calibration curve for the sought zero position (ZP). An example of the two original curves and the interpolated curve is shown in Figure 4.4.
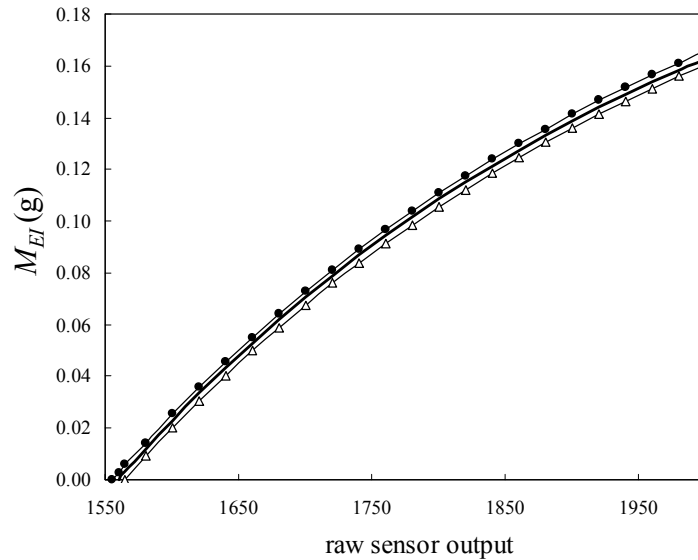
Figure 4.4: An example of interpolation of two calibration curves to get a new curve starting at the sought zero position (ZP_O, solid line). The ZP_{HO} and ZP_{LO} are represented by black circles and white triangles, respectively.

After the calibration curve has been applied to the raw sensor readings and the values of effective immersed masses (M_{EI}) obtained at the different instants of times (t), a curve is fitted to the calculated M_{EI} points. A MMF (Morgan and Mercer model; Hyams, 2001) model was adjusted to the observed data and forced to pass through the origin, as shown in Figure 4.5. The exponential model, described by $y = a \cdot (b - \exp(-cx))$, was also applied to a few cycles, since it produced a better fitting. Curves fitted to the data sampled at the different cycles of measurement had $r^2 > 0.9$, excepting five cycles where $0.53 < r^2 < 0.85$. The adjusted curves represent the mass accumulation of particles settled on the balance plate as a

function of time. The values estimated by these models at the different instants of time were used in the calculations of dry-masses and settling velocities of SPM, as described below.
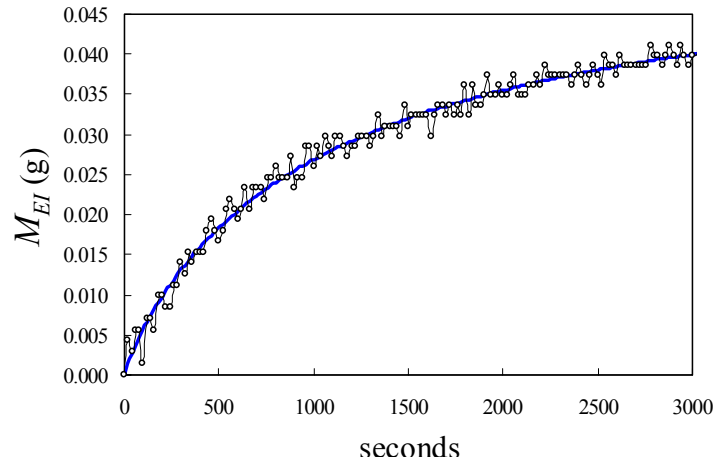
Figure 4.5: Variation in the effective immersed masses (M_{EI}, g) as a function of sedimentation time (open circle) and the adjusted MMF model to the measured values (blue line). The adjusted model corresponds to $y = (a \cdot b + c \cdot x^d)/(b + x^d)$, and $r^2 = 0.99$.

4.3.1. Calculations of dry-mass and concentration of particulate matter (PM) from SEDVEL measurements

The dry weight of particulate matter (P_{PM}) is equal to the immersed weight of particulate matter (P_I) plus its buoyancy ($B = \rho_w V_w g$):

$$P_{PM} = P_I + B, \tag{4.6}$$

which can be written as:

$$M_{PM} g = M_{EI} g + \rho_w V_w g, \tag{4.7}$$

where M_{PM}, M_{EI}, ρ_w, V_w and g are the dry mass of particulate matter (*PM*), the effective immersed mass of *PM*, water density, the volume of water displaced by the particles and gravitational field strength, respectively. Even though the total mass is the same whatever the material is immersed or not, the effective immersed mass (M_{EI}) was used for the SEDVEL calibration since it allows relating the instrument output to mass regardless the kind of

material (i.e. its density). Based on the M_{EI}, the density of *PM* and its dry-mass can be estimated (see Sections 4.3.1 and 4.3.2).

Adopting $V_w = V_{PM} = M_{PM} / \rho_{PM}$, the dry-mass of particulate matter (M_{PM}) corresponds to:

$$M_{PM} = M_{EI} / (1 - \rho_w / \rho_{PM}) = M_{EI} / f , \qquad (4.8)$$

where V_{PM} is the volume of particles/flocs and ρ_{PM} is the dry density of *PM*. The factor ($f = 1 - \rho_W / \rho_{PM}$) was calculated by taking into account the estimated *PM* densities (see Section 4.3.2) and water densities for each experimental cycle.

The 'dry concentration' of particulate matter ($C_{(PM)_{dry}}$, mg l^{-1}) of the water samples confined inside the tube were calculated by:

$$C_{(PM)_{dry}} = M_{PM} / V , \qquad (4.9)$$

V is the volume of the parcel of water above the balance plate, i.e., the plate area (0.0071 m^2) multiplied by the tube height (0.321 m). Applying M_{EI} to the above equation, the 'wet concentrations' of *PM* ($C_{(PM)_{wet}}$, mg l^{-1}) can be calculated.

4.3.2. Aggregate density estimate

Densities of the particulate matter (*PM*) were determined by the following procedure: a large container (i.e. 30 l) was filled with a water sample taken in the environment and kept still, allowing the SPM to settle on the bottom (i.e. *PM*). Four subsamples were withdrawn with a syringe from the material deposited on the bottom. Effective immersed masses of each sub-sample were obtained by using a high precision analytical balance (0.0001 g) equipped with a standard built-in underhook. A balance plate was hung on the hook and worked immersed in a container filled with filtered salt water. A Petri dish was placed on the balance plate and the system recalibrated, after which the *PM* sample was gently delivered with a syringe onto the Petri dish and its effective immersed mass recorded (hydrostatic weighing). After, the Petri dish was carefully removed, the sample was washed with distilled water in a pre-weighed

filter (fibreglass, Whatman, GF/F) that was used to quantify the dry-mass and organic content of *PM*. Water salinity and temperature were measured for density calculations. Organic matter content was quantified by weighing the fibreglass filters (plus SPM) before and after their combustion for 3 hours at 550°C. The *PM* volume of each sub-sample was calculated as the difference between the dry and immersed weights divided by the water density. The dry density of *PM* (ρ_{PM}) was estimated by dividing the dry-mass of *PM* by its volume, similar results are obtained if the Equation 4.7 is applied. The organic matter content (*OM*) was calculated by dividing the mass of organic matter by the dry mass of *PM* (*OM* = M_{OM}/M_{PM}).

An exponential decay of sediment densities with organic matter content has been established (Mann and Wetzel, 2000; Wüst, 2001). A sigmoidal model was adjusted to relate M_{OM}/M_{PM} ratio and *PM* density as depicted in Figure 4.6. Before fitting a curve to the data, upper and lower limits of 2.6 g cm^{-3} and 0.8 g cm^{-3} were assumed for M_{OM}/M_{PM} equal to 0 and 1, respectively. The upper limit corresponds to the minerals' dry density, and the lower limit was based on measurements of the dry density of sediment with different organic contents presented in Wüst (2001; see Figure 4.15). The final *PM* density estimates vary less than 10% for *OM* < 0.4 if a density of 1.03 g cm^{-3} is used as organic dry density, as proposed by Fennessy et al. (1997). In the SEDVEL data analysis, densities of *PM* (ρ_{PM}) for each cycle of measurement were estimated, based on the measured organic matter content by applying the following equation ($r^2 = 0.99$):

$$\rho_{PM} = 0.67 /(1 - 0.74 \cdot e^{(-1.59 \cdot OM)}) . \qquad (4.10)$$
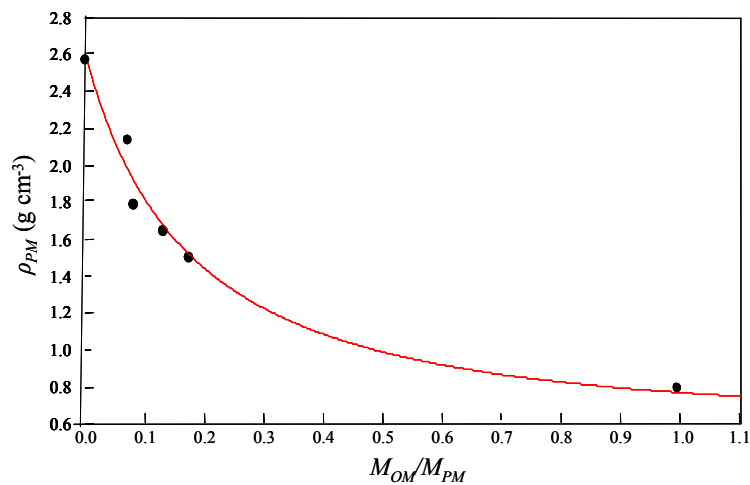
Figure 4.6: Relationship between *PM* density and the organic matter content (*OM*) expressed by M_{OM}/M_{PM} ratio (1.0 = 100 wt-%).

4.3.3. Calculations of deposition rates and settling velocities from SEDVEL measurements

The values corresponding to the total mass derivative ($d\,M/dt$), the partially settled fraction ($M_{PS}(t)$) and the completely settled fraction ($M_{CS}(t)$) were calculated for each time interval in order to obtain the frequency distribution of concentration or mass for each settling class considered. The derivative of the total mass in each instant of time ($d\,M_i/dt$) was estimated by the derivative of the MMF curve, adjusted to the measured points represented in Figure 4.5, as following:

$$dM_i/dt = [t_i^{(d-1)} \cdot bd(c-a)]/[(b+t_i^{d})^2],\qquad(4.11)$$

or by the derivative of the exponential model:

$$dM_i/dt = a\,c \cdot \exp(-c\,t_i),\qquad(4.12)$$

where t is the instant of time and a, b, c and d are the model constants calculated for each cycle of measurement. Then, the partially settled mass M_{PS_i} at each instant of time t_i is given by:

$$M_{PS_i} = \frac{dM_i}{dt}\cdot t_i\,.\qquad(4.13)$$

As shown in the Figure 4.2, the completely settled fraction in each instant of time (M_{CS_i}, equivalent to the OB_i distance) can be calculated by:

$$M_{CS_i} = M_i - M_{PS_i}\,.\qquad(4.14)$$

The index i represents the different instants of time, and the classes of settling velocity were determined by two consecutive instants of time. The first instant of time t_1 was fixed at 20 s, which corresponds to the minimum instrumental sampling rate. As demonstrated in Figure 4.2b, the mass in each settling class (m_i), defined by the interval of time between t_i and t_{i-1},

can be obtained by subtracting successive values of the accumulative curve of mass representing the completely settled material at each instant of time (M_{CS_i}, the OB_i distance):

$$m_i = M_{CS_i} - M_{CS_{i-1}}, \tag{4.15}$$

with $i = 1, 2 \ldots n$.

The concentration of *PM* (C_i) in each class i is given by the mass within that class (m_i) divided by the volume of the water parcel above the pan ($V = 2.3$ l):

$$C_i = \frac{m_i}{V}. \tag{4.16}$$

The settling velocity in each class i (W_{S_i}) is obtained by dividing the settling distance ($h = 32.1$ cm) by time at each instant of time t_i:

$$W_{S_i} = h / t_i. \tag{4.17}$$

This means that at the instant t_i all particles with settling velocity W_{S_i} or higher have reached the bottom. At the instant t_{i+1} all particles with settling velocity smaller than W_{S_i} and bigger or equal to $W_{S_{i+1}}$ have certainly reached the bottom of the settling tube, and so on.

A frequency histogram in percentage was obtained for each cycle, relating the percentage of the total concentration ($C = \sum_{i=1}^{n} C_i$) present in each settling velocity class interval (i.e. $C_i / C \cdot 100$). Note that percentage of total concentration is equivalent to the percentage of total mass. A time interval of 5 s was adopted in order to calculate the histogram of concentration/mass versus W_s. All settling velocity and concentration calculations were based on the effective immersed masses in order to avoid the errors accumulating due to the conversion to dry masses and concentrations. The frequency distribution would not change if the dry-mass values were considered. At the end of each experiment, deposition rates represent the maximum sedimentation achieved in quiescent conditions inside the tube, when

almost no *PM* is left in suspension. They do not represent actual deposition rates in the environment, which are dependent upon the shear stress in the water column.

A single value of settling velocity for each cycle of measurement was obtained by calculating the concentration-weighed settling velocity ($\langle W_S \rangle$, mm s^{-1}) as:

$$\langle W_S \rangle = \frac{\sum_{i=1}^{n} C_i W_{si}}{\sum_{i=1}^{n} C_i} , \qquad (4.18)$$

where C_i is the mass concentration of the class i and W_{si} is the settling velocity of the class i, with $i = 1,2,...n$ (Zaneveld et al., 1982; Van Leussen, 1996).

4.4. Laboratory experiments

4.4.1. Experiments set-up

A few experiments were run in the laboratory to test the SEDVEL performance. In these experiments, the settling behaviour under quiescent conditions of sediment particles and glass beads spheres was analysed for diverse initial concentrations (as summarized in Table 4.1).

Table 4.1. Resume of experimental conditions, including the average temperature and salinity, kind of particle used and the initial concentration (*IC*, mg l^{-1}).

	temperature (°C)	salinity	particles (type)	IC (mg l^{-1})
Series *A*				
A3	24.2	0	sediment	11
A4	24.8	0	sediment	26
A5	24.3	0	sediment	51
A6	24.8	0	sediment	102
A7	24.6	0	sediment	204
Series *S*				
S1	25.4	35.9	sediment	7
S3	24.7	35.9	sediment	27
S4	25.5	36.0	sediment	50
S5	25.7	36.0	sediment	102
S6	25.6	35.9	sediment	204
Series *GB*				
GB3	24.3	36.1	glass beads	54
GB4	25.0	36.1	glass beads	106
GB5	24.7	36.1	glass beads	205

In the laboratory configuration, the inlets of the SEDVEL settling tube, located at its bottom, were closed and all pumps removed. The settling tube was opened at its top for the sample introduction (Figure 4.7).
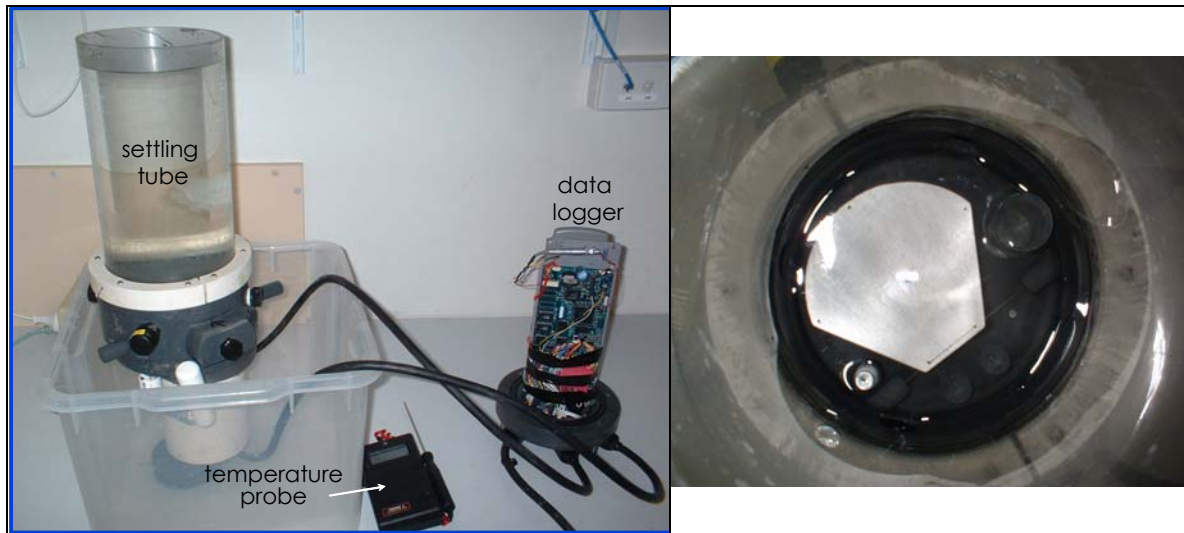
Figure 4.7: (*a*) Schematic representation of SEDVEL settling tube set-up for the laboratory experiments (*b*) photo of the balance plate covered by a thin layer of sediment. Three vials glued to the tube bottom are also shown.

At the beginning of each experiment, the tube was filled to a set level (settling height = 31.2 cm) with water free of particles and of a known salinity. Experiments were performed both in saltwater (salinity of 36.1±0.2) and freshwater (salinity zero) (Table 4.1). Water temperature and salinity were measured at the beginning and at the end of the experiments using a temperature (Therma2, E.T.I Ltda) and a conductivity meter (Model 130, ATI-Orion) probes. Water temperature was kept as constant as possible, but variations between 0.3 and 1.5°C were observed during the experiments, especially if a long period of sedimentation (e.g. above 3 h) was considered. As these variations were high enough to interfere with the instrument response, just the first hour of sedimentation was considered for the settling velocity and masses calculations. The exception was the experiments with very fine glass beads for which a longer settling period was used (i.e. 12 h).

Sediment used in the experiments was collected in Cleveland Bay close to the Townsville Harbour. The bottom sediment was dried, disaggregated and sieved. The fraction that passed through the 63 μm mesh was used in the experiments of series *A* and *S*, while glass beads with nominal diameter less than 10 μm were used in the series *GB* experiments (Table 4.1).

Subsamples of sediment and glass beads used in the experiments were analysed in the laboratory through a laser particle sizer (Malvern Mastersizer) for a size range between 0.5 and 600 μm (300 mm lens). This instrument relies on the laser diffraction technique to measure particle size distribution per unit of volume concentration (Rawle, 2005). Each subsample was run with and without applying the ultrasonic treatment (20 seconds of sonification) for comparison of the resultant size distribution by percent of volume. During the laser particle sizer analysis, either with or without ultrasonic treatment, samples were kept under vigorous mixing (stirring paddles) in the chamber where the sample is placed to perform the size analysis.

A constant percentage of organic matter (i.e. $OM = 6.5\%$) was adopted for all experiments using sediment. This organic matter content corresponded to an average of the values of OM obtained for three subsamples extract from the same lot of sediment used in all experiments. The organic matter fraction was quantified by combusting the sediment samples for 3 h at 550ºC. Organic matter percentage is an input to Equation 4.10 used to estimate the sediment density and convert effective immersed mass into dry mass (see Sections 4.3.2 and 4.3.3). A density of 2.6 g cm^{-3} was employed for the glass beads that consisted of purely inorganic particles. No defloculants were used in the experiments.

Before starting each experiment, the zero position was set-up within the 1490 to 1500 interval. A pre-weighed amount of sediment was then spread on the top of a thin PVC sheet and lowered into the water. The sediment was mixed through the water column by moving a spatula in a zigzag motion, avoiding water spinning that could result in a non-homogeneous distribution. Visual observations showed a well-distributed layer of particles on the pan (Figure 4.7b). The pan was kept in vertical position during mixing, being quickly lowered back to the horizontal position afterwards. After the turbulence inside the tube had been damped, the settling behaviour of sediment was monitored for at least 2 h. The initial concentration (IC) used in each experiment was calculated by dividing the total amount of material introduced in the tube by the volume of water used in each experiment. The IC values are summarized in the Table 4.1.

Three small vials were glued to the base of the tube in order to collect the settled material. These vials were carefully retrieved at the end of each experiment. The excess of water inside them was extracted with a syringe, and the collected particulate material was oven dried at

60°C. The net weight of the settled material inside each vial was divided by the vial opening area, and expressed in g cm^{-2}. This was compared with the estimated dry-mass of particulate material per unit of the pan area (also in g cm^{-2}) obtained from SEDVEL measurements. This comparison was only performed for the Series *A* (freshwater experiments). The material collected in the vials in the saltwater experiments also included a portion of dried salt. Attempts to correct the mass of salt showed that these measurements were subjected to a large error, and therefore they were not considered.

For each experiment, variations of SEDVEL output with time was analysed, as described in the Section 4.3, in order to estimate the effective immersed and dry masses of *PM* as well as to compute the concentration/mass frequency distribution of settling velocity.

4.4.2. Experiments results

It was observed in all experiments that both sediments and especially the very fine glass beads flocculated when introduced in the water. Figures 4.8a and b show the size distribution of natural sediment and glass beads with and without sonification, respectively. It can be observed that coarse fractions were substantially reduced after sonification, especially for the glass beads particles. The mean diameter of the particles of sediment dropped from 32.3 to 20.3 μm after sonification, and the main mode shifted from 44 to 15 μm. The sediment used in the experiments consisted mostly of silt and clay. The clay fraction increased from 10 to 19% after the ultrasonic treatment, while the silt fraction dropped from 81 to 76%. A tri-modal size distribution (modes at 7, 72 and 269 μm) was observed for the glass beads before the ultrasonic treatment. After sonification, the large flocs (between 100 and 500 μm) broke up resulting in only one mode at 7 μm, and the mean size dropped from 57.7 to 15.7 μm.

This shows that some large flocs resist the vigorous mixing applied during the size analysis in the laser particle sizer, being only broken by the ultrasonic treatment. The manual mixing applied to the suspended particles at the beginning of each experiment was less vigorous than that applied in the size analysis, and therefore it is expected that a number of flocs coarser than the primary particle size were present in all experiments. Moreover, it is also likely that a fraction of the coarse material that settled quickly to the bottom of the tube as soon as the sample was introduced, and it was not further resuspended by mixing. In addition, some large

material could have settled during the first 5−10 seconds needed to place the balance plate back to its horizontal position.
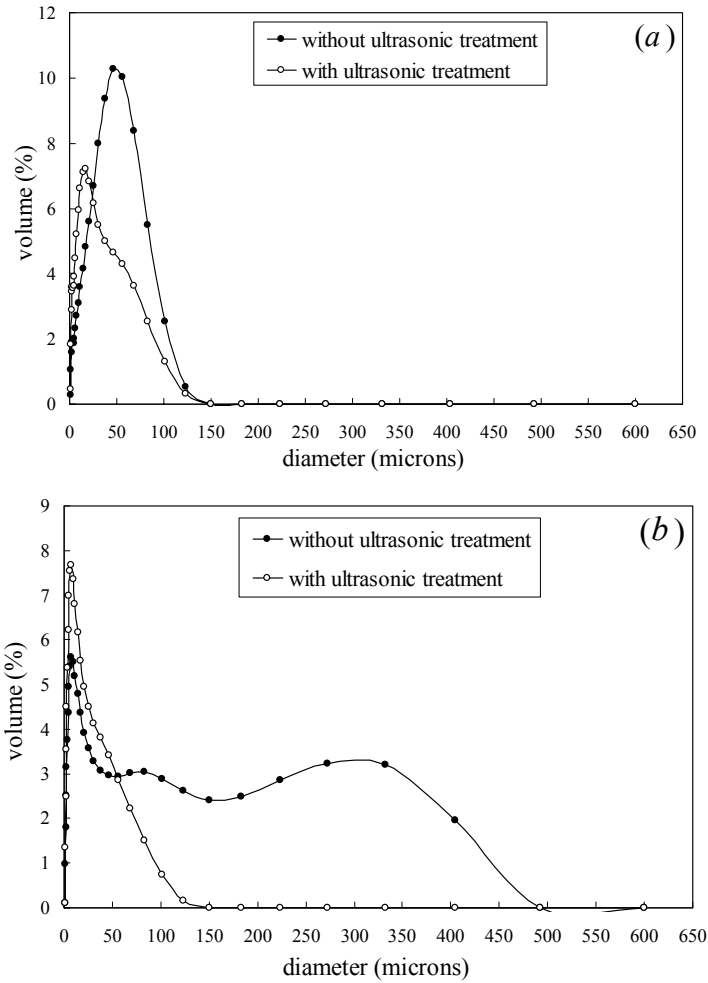
Figure 4.8: Grain size distribution expressed as percent of the volume concentration analysed in the laser particle sizer (Malvern Mastersizer) of (*a*) the natural sediment collected at the Townsville Harbour and (*b*) glass beads particles.

Therefore, the given initial concentration of particles for each experiment (*IC*, Table 4.1) represents a reference concentration, and the actual mass of the particulate material settled on the pan is expected to be smaller than *IC*. Even though *IC* values are not an exact representation of the amount of material settled on the pan, they were compared with the maximum dry concentrations estimated for each experiment. The *IC* values were considered more reliable than the estimates obtained from the weighing of the material collected inside the vials in the saltwater experiments. The reduced size of the vials and of the amount of material trapped inside them, as well as inaccuracies inherent in the measurements of small volumes of water left to dry in each vial, led to errors in the estimate of the mass of salt that

should be subtracted from the total mass in each vial to furnish the mass of *PM*. However, for the experiment of Series *A* run in freshwater, a comparison between the estimated dry mass per unit of area settled on the balance plate and the mean dry-mass per unit of area collected in the 3 replicates vials yielded good results and it is subsequently presented.

The relationship between the calculated dry-concentration, based on the maximum estimated dry-mass settled on the SEDVEL pan at the end of each experiment, and the initial concentration (*IC*) is presented in Figure 4.9. The linear regression fitted between these two parameters (r^2 = 0.90, *p* < 0.01) is also shown. In general, SEDVEL measurements overestimated the *IC* at low concentrations (less than 50 mg l^{-1}) and underestimated the *IC* at high concentrations (50 < *IC* < 200 mg l^{-1}) (Table 4.2). At very low concentrations (less than 10 mg l^{-1}), ratios between the SEDVEL estimates and the *IC* ranged between 1.7 and 2.2. This overestimation can be related to the lower instrument sensitivity at low concentrations. Also, the observed temperature oscillations during the experiments could change the pan position; these changes will represent a relatively bigger error when small masses have been measured then would be expected for large masses.
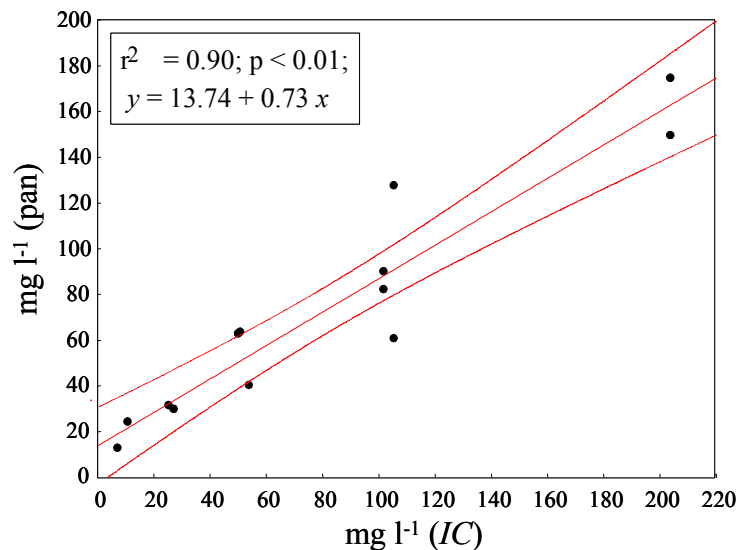
Figure 4.9: Relationship between the estimated dry-concentration of *PM* based on the maximum masses measured on the pan and the initial reference concentration (*IC*). The adjusted equation, r^2 and *p* values are given in the inset.

Conversely, the largest underestimation occurred for the Series *GB* experiments (Table 4.2). Based on the size distribution presented in Figure 4.8b, the percentage of glass beads flocs bigger than 100 μm added to 21% of the total for the flocculated sample (no ultrasonic

treatment applied). Based on The Stokes Law, glass spheres of 100 and 400 μm can reach the tube bottom in 31 and 4.5 seconds, respectively. Therefore, some of the largest flocs could have settled to the tube bottom while lowering the balance plate to its horizontal position. This can represent a significant part of the material, which was not accounted into the pan measurements.

Table 4.2: Resume of the water density, initial dry-concentration (*IC*), dry concentration estimated from SEDVEL measurements (pan), the ratio between these two dry concentrations (pan/*IC*), wet concentrations calculated based on the measured effective immersed masses, and the averaged settling velocity ($\langle W_S \rangle$, see Equation 4.18) calculated using time intervals of 20 ($\Delta t = 20$ s) and 5 s ($\Delta t = 5$ s) and the ratio between them, i.e. $\langle W_S \rangle_{(5s)} / \langle W_S \rangle_{(20s)}$.

experiment	density kg m^{-3}	dry concentration *IC* (mg l^{-1})	dry concentration pan (mg l^{-1})	ratio pan/IC	wet concentration mg l^{-1}	$\langle W_S \rangle$ $\Delta t = 20$ s (mm s^{-1})	$\langle W_S \rangle$ $\Delta t = 5$ s (mm s^{-1})	Ratio $\langle W_S \rangle_{(5s)} / \langle W_S \rangle_{(20s)}$
A3	997.25	10.93	24.05	2.20	12.93	1.86	1.97	1.06
A4	997.10	25.50	31.15	1.22	16.75	2.01	2.14	1.06
A5	997.22	50.99	63.29	1.24	34.04	2.46	2.65	1.08
A6	997.10	101.98	89.69	0.88	48.24	2.39	2.57	1.08
A7	997.16	203.96	149.41	0.73	80.35	2.24	2.43	1.08
S1	1023.93	7.28	12.59	1.73	6.60	1.04	1.10	1.05
S3	1024.11	27.32	29.60	1.08	15.51	2.09	2.21	1.06
S4	1023.94	50.26	62.55	1.24	32.78	2.53	2.70	1.07
S5	1023.88	101.98	81.92	0.80	42.93	1.89	2.04	1.08
S6	1023.87	203.96	174.37	0.85	91.38	1.55	1.68	1.08
GB3	1024.38	54.09	39.96	0.74	25.57	1.68	1.76	1.05
GB4	1024.18	105.62	60.47	0.57	38.70	2.68	2.78	1.04
GB5	1024.26	204.51	127.35	0.62	81.50	1.22	1.29	1.06

Apart from the dry *IC* and maximum estimated concentrations and their ratio, Table 4.2 also presents the maximum concentration of effective immersed mass (for reference), and the time averaged settling velocity weighed by the concentration ($\langle W_S \rangle$, Equation 4.18). In the calculation of $\langle W_S \rangle$ values, the difference in the concentration between the instant i and i-1 was multiplied by the maximum settling velocity (W_{S_i}) in each class interval. Evidently, this calculation consists of an approximation since each class interval contains its own settling velocity distribution. Therefore, if the adopted time interval (Δt) is reduced, the error associated with this approximation also decreases. In order to evaluate the magnitude of this error, the $\langle W_S \rangle$ values were calculated using two different time intervals, i.e. 5 s and 20 s.

However, the first time t_1 was considered to be 20 s for both calculations, which corresponds to the minimum sampling rate of the instrument. Reducing time interval from 20 to 5 s increased the calculated $\langle W_S \rangle$ in less than 8% (Table 4.2, ratio: $\langle W_S \rangle_{(5s)} / \langle W_S \rangle_{(20s)}$). However, the $\Delta t = 5$ s was used to compute the histogram of frequency of settling velocity versus percent of mass concentration presented below.

Figure 4.10a shows the variation in time of the effective immersed masses of sediment measured with SEDVEL at different concentrations for the experiment of Series A run in freshwater. A fast rise in mass is observed within the first 10 minutes, followed by a slower increment until reaching almost constant values at the end of each experimental cycle. Figure 4.10b shows the relationship between the total sediment settled to the pan at the end of the experimental cycle and the averaged amount of sediment collected in the vials placed on the tube bottom, both in g cm^{-2} of dry material.

A good linear agreement was observed between these two independent measurements ($r^2 = 0.97$, $p < 0.01$), indicating that SEDVEL was able to consistently measure the sediment masses and the use of the organic matter content to calculate the sediment density consisted of a good approximation.

The settling behaviour of the sediment in saltwater (Series S) was very similar to that in freshwater (Series A) (Figure 4.10a,c), since the same kind of sediment was used in both experimental series. However, the average of the $\langle W_S \rangle$ values calculated for experiments of the Series A (i.e. 2.35 mm s^{-1}) was 20% higher (t test, $p = 0.21$) than the averaged $\langle W_S \rangle$ values for all experiments of Series S (i.e. 1.95 mm s^{-1}). This may be related to differences in the fluids' properties. Applying averaged values of fluid density and kinematic viscosity for the experiments of Series A and S to the Stokes Law (Equation 4.1) produces settling velocities 8% faster in freshwater mediums for equivalent particles diameters. Furthermore, differences in the flocculation process between the freshwater and saltwater mediums could lead to the formation of flocs with different sizes. Lick and Huang (1993) observed a steady-state diameter 33% higher for flocs formed in freshwater compared with those produced in saltwater under a shear of 100 s^{-1} and concentrations of 100 mg l^{-1}. The percentage of mass of flocs with $W_s > 2$ mm s^{-1} was on averaged 17% higher for the experiment of Series A than for the Series S. Also, the percentage of mass of flocs with $W_s < 2$ mm s^{-1} was 5% smaller for the

experiment of Series *A* compared with the Series *S*. These differences, although small, could account for the higher average of $\langle W_S \rangle$ calculated for the Series *A* experiments.
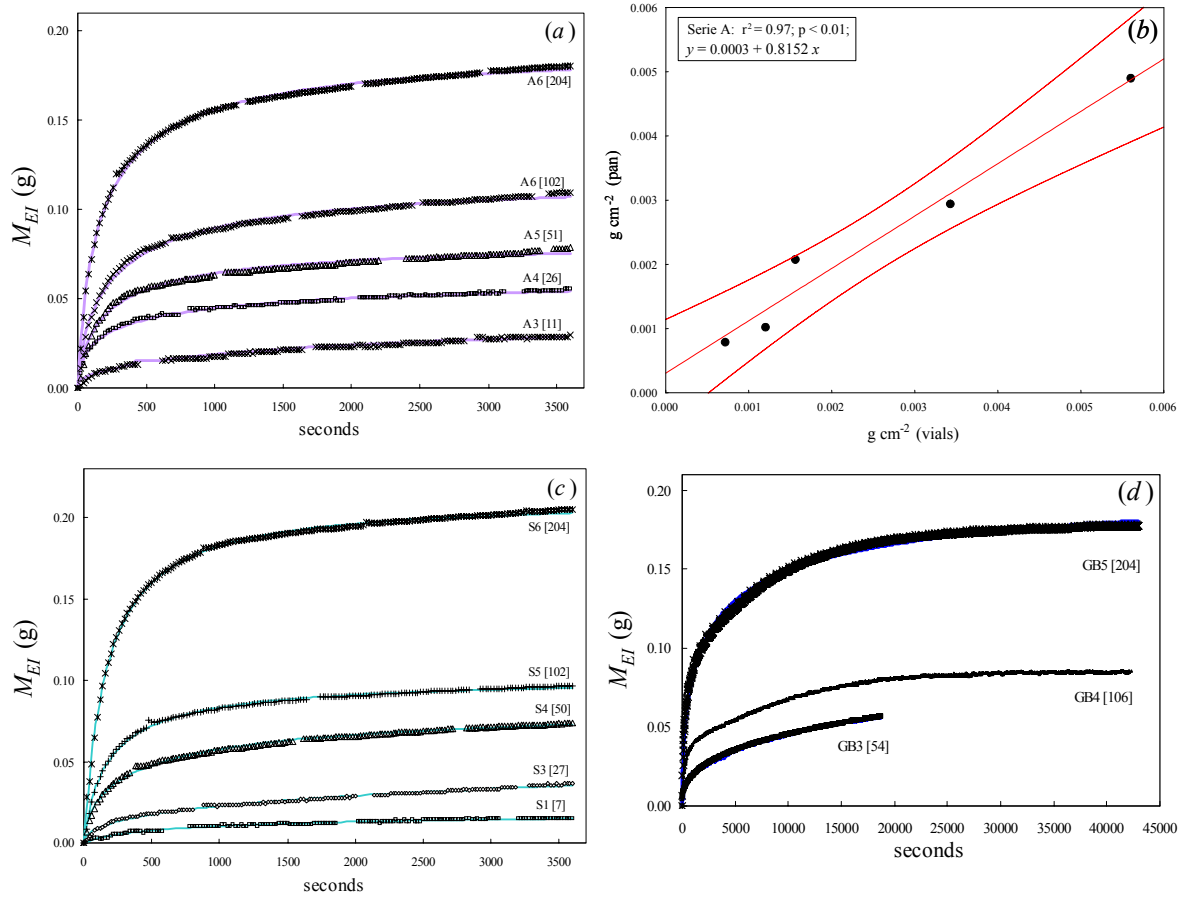
Figure 4.10: (*a*) Experiments with natural sediment run in freshwater (Series *A*) at different initial sediment concentrations ([*IC*], mg l^{-1}) as indicated on the picture, (*b*) linear regression between the averaged dry-mass of sediment (g cm^{-2}) collected inside the vials and the dry-mass of sediment settled on the pan (g cm^{-2}), (*c*) experiments with sediment run in saltwater (Series *S*) at different initial sediment concentrations ([*IC*], mg l^{-1}) and (*d*) experiments with glass beads (Series *GB*) run in saltwater at different initial sediment concentrations ([*IC*], mg l^{-1}). Points represent the original data and the lines the curves fitted to them.

Plots of the percent of concentration versus W_s in each class interval of the settling particles showed a very comparable pattern of distribution for the experiments of Series *A* and *S* carried out at similar particle concentrations (Figure 4.11a,b). However, the frequency of mass distribution in each class of settling velocity varied among the different concentrations in both Series *A* and *S* experiments. For concentrations below 50 mg l^{-1}, the main mode situated at $0.12 \leq W_s < 0.25$ mm s^{-1}, while for concentrations between 50 and 200 mg l^{-1}, the main mode was at $0.5 \leq W_s < 1.0$ mm s^{-1} and a second mode was present at $2.0 \leq W_s < 3.0$ mm s^{-1}. These differences led to a significantly (*t* test, $p = 0.13$) lower averaged value of $\langle W_S \rangle = 1.8$ mm s^{-1}, for the low concentration experiments (i.e., A3, A4, S1, S3), compared

with the average of $\langle W_S \rangle$ = 2.3 mm s^{-1}, calculated for the high concentration experiments (i.e., A5, A6, A7, S4, S5, S6).
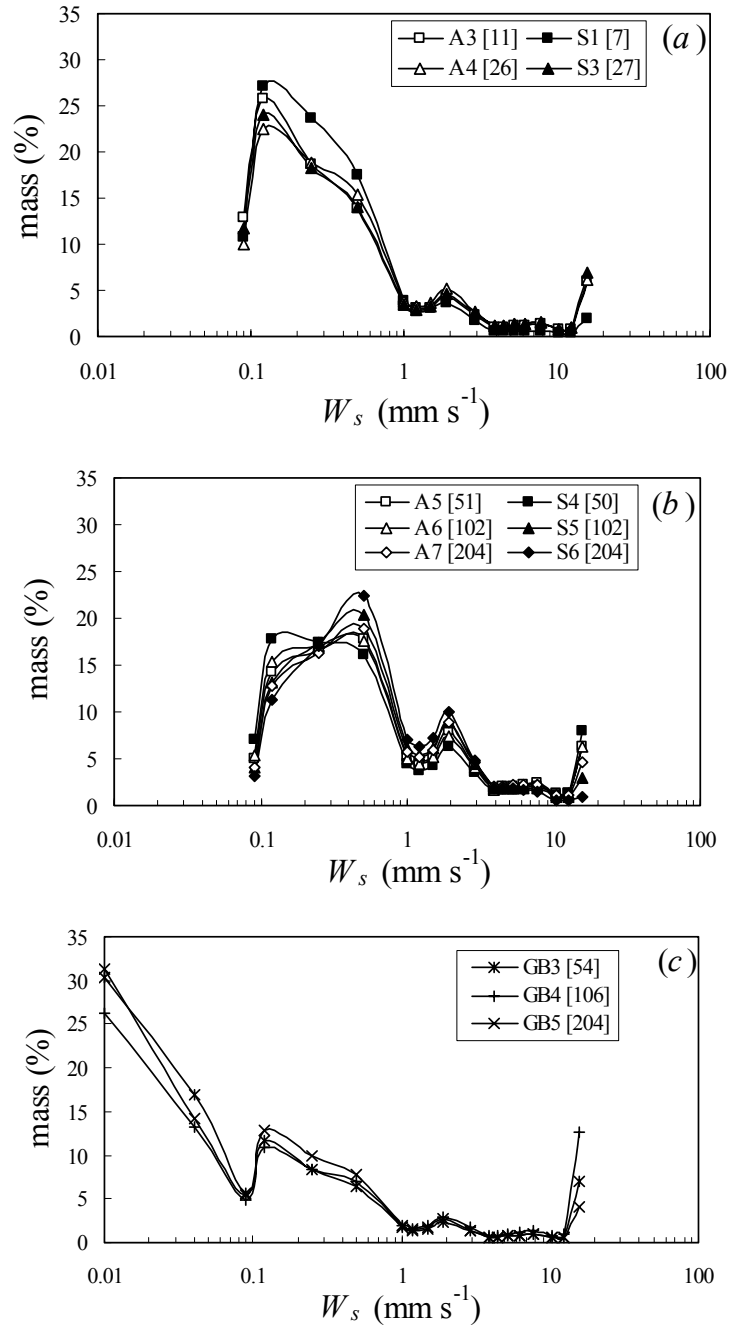
Figure 4.11: Percent of mass plotted against the minimum settling velocity in each settling class for (*a*) initial sediment concentrations less than 50 mg l^{-1} for the experiments of Series *A* and *S*, (*b*) for concentrations above 50 mg l^{-1} for the experiments of Series *A* and *S*, and (*c*) for concentrations above 50 mg l^{-1} for the experiments of Series *GB*.

Different factors could lead to the observed differences between the low ($C < 50$ mg l^{-1}) and high ($50 < C < 200$ mg l^{-1}) concentrations experiments, such as the usually observed

influence of the concentration on settling velocities, differential settling and floc formation, as discussed below.

The fall velocity frequency distribution for the experiment of the Series *GB* differed from the previous series, since they showed a large portion (55 to 65%) of slow falling particles, i.e. $W_s < 0.25$ mm s^{-1} (Figure 4.11c). Most of the particles/flocs had $W_s < 1$ mm s^{-1} (71 to 82%), while the fraction of large flocs ($W_s > 15.6$ mm s^{-1}) represented 4 to 13% of the total. This is consistent with the small particle size used in the experiments (mode of 7 μm). The larger fraction of slow-settling particles may also be associated with the greater settling time adopted in the experiments of the Series *GB*. The mode around 2 mm s^{-1} was not marked in the experiment of the Series *GB*. Therefore, if there was some reflocculation within the settling column, it only led to the formation of small flocs. The lack of measurements at low concentrations (< 50 mg l^{-1}), makes it difficulty to evaluate the reflocculation effect.

A large variation in the percent of the first class of $W_s \geq 15.6$ mm s^{-1} was verified in all experiments. This can be related to differences in the initial amount of large flocs present in each experiment as well as with the uncertainties in for estimating the starting zero position.

4.4.3. Reflocculation within settling columns and SEDVEL measurements in the laboratory

The flocculation of individual particles depends on their cohesiveness and on the frequency of particle collisions. The frequency of collisions depends on the SPM concentration and the movement of particles relative to each other (Puls et al., 1988). The main processes promoting collision are: (*i*) Brownian motion, which is only important for very fine particles (< 2 μm) at the beginning of flocculation or at SPM concentrations higher than 10 g l^{-1}; (*ii*) differential settling that occurs when a faster aggregate (larger and denser) collides with a floc of slower fall velocity (smaller or lighter) and they coalesce, and (*iii*) turbulence that can promote both aggregation or disaggregation depending on the flow shearing intensity, floc size and strength of cohesion (Burt, 1986; Krone, 1986; Mehta, 1986, 1994; Van Leussen, 1988). The maximum aggregate size (terminal size) and settling velocity are reached, when the fluid shear exerted on it equals its inter-particle strength (Burt, 1986).

The sediment used in the experiments of Series *A* and *S* consisted of single particles and shear-resistant flocs, since they were not broken by vigorous mixing only by sonification (see

Figure 4.8). Small flocs probably were not broken during the manual mixing of sediment (of about a minute) that occurred after its introduction in the settling column. Contrarily, new flocs could be formed by an increasing collision frequency within this period. However, as the mixing period was short it is believed that only a few new flocs were formed and they did not have enough time to reach a terminal size. According to Lick and Huang (1993), flocs subjected to a high shear (i.e. 100 s^{-1} at concentrations of 100 mg l^{-1}) reached a stable size after 5 to 10 minutes in saltwater and after 50 to 80 minutes in the freshwater. As in the present experiments, the mixing intensity and duration were smaller; it is believed that the effect of shear in floc formation or break-up was also small.

As mentioned in the introduction, at moderate concentrations, aggregation causes W_s to increase with concentration, i.e. $W_S = kC^n$. This is especially important in the laboratory settling column experiments, where the aggregation is usually well-advanced as result of high rates of inter-particle collisions, and there is no break-up since shearing is negligible (Mehta, 1986). Further, in fine sediment suspensions, the flocculation rate scales with the square of concentration, rapidly increasing as concentration increases (Curran et al., 2003). Even though, there was no clear relationship between the averaged settling velocity ($\langle W_s \rangle$) and initial concentration (*IC*) (r^2 = 0.17, *p* = 0.2; Figure 4.12a), considering all experiments of Series *A* and *S*; the influence of suspended sediment concentration was evident on the mass frequency distribution of settling velocity (Figures 4.11a,b). This effect is corroborated by the fact that significant power correlations were found for the relationship between *IC* and the mass percent of flocs with the class $0.5 \leq W_S < 1.0$ mm s^{-1} (r^2 = 0.55, *p* < 0.02; Figure 4.12b), and especially, *IC* and the mass percent of flocs with the class $2.0 \leq W_S < 3.0$ mm s^{-1} (r^2 = 0.90, *p* < 0.01; Figure 4.12c).

An increasing aggregation rate at high sediment concentrations could have occurred in the experiments of Series *A* and *S*, especially within the first 10 minutes of settling which contain the two main settling modes (i.e., at 1.7 to 2.6 and 5.2 to 10.4 minutes). In contrast, the reflocculation effect was not evident in the glass bead experiments, suggesting not only collision frequency but also cohesiveness contributed to floc formation. Kranck (1986) asserted that a mixture of 50% inorganic and 50% organic matter, allowed to flocculate together, exhibited a settling rate an order of magnitude higher than that of inorganic matter itself.
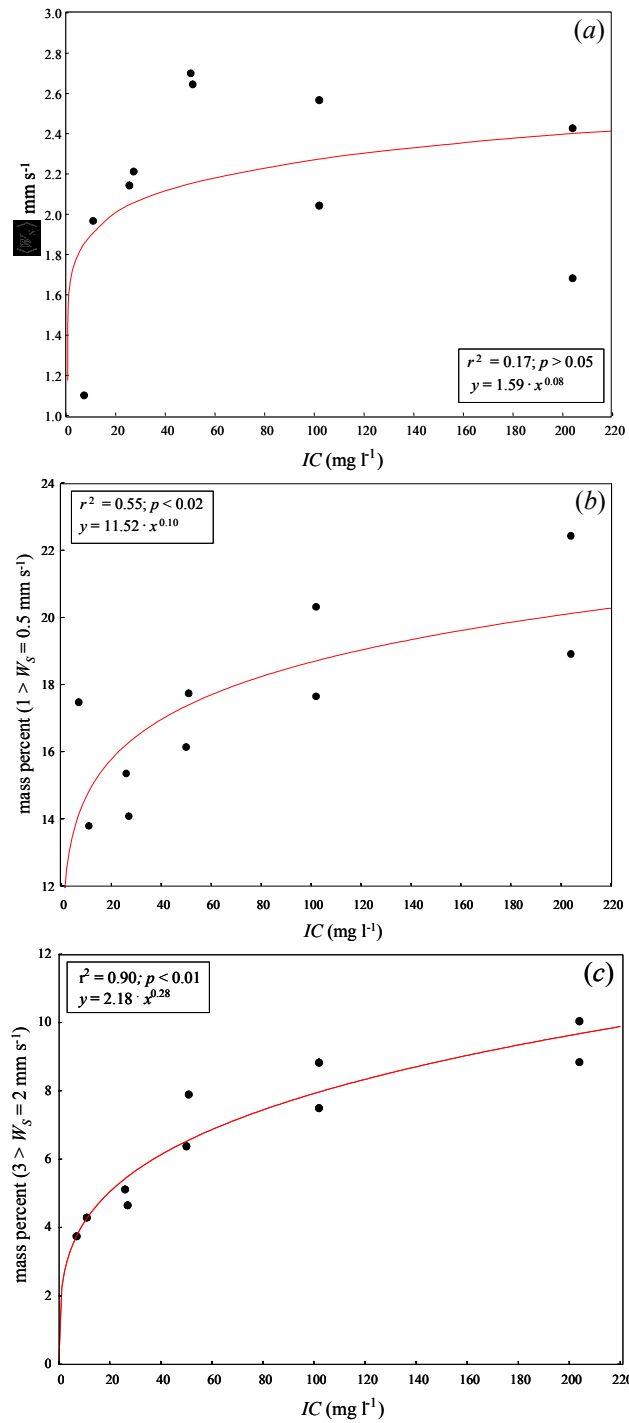
Figure 4.12: (*a*) Power correlation between the initial concentration of sediment (*IC*, mg l^{-1}) and the $\langle W_S \rangle$ (mm s^{-1}) for the experiments of Series *A* and *S*, (*b*) power correlation between the initial concentration of sediment (*IC*, mg l^{-1}) and mass percent of flocs with $0.5 \leq W_S < 1.0$ mm s^{-1} for the experiments of Series *A* and *S*, and (*c*) power correlation between the initial sediment concentration (*IC*, mg l^{-1}) and mass percent of flocs with $2.0 \leq W_S < 3.0$ mm s^{-1} for the experiments of Series *A* and *S*. All correlations were performed at 0.5% level of significance, the equations, r^2 and *p* values are given in the inlets.

In addition, porous aggregates, with porosities typical of large marine flocs, have collision efficiencies one to two orders of magnitude higher than impermeable spheres, because there

is sufficient flow across the sinking large aggregate surface to shift the trajectories of small particles, so that they pass through the aggregate, making possible collisions that might otherwise not occur (Stolzenbach, 1993; Stolzenbach and Elimelech, 1994; Kim and Stolzenbach, 2004).

Another process which can lead to an increase in W_s at slow fluid shear velocities or still conditions, as verified inside settling columns, is the differential settling. This process is enhanced with increasing SPM concentrations. Differential settling may have occurred at concentrations higher than 50 mg l^{-1} in the experiments of Series A and S, which could have produced higher averaged settling velocities and a second mode of W_s in relation to the low concentrations (<50 mg l^{-1}) experiments. Modelling of the differential settling inside settling tubes has shown that this process can lead to increases in the median settling velocities by a factor of 1.3 times, for concentrations of 100 mg l^{-1}, and by a factor of 2−4.4 times, for concentrations of 700−800 mg l^{-1} (Puls et al., 1988; Puls and Kühl, 1996).

In addition, the higher settling velocities (second mode), observed at high concentrations (above 50 mg l^{-1}) in the experiments of Series A and S, can also be associated with a higher flocculation rate at high concentrations that could lead to a formation of a larger number of flocs. Some authors claim that the still-water environment of a closed settling column can enhance floc growth as turbulent-shear values decrease (Milligan, 1995; Fugate and Friedrichs, 2002). For example, Milligan and Hill (1998), using a camera within a inverting column flocculator to test the importance of turbulence, composition and concentration on the maximum floc size, found that increased concentrations (50 to 250 mg l^{-1}) resulted in more rapid floc formation and higher settling velocity in still water, but equilibrium floc size did not change with increased concentration. In addition, Curran et al. (2003), investigating the evolution of floc size and settling velocities of marine clays in an invertible column using both sample withdrawal and video analysis, verified that the presence of a initial fast-sinking (1−4 mm s^{-1}) floc population, followed by a second low-density (and settling rate) floc population after 15 minutes of settling due to the aggregation of stranded particles via differential settling. Faster re-aggregation within the first 3 to 6 minutes after ceasing turbulence has also been reported (Milligan, 1995; Dearnaley, 1996).

The experiments carried out in this study suggested a more accentuated floc formation and superior averaged settling velocities at high sediment concentrations, i.e. 50 to 200 mg l^{-1},

compared with low concentrations (less than 50 mg l^{-1}) experiments. Milligan (1995) observing the settling behaviour in a mesocosm carousel flume, observed a rapid settling of the largest and inorganic-rich flocs followed by a slower-settling population of more organic-rich particles. In the present experiments, the organic fraction of sediment represented about 6%. Therefore, it is reasonable to assume that fast single inorganic grains and large flocs settled within the first minute or two. Next, a second floc population, with settling velocities between 2 and 3 mm s^{-1}, reached the bottom in 1.7 to 2.7 minutes, which was followed by a population of slower-settling smaller particles or large low-density flocs that were deposited after 5 to 10 minutes. However, the lack of simultaneous measurements of other floc properties (e.g. size, volume, shape) or video images makes difficulty to conclude exactly which process (or combination of processes) was responsible for the floc formation and settling velocities enhancement observed in the high-concentration experiments.

4.5. SEDVEL assessment *in situ*

4.5.1 Site of study

SEDVEL field trials were carried out in Cleveland Bay (Townsville, Australia). Cleveland Bay is a small (325 km^2) and shallow (5–15 m) embayment that lies on the north coast of Queensland. It is enclosed by mainland on its southern and eastern boundaries, and bounded by Magnetic Island on its northwest side. The West Channel separates Magnetic Island from the main land and has maximum depth of 4 m (Figure 4.13). The SEDVEL deployments took place at two locations: the Strand beach (0.8 to 4 m deep) and the Townsville Harbour (8 to 10 m deep). At the Strand beach, SEDVEL was deployed close to the Pier headland, about 30 m from the shore. At the Townsville Harbour, SEDVEL was moored at Berth 11 (Figure 4.13).

The climate in the Townsville region is defined as hot, humid and tropical with a summer rainfall peak. The mean annual precipitation in the region is 1125 mm, around 78% of which falls in the wet season (December to March) (Bureau of Meteorology, mean from 1940 to 2003 for the Townsville Airport Station). In the Townsville region, the dominant winds are from southeast or northeast, showing major direction variability during the summer (Wolanski, 1994). Tides in Cleveland Bay and adjacent areas are semi-diurnal with diurnal

inequality. Tidal height varies between 0.3 and 3.8 m, and tidal currents reach 0.4 m s^{-1} during the springs. The flood tidal currents are directed inshore, and the ebb tidal flow directed offshore (Lou, 1995). However, both wind-driven and tidal circulations control current velocity and direction; the wind-driven circulation is dominant in most of the bay, excepting near the West Channel where the tidal influence is greater (Lou, 1995).
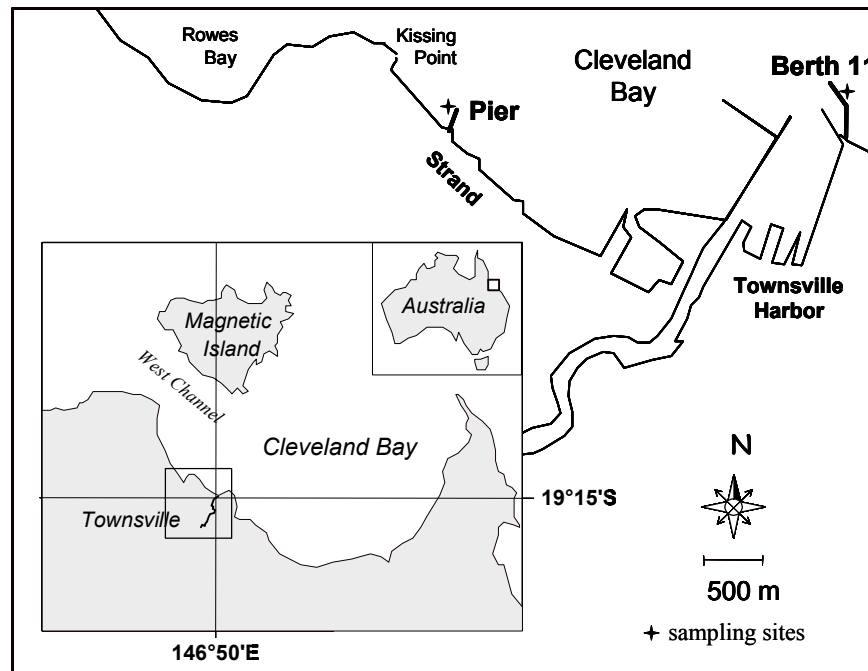
Figure 4.13: (*a*) Cleveland Bay located in Townsville (Australia), showing a detail of the two sampling areas: Berth 11 at the Townsville Harbour (right) and the Pier at the Strand Beach (left) (top map) and a photo of the Pier at the Strand Beach (bottom). The blue star indicates the site where the instruments were deployed.

The major cause of sediment resuspension in the bay are waves. Swell waves heights and periods in the coastal region mostly range from 0.5−1.5 m and 5−8 s, respectively (Carter and Larcombe, 2002). Waves in the bay consist of two parts: locally generated wind waves (period $T < 7s$) and swell waves (period, $T > 7s$) propagated from offshore deep water (Larcombe et al., 1995). Cleveland Bay is protected from the dominant south-easterly trade wind by Cape Cleveland, but it lies opened to northerly and north-easterly winds (Carter and Larcombe, 2002). Cleveland Bay consists of bioturbated muddy sands and sandy muds, and most of the bottom sediments are mixtures of four dominant grain size modes: 7 μm, 30 μm, 110 μm and 900 μm (Larcombe et al., 1995).

4.5.2. Field procedure and methods

SEDVEL was mounted on a tripod fixed to a triangular wood base and carefully placed on the seabed. Inlets for sample withdrawal were located about 0.4 m above the bed. More details of the SEDVEL deployment procedure were given in the Section 3.4.7. During each SEDVEL deployment, current speed and direction were monitored every 2 to 5 minutes by using an Anderaa current meter moored about 1 m above the bottom. Vertical profiles of salinity and temperature were measured every hour by using a CTD (Seabird), with sampling rate of 0.5 s. A Van-Dorn bottle was used to hourly collect water samples about 0.5 m above the bottom. The sampling times were coincident with the beginning of each cycle of measurement. Water samples were analysed in the laboratory for the determination of the concentration, size and organic content of SPM. The organic matter values determined for each cycle of measurement were used as an input to the Equation 4.10 and 4.9 to calculate the dry-density and dry-concentrations of SPM (Section 4.3.2). Water densities were calculated for each experimental cycle by applying the measured values of salinity and temperature to the UNESCO (1983) equations. In addition, visual observations of wave height and direction were carried out hourly. Measurements of tidal height variations (every 10 minutes) at the Townsville Harbour were kindly furnished by the Townsville Port Authority, and were referenced to mean sea level (MSL). Hourly data of wind direction and intensity at the Townsville Airport was provided by EPA (Environmental Protection Agency). Data of significant wave height (Hs) measured by the offshore Waverider buoy (close to Cape Cleveland) was kindly made available by the Coastal Sciences Unit of the Environmental Protection Agency (Environmental Sciences Division).

The mass-concentrations of SPM of the water samples collected in the field were determined by filtration through preweighed glass fibre (Whatman, GF/F, nominal retention of 0.8 μm). The filters were washed five times with deionized water to remove the excess of salt, and then oven dried for 5 h at 60ºC. Subsequently they were allowed to adjust to room temperature and weighed with a precision of 0.1 mg. The SPM organic matter fraction was quantified by combusting the filters for 3 h at 550ºC. Blanks were used for correcting mass losses of the glass-fibre filters during combustion. The size of SPM was analysed in the laboratory through the laser particle sizer (Malvern Mastersizer) for a size range between 0.5 and 600 μm (300 mm lens). A sub-aliquot of the water samples used for the quantification of SPM concentrations was analysed to determine size distribution of SPM.

SEDVEL was deployed at the Strand beach in Cleveland Bay (Townsville, Australia) during October and November 2003 (first SEDVEL version) and August and September 2004 (second SEDVEL version). Because water samples were taken at only a few occasions during SEDVEL deployment at Berth 11, only a small number of cycles are presented. SEDVEL measurements were only reported for the 2004 deployments, where the second SEDVEL version was used. The duration of the cycles of measurements of SEDVEL was 60 minutes, and the adopted sampling rate 20 s, giving an average of 5000 scans within this log interval. The adopted pumping period ranged from 1.5 to 2.5 minutes. Greater pumping periods (i.e. 2.5 minutes) were used in rough sea conditions and high SPM concentrations, since shorter time intervals proved to be insufficient for proper pan cleaning.

4.5.3. SEDVEL estimates of the dry-mass concentrations versus measurements

Assessment of SEDVEL performance *in situ* was realized by comparing the values of the dry-concentrations of SPM (mg l^{-1}) estimated from SEDVEL measurements ($C_{(PM)_{dry}}$, Sections 4.3.1 and 4.3.2) with the dry-concentrations of SPM obtained from the gravimetric analysis of the water samples (mg l^{-1}) taken at the beginning of each cycle of measurement. The conversion between effective immersed mass and dry-mass was performed to test SEDVEL's accuracy, since there is not any other method available to directly measure effective immersed masses of *PM in situ*.

The relationship between the dry-concentrations of SPM estimated from SEDVEL results and the measured dry-concentrations of SPM for 42 cycles of measurements is shown in Figure 4.14. These data included concentrations varying from 5 to 170 mg l^{-1}. Although the SEDVEL was able to reproduce the general tendency of the measured SPM concentrations ($r^2 = 0.65$, p < 0.01), a large scatter in the data was observed. Ratios between the estimated ($C_{(PM)_{dry}}$) and the measured SPM concentrations varied from 0.35 to 2.8. Differences between the estimated and the measured values were less than ±30% in 48% of the cycles, and less than ±50% in 69% of the measurements. The SEDVEL results overestimated the measured concentrations in 69% of the analysed cycles.
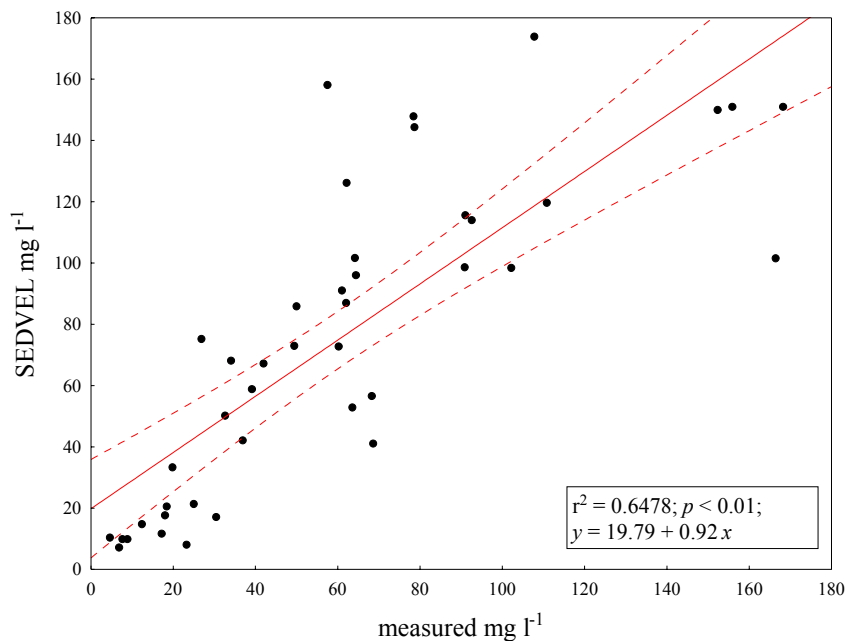
Figure 4.14: Relationship between the dry mass concentrations of SPM ($C_{(PM)_{dry}}$, mg l^{-1}) estimated from SEDVEL measurements and those measured from the water samples collected concomitantly *in situ*. The adjusted equation, r^2 and *p* values are shown in the inlet.

A number of factors can be responsible for the discrepancies between the measured and estimated concentrations, including errors associated with: (*i*) an eventual non-homogeneous distribution of particles on the balance plate, (*ii*) the determination of the starting zero position, (*iii*) errors associated with the gravimetric method used to determine mass-concentrations and organic content of SPM and (*v*) conversions of effective immersed masses in dry masses. Each one of these factors is discussed next.

If a large and heavy particle eventually settles in one particular position on the pan, it can result in a sensor reading larger or smaller than its actual mass. Also, if flocs of different sizes are not homogeneously distributed on the balance plate, this can produce a sensor output different from that expected if particles were deposited on the balance centre of mass. The error expected by a non-homogeneous distribution of particles in the pan depends on the starting zero position (Section 3.4.4). As pointed out in Section 3.4.4, maximum errors associated with a non-homogeneous distribution of particles, for a zero position of 1557, represented increases of +21% or decreases of -13% in relation to the values measured at the pan centre of mass, depending if particles were deposited further from or close to the pan support, respectively. It is reasonable to expect that particles settled both close to and further from the pan support (suspension system), and therefore, part of this error will be cancelled out. In the field, the actual error caused by a non-homogeneous distribution of particles on the balance plate is difficult to predict. In addition, even though the zero position changed usually by less than 5% (maximum of 15%) between the different cycles of measurement within a same deployment, a great variation in the zero positions took place between the different deployments (i.e. from 1380 to 1830). Therefore, distinct cycles of measurement likely experienced errors of different magnitudes due to an eventual non-homogeneous distribution of particles on the pan.

Another factor to consider is that there is some subjectivity associated with the selection of the starting zero position (*ZP*). The adopted *ZP* corresponded to the position where a continuous and consistent increase of the mass could be observed, it was usually situated 4 to 6 measurements after the top pump have stopped. The choice of the starting zero position is particularly critical because, as mentioned before, even small variations of *ZP* can promote significant changes in the estimated mass (Section 3.5.3). The location of *ZP* is particularly crucial at high sediment concentrations, when the SEDVEL output can increase considerably between two successive reading (Δt = 20 s). Errors associated with *ZP* determination could have been significant at some cycles of measurement, but generally a reduction of the sampling noise and a consistent pattern of deposition, i.e., a continuous increase of the readings and a well defined pattern of deposition were observed in most of the cycles.

In addition, bottle sampling and the gravimetric method applied in the quantification of the mass-concentration and organic content of SPM, used as a standard for comparison with SEDVEL estimates, may accumulate errors in sample collection and computation as large as

20% (Wren et al., 2000). Furthermore, even though the water samples were taken approximately at the same time and very close to the SEDVEL instrument, small scale spatial variability in the concentrations and organic content of SPM can occur.

Another source of error in the computation of SEDVEL dry-masses is related to uncertainties in the estimation of the density of *PM* needed to convert the effective immersed masses into dry masses. In this conversion, a relationship between the organic content and density of SPM was used (Section 4.3.2). The measured organic matter content (*OM*) varied from 3 to 28% in the 42 analyzed cycles, corresponding to *PM* densities of about 2.3 and 1.3 g cm^{-3}, respectively. These densities produced factors *f* (used in Equation 4.8) ranging from 0.2 to 0.6. Therefore, dry masses of *PM* (M_{PM}) were obtained by multiply the effective immersed masses (M_{EI}) by factors between 1.7 and 5. This variation arises because the estimate of the density of SPM is very sensitive to *OM* contents below 0.3 (i.e. 30%), as showed in the Figure 4.6. For example, adopting a value of *OM* = 0.19 produces dry-mass concentrations of SPM 56% higher than if a value of *OM* = 0.07 was considered. A similar range of variation in the *OM* values was verified among different cycles of measurement in the same day of deployment, although a much smaller variation was usually observed between two consecutive measurements. Therefore, small spatial and temporal variations in *OM* may result in large variations in the estimated mass of *PM*.

According to Fennessy et al. (1997), the calculation of the floc bulk mass ($m_f = V_f \rho_f$) integrate the diverse components of floc density, i.e. the dry-density of the mineral component of SPM (ρ_m), the dry-density of the organic component of SPM (ρ_o) and density of the floc interstitial water (ρ_{iw}, usually equivalent to the density of the ambient water) and their respective volumes, as following: $V_f \rho_f = V_m \rho_m + V_o \rho_o + V_{iw} \rho_{iw}$. If flocs are highly consolidated aggregates, with hardly any interstitial water, then $V_{iw} \approx 0$; contrarily, if flocs present an extremely low effective density ($\rho_e = \rho_f - \rho_w$), then $V_{iw} \approx V_f$ (Fennessy et al., 1997). They also concluded that when estimating the dry-mass of flocs, the equation:

$M_{dry_f} \cong \dfrac{\pi d^3 \rho_e}{6}$ should be replaced by $M_{dry_f} = \dfrac{\pi d^3}{6} \dfrac{\rho_e \rho_{mo}}{(\rho_{mo} - \rho_w)}$, where the mean dry-density

of SPM is $\rho_{mo} = (V_m \rho_m + V_o \rho_o)/V_{mo}$ and V_{mo} is the dry-volume of SPM. In the second

equation, the dry mass is computed based on the volume of flocs discounting the volume of the interstitial water, i.e. $V_f\rho_f - V_{iw}\rho_{iw}$.

In this work, the hydrostatic weighing method was applied to determine the dry density of *PM* used to obtain the dry-mass and concentration of *PM*. By this method, the volume of a solid sample is determined by comparing the weight of the sample in air to the weight of the sample immersed in a liquid of known density (Webb, 2001). Therefore, the interstitial volume of water is excluded from the calculations because the pore volume is likely filled with water of the same density as the surrounding fluid medium, used to determine the immersed weight of the sample. The hydrostatic weighing method was used because it measures the immersed weight of *PM* in an analogous way to that used in SEDVEL immersed weight measurements. However, in this approach, a constant density is assumed for the whole population of flocs in suspension, but in fact aggregates within a sampling population can present different densities. It has been well documented that the average density and the strength of aggregates decreases with increasing size and order of aggregation (Partheniades, 1993; Fennessy et al., 1994; Mikkelsen and Pejrup, 2001).
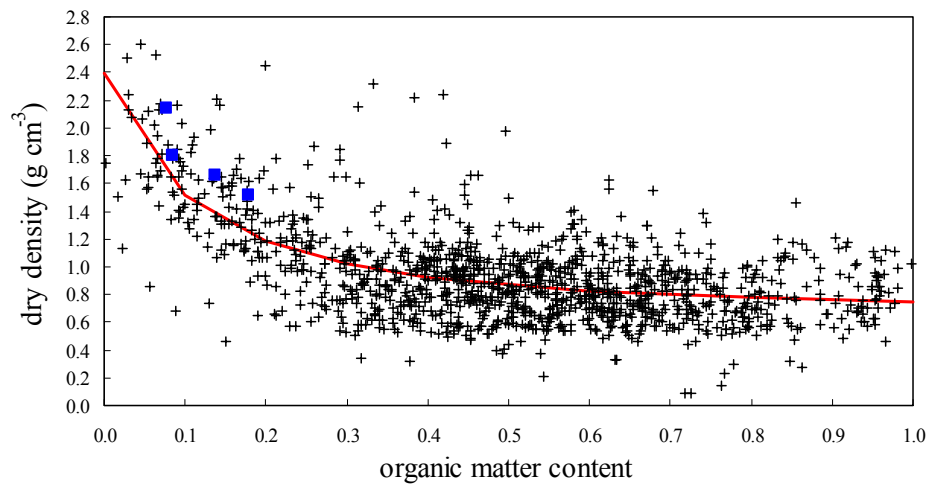
Figure 4.15: Relationship between dry density (g cm^{-3}) and organic matter content (*OM*, 1.0 = 100 wt-%) of over 1230 sediment and peat samples (+) from a lake system in Malaysia (Wüst, 2001). The regression curve fitted to the data is represented by the red line ($0.72/(1-0.70\cdot\exp(-2.84\cdot OM))$), r^2 = 0.42). Measurements of SPM density effectuated in this work were not include in the regression, but are presented in the figure (blue squares) for comparison.

Relationships between density and organic content are usually established for measurements of the bulk density of the bottom sediment, and generally exponential relationships can be found between these two parameters (Mann and Wetzel, 2000; Wüst, 2001). However, plots

of the density of the bottom sediment against its organic matter content can show a large scatter (Wüst, 2001; Figure 4.15). The dry-densities of SPM measured in this work are presented in Figure 4.15 (blue squares), and the values showed the same tendency of variation as observed for Wüst (2001) measurements.

Alternatively, the aggregate volume based on particle size measurements could be used to calculate the density and dry-mass concentration of *PM*. However, these volumes are usually obtained by applying simultaneous measurements of floc size and settling velocities to the Stokes Law. The Stokes Equation assumes that the particle (floc) is spherical, and includes the volume of the interstitial water in the total floc volume. According to Fennessy et al. (1997), the Stokes density notation is appropriate when dealing with single grains composed of single density and which have no interstitial water (e.g. quartz spheres). However a better approach is needed when calculating the bulk densities of estuarine/marine aggregates, which are composed of mineral and organic particulates as well as interstitial water. Nevertheless, aggregates can present different densities for the same particle size/volume, which lead to different settling velocities. For example, Van der Lee (2000) found no relationship between the density of flocs and their size, a fact attributed to differences in floc densities for the same particle size, which can vary from highly organic or porous flocs to almost sand grains. Even though relationships between the excess density and the diameter of particles (usually the equivalent spherical diameter) have been established for different environments, they usually present a large scatter (Fennessy et al., 1994; Ten Brinke, 1994). Further, they are found to vary considerably for different environments and seasonally for a particular site (Kranck et al., 1993). For example, Sternberg et al. (1999) applied relationships between the excess density and size of flocs proposed for different authors in order to estimate the settling velocity of the aggregates, and encountered one order of magnitude deviations from the measured values.

In the present work, the size of the SPM was analysed through a laser particle-sizer in the laboratory. The obtained results furnish a general indication of the size distribution of the particles, but obviously do not represent actual *in situ* aggregate sizes, since floc disruption is likely to occur during sampling and analysis (see Section 4.4). Also, the laser-diffraction technique represents the size distribution of the particles based on their volumetric concentrations, while SEDVEL measurements are based on their mass distribution. The volume distribution is comparable to a weight distribution if density is constant (Rawle,

Malvern instruments). A uniform density, usually based on an inorganic grain, is adopted in the laser diffraction size analysis. However, density of aggregates in nature is seldom constant and it may vary considerably from the density of inorganic particles. In conclusion, it is believed that even though the use of organic matter content to estimate the dry density of *PM* may not be the best approach, it will be more representative of the aggregate density than those that could be obtained by estimating an aggregate volume based on the measured SPM size in the laboratory. Refinements of this estimate could be obtained by measuring the particles size *in situ* simultaneously with SEDVEL measurements.

4.5.4. SEDVEL estimates of mass distribution of settling velocity

Results of the mass-weighed average settling velocity and the mass distribution of settling velocity were produced for each day of deployment, which generally included 3 to 6 cycles of measurement. Cycles that did not demonstrate a clear pattern of deposition (as shown in Figures 3.30 and 3.32d) were not considered. A few cycles (less than five) were eliminated including: (*i*) those that presented a continuous and steep rising in the mass from the beginning to the end of the monitoring period, which likely resulted from improper sealing of the tube and (*ii*) cycles that showed a very quick saturation of the balance, possibly related to the falling of a very heavy particle at the beginning of measurements.

The maximum and minimum setting classes included in the analysis consisted of flocs with $W_S \geq 16.0$ mm s^{-1} and $0.09 \leq W_S < 0.12$ mm s^{-1}, respectively. Plots of concentration/mass percentage versus minimum W_s in each class interval of the settling velocity are shown in Figures 4.16 and 4.17 for the deployments carried out at the Pier (Strand Beach), and in Figure 4.24, for the Berth 11 deployments. The size distributions of SPM obtained from the laser particle sizer analysis are also shown in these pictures. Even though these values do not represent the actual *in situ* aggregate size distribution due to a possible disruption of the flocs, during sampling and analysis, they can act as indicators of temporal changes in the SPM size composition.

4.5.4.1. Pier (Strand Beach)

The percentage of mass in each settling velocity class and size distributions during seven days of deployment at the Pier (Strand Beach) is shown in Figure 4.16 (for the neap cycles) and Figure 4.17 (for the spring cycles). The date, starting time and SPM concentrations (inside brackets) at each cycle of measurement are indicated in these Figures. The SPM concentrations for the different cycles measured at the Pier ranged from about 5 to 170 mg l^{-1}, with 3 to 19% of organic matter. Most of the cycles presented a main mode of relatively slow-settling particles/flocs within $0.09 \leq W_s < 0.5$ mm s^{-1}, and usually a second mode of $1.5 \leq W_s < 3.0$ mm s^{-1}.
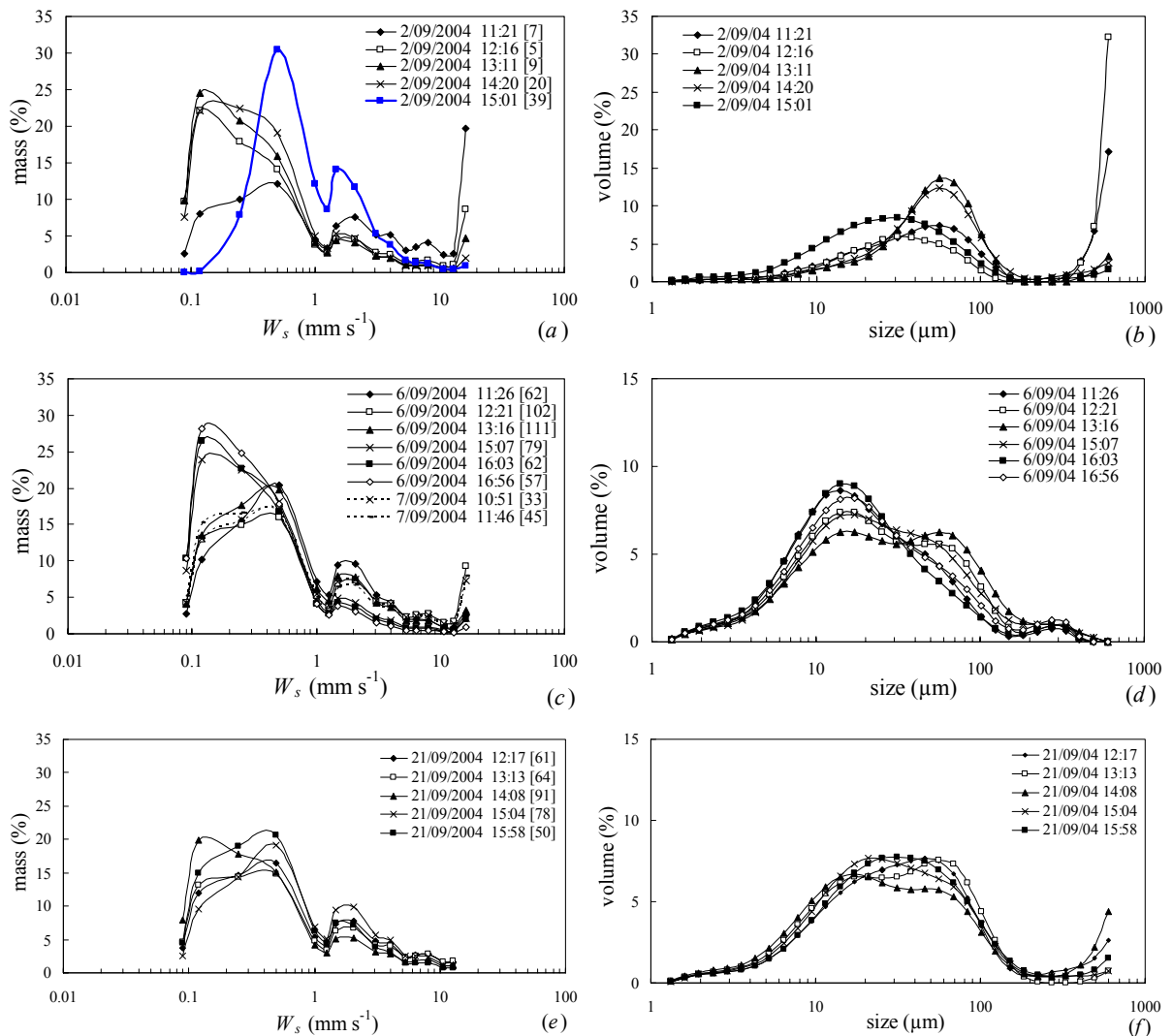
Figure 4.16: Percentage of mass distribution in each settling class for the deployments at the Pier (Strand Beach) (left) and size distribution of SPM (right), determined by the laser particle sizer in the laboratory. Deployment dates, the starting times and concentrations of SPM for each cycle of measurement are shown in the inlets. These cycles were measured during the neap tide.

Fastest settling particles ($W_s \geq 16$ mm s^{-1}) occurred at some cycles. However, these particles represented less than 5% of the total mass in most of the cycles, and between 5 and 20% in a few cycles (Figures 4.16 and 4.17). For example, the cycles started at 11:21 and 12:16 on 02/09/04 exhibited relatively high percentage of the class $W_s \geq 16$ mm s^{-1}, and coincidently, they showed a greater portion of large particles (500−600 μm) (Figure 4.16a,b). However, the variability, often observed among cycles for the same day of deployment, in the fastest settling particles can be related to uncertainties in the definition of the starting settling time.

The size spectra, obtained from the laser particle sizer analysis, exhibited one mode in most of the cycles sampled at the Pier, although a bimodal distribution occurred in some cycles. Around 76% of the sampled cycles presented a main mode with particles between 13 and 30 μm, and 24% of the cycles showed main modes between 39 and 64 μm. Particles with diameter less than 150 μm composed 90−98% of the size spectra, except two cycles in which they summed less than 73%. The percentage of particles/flocs smaller than 56 μm varied from 50 to 89%, while the size fraction between 56 and 150 μm represented 6 to 30%. The large amount of small particles/flocs (<56 μm) is consistent with the high percent of mass (i.e. usually 40−96%) encountered for particles/flocs falling at speeds less than 1 mm s^{-1}.

The bottom around the Pier headland is mainly composed of sand (diameter of 62 to 1000 μm), with small amounts of silt ($d < 62$ μm, 2−22%) (Muller, 2002). In this work, the size measurements of the SPM showed that the sediment particles or flocs in suspension presented diameter smaller than 150 μm, and most of the particles/flocs had diameter less than 56 μm. This agrees with Larcombe et al. (1995) who commented that the larger sediments (sizes between 110 and 900 μm) will only be placed in suspension by long period swells or during storms, while fine modes (7 and 30 μm) will be in near permanent suspension or released from spaces between larger grains during resuspension events.
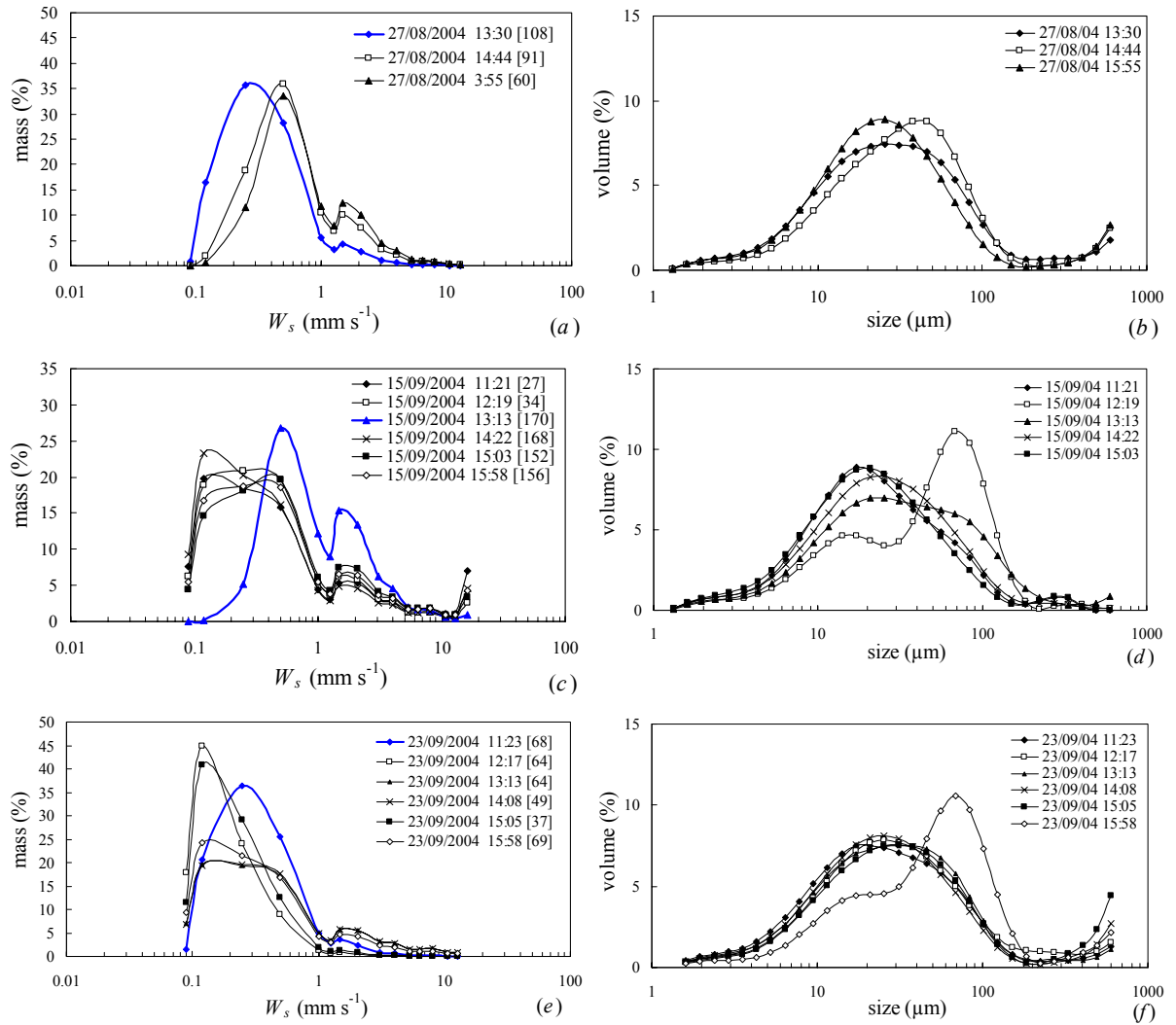
Figure 4.17: Percentage of mass distribution in each settling class for the deployments at the Pier (Strand Beach) (left) and size distribution of SPM (right), determined by the laser particle sizer in the laboratory. Deployment dates, the starting times and concentrations of SPM for each cycle of measurement are shown in the inlets. These cycles were measured during the spring tide.

The Stokes Law (Equation 4.1) was used to test the consistency between the measured particles sizes and the settling velocities. Average values of water density, floc density (c.a. 1.8 g cm^{-3}) and kinematic viscosity were computed considering all cycles of measurement carried out at the Pier. Inputting these parameters to the Stokes Equation, resulted in settling velocities of 0.8 and 5.6 mm s^{-1}, for particles with sizes of 56 and 150 μm, respectively. Mineral particles of equivalent size range would settle at around 1.07 and 7.7 mm s^{-1}. Although both estimates encompass the range of fall velocities measured for the second settling mode ($1.5 \leq Ws < 3.0$ mm s^{-1}), but the lower and upper limits are broader, indicating that the population of particles represented by the second mode must be mainly composed of particles smaller than 150 μm and bigger than 56 μm. For example, fall velocities around 3

mm s^{-1} can be reached by an inorganic particle of about 95 μm as well as by flocs around 110 μm (ρ_f = 1.8 g cm^{-3}) and 130 μm (ρ_f = 1.5 g cm^{-3}). Alternatively, flocs with sizes ranging from 110−160 μm and densities of 1.3 g cm^{-3} could also reach settling velocities between 1.5 and 3.0 mm s^{-1}. In addition, the main modal sizes of 13−30 μm correspond to settling velocities of 0.04−0.23 mm s^{-1} for an average floc density of 1.8 g cm^{-3} and 0.06−0.31 mm s^{-1} for mineral grains (ρ_f = 2.6 g cm^{-3}). These calculations, although generic, indicate that the slow-settling population (0.09 ≤ W_s < 0.5 mm s^{-1}) may be composed of either small inorganic particles (13−40 μm; W_s = 0.06−0.55 mm s^{-1}) or microflocs with lower densities and bigger sizes than mineral particles.

Despite the general consistency in the form of settling spectra among the monitored cycles (Figure 4.16 and 4.17), some differences among cycles of the same day of deployment were detected. These differences were related to changes in tidal/waves conditions and SPM concentrations/size during the day. For example, during the neap of 02/09/04, a relatively small amount (i.e. 12%) of the slow-settling flocs (mode of 0.5 ≤ W_s < 1.0 mm s^{-1}), and a larger amount of flocs with W_s > 1 mm s^{-1} occurred during the first cycle of measurement (cycle 11:21) performed at the high tide (Figure 4.16 a). During the ebb (cycles 12:16, 13:11, 14:20), the settling spectra was similar, with the main settling mode of 0.09 ≤ W_s < 0.5 mm s^{-1} representing about 22−25% of the total mass, and the settling class of 1.5 ≤ W_s < 3.0 mm s^{-1} representing about 4.5−7.5% (Figure 4.16a).

During the ebb cycles, low SPM concentrations (5 to 20 mg l^{-1}) and tidal levels between 1.5 and 2.4 m were observed. Relatively calmer sea conditions occurred during the ebb cycles, i.e. small local wave heights (H = 0.15−0.3 m) and slow currents (around 2 cm s^{-1}). After 13:30, local wave heights and currents intensities increased, reaching, respectively, values of H = 0.3−0.5 m and 2.3−5.5 cm s^{-1} in the afternoon (Figure 4.18d,e). These increases were related to a constant and strong NE winds (up to 30 km h^{-1}) during this period (Figure 4.18b,c). Consequently, increasing SPM concentrations were observed in the afternoon, reaching a maximum of ≈130 mg l^{-1} (Figure 4.18f). The cycle measured at the low tide (around 15:00) presented a particular settling spectrum. In this cycle, there was a shift in the main settling mode to 0.5 ≤ W_s < 1.0 mm s^{-1}, which represented 30% of the total, and an increase in the amount of particles within 1.5 ≤ W_s < 3.0 mm s^{-1} interval (i.e. 14%) (Figure 4.16a; 02/09/04 15:01).
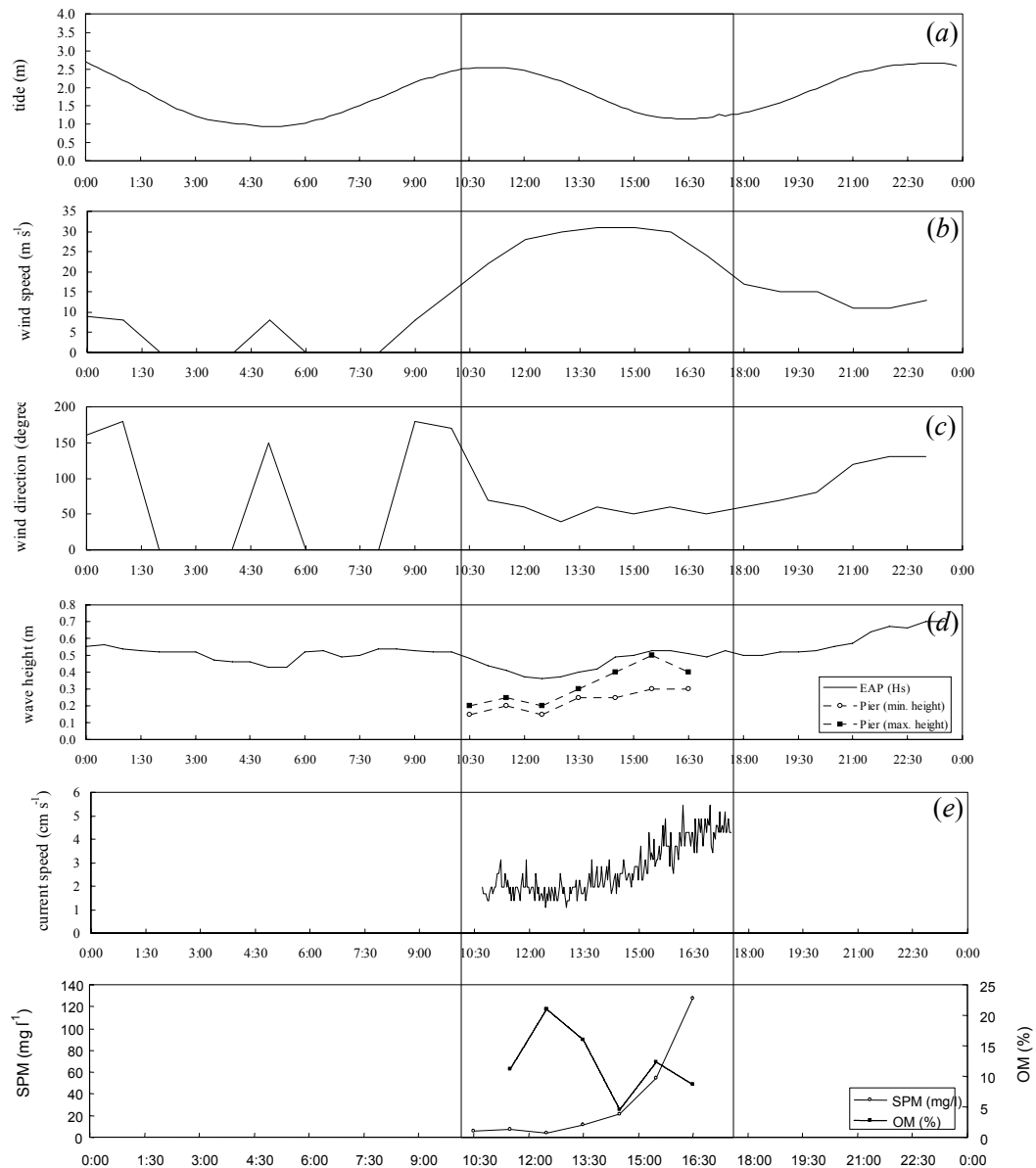
Figure 4.18: Variation during the day of the tidal range (*a*), wind speed (*b*) and direction (*c*), and the significative wave height measured at Cape Cleveland (EAP, *Hs*) (*d*). Variation during the period of monitoring of the minimum and maximum wave heights at the Pier (visual observations, *d*), the current intensity (*e*) and the concentration (SPM, mg l⁻¹) and organic matter content (OM, %) of SPM (*f*) on 02/09/04 (neap tide).

On the 06/09/04, north-east swell waves, with *Hs* = 0.8―1.0 m, and moderate local waves at the Pier (*H* = 0.3−0.6 m) were observed at the beginning and through the monitoring period (Figure 4.19d). The first three cycles of measurements on 06/09/04 (i.e. 11:26, 12:21 and 13:16) were performed during low tide and the beginning of flood and presented relatively high SPM concentrations 62−111 mg l⁻¹ (Figure 4.19a,f). Currents situated mainly within the 2.5−3 cm s⁻¹ interval, with maximum around 6 cm s⁻¹ (Figure 4.19e). At these cycles, the settling spectra had a main mode of $0.5 \leq W_s < 1.0$ mm s⁻¹, which represented 20−26% of the total mass, and a secondary mode around $1.5 \leq W_s < 3.0$ mm s⁻¹, comprising 7−10% of the

139

total mass. The last three cycles were performed during the rising tide and high water, and they exhibited SPM concentrations between 50 and 80 mg l^{-1}. At these cycles, the main settling mode changed to $0.12 \leq W_s < 0.25$ mm s^{-1} (24−28%), and the second mode ($1.5 \leq W_s < 2.0$ mm s^{-1}) was less pronounced (4−5%) (Figure 4.16c).
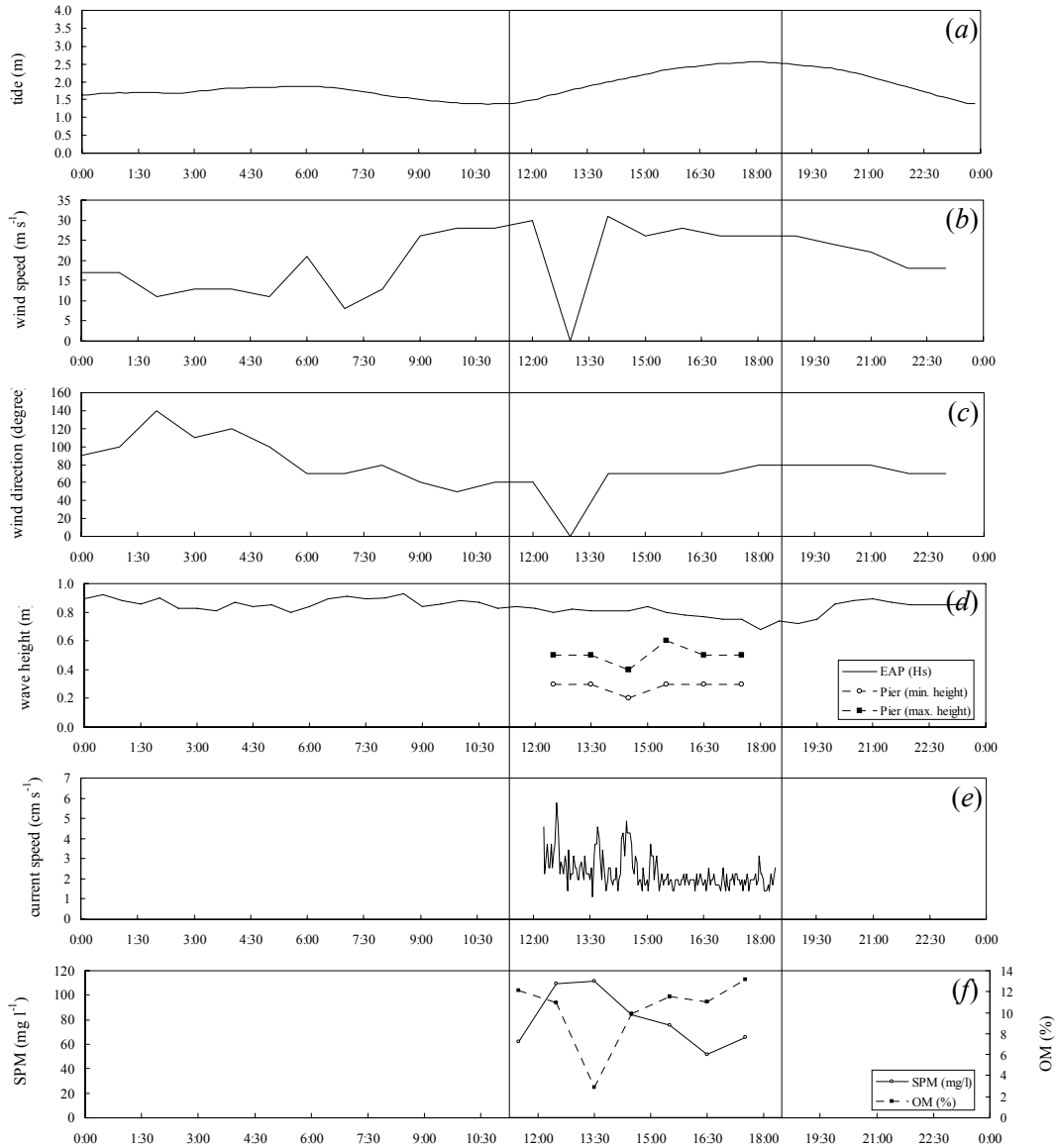
Figure 4.19: Variation during the day of the tidal range (*a*), wind speed (*b*) and direction (*c*), and the significative wave height measured at Cape Cleveland (EAP, *Hs*) (*d*). Variation during the period of monitoring of the minimum and maximum wave heights at the Pier (visual observations, *d*), the current intensity (*e*) and the concentration (SPM, mg l^{-1}) and organic matter content (OM, %) of SPM (*f*) on 06/09/04 (neap tide).

The concentrations of SPM concentrations were relatively high on this neap (> 60 mg l^{-1}), even during the high tide, which indicates that there were relatively high quantities of material in suspension in the waters advected from the offshore direction. High significative heights ($H_S = 0.8−0.9$m) were observed for the swell waves since the morning (Figure 4.19d),

and this long period of rough sea conditions likely led to an increase of the suspended load in the bay. Only two cycles were monitored on 07/06/04 and they presented a remarkably similar settling behaviour to those measured on 06/09/04.

On the neap of 21/09/04 measurements were performed during the rising tide and high water. During these measurements, wave heights at the Pier ranged from 0.2 to 0.4 m, the currents intensities oscillated between 1.4−7.2 cm s^{-1} and the SPM concentrations varied between 50 and 91 mg l^{-1}. The settling behaviour on 21/09/04 was close to those measured on the 06/09/04 neap. The observed consistency of the settling behaviour on the 21/09/04 neap (Figure 4.16e) is corroborated by the similarity in the measured particle sizes among the different cycles (Figure 4.16f).

The spring of 15/09/04 also presented a pattern of settling similar to the 06/09/04 and 21/09/04 neaps, excepting the cycle started at 13:13 (Figure 4.17c). This cycle was performed during the low tide (tidal level around 1 m) and presented a high SPM concentration ($\approx$ 170 mg l^{-1}; maximum of 220 mg l^{-1} at 13:30). Within this cycle, the main settling velocity mode shifted towards $0.5 \leq W_s < 1.0$ mm s^{-1}, representing 27% of the total mass. There was also an increase in the percentage of mass (i.e. 15%) in the $1.5 \leq W_s < 2.0$ mm s^{-1} mode. The relatively higher settling velocities for this cycle are consistent with the shift in the size mode towards a coarser particle diameter observed for the water sample collected at the same time (Figure 4.17d). On the 15/09/04 spring, concentrations around 30 mg l^{-1} occurred during the ebb period (i.e. 10:30−12:30) under tidal levels of 1.4−2.4 m. During the low water (i.e. 13:30−16:30), SPM concentrations increased considerably reaching values of 140−220 mg l^{-1} (Figure 4.20f). During the low tide and beginning of the flood, there was also an enhancement of the local wave heights from 0.2−0.3 to 0.2−0.5 m and the current speeds from 1.4−4.3 to 2.0−6.3 cm s^{-1} (Figure 4.20d,e). Again, this intensification was related to constant and strong NE-winds (up to 30 km h^{-1}) blowing during the afternoon.
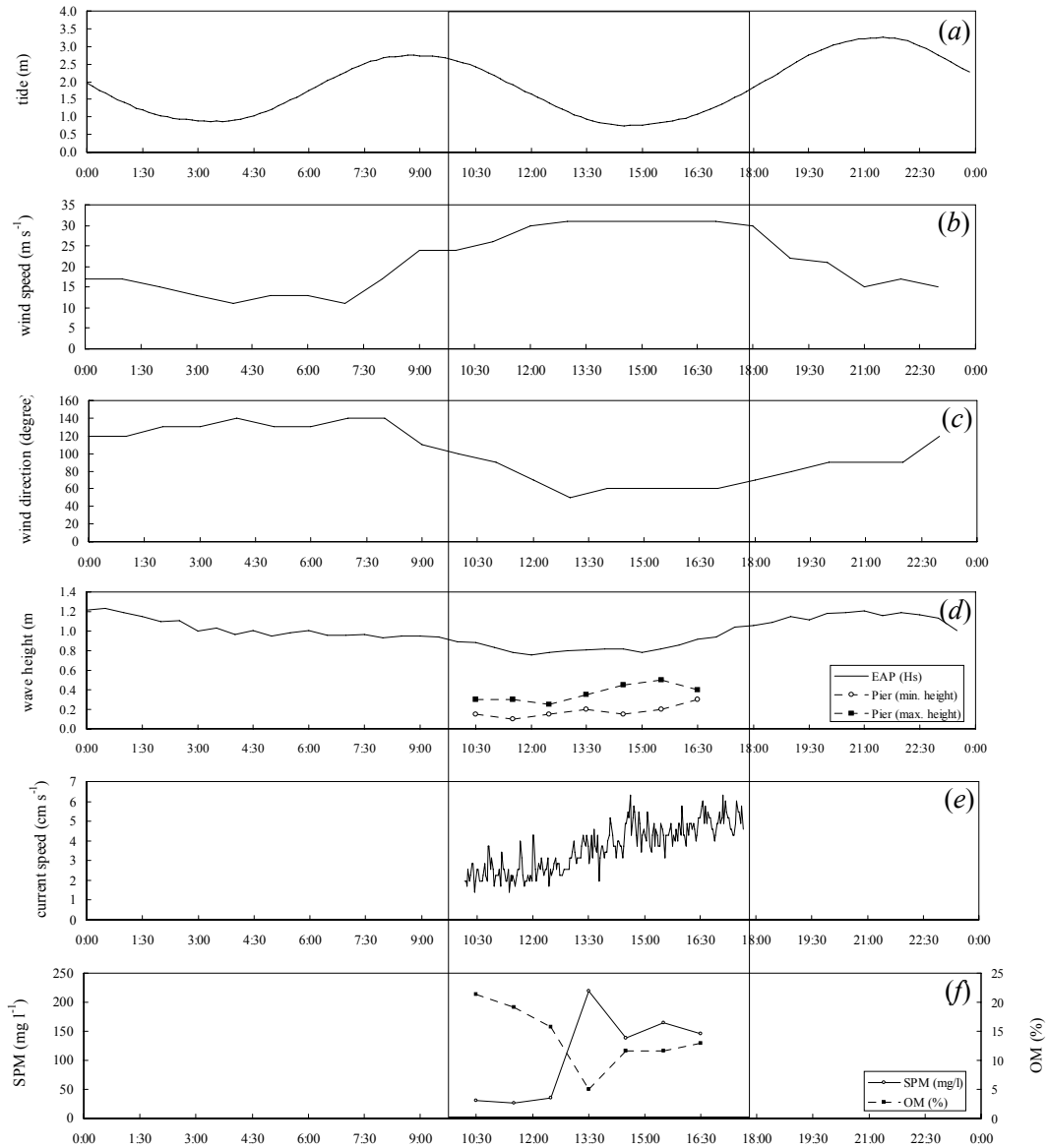
Figure 4.20: Variation during the day of the tidal range (*a*), wind speed (*b*) and direction (*c*), and the significative wave height measured at Cape Cleveland (EAP, *Hs*) (*d*). Variation during the period of monitoring of the minimum and maximum wave heights at the Pier (visual observations, *d*), the current intensity (*e*) and the concentration (SPM, mg l⁻¹) and organic matter content (OM, %) of SPM (*f*) on 15/09/04 (spring tide).

Most of the cycles monitored during the springs of 27/08/04 and 23/09/04 presented more marked main mode of settling velocity than the previously analysed cycles (Figure 4.17a,e). The cycles measured on 27/08/04 showed a sharp mode within the $0.25 \leq W_s < 1.0$ mm s⁻¹ interval particles (33−36%) and a less conspicuous second mode of $1.5 \leq W_s < 2.0$ mm s⁻¹ (4−12%) (Figure 4.17a). A very low tidal level of 0.28 m, waves heights of 0.2−0.3 m and currents mostly around 3−4 cm s⁻¹ were observed at the first cycle (i.e. 27/08/04, 13:30), associated with high SPM concentrations ($\approx$ 110 mg l⁻¹) (Figure 4.21a,d,e,f). About 81% of the flocs presented $W_s < 1$ mm s⁻¹ for the cycle started at 13:30, while this percentage dropped to 46−57% during the other two cycles measured during the beginning of the flood.
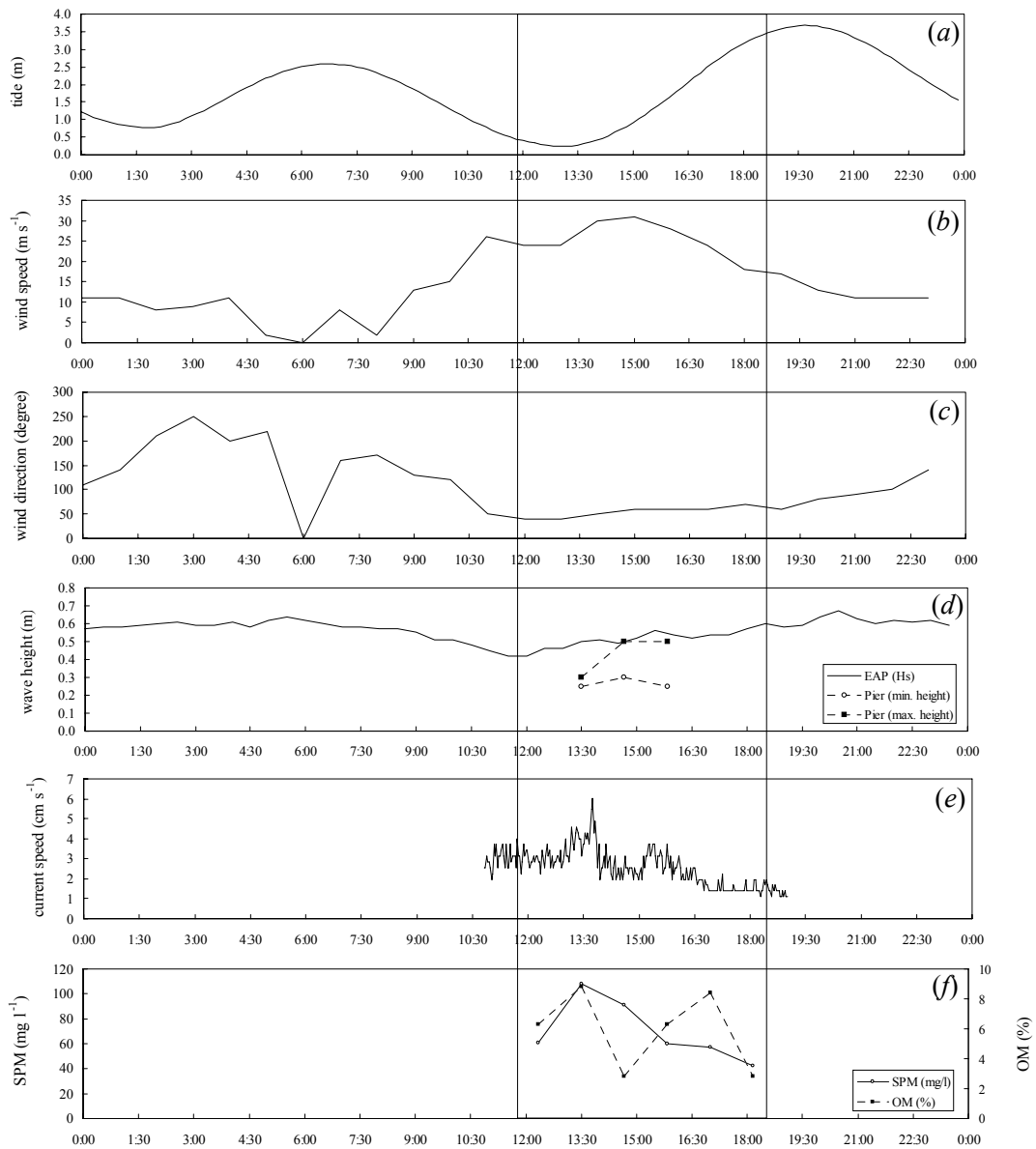
Figure 4.21: Variation during the day of the tidal range (*a*), wind speed (*b*) and direction (*c*), and the significative wave height measured at Cape Cleveland (EAP, *Hs*) (*d*). Variation during the period of monitoring of the minimum and maximum wave heights at the Pier (visual observations, *d*), the current intensity (*e*) and the concentration (SPM, mg l^{-1}) and organic matter content (OM, %) of SPM (*f*) on 27/08/04 (spring tide).

The cycle measured on the 27/08/04 at the minimum tidal level presented a settling spectrum very similar to that observed at the low tide of the 23/09/04 spring (Figure 4.17e; cycle of 11:23) subjected to a relatively lower SPM concentration (i.e. 68.3 mg l^{-1}). The other cycles measured on 23/09/04, presented a main mode of $0.12 \leq W_s < 0.25$ mm s^{-1} (19−45%) and a less notable second mode of $1.5 \leq W_s < 2.0$ mm s^{-1} (0.8−6%) for SPM concentrations ranging between 37 and 69 mg l^{-1} (Figure 4.17e). Again cycles measured during the flood (i.e. 13:13,

14:08, 15:58) presented similar mass distribution of settling velocity and distinct from cycles measured during the low-tide, excepting one cycle (i.e. 15:05).

4.5.4.2. Environmental conditions at the Pier and the settling spectrum

In general the settling behaviour at the Pier was similar in the different analysed cycles, with a large portion (30−97%) of particles with $W_s < 1$ mm s^{-1}, followed by a second mode (2−50%) of $1.0 \leq W_s < 2.0$ mm s^{-1}, and a smaller amount of faster settling flocs. In addition, rapid variations in the settling behaviour could be observed between the different analysed cycles. Such variations were attributed to the process of settling, resuspension and advection that continuously change the concentration and characteristics of SPM in the water column. Considering that the water samples used in SEDVEL analysis were withdrawn 0.4 m above the seafloor, even the slow-settling particles, e.g. with $W_s = 0.12$ mm s^{-1}, could reach the floor within about 55 minutes (about the sampling interval) under conditions of reduced shear stresses in the water column. Faster falling flocs would settle to the bottom in a few minutes. Similarly, resuspended particles in the bottom layer could be easily be sampled.

Even though a similar pattern of settling could be observed under different environmental conditions, a few cycles of measurement presented a particular settling behaviour when compared with the other cycles measured in the same day of deployment. These cycles comprised measurements carried out during the low tide on the springs and on the neap of 02/09/04, in which minimum water levels (*MWL*) ranged from 0.3 to 1.3 m (highlighted cycles in Figures 4.16 and 4.17). The *MWL* cycles typically presented a marked mode of flocs (27−36%) with settling intervals of $0.25 \leq W_s < 0.5$ mm s^{-1} or $0.5 \leq W_s < 1.0$ mm s^{-1}, and a sharper settling distribution than the other cycles measured in the same day. They also had the particularity of presenting SPM concentrations usually higher than measured in the other cycles of the same day of deployment, and relatively low organic contents (i.e. 3−9%). The Stokes Equation was used to estimate the equivalent spherical diameter corresponding to the main mode of settling velocity observed in the *MWL* cycles. Averaged values of water density, floc density (1.92 g cm^{-3}) and kinematic viscosity at these cycles were applied to the Stokes Equation, resulting in floc sizes of about 30−60 μm for $W_s = 0.25$−1.0 mm s^{-1}. These values are consistent with the main size mode measured for these cycles of 15−64 μm.

Considering all the sampled days at the Pier (total of 20 days), relatively higher SPM concentrations occurred during the low tides compared with those measured during the flood and high water in most of the monitored days, especially during the spring tides subjected to larger tidal ranges. This was verified even when the waves and currents conditions did not change considerably between the high and low tides (e.g. Figure 4.19 and 4.21). Although this effect was intensified when the low tide was coincident with a period of enhancement in the amplitude of the waves and current speeds (e.g. Figures 4.18 and 4.20).

The measured increase in the SPM concentrations during low tides was likely resultant from an intensification of the bottom shear stress and resuspension under reduced water depths. Decreases in the water depth lead to an increase in the maximum orbital velocity of the wave and, consequently, to an increase in the shear stress at the sea-bed and in the potential for sediment movement (OUCT, 1989). Similarly, reductions in the SPM concentrations as the water depth increases can result from (*i*) a reduction in the wave shear stresses and consequently in the resuspension, (*ii*) a dispersion of the previously resuspended material through a relatively wider water column and (*iii*) change in the water masses by the advection of an offshore water. Orpin et al. (1999), analysing simultaneous records of SPM concentrations, significative wave height and period from a 21 m deep site (off Cape Cleveland), did not observe significant resuspension of the mud fraction at *Hs* up to 1 m. Larcombe et al. (1995) demonstrated that in the shallow reef embayments sediment is resuspended by even small amplitudes wind-waves, which do not mobilize sediment in deeper offshore water.

In addition, a non-linear relationship was found between the SPM concentrations and the organic matter content ($r^2 = 0.5$, $p < 0.01$) as shown in Figure 4.22; where the lower the organic content, the higher is the SPM concentrations.

Even though the organic matter does not cause the bottom resuspension or deposition, it can probably be used as an indicator of the predominance of resuspension, deposition or advection processes that controls the SPM dynamics. At the events of resuspension, the water turbidity at the mooring site (close to the headland) was often higher than that observed at the end of the Pier or for offshore waters (e.g. Figure 4.23). This is probably related to an intensification of the erosion around the rock headlands and shallow areas close to the shore. In conclusion, high SPM concentrations (and low *OM*) were usually associated with the

intensification of the resuspension of the bottom sediments in shallow waters, while low SPM concentrations and high organic content were associated with the advection of relatively clearer offshore water to the site of measurement.
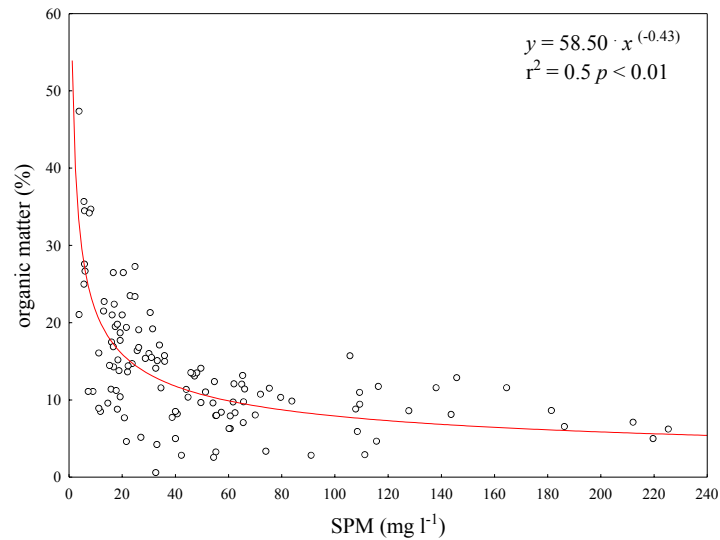
Figure 4.22: Relationship between SPM concentrations (mg l^{-1}) and organic matter percentage considering all measurements effectuated at the Pier during 2003 and 2004.
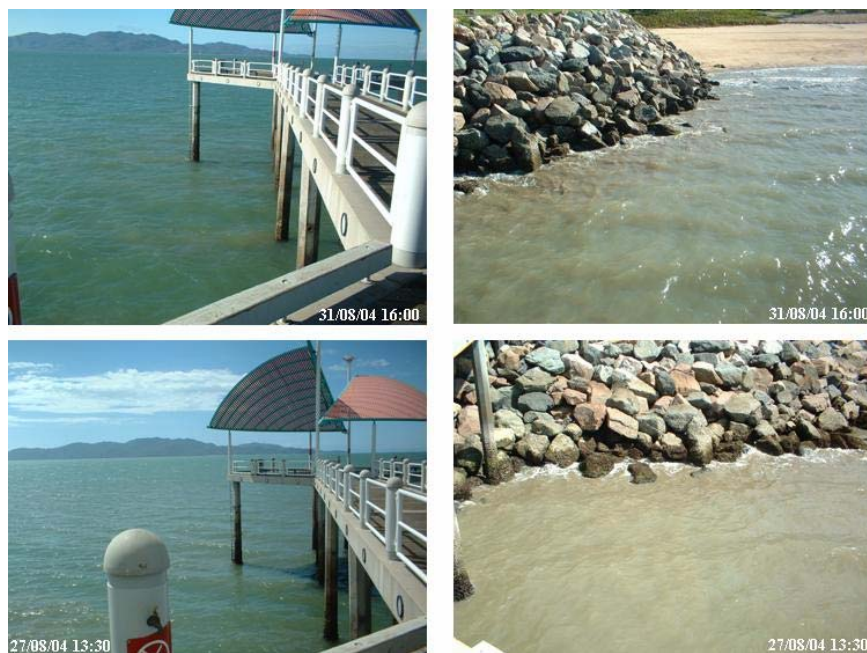
Figure 4.23: Photographs taken at the Pier for comparison of the water turbidity close to the rock headland at the sampling site and at end of the Pier and offshore waters at the low-water of two spring tides: the spring of 31/08/04 (top) and the spring 27/08/04 (bottom).

The SPM, measured at the *MWL* cycles, usually presented a reduced organic content, which indicates the preponderance of inorganic particles. As the bottom at the pier is mainly

composed by sand (Muller, 2002), with small amounts of silt and clay, its cohesiveness is expected to be low; and then particles could possibility be easily put in suspension when a critical shear stress for erosion was exceeded. Therefore, it is likely that the settling spectra measured in the *MWL* cycles suffered the influence of a population of particles resuspended from the bottom, which added some variability to the mass distribution of settling velocities compared with the other cycles measured in the same deployment.

At two of these *MWL* cycles (i.e. 02/09/04 15:01 and 15/09/04 13:13), the settling mode shifted slightly towards a faster settling velocity, and the amount of particles/flocs with $W_S <$ 1 mm s^{-1} dropped to 32−38% compared with percentages of 57−72% verified in the other cycles measured during these two days. These measurements were performed under moderate local waves ($H = 0.2- 0.5$ m), water levels between 1.1−1.3 m and current speeds around 2−4 cm s^{-1}. Conversely, the *MWL* cycles measured on the springs of 27/08/04 and 23/09/04, presented higher percentages of flocs with $W_S < 1$ mm s^{-1} (i.e. 81−84%) than the other cycles monitored during these days (i.e. 46−72%). These springs were subjected to relatively smaller waves heights (i.e. $H = 0.1-0.3$ m) than the other two cycles, comparable current speeds (2−4.6 cm s^{-1}), but lower *MWL* (i.e. 0.3−0.9 m). During these two springs, large flocs may have been disrupted due to an increased shear close to the bed under relatively smaller depths, resulting in a decrease of fast sinking particles in the settling spectra. It is unlikely that increasing SPM concentrations led to an increase in the flocculation of particles, since a very similar settling behaviour was verified at different concentrations, for instance at 40 mg l^{-1} on 02/09/04 and 170 mg l^{-1} on 15/09/04 (Figure 4.16a and 4.17c). But, similar aggregation/disaggregation processes could have taken place close to the bottom at similar levels of shear stress, which could also lead to the resuspension of sediment grains with a similar size.

To finalize, the settling spectra measured during the low-tide cycles (*MWL* cycles) were influenced by the presence of a "resuspension population". The size, density and aggregation level of this population probably varied as a function of the shear stress on the bottom. During the flood periods, fine particles and small flocs may be brought in suspension to the sampling site from offshore areas. At these periods, both particles locally resuspended or advected from offshore may compose the SPM and cause changes in floc size and settling velocity distribution. The offshore waters usually presented lower SPM concentrations and

higher organic content, which may lead to differences in the floc formation, in the degree of aggregation and floc densities.

4.5.4.3. Berth 11

The measured settling spectra at the Berth 11 were remarkably consistent in form for the eight cycles of measurement (Figure 4.24). The population in suspension consisted mainly of slow-settling particles/flocs, showing only one mode of settling velocities with $0.09 \leq W_S < 0.12$ mm s^{-1}. The measured SPM concentrations ranged from 8 to 30 mg l^{-1} within these cycles. Suspended particulate matter (SPM) presented a relatively high organic content (between 17 and 28%) in most of the cycles, excepting one cycle in which a value of 9% was measured. Estimated floc densities from Equation 4.10 varied from 1.3 to 1.9 g cm^{-3}, and their main size mode ranged from 12 to 39 µm. It was observed in the field that the bottom at this sampling station is composed of a very soft mud with high cohesion. Samples of the bottom sediment presented a mean size of 20 µm and main mode of 10 µm.
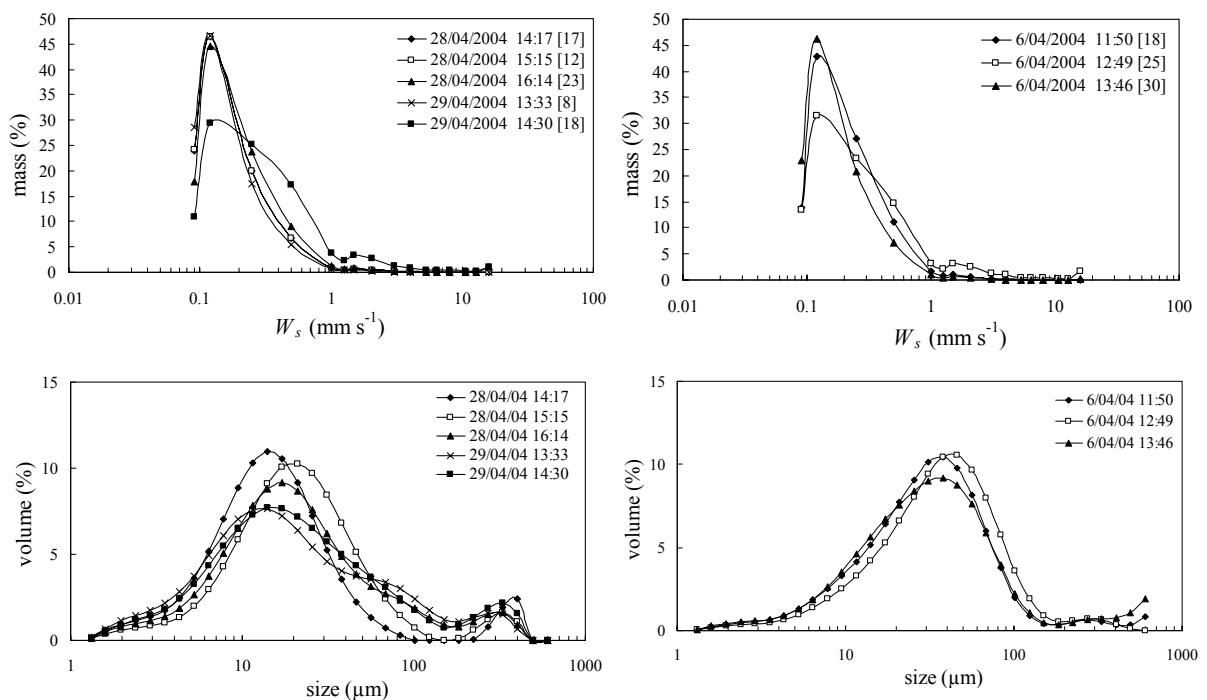
Figure 4.24: Percentage of mass distribution in each settling class for the Berth 11 deployments (upper graphics) and size distribution of SPM (lower graphics), determined by the laser particle sizer in the laboratory. Deployment dates, the starting times and concentrations of SPM for each cycle of measurement are shown in the inlets.

Averaged values of water density and kinematic viscosity for the eight cycles of measurement and a mineral density of 2.6 g cm^{-3} were applied to the Stokes Law (Equation 4.1) in order to estimate the settling velocities of particles with diameters of 12 and 39 μm, correspondent to the main size modes of the SPM. The estimated settling velocities ranged between 0.13 and 1.38 mm s^{-1}, which are higher than the measured settling velocity mode. However, if mean value for the estimated floc densities at these cycles (c.a. 1.5 g cm^{-3}) is applied to the Stokes Equation considering the same size range, it results in settling velocities between 0.03 and 0.29 mm s^{-1}, which encompasses the measured mode of settling velocity, with $0.09 \leq W_s < 0.12$ mm s^{-1} interval. Therefore, if the modal values for size and settling velocity correspond to the same population, particles/flocs must be of lower mean density than inorganic mineral grains. The estimated mean density of flocs, 40% smaller than the density of inorganic particles, represented better the settling mode measured at Berth 11. Hence, the SPM at Berth 11 was probably comprised of microflocs composed both of organic and inorganic material, and with densities lower than the density of mineral particles, plus small inorganic particles (5–15 μm) resuspended from the bottom. Large and weak flocs may have been disrupted by pumping water during the sample replacement at the beginning of each cycle, even though small and stable flocs seemed to have resisted the procedure of water withdrawal. Nevertheless, fast falling flocs were present in the settling spectra measured at the Pier, where the same water withdrawal procedure was used. Thus, the amount of instrument-induced floc break-up needs further investigations.

4.5.4.4. Mass-weighed average of settling velocities versus SPM concentrations

The mass-weighed average of settling velocities ($\langle W_S \rangle$) ranged from 0.3 to 5.5 mm s^{-1} (mean of 2.1 mm s^{-1}) at the Pier, and they varied from 0.2 to 1.0 mm s^{-1} (mean of 0.5 mm s^{-1}) at Berth 11. Considering all 42 analysed cycles at these two locations, there was no correlation between the mean or median settling velocities and the SPM concentrations. Correlations between these two parameters have been established for several environments (Eisma et al., 1997). The lack of correlation observed in the present work may be related to: (*i*) uncertainties in the definition of the settling classes and (*ii*) characteristic of the sampling sites.

The lack of correlation between settling velocity and SPM concentration may be associated with uncertainties in the computation of the first and last classes of settling velocities. Errors in the amount of fast settling particles may be associated to uncertainties in the definition of the zero position and in the extrapolation of the fitted curve to the zero, and consequently in the determination of amount of mass allocated for the first settling class. In addition, the cycle of measurement was restricted to one hour (minimum settling velocity of 0.09 mm s^{-1}), and therefore a background population of very slow settling particles was not included in the analysis.

However, the lack of correlation between the mean/median settling velocities and the SPM concentrations is more likely a characteristic of the sampling sites. Most of the measurements were carried out at the Pier, where similar settling patterns were observed at different SPM concentrations. High settling velocities also occurred at relatively low concentrations and relatively low settling speeds were observed at high concentrations. At the Pier, the settling velocity is likely to be determined by erosion and deposition of microflocs/particles from and to the bed near the headland, controlled by the combined action of water depth, local waves and currents as well as by advection of offshore floc populations during the rising tide. At Berth 11 measurements encompassed eight cycles of low concentrations (8−30 mg l^{-1}) of an organically-rich SPM, which is likely aggregated in a form of microflocs of low-density and slow settling velocities. The absence of a relationship between SPM concentrations and median settling velocities has also been identified in other environments (e.g. Mikkelsen and Pejrup, 1998; Van der Lee, 2000; Sanford et al., 2004). Van der Lee (2000) pointed out that a correlation between settling velocity and SPM concentration occurs in a specific location in an estuary during a short period of time (e.g. tidal cycle), and this relationship cannot be generalized. In addition, Mehta (1994) suggests that the inter-particle collision is an important factor increasing aggregation and leading to higher settling velocities at concentrations above 100−300 mg l^{-1}, being the mutual interference among particles minimal below these concentrations (free settling). The sampled concentrations at the Pier were usually less than 100−200 mg l^{-1}, and therefore the free settling regime may have prevailed.

Further, the lack of correlation between W_s and concentration suggest that particle reflocculation induced by the settling column, as identified in the laboratory (Section 4.4.2), did not occur in the field. Particle flocculation in the tube itself due to differential settling would result in strong correlations between settling velocity and SPM concentration (Sanford

et al., 2004). In addition, Mikkelsen et al. (2004) did not observe floc alteration inside a settling column when comparing *in situ* data simultaneously obtained by a digital floc camera (outside the column) and a video camera mounted inside the settling column, even in relatively energetic environments.

Considering measurements carried out at the Pier, variations in SPM concentrations could explain 50% of the variability in the organic matter percentage, as indicated by a negative power relationship between these two parameters (Figure 4.22). This relationship showed a general tendency of decreasing the organic content at high concentrations, especially above 60 mg l^{-1}. Therefore, even though the collision efficiency between particles may have increased at high SPM concentrations, the reduced amount of organic material may indicate a limited efficiency in the biological binding of particles (Van der Lee, 2001).

In nature, aggregation of particles depends on: (*i*) collision frequency that is determined by the shear within the water column and by the concentration of SPM and (*ii*) collision efficiency that varies as a function of water properties and mud, such as salinity and presence of gluey substances (e.g., organic coatings and biopolymers) (Van der Lee, 1998; 2001). Therefore, temporal variations not only in the quantity but also in the quality of the organic matter are important in determining aggregation and floc size. Polymeric substances that increase collision and aggregation efficiency consist mainly of polysaccharides produced by plankton, benthos and bacteria (Van der Lee, 2001). At the Pier, the presence of seagrass detritus and algae filaments was observed at several occasions during instrument deployment in the region. Further, several events of red tide took place close to the shore during the monitored months in 2003. Therefore, temporal variations in quality of biological communities (e.g. diatoms, bacteria) may also have contributed to the observed variability in the organic matter content for the same concentration of SPM (Figure 4.24) and biological binding efficiency, and consequently, to changes in floc sizes and settling velocities.

4.6. General assessment and conclusions

SEDVEL instrument presented consistent and reproducible results, when testing similar materials in the laboratory. Errors in the maximum estimated dry-masses may be related to uncertainties in the density of aggregates and in the definition of the zero position as well as

to superimposed changes in the instrument response due to variation in the water density during the experiments. However, results also suggested that some alteration of the floc population can take place under quiescent conditions generated inside the settling tube, especially at concentrations higher than 50 mg l^{-1}. Some authors recommend that estimation of settling velocities with the Owen-kind settling columns should be made within the first minutes after sampling in order to minimize floc alteration (Milligan, 1995; Dearnaley, 1996; Curran et al., 2003). SEDVEL measurements carried out in the laboratory suggested that measurements should take place at least for 15 minutes, especially at high concentrations (i.e. 200 mg l^{-1}) of fine sediment, until a slower-settling population is observed. Short periods of measurement could overestimate the average settling velocity of the population of particles and aggregates.

The majority of the devices used to measure settling velocities *in situ* are flow-intrusive (see Chapter 2). They usually confine or enclose a water volume to measure particles size and/or settling velocity, that eliminates or drastically reduces natural turbulence levels (Berlamont et al., 1993). Generating still conditions can induce diverse processes that alter aggregates' size or settling in relation to their behaviour in the undisturbed environment, as previously discussed (Section 2.6). Particularly for the SEDVEL instrument, still conditions are crucial for the proper functioning of the mass balance, since it is very sensitive to micrometric alterations in the pan position produced, e.g. by vibrations. Therefore, a better understanding of the processes going on inside of settling columns and simultaneous comparisons with processes taken place in the environment under similar shear stress conditions is needed in order to propose correction procedures to counteract effects generated by the apparatus.

In addition, small tube vibrations verified *in situ* during SEDVEL measurements and the existence of small secondary circulation inside the tube a few minutes after the pump has stopped can led to changes in the settling velocity of the aggregates. Also, the existence of residual turbulence from the fill-in period compromises the measurement of settling velocity of the largest particles (Agrawal and Pottsmith, 2000). For the SEDVEL instrument, the observed residual turbulence for about 1−2 minutes after the top pump has stopped compromises both the measurements of the fastest falling particles and the accurate determination of the zero position (*ZP*). Restricting the pan movement or fixing the balance plate during pan cleaning and water replacement could reduce the amount of time needed for the pan returning to its horizontal position and make the definition of *ZP* more precise.

Laboratory experiments reproduced better measured dry-concentrations than deployments carried out *in situ*. They were also subjected to less noise in the sensor output. The better performance of SEDVEL in the laboratory can be related to a number of factors, including: (*i*) higher homogeneity of the tested material in the laboratory in terms of grain size and organic matter content than occurred *in situ*, (*ii*) the use of controlled salinity and temperature conditions in the laboratory; (*iii*) the balance was recalibrated at the beginning of each experiment in the laboratory, while *in situ* the balance was calibrated only at the beginning of the deployment and small changes in the zero position occurred among the different cycles of measurement; (*iv*) a better definition of the starting zero position and a shorter time to the pan return to its horizontal (*ZP*) position was achieved under laboratory conditions and also; (*v*) in the laboratory the instrument was kept completely still, and hence, there was a minimal noise in the DVRT sensor readings, while *in situ* small high-frequency vibrations of the settling tube produced a relatively higher noise.

Although the field estimates of the dry-concentrations showed a larger scatter than observed in the laboratory (see Figures 4.9, 4.10 and 4.14), the computed settling spectra of mass distribution presented a consistent and reproducible behaviour among the different analysed cycles. Also, distinct settling behaviours were observed for the two sites of measurement, which where mainly attributed to differences in the floc population. It is worthwhile to note that the effective immersed masses were applied in the calculations of the mass distribution of settling velocity, and therefore, they were not subjected to errors inherent in the estimate of the density of flocs, which is the case for the dry-concentrations computation.

Another point to consider is that the pumping withdrawal system used in the SEDVEL instrument can possibly lead to some break-up of the largest fragile flocs (see Figure 4.21b), even though this problem was possibly minimized by sucking the water out of the tube and avoiding the sample passing through the pump (see Section 3.7). Future refinements of SEDVEL instrument should reduce the potential of floc break-up during sampling by replacing pumping for a less disruptive system. Problems associated with flocs disruption and changes in the natural turbulence levels due to water withdrawal and confinement are inherent to most devices used to measure the settling velocity in a flow-intrusive way. For example, the VISTA system (see Section 2.2.2) uses an on-deck pump to pull water through a 90-degree turn and up to a vertical section of a settling tube where a video camera is located

(Sanford et al., 2004). Measurements performed with VISTA *in situ* to estimate the settling velocities of aggregates, suggested that the adopted sampling withdrawal procedure disrupted the largest, weakest flocs. Another example is the LISST-ST (see Section 2.3.2), which uses a propeller to clean the settling column and the optic windows and filling the tube with a new fluid: within this system a faster suppression of the turbulence was achieved by using a narrow rectangular column (1 cm wide) inside the settling tube (Agrawal and Pottsmith, 2000). However, these authors did not address the possible effect of a shear induced break-up within the narrow measurement path nor a possible floc disruption induced by the propeller system. Even though several authors suggested a possible disruption of flocs due to an instrument induced turbulence for different kind of devices used to measure the settling velocity and size of aggregates *in situ* (e.g Dearnaley, 1997; Van der Lee, 1998; Sanford et al., 2004), the total amount of the disruption is difficulty to quantify (see Section 2.6).

In the future, the attachment of an underwater video camera to the settling column would permit the determination of the nature, shape and size of aggregates and the improvement of the estimates of particle volume. Further, a video system could also help to address the amount of instrument-induced floc disruption (during sampling) or reflocculation (during measurements). Further, measurements of mass together with the estimates of volume could be used to determine the density of the flocs and the excess density. Uncertainties remain in the assumptions on the three dimensional structure of the aggregates and on the volume of the interstitial water. The use of indirect fractal analysis or direct techniques to measure the aggregates' volume (e.g. holographic and shadowgraph method) can improve these measurements. Volume concentrations can also be obtained with laser diffraction techniques. An alternative approach that could be used to calculate the SPM volume is to use a sediment trap carousel to collect the material settled in a tube that contains an underwater balance. This set-up would permit the measurement of both the effective immersed (M_{EI}) and dry masses (M_{spm}) of SPM, and the particle volume (V_{spm}) could be calculated by assuming V_{spm} is equal to the volume of water displaced by the particles (V_w) at a known water density (ρ_w) through the relationship: $M_{spm} = M_{EI} + \rho_w V_w$. In all the above cases, simultaneous and direct measurements of the mass and volume of particles would considerably improve the aggregates density determination and the conversion of effective immersed masses into dry masses.

5. Summary and conclusion

The concentration and settling velocity of suspended particulate matter (SPM) are key parameters in the advection-diffusion model applied to describe the SPM mass transport, and their accurate determination has been regarded as a top priority in improving numerical models of cohesive sediment transport (Mcanally and Mehta, 2001). The determination of settling velocity *in situ* is essential because: (*i*) cohesive SPM occurs as aggregates of organic and inorganic particles, (*ii*) aggregates easily break up when sampled and manipulated, (*ii*) their settling velocity changes in space and time and (*iii*) their settling velocities are drastically different from those estimated on the basis of theoretical calculations for spherical inorganic particles. In the last four decades, a broad variety of techniques has been developed to measure the settling velocity of aggregates in the field, ranging from simple manually-operated devices to sophisticated automatic instrumentation. These techniques were reviewed in the Chapter 2. A brief description of the different devices, their working principle and their principal issues and advantages was presented, finalizing with an assessment of which factors should be taken into account when designing/building new devices for settling velocity measurements in the environment.

The discussion about the strength and weaknesses associated with each technique led to the conclusion that further instrumentation development is needed to automatically measure *in situ* the mass distribution of settling velocity and density of SPM. There is also a need to develop new mechanisms to enclose and replace water samples inside the settling columns in order to reduce the break-up of fragile flocs. Direct devices, which apply straightforward calibration to obtain SPM mass and settling velocity, have the advantage of reducing build-up errors that occur during data calibration and the mathematical procedures adopted for data analysis of the output of indirect devices. Settling tubes are the only devices available for directly quantifying the mass distribution of settling velocity. Further, direct measurements of SPM mass-concentration are only possible by collecting water samples through manually or automatically triggered bottles or through pumping. All these techniques require further laboratory analysis for gravimetric quantification of SPM mass-concentration, and therefore are labour intensive.

A new approach to directly measure the mass distribution of settling velocity of aggregates and mass-concentration of SPM in the field was designed and built. This new instrument (SEDVEL–Sedimentation Velocity) measures *in situ* the mass-concentration and settling velocity of particles and aggregates and consists of an automated mass balance that can work under water. SEDVEL directly measures the variation in time of the immersed weight of particulate matter (*PM*) as it settles on a plate located at the bottom of a settling tube, which is filled with water taken in the environment and kept under quiescent conditions. This instrument works under water and is fully automatic in terms of sampling, measurement, and data storage. Even though the SEDVEL working principle was based on that of the existent analytical mass balance for laboratory use, there are no other similar instruments able to measure mass of SPM *in situ*. It represents an innovation for its field of application and offers an alternative to measurement of the mass-distribution of settling velocities of cohesive sediment *in situ*. SEDVEL works moored to the seabed and it does not require extraction of subsamples to obtain sediment mass. This avoids the floc break-up and settling velocity alterations that are observed, e.g. in the Owen-kind tubes due to the development of small circulation inside the tube during the subsamples withdrawal and manoeuvring of the tube during its retrieval to the surface.

SEDVEL consists of a mass balance, which uses a magnetic spring system and a high-resolution displacement sensor that detects micrometric variations in the balance plate equilibrium position as particles/flocs settle on it. These changes are proportional to the immersed weight of the sediment, and the actual sediment mass can be obtained by calibration with known masses. The balance zero position (*ZP*, equilibrium position) corresponds to the initial distance between the balance plate (held in a horizontal position) and the head of the displacement sensor, which is set up by changing the relative distance between the pair of magnets (i.e. changing the repulsive force). The balance plate is made of aluminium and works as a conductive target for the displacement sensor.

The main body of the instrument consists of a settling tube and a sensor case which is connected to a data logger/controller unit and a battery case. These components are arranged on a tripod frame to be moored on the seabed. It also incorporates: (*i*) a pumping system for cleaning the balance plate and the settling tube, and a separate pump for replacing the water samples after each cycle of measurement and, (*ii*) a sealing tube system composed of two

sequential one-way silicone valves fitted to all tube inlets and outlets. These valves constituted a very simple and efficient system of closing the tube, since little turbulence is caused during the valves closure. It has also the advantage of not requiring complex and battery-powered mechanisms for the tube closure. However, the pumping system used for the water replacement generates turbulence and keeps a homogeneous mixing inside the tube, which can potentially lead to some floc break-up. The amount of floc disruption due to turbulence was not quantified and needs further investigation.

The total settling period used in each cycle of measurement can be set as required from a few minutes to many hours, with a minimum sampling interval of 20 s. The deployment period is limited by the capacity of the battery used to drive the pumps to a maximum of 3 to 5 days, depending on the period of time the pumps stay activated. SEDVEL can operate in concentrations ranging from 5 to about 200–500 mg l^{-1}, with a resolution better than 0.01 g. This upper limit of measurement can be extended to concentrations of 800−1000 mg l^{-1} by slightly changing the balance plate effective immersed mass and the relative distance between the pair of magnets, but with a smaller resolution. Settling velocities ranging from 0.09 to 16 mm s^{-1} can be measured if a settling period of 60 minutes is adopted.

Compared with other automated instruments, SEDVEL has a relatively simple working principle, calibration and data analysis procedure. Its calibration is straightforward, being performed by relating the balance plate (pan) displacement to the effective immersed mass of a standard weight (of known mass and density) placed on the top of the pan. As the balance plate is submerged its buoyancy, and hence the balance calibration, can change in different water densities. Considering a constant water density, a family of calibration curves can be obtained by adopting different zero positions. The greater the value of the zero position, the higher is the instrument sensitivity; but as the sensitivity increases the measurement range narrows. Further, it was found that the balance resolution increases as the accumulative weight on the pan increases. This is because the displacement sensor has a non-linear response with an increasing sensitivity as the distance between the sensor head and the target (i.e. pan) diminishes.

SEDVEL calibration has the advantage of not requiring multiple parameter calibrations and indirect mass estimation, and the size and shape of aggregates do not influence the instrument response, as occurs, e.g., with the optical sensors. Although calibration depends on the

medium density (salinity and temperature), these parameters can be easily measured in order to apply the correct calibration curve. A good reproducibility of the calibration was achieved for a given zero position. However, the instrument probably would not work efficiently in environments subjected to drastic variations in the SPM concentrations, ranging, for example, from a few milligrams per litre to a few grams per litre. This is because measurements at low SPM loads require high instrumental sensitivity, which leads to a narrower measurement range; while a lower sensitivity and a wider measurement range are recommended for areas with high SPM concentrations. Therefore, a wide range of concentrations could not be measured in a set of consecutive measurements, without sacrificing the instrument resolution.

The final balance sensitivity depends on a complex interaction of the following factors: (*i*) the relative force between the pair of magnets composing the balance magnetic spring system, which is dependent on the distance that they are set apart, (*ii*) the distance between the aluminium target (pan) and the DVRT sensor head, (*iii*) the balance plate mass (and buoyancy), and (*iv*) the torque exerted on the pan due to the suspension system. A good reproducibility of measurements can be achieved if the instrument configuration (e.g. balance plate material and position, suspension system, zero starting position) is kept constant among different cycles of measurement. Further research is needed to better understand the interactions among the factors listed above that can influence the balance resolution and calibration.

Apart from the adopted zero position, the homogeneity of settled material on the balance plate also interferes with the balance reading. This is because the balance plate works held by its smallest side, and the torque produced by a certain mass placed on the pan increases the further a particle (mass) is deposited from the pan support (suspension system). Maximum errors associated with an eventual non-homogeneous distribution of flocs on the pan were found to be around 20%. Additionally, the bigger the balance sensitivity, the larger is the absolute error associated with a non-homogeneous distribution. An eventual non-homogeneous distribution of flocs on the pan can affect the accuracy of the balance, while changes in the adopted zero position influences its sensitivity (resolution) and its range of measurement.

The zero position changes as a function of the water (fluid medium) density, presence of air bubbles and a non-complete cleaning of the material deposited on the pan in the previous

cycle of measurement. Variations in the density of the water among the different cycles of measurement can cause the *ZP* to change in relation to its position at the beginning of the deployment. It was observed in the laboratory that variations in salinity from 36 to 0 cause the zero position to rise up to $3-26\%$, depending on the starting zero position. Even small variation in the *ZP* can cause considerable variations in the estimate of the effective immersed mass, if the right calibration is not applied. Bubbles may be accidentally introduced in the tube during the tube filling before its deployment. If bubbles adhere to balance plate, they change the plate buoyancy and alter the *ZP* set-up, leading to a reduction in the sensitivity of the instrument. When bubbles were introduced to the tube they ruled out the first few cycles of measurement, after which they were usually eliminated and measurements could be performed.

SEDVEL can work both in freshwater and saltwater environments provided it has been calibrated at the environmental water density and an appropriate calibration curve has been adopted. Measurements could probably still be performed in environment subjected to large and fast variations in salinity (e.g. estuaries), but it is expected that the instrument *ZP* (and sensitivity) would change considerably among the experimental cycles, requiring a demanding calibration. A system that permitted the balance to be re-calibrated at the beginning of each cycle of measurement would considerably reduce the post-calibration effort and minimize the problem of the zero position drifting among the different cycles of measurement.

SEDVEL data analysis involved a few steps, namely: (*i*) the adoption of the zero starting position; (*ii*) the conversion of the raw sensor output to effective immersed mass by applying the appropriate calibration curve considering the zero position and the water densities at the beginning of each cycle of measurement, and (*iii*) fitting a curve to the cloud of measured points and extrapolating it to zero. Both the calibration curves and the curves fitted to the data presented, usually, $r^2 > 0.9$. In addition, the Odén's theory of sedimentation of polydisperse systems was applied to convert the accumulative effective immersed masses obtained from SEDVEL measurements into a frequency distribution of mass in each settling class.

The choice of the zero position is critical, since some subjectivity is involved in this process. This is because the residual turbulence inside the tube, when the top pump used to replace the

water sample stops, cause the balance plate to oscillate for about 2 minutes before its equilibrium position is reached and the measurements can be properly done. The observed residual turbulence compromises not only the accurate determination of the *ZP* but also the measurements of the settling velocity of the fastest falling aggregates. In addition, variations in the *ZP* among the different cycles of measurement in relation to that set-up at the beginning of the experiments also represented a problem, because this changes the instrument sensitivity and requires a demanding calibration procedure.

Because SEDVEL measures the effective immersed mass of particles and aggregates, their conversion to dry-masses demands knowing the floc density (ρ_f). As mentioned above there is no instrumentation available to directly measure the floc density *in situ*. Thus, the floc density has been mostly determined by estimating the effective density ($\rho_e = \rho_f - \rho_w$) by applying to the Stokes Law the values of size and settling velocity simultaneously measured *in situ*. In these calculations, a spherical particle shape is usually adopted and the volume of the interstitial water is computed in the total floc volume. An alternative approach to estimate floc density was applied to the SEDVEL data that relates the measured density of particulate matter (*PM*) to its organic content. Densities of *PM* were obtained in the laboratory through a hydrostatic weighting method. This method was used because it measures the immersed weight of *PM* in an analogous way to that used in SEDVEL immersed weight measurements. However, in this approach, a constant density is assumed for the whole population of flocs in suspension, but in fact aggregates within a sampling population can present different densities. The conversion of effective immersed mass in dry-mass was performed in order to compare SEDVEL estimates with dry-mass concentrations of SPM taken concomitantly in the field and quantified by the gravimetric method.

The performance of SEDVEL was tested both in the laboratory and in the field. In the laboratory, patterns of deposition of fine sediments and glass beads were analysed. SEDVEL gave consistent and reproducible results, when measuring similar particles type in the laboratory. It was able to reproduce the initial particles concentrations ranging from 7 to 200 mg l^{-1} ($r^2 > 0.9$, $p < 0.01$) in 13 laboratory experiments. Results also suggested that some particle reflocculation induced by the settling column can take place for concentrations higher than 50 mg l^{-1} in the laboratory conditions. A better understanding of the processes going on inside of settling columns and simultaneous comparisons with processes taken place

in the environment under similar shear stress conditions is needed in order to propose correction procedures to counteract effects generated by the apparatuses.

Field trials of SEDVEL were carried out at two locations in Cleveland Bay: the Pier (Strand Beach) and Berth 11 (Townsville Harbour). Although SEDVEL reproduced the general tendency of the SPM concentrations as measured from water bottle samples ($r^2 = 0.65$, $p <$ 0.01) in 42 cycles of measurement, a large scatter in the data was observed. Ratios between the dry-concentrations of SPM estimated from SEDVEL measurements and measured by gravimetric quantification of the water samples varied from 0.35 to 2.8. A number of factors were identified as causing the differences between the two methods, such as errors associated with: (*i*) an eventual non-homogeneous distribution of particles on the balance plate, (*ii*) the determination of the starting zero position, (*iii*) the gravimetric method used to determine mass-concentrations and organic content of SPM, and especially, (*v*) the conversions of effective immersed masses in dry masses.

Laboratory experiments reproduced better the measured dry-concentrations than deployments carried out in the field. They were also subjected to less noise in the sensor output. The better performance of SEDVEL in the laboratory can be also related to a number of factors, especially to: the higher homogeneity of the tested material in the laboratory in terms of grain size and organic matter content than occurred in the field, recalibration of the balance at the beginning of each experiment in the laboratory, while in the field the balance calibration occurs only at the beginning of the deployment although small changes in the zero position occurred among the different cycles of measurement, and a better definition of the starting zero position.

At the Pier, SPM concentrations ranged from about 5 to 170 mg l^{-1} in the measured cycles, with 3 to 19% of organic matter. Settling velocities presented a main mode of relatively slow-settling particles/flocs within $0.09 \leq W_s < 0.5$ mm s^{-1}, and usually a second mode of $1.5 \leq W_s$ < 3.0 mm s^{-1}. The settling dynamics at this location was mainly determined by erosion and deposition of sediment particles from and to the bed near the headland as well as by advection of offshore flocs populations during the rising tide. The measurements performed at Berth 11 encompassed low concentrations (8−30 mg l^{-1}) of an organically-rich (17−28%) suspended particulate matter, which showed only one mode of settling velocities between 0.09 and 0.12 mm s^{-1}. At this location, aggregates were composed mainly of microflocs of

low-density and slow settling velocities. The field trials proved that SEDVEL is a useful instrument to measure settling velocity of aggregates *in situ*.

5.1. Suggestions for future SEDVEL improvements

The work to date has produced "from scratch" a useful prototype instrument. Many different problems with the development have been overcome, and with the field and the laboratory trials carried out, significant improvements to the design have been identified. These improvements are listed below:

- Better definition of the zero position (*ZP*) at the beginning of each cycle of measurement could be achieved either holding the balance plate still during the cleaning or restricting its movement. This could reduce the amount of time needed to the pan return to its horizontal position and could make *ZP* definition more precise. This improvement if also associated with the use of a taller settling column, so the fastest particles would take longer to reach the bottom, would permit the measurement of a wider range of velocities, especially the larger velocities.

- The amount of time need to damp the turbulence inside the tube should be reduced in order to better delineate the settling behaviour of the fastest settling particles. Ideally zero or little turbulence should be generated during the water replacement. It is advisable to change the pumping system for a less disruptive system of sample withdrawal. This system has to be able of producing a homogeneous distribution of particles inside the tube without breaking the fragile flocs and generating little turbulence that could be quickly damped. A new system where the whole tube could open and close (or move up and down) could be tried.

- Simple design solutions such as making a shorter pan, and attaching the small magnets on the centre of mass of the pan could increase the SEDVEL accuracy by reducing problems associated with a non-homogeneous distribution of particles. Also, reducing the balance plate volume while keeping the same weight would reduce its buoyancy, and therefore, the balance would suffer less influence of medium density

on its calibration, and the amount of variation of the zero position among the different cycles of measurement would diminish.

- Both a high sensitivity and a broad range of measurements could be achieved by using two different balance plates (with distinct buoyancies) inside a bigger tube or two small tubes.

- A re-calibration of the SEDVEL balance at the beginning of each cycle of measurement would considerably reduce the post-calibration effort and minimize the problem of zero position drifting among the different cycles of measurement. This could be done by relating the distance between the two magnets to the immersed weight of the pan at different water densities and at a particular zero position. Therefore, if the water density was determined at the beginning of each experimental cycle in the field, a feedback system within the data logger could control the necessary number of turns of the magnet motor to bring it back to its original position, i.e. a constant *ZP* regardless the water density.

- The use of a displacement sensor with a linear calibration, if existent, would permit a constant instrument resolution for the whole range of measurements, since the displacement of the balance plate as a function of the accumulative mass shows a linear behavior.

- The integration of the underwater balance with video/holographic techniques would allow direct measurements of three main aggregates characteristics: mass, settling velocities and size. Further, measurements of mass together with the estimates of volume could be used to determine the density of the flocs and the excess density. Care must be taken however because devices that measure mass give an integrated mass distribution for the whole aggregate population, while video image techniques analyse floc by floc within a size range depending on instrument resolution. Further, a video system could also help to address the amount of instrument-induced floc disruption (during sampling) or reflocculation (during measurements).

- The whole device should be more portable to facilitate deployment and more robust to reduce tube vibrations. A double-walled tube fitted with some insulating material could be used to both absorb and damp some vibrations caused by the water turbulence and thermal insulation. The thermal insulation is highly recommended for avoiding changes of the water temperature during calibration, while SEDVEL is still outside of the water, as well as during the underwater measurements. The introduction of bubbles to the settling tube should be reduced by trying different designs of the filling system.

- A tripod incorporating an automatic levelling and locking system, in which the main body of the instrument (with a heavy base) could pivot to be adjusted to work in the vertical position, would avoid sloping of the balance plate and reduce the instrument bias.

References

Adams, A.T. 1971. Electromagnetics for engineers. The Ronald Press Company, New York.

Adams, E.E., Stolzenbach, K.D., Lee J.J., Caroli, J., Funk, D. 1998. Deposition of contaminated sediments in Boston Harbor studied using fluorescent dye and particles tracers. Est. Coast. Shelf Sci. 46, 371-382.

Agrawal, Y.C., Pottsmith, H.C. 2000. Instruments for particle size and settling velocity observations in sediment transport. Mar. Geol. 168, 89-114.

Allen, T. 1981. Particle size measurement (3rd Edition). Chapman and Hall, London, 678 p.

Allersma, E. 1980. Mud in estuaries and along coasts. Proc. Int. Symp. Riv. Sedim. Beijing, China, pp. 663-685.

Arms, S. 2004. MicroStrain, Steven Arms (President), Inc.310 Hurricane Lane Suite #4, Williston, VT 0549, U.S.A., http://www.microstrain.com/NCDVRT.htm (noncontacting_flier_r3.pdf).

Asper, V.L. 1996. Particle flux in the ocean: oceanographic tools. In: Particle Flux in the Ocean. Ittekkot, V., Schafer, P., Depetris, P.J. (Eds.), John Wiley & Sons Ltd, pp. 71-84.

Ayukai, T., Wolanski, E. 1997. Importance of biologically mediated removal of fine sediments from he Fly River plume, Papua New Guinea. Est. Coast. Shelf Sci. 44, 629-639.

Bale, A.J. 1996. In situ laser optical particle sizing. J. of Sea Res., 36 (1-2), 31-36.

Bartz, R., Zaneveld, J.R.V., McCave, I.N., Hess, F.R., Nowell, A.R.M. 1985. Rost and Beast: devices for in-situ measurement of particle settling velocity. Mar. Geol. 66, 381-395.

Berlamont, J., Ockenden, M., Toorman, E., Winterwerp, J. 1993. The characterisation of cohesive sediment properties. Coastal Engineering 21, 105-128.

Boss, E., Pegau, W.S., Gardner, W.D., Zaneveld, J.R.V., Barnard, A.H., Twardowski, M.S., Chang, G.C., Dickey, T.D. 2001. Spectral particulate attenuation and particle size distribution in the bottom boundary layer of a continental shelf. J. Geophys. Res. 106 (C5), 9509-9516.

Burt, T.N. 1986. Field settling velocities of estuary muds. In: Estuarine cohesive sediment dynamics. Lecture Notes on Coastal and Estuarine Studies. Mehta, A.J. (Ed.), Springer-Verlag, Chapter VII, pp. 126-150.

Carder, K.L., Steward, R.G., Betzer, P.R. 1982. In situ holographic measurements of the sizes and settling rates of oceanic particulates. J. Geophys. Res. 87 (C8), 5681-5685.

Carter, R.M. and Larcombe, P. 2002. Geology and sedimentary characteristics of Cleveland Bay. In: Cleveland Bay consortium, http://www.clevelandbayconsortium.com, pp. 37-54.

Chalvidan, V., Chambard, J.P., Craig, G., Diard, A., Foresti, G.L., Forre, B., Gentili, S., Hobson, P.R., Lampitt, R.S., Maine, P., Malmo, J.T., Nareid, H., Pescetto, A., Watson, J. 1998. High-resolution in situ holographic recording and analysis of marine organisms and particles (HOLOMAR). IEEE, Piscataway, NJ (USA) Ocean Engineering Soc. Oceans 98 – Engineering for sustainable use of the oceans: Conference proceedings 28 September – 1 October 1998, Nice (France). Vol. 3, pp. 1599-1603.

Chen, S., Eisma, D. and Kalf, J. 1994. In situ size distribution of suspended matter during the tidal cycle in the Elbe estuary. Neth. J. Sea Res. 32 (1), 37-48.

Cornelisse, J.M. 1996. The field pipette withdrawal tube (FIPIWITU). J. of Sea Res., 36 (1-2), 37-39.

Costello, D.K., Carder, K.L., Betzer, P.R., Young, R.W. 1989. In situ holographic imaging of settling particles: applications for individual particle dynamics and oceanic flux measurements. Deep-Sea Res. 36 (10), 1595-1605.

Curran, K.J., Hill, P.S., Milligan, T.G. 2003. Time variation of floc properties in a settling column. J. Sea Res. 49, 1-9.

Dearnaley, M.P. 1996. Direct measurements of settling velocities in the Owen tube: a comparison with gravimetric analysis. J. of Sea Res. 36 (1-2), 41-47.

Dearnaley, M.P. 1997. Direct measurements of settling velocities in the Owen tube: a comparison with gravimetric analysis. In: Burt, N., Parker, R., Watts, J. (Eds.), Cohesive Sediments. John Wiley & Sons Ltd, pp. 75-85.

Design Guide 2000. Total magnetic solutions, http://www.magnetsales.com/Design/ DesignG_frames/ frame_dgbod2.htm#modernmag.

Dietrich, W.E. 1982. Settling velocity of natural particles. Water Resources Res. 18 (6), 1615-1626.

Dobbs, E.R. 1984. Electricity and Magnetism. Student Physics Series, IBM PressRoman, 128 p.

Douglas, R.W., Rippey, B., Gibson, C. 2003. Estimation of the in-situ settling velocity of particles in lakes using a time series sediment trap. Freshwater Biology 48, 512-518.

Dreisbach, F. and Lösch, H.W. 1999. A new type pf magnetic suspension balance for gravimetric measurements of ad- and desorption processes in fixed adsorbent beds 4th Topical conference on separations science and technology, 1-7.

Dreisbach, F. and Lösch, H.W. 2000. Magnetic suspension balance for simultaneous measurement of a sample and the density of the measuring fluid. Journal of Thermal Analysis and Calorimetry, 62, 515-521.

Duffin, W.J. 1980. Electricity and magnetism (3rd Edition), McGraw-Hill Book Company, UK, Chapter 12, pp. 331-363.

Dyer, K.R. 1986. Coastal and estuarine sediment dynamics. John Wiley & Sons Ltd, 341 p.

Dyer, K.R. 1995. Sediment transport processes in estuaries. In: Perillo, G.M.E. (Ed.), Geomorphology and sedimentology of estuaries. Developments in sedimentology. Elsevier Science B.V., pp. 423-449.

Dyer, K.R., Cornelisse, J., Dearnaley, M.P., Fennessy, M.J., Jones, S.E., Kappenberg, J., McCave, I.N., Pejrup, M., Puls, W., Van Leussen, W. and Wolfstein, K. 1996. A comparison of in situ techniques for estuarine floc settling velocity measurements. J. Sea Res. 36 (1-2), 15-29.

Eisma, D., Kalf, J. 1996. In situ particle (floc) size measurements with the NIOZ in situ camera system. J. of Sea Res. 36 (1-2), 49-53.

Eisma, D. 1986. Flocculation and de-flocculation of suspended matter in estuaries. Neth. J. Sea Res. 20 (2/3), 183-199.

Eisma, D., Bale, A.J., Dearnaley, M.P., Fennessy, M.J., Van Leussen, W., Maldiney, M.A., Pfeiffer, A., Wells, J.T. 1996. Intercomparison of in situ suspended matter (floc) size measurements. J. of Sea Res. 36 (1-2), 3-14.

Eisma, D., Bernard, P., Cadée, G.C., Ittekkot, V., Kalf, J., Laane, R., Martin, J.M., Mook, W.G., Van Put, A., Schuhmacher, T. 1991. Suspended-matter particle size in some West-European estuaries; Part I: particle-size distribution. Neth. J. Sea Res. 28 (3), 193-214.

Eisma, D., Dyer, K.R., Van Leussen, W. 1997. The in situ determination of the settling velocities of suspended fine-grained sediment–a review. In: Burt, N., Parker, R., Watts, J. (Eds.), Cohesive Sediments. John Wiley & Sons Ltd, 17-44.

Eisma, D., Li, A. 1993. Changes in suspended-matter floc size during the tidal cycle in the Dollard estuary. Neth. J. Sea Res. 31 (2), 107-117.

Eisma, D., Schuhmacher, T., Boekel, H., Van Héerwaarden, J., Franken, H., Laan, M., Vaars, A., Eijgenraam, F., Kalf, J. 1990. A camera and image-analysis system for in situ observations of flocs in natural waters, Neth. J. Sea Res. 27 (1), 43-56.

Ellis, K.M., Bowers, D.G., Jones, S.E. 2004. A study of the temporal variability in particle size in a high-energy regime. Est. Coast. Shelf Sci. 61 (2), 311-315.

Fennessy, M.J., Dyer, K.R. 1996. Floc population characteristics measured with INSSEV during the Elbe estuary intercalibration experiment. J. of Sea Res. 36 (1-2), 55-62.

Fennessy, M.J., Dyer, K.R., Huntley, A., Bale, A.J. 1997. Estimation of settling flux spectra in estuaries using INSSEV. In: Burt, N., Parker, R., Watts, J. (Eds.), Cohesive Sediments. John Wiley & Sons Ltd, pp. 87-104.

Fennessy, M.J., Dyer, K.R., Huntley, D.A. 1994. INSSEV: an instrument to measure the size and settling velocity of flocs in situ. Mar. Geol. 117, 107-117.

Fischer, M.A., Odén, S. 1923-24. The theory of the mechanical analysis of sediments by means of the automatic balance. Proceedings of the Royal Society of Edinburgh, Vol. 44, pp. 98-115.

Fugate, D.C., Friedrichs, C.T. 2002. Determining concentration and fall velocity of estuarine particle populations using ADV, OBS and LISST. Cont. Shelf Res. 22, 1867-1886.

Fugate, D.C., Friedrichs, C.T. 2003. Controls on suspended aggregate size in partially mixed estuaries. Est. Coast. Shelf Sci. 58, 389-404.

Gartner, J.W. 2002. Estimation of suspended solids concentrations based on acoustic backscatter intensity: theoretical background. Turbidity and other sediment surrogates workshop, Reno, NV.

Gibbs, R.J. 1985. Estuarine flocs: their size, settling velocity and density. J. Geophys. Res. 90 (C2), 3249-3251.

Group Arnold, 2000. Soft magnets application guide. Group Arnold, the magnetic products group of SPS technologies, www.grouparnold.com, 11p.

Hamm, L., Migniot, C. 1994. Elements of cohesive sediment deposition, consolidation and erosion. In: Coastal, estuarial and harbour engineers' reference book. Abbott, M.B., Price, W.A. (Eds.), E & FN Spon, Melbourne, Chapter 7, pp. 93-106.

Hatcher, A., Hill, P., Grant, J., Macpherson, P. 2000. Spectral optical backscatter of sand in suspension: effects of particle size, composition and colour. Mar. Geol., 168, 115-128.

Heffler, D.E., Syvitski, J.P.M., Asprey, K.W. 1991. The floc camera. In: Syvitski, J.P.M. (Ed.). Principles, methods and application of particle size analysis. Cambridge University Press, New York, pp. 209-221.

Hill, P.S., Sherwood, C.R., Sternberg, R.W., Nowell, A.R.M. 1994. In situ measurements of particle settling velocity on the northern California continental shelf. Cont. Shelf Res. 14 (10/11), 1123-1137.

Hill, P.S., Syvitski, J.P., Cowan, E.A., Powell, R.D. 1998. In situ observations of floc settling velocities in Glacier Bay, Alaska. Mar. Geol. 145, 85-94.

Hill, P.S., Milligan, T.G., Geyer, W.R. 2000. Controls on effective settling velocity of suspended sediment in the Eel River flood plume. Cont. Shelf Res. 20, 2095-2111.

Holdaway, G.P., Thorne, P.D., Flatt, D., Jones, S.E., Prandle, D. 1999. Comparison between ADCP and transmissometer measurements of suspended sediment concentration. Cont. Shelf. Res. 19, 421-441.

Hyams, D. 2001. CurveExpert Version 1.38. A curve fitting system for Windows, double precision, 32 bit-package.

Jackson, G.A., Maffione, R., Costello, D.K., Alldredge, A.L., Logan, B.E., Dam, H. G. 1997. Particle size spectra between 1 um and 1 cm at Monterey Bay determined using multiple instruments. Deep-Sea Res. I 44 (11), 1739-1767.

Jago, C.F., Jones, S.E. 1998. Observation and modelling of the dynamics of benthic fluff resuspended from a sandy bed in the southern North Sea. Cont. Shelf Res. 18, 1255-1282.

Jiles, D. 1991. Introduction to magnetism and magnetic materials, Chapman & Hall (Ed.), 440 p.

Johnson, C. P., Xiaoyan, L., Logan, B. E. 1996. Settling velocities of fractal aggregates. Environ. Sci. Technol. 30, 1911-1918.

Jones, S.E., Jago, C.F., Bale, A.J., Chapman, D., Howland, R.J.M., Jackson, J. 1998. Aggregation and resuspension of suspended particulate matter at a seasonally stratified site in the southern North Sea: physical and biological controls. Cont. Shelf Res. 18, 1283-1309.

Jones, S.E., Jago, C.F. 1996. Determination of settling velocity in Elbe estuary using QUISSET tubes. J. of Sea Res. 36 (1-2), 63-67.

Katz, J., Donaghay, P.L., Zhang, J., King, S., Russel, K. 1999. Submersible holocamera for detection of particle characteristics and motions in the ocean. Deep-Sea Res. Part I: Oceanographic Research papers 46 (8), 1455-1481.

Kawanisi, K., Yokosi, S. 1997. Characteristics of suspended sediment and turbulence in a tidal boundary layer. Cont. Shelf Res. 17 (8), 859-875.

Kim, A.S., Stolzenbach, K.D. 2004. Aggregate formation and collision efficiency in differential settling. Journal of Colloid and Interface Science 271, 110-119.

Kineke, G.C., Sternberg, R.W. 1989. The effect of particle settling velocity on computed suspended sediment concentration profiles. Mar. Geol. 90, 159-174.

Kineke, G.C., Sternberg, R.W., Johnson, R. 1989. A new instrument for measuring settling velocities in situ. Mar. Geol. 90, 149-158.

Knowles, S.C., Wells, J.T. 1996. Suspended aggregate analyses using ISAAC, Elbe river, 9-10 June 1993. J. of Sea Res. 36 (1-2), 69-75.

Kranck, K. 1986. Settling behavior of cohesive sediment. In: Mehta, A.J. (Ed.), Estuarine cohesive sediment dynamics. Lecture Notes on Coastal and Estuarine Studies. Springer-Verlag, Chapter VIII, pp. 150-169.

Kranck, K., Petticrew, E., Milligan, T.G., Droppo, I.G. 1993. In situ particle size distributions resulting from flocculation of suspended sediment. In: Mehta, A. J. (Ed.), Coastal

and estuarine studies. Nearshore and estuarine cohesive sediment transport. American Geophysical Union, Washington, pp. 60 –74.

Krishnappan, B.G., 2000. In situ size distribution of suspended particles in the Fraser River. Journal of Hydraulic Engineering 126 (8), 561-569.

Krone, R.B., 1986. The significance of aggregate properties to transport processes. In: Mehta, A.J. (Ed.), Estuarine cohesive sediment dynamics. Lecture Notes on Coastal and Estuarine Studies. Springer-Verlag, Chapter IV, p: 66-84.

Krone, R.B., 1993. Sedimentation revisited. In: Mehta, A. J. (Ed.), Coastal and estuarine studies. Nearshore and estuarine cohesive sediment transport. American Geophysical Union, Washington, pp. 108 –126.

Krumbein, W.C., Pettijohn, F.J. 1938. Manual of sedimentary petrography. Appleton Century Crofts, Inc, Chapter 5, pp. 91-134.

Larcombe, P., Ridd, P.V., Prytz, A., Wilson, B. 1995. Factors controlling suspended sediment on inner-shelf coral reefs, Townsville, Australia. Coral Reefs, 14: 163-171.

Law, D.J., Bale, A.J. 1998. In situ characterization of suspended particles using focused-beam laser reflectance particle sizing. In: Black, K.S., Paterson, D.M., Cramp, A. (Eds.), Sedimentary processes in the intertidal zone, Geological Society, London, Special Publications, 139, pp. 57-68.

Law, D.J., Bale, A.J., Jones, S.E. 1997. Adaptation of focused beam reflectance measurement to in-situ particle sizing in estuaries and coastal waters. Mar. Geol. 140, 47-59.

Lick, W., Huang, H. 1993. Flocculation and the physical properties of flocs. In: Mehta, A.J. (Ed.), Nearshore and estuarine cohesive sediment transport, Coastal and Estuarine Studies 42. American Geophysical Union, pp. 21-39.

Lorrain, P., Corson, D.R. 1970. Electromagnetic fields and waves (2nd Edition), W.H. Freeman and Company, San Francisco.

Lou, J. 1995. Modelling of hydrodynamics and suspended sediment transport in coastal areas. Thesis for degree of Doctor in Philosophy in the Department of Physics at James Cook University, 243 p.

Lovell, C.J., Rose, C.W. 1991a. Wake-capture effects observed in a comparison of methods to measure particle settling velocity beyond Stokes' range. Journal of Sedimentary Petrology 61 (4), 575-582.

Lovell, C.J., Rose, C.W. 1991. The effects of sediment concentration and tube-diameter on particle settling velocity measured beyond stokes range: experiment and theory. Journal of Sedimentary Petrology, 61 (4), 583-589.

Lynch, J.F., Irish, J.D., Sherwood, C.R., Agrawal, Y.C. 1994. Determining suspended particle size information from acoustical and optical backscatter measurements. Cont. Shelf Res. 14 (10/11), 1139-1165.

Malkiel, E., Alquaddoomi, O. Katz, J. 1999. Measurements of plankton distribution in the ocean using submersible holography. Meas. Sci. Technol. 10, 1142-1152.

Mann, C.J., Wetzel, R.G., 2000. Hydrology of an impounded lotic wetland–wetland sediment characteristics. Wetlands 20 (10), 23-32.

Manning, A.J., Dyer, K.R. 2002a. The use of optics for the in situ determination of flocculated mud characteristics. J. Opt. A: Pure Appl. Opt. 4, S71-S81.

Manning, A.J., Dyer, K.R. 2002b. A comparison of floc properties observed during neap and spring tidal conditions. In: Winterwerp, J.C, Kranenburg, C. (Eds.), Fine Sediment Dynamics in the Marine Environment, Elsevier Science B, 233-250.

Manning, A.J., Dyer, K.R. 1999. A laboratory examination of floc characteristics with regard to turbulent shearing. Mar. Geol. 160, 147-170.

Mantovanelli, A., Noernberg, M.A., Marone, E., Silva, E.T., 1999. Evaluation of turbidity sensor response in different concentrations and sizes of sediment and comparison with field measurements. Boletim Paranaense de Geociências, 47, 101-109.

Markofsky, M., Lang, G., Schubert, R. 1986. Suspended sediment transport in rivers and estuaries. In: Van de Kreeke, J., Physics of Shallow Estuaries and Bays, Notes Coastal Estuarine Stud., vol. 16, Springer, New York, pp. 210–227.

Mcanally, W.H., Mehta, A.J., 2001. Coastal and estuarine fine sediment processes. Proceedings in Marine Science 3, Elsevier, 507 p.

McCave, I.N. & Gross, T.F., 1991. In-situ measurements of particle settling velocity in the deep sea. Mar. Geol. 99, 403-411.

Mehta, A., McAnally Jr., W.H., Hayter, E.J., Teeter, A.M., Schoellhamer, D., Heltzel, S.B., Carey, W.P., 1989. Cohesive sediment transport II: application. J. Hydraulic Eng. 115 (8): 1094-1112.

Mehta, A.J. 1986. Characterization of cohesive sediment properties and transport processes in estuaries. In: Mehta, A.J. (Ed.), Estuarine cohesive sediment dynamics. Lecture Notes on Coastal and Estuarine Studies. Springer-Verlag, Chapter XV, pp. 290-325.

Mehta, A.J. 1988. Laboratory studies on cohesive sediment deposition and erosion. In: Dronkers, J., Van Leussen (Eds.), Physical processes in estuaries. Springer-Verlag, Berlin, pp. 427-445.

Mehta, A.J. 1994. Cohesive sediments in coastal engineering applications. In: Abbott, M.B., Price, W.A. (Eds.), Coastal, estuarial and harbour engineers' reference book. E & FN Spon, Melbourne, pp. 597-613.

Mikkelsen, O. A., Milligan, T.G., Hill, P.S., Moffatt, D. 2004. INSSECT-an instrument platform for investigating floc properties close to the seabed. Limnol. Oceanogr.: Methods 2, 226-236.

Mikkelsen, O. A., Pejrup, M. 2000. In situ particle size spectra and density of particle aggregates in a dredging plume. Mar. Geol. 170, 443-459.

Mikkelsen, O. A., Pejrup, M. 2001. The use of a LISST-100 laser particle sizer for in-situ estimates of floc size, density and settling velocity. Geo-Marine Letters 20, 187-195.

Mikkelsen, O., Pejrup, M. 1998. Comparison of flocculated and dispersed suspended sediment in the Dollard estuary. In: Black, K.S.; Paterson, D.M., Cramp, A. (Eds.), Sedimentary processes in the intertidal zone, Geological Society, London, Special Publications 139, pp. 199-209.

Milligan, T.G. 1995. An examination of the settling behaviour of a flocculated suspension. Neth. J. Sea Res. 33 (2), 163-171.

Milligan, T.G. 1996. In situ particle (floc) size measurements with the benthos 373 plankton silhouette camera. J. of Sea Res. 36 (1-2), 93-100.

Milligan, T.G., Hill, P.S. 1998. A laboratory assessment of the relative importance of turbulence, particle composition, and concentration in limiting maximal floc size and settling behaviour. J. Sea Res. 39, 227-241.

Muller, J. 2002. Sediment transport on the Strand, Rowes Bay and Pallarenda beaches, Townsville, Australia. B.Sc. (Hons.) Thesis, James Cook University, Townsville.

Murray, P.B., McCave, I.N., Owen, T.R.E., Mason, M. and Green, M.O. 1996. A robust in situ settling velocity box for coastal seas. J. of Sea Res. 36 (1-2), 101-107.

NDT 2004. Resource Centre. http://www.ndt-ed.org/index_flash.htm.

Nichols, M.M. 1986. Effects of fine sediment resuspension in estuaries. In: A.J. Mehta (Ed.), Estuarine cohesive sediment dynamics. Lecture Notes on Coastal and Estuarine Studies. Springer-Verlag, Chapter II, pp. 5-42.

Odd, N.V.M. 1988. Mathematical modelling of mud transport in estuaries. In: Dronkers, J., Van Leussen, W. (Eds.), Physical processes in estuaries. Springer-Verlag, pp. 503-531.

Orpin, A.R., Ridd, P.V., Stewart, L.K. 1999. Assessment of the relative importance of major sediment-transport mechanisms in the central Great Barrier Reef lagoon. Australian Journal of Earth Sciences 46, 883-896.

Osborne, P.D., Vincent, C.E., Greenwood, B. 1994. Measurement of suspended sand concentrations in the nearshore: field intercomparison of optical and acoustic backscatter sensors. Cont. Shelf Res. 14 (2/3), 159-174.

OUCT, 1989. Waves, tides and Shallow-water processes. The Open University Course Team. Oceanography Course Team, Vol. 4, 187 p.

Owen, M.W. 1971. The effect of turbulence on the settling velocities of silt flocs. Proc. 14th Congres. Of IAHR, Paris 4, D4-1-D4-5.

Owen, M.W. 1976. Determination of the settling velocities of cohesive muds. Hydraulic Research Station, Wallingford, Report N° IT 161, pp. 1-8.

Owen, R.B., Zozulya, A.A. 2000. In-line digital holographic sensor for monitoring and characterizing marine particulates. Opt. Eng. 39 (8), 2187-2197.

Partheniades, E. 1993. Turbulence, flocculation and cohesive sediment dynamics. In: Mehta, A.J. (Ed.), Coastal and estuarine studies. Nearshore and estuarine cohesive sediment transport. American Geophysical Union, Washington, pp. 40 -59.

Pejrup, M., Edelvang, K. 1996. Measurements of in situ settling velocities in the Elbe estuary. J. of Sea Res. 36 (1-2), 109-113.

Pejrup, M. 1988. Flocculated suspended sediment in a micro-tidal environment. Sed. Geol. 57 (3-4), 249-256.

Puls, W., Kühl, H. 1996. Settling velocity determination using the BIGDAN settling tube and the Owen settling tube. J. of Sea Res. 36 (1-2), 119-125.

Puls, W., Kuehl, H., Heymann, K. 1988. Settling velocity of mud flocs: results of field measurements in the Elbe and Weser Estuary. In: Dronkers, J., Van Leussen, W. (Eds.), Physical processes in estuaries. Springer-Verlag, Berlin, pp. 405-425.

Rawle, A. 2005. Basic principles of particle size analysis. Malvern Instruments, http//www.malvern.co.uk.

Renagi, O., 1999. Optical instrumentation for measuring sediment siltation rates. Master Thesis of Science in Department of Physics, James Cook University of North Queensland, 90 p.

Richards, S.D. 1998. The effect of temperature, pressure, and salinity on sound attenuation in turbid seawater. J. Acoust. Soc. Am. 103 (1), 205-211.

Ridd, P., Larcombe, P. 1994. Biofouling control for optical backscatter suspended sediment sensors. Mar. Geol. 116 (3-4), 255-258.

Ridd, P., Day, G., Thomas, S., Harradence, J., Fox, D., Bunt, J., Renagi, O., Jago, C. 2001. Measurement of sediment deposition rates using an optical backscatter sensor 2001. Est. Coastal and Shelf Sci. 52, 155-163.

Rigler, J.K., Collins, M.B., Williams, S.J. 1981. A high precision, digital-recording sedimentation tower for sands. Journal of Sedimentary Petrology, 51 (2), 642-644.

Rose, C.P., Thorne, P. D. 2001. Measurements of suspended sediment transport parameters in a tidal estuary. Cont. Shelf Res. 21, 1551-1575.

Rouse, H. 1937. Modern conceptions of the mechanics of fluid turbulence. Transactions of the America Society of Civil Engineers 102, 463-541.

Sanford, L.P., Dickhudt,P.J., Rubiano-Gomez, L., Yates, M., Suttles, S.E., Friedrichs, C.T., Fugate, D.D. and Romine, H. 2004. Variability of suspended particle concentratations, sizes and settling velocities in the Chesapeake Bay turbidity maximum. In: Droppo, I.G., Leppard, G.G., Liss, P., Milligan, T., Flocculation in natural and engineered environmental systems. CRC Press, LLC, Boca Raton, Florida, in press.

Sequoia Scientific. Application Note L002. Measuring the volume scattering function using Lisst-100. WWW Page, http://www.sequoiasci.com.

Sequoia Scientific. Application Note L007. The size resolution of the LISST series of instruments. WWW Page, http://www.sequoiasci.com.

Sequoia Scientific. Application Note L008. estimating the size-dependent settling velocity of suspended particles using the LISST-ST. WWW Page, http://www.sequoiasci.com.

Serra, T., Casamitjana, X., Colomer, J. 2002. Observations of the particle size distribution and concentration in a coastal system using an in situ laser analyzer. Mar. Technol. Soc. J. 36 (1), 59-69.

Sheng, J., Hay, A.E. 1988. An examination of the spherical scatterer approximation in aqueous suspensions of sand. Journal of the Acoustic Society of America 83 (2), 598-610.

Skinner, J. 2000. Pipet and x-ray grain-size analysers: comparison of methods and basic data. Federal interagency sedimentation project, Report 00, Vicksburg, WWW Page, http://fisp.wes.army.mil.

Smith, C.J. 1960. A degree physics. Part V. Electricity and magnetism, Edward Arnold (Publishers) Ltd., London.

Sternberg, R.W., Berhane, I., Ogston, A.S. 1999. Measurement of size and settling velocity of suspended aggregates on the northern California continental shelf. Mar. Geol. 154, 43-53.

Sternberg, R.W., Ogston, A., Johnson, R. 1996. A video system for in situ measurement of size and settling velocity of suspended particulates. J. of Sea Res. 36 (1-2), 127-130.

Stokes, G.G. 1851. On the effect of the internal friction of fluids on the motion of pendulums. Transactions of Cambridge Philosophical Society, Vol. IX: 8-106. Reprinted in Mathematical and Physical Papers, 2nd ed., Vol. 3Johnson Reprint Corp., p1, 1966.

Stolzenbach, K.D. 1993. Scavenging of small particles by fast-sinking porous aggregates. Deep-Sea Res. I 40 (2), 359-369.

Stolzenbach, K.D., Elimelech, M. 1994. The effect of particle density on collisions between sinking particles: implications for particle aggregation in the ocean. Deep-Sea Res. I 41 (3), 469-483.

Subcommittee on Sedimentation 1943. A study of methods used in measurement and analysis of sediment loads in streams. A study of new methods for size analysis of suspended sediment samples, Report 7. Published by Project Offices of Cooperating Agencies at St. Paul U.S. Engineer District Sub-Office Hydraulic Laboratory, University of Iowa, Iowa City, Iowa, 102 p.

Subcommittee on Sedimentation 1953. A study of methods used in measurement and analysis of sediment loads in streams. Accuracy of sediment size analysis made by the bottom withdrawal tube method, Report 10. Published by Project Offices of Cooperating Agencies, 115 p.

Sutherland, T.F., Lane, P.M., Amos, C.L., Dowing, J. 2000. The calibration of optical backscatter sensors for suspended sediment of varying darkness levels. Mar. Geol. 162, 587-597.

Syvitski, J.P.M. and Hutton, E.W.H. 1996. In situ characteristics of suspended particles as determined by the floc camera assembly FCA. J. of Sea Res. 36 (1-2), 131-142.

TDK 2003. Neorec Series. http://www.tdkchina.com/pdf/e331.pdf.

Teisson, C. 1997. A review of cohesive sediment transport models. In: Burt, N., Parker, R., Watts, J. (Eds.), Cohesive sediments. John Wiley & Sons Ltd., pp. 367-381.

Ten Brinke, W.B.M. 1994. In situ aggregate size and settling velocity in the Oosterschelde tidal basin (The Netherlands). Netherlands Journal of Sea Research 32 (1), 23-35.

Ten Brinke, W.B.M. 1997. Temporal variability in aggregate size and settling velocity in the Oosterschelde (The Netherlands). In Burt, N.; Parker, R., Watts, J. (Eds.), Cohesive sediments. John Wiley & Sons Ltd., pp. 63-73.

Thomas, S., Ridd, P. V. 2004. Review of methods to measure short time scale sediment accumulation. Mar. Geol. 207 (1-4), 95-104.

Thorne, P.D., Hanes, D.M. 2002. A review of acoustic measurement of small-scale sediment processes. Cont. Shelf Res. 22, 603-632.

Thorne, P.D., Vicent, C.E., Hardcastle, P.J., Rehman, S., Pearson, N. 1991. Measuring suspended sediment concentrations using acoustic backscatter devices. Mar. Geol. 98, 7-16.

Traykovski, P., Latter, R.J., Irish, J.D. 1999. A laboratory evaluation of the laser in situ scattering and transmissometery instrument using natural sediments. Mar. Geol. 159, 355-367.

Trout, S.R. 2003. Understanding permanent magnet materials: an attempt at universal magnetic literacy. Arnold Magnetic Technologies Corporation, WWW Page, www.grouparnold.com.

UNESCO 1983. International Oceanographic tables. Unesco Technical Papers in Marine Science, Algorithms for computation of fundamental properties of seawater, No. 44.

Van Der Lee, W.T.B. 1998. The impact of fluid shear and suspended sediment concentration on the mud floc size variation in the Dollard estuary, The Netherlands. In: Black, K.S.; Paterson, D.M., Cramp, A. (Eds), Sedimentary processes in the intertidal zone. Geological Society, London, Special Publications 139, pp. 187-198.

Van der Lee, W.T.B. 2000. Temporal variation of floc size and settling velocity in the Dollard estuary. Cont. Shelf Res. 20, 1495-1511.

Van der Lee, W.T.B. 2001. Parameters affecting mud floc size on a seasonal time scale: The impact of a phytoplankton bloom in the Dollard estuary, The Netherlands. In: McAnally, W.H., Mehta, A.J. (Eds.), Coastal and Estuarine Fine Sediment Processes, Elsevier Science B.V., Berlin, pp. 403-421.

Van Leussen, W. 1988. Aggregation of particles, settling velocity of mud flocs. A review. In: Dronkers, J., Van Leussen, W. (Eds.), Physical processes in estuaries. Springer-Verlag, Berlin, pp. 347-403.

Van Leussen, W., Cornelisse, J.M. 1996. The underwater video system VIS. J. of Sea Res. 36 (1-2), 77-81.

Van Leussen, W., Dronkers, J. 1988. Physical processes in estuaries: an introduction. In: Dronkers, J., Van Leussen, W. (Eds.), Physical processes in estuaries. Springer-Verlag, Berlin, pp. 1-18.

Van Leussen, W. 1996. The RWS field settling tube. J. Sea Res. 36 (1-2), 83-86.

Van Leussen, W.V., Cornelisse, J.M. 1993a. The determination of the sizes and settling velocities of estuarine flocs by an underwater video system. Neth. J. Sea Res. 31 (3), 231-241.

Van Leussen, W., Cornelisse, J.M. 1993b. The role of large aggregates in estuarine fine-grained sediment dynamics. In: Mehta, A.J. (Ed.), Nearshore and estuarine cohesive sediment transport, Coastal and Estuarine Studies 42. American Geophysical Union, pp. 75-91.

Van Rijn, L.C., Nienhuis, L.E.A. 1985. In situ determination of fall velocity of suspended sediment. Proc. 21st Congress IAHR, Melbourne, Australia 4: 144-148.

Vincent, C.E., Downing, A. 1994. Variability of suspended sand concentrations, transport and eddy diffusivity under non-breaking waves on the shoreface. Cont. Shelf Res. 14 (1/2), 223-250.

Voulgaris, G., Meyers, S.T. 2004. Temporal variability of hydrodynamics, sediment concentration and sediment settling velocity in a tidal creek. Cont. Shelf Res. 24, 1659-1683.

Watson, J., Craig, G., Chalvidan, V., Chambard, J.P., Diard, A., Foresti, G.L., Forre, B. Gentili, S. Hobson, P.R., Lampitt, R.S., Maine, J.T., Malmo, J.T., Nareid, H., Pieroni, G. 1999. High-resolution in situ holographic recording and analysis of marine organisms and particles. Third European marine science and technology conference (MAST conference), Lisbon, 23-27 May 1998: Conference proceedings, 104-105.

Webb, P.A. 2001. Volume and density determinations for particle technologists. In Micromeritics Instrument Crop. 16 February 2001, pp. 1-16.

Welsby, S.D. and Hitz, T. 1997. True position measurement with eddy current technology. http://www.sensorsmag.com/articles/1197/eddy1197/main.shtml, Sensor Magazine, November 1997.

Widdows, J.; Brinsley, M. and Elliott, M. 1998. Use of in situ flume to quantify particle flux (biodeposition rates and sediment erosion) for an intertidal mudflat in relation to changes in current velocity and benthic macrofauna. In: Sedimentary processes in the intertidal zone, Black, K.S.; Paterson, D.M. & Cramp, A. (eds), Geological Society, London, Special Publications 139, p: 85-97.

Wikipedia, 2002. www Page: http://www.absoluteastronomy.com.

Williams, J.J., Rose, C.P., Thorne, P.D., O'Connor, B.A., Humphery, J.D., Hardcastle, P. J., Moores, S.P., Cooke, J.A., Wilson, D. J. 1999. Field observations and predictions of bed shear stresses and vertical suspended sediment concentration profiles in wave-current conditions. Cont. Shelf Res. 19, 507-536.

Williams, J.J., Rose, C.P., Thorne, P.D. 2002. Role of wave groups in resuspension of sandy sediments. Mar. Geol. 183, 17-29.

Wolanski, E. 1994. Physical oceanographic processes of the Great Barrier Reef. CRC Press, Inc. Marine Science Series. Michael J. Kennish & Peter L. Lutz (Eds.), 194p.

Wolanski, E., Gibbs, R., 1992. Resuspension and clearing of dredge spoils after dredging, Cleveland Bay, Australia. Water Environment Res. 64 (7), 910-914.

Wolfstein, K. 1996. Fractionation and measurements of settling velocities of suspended matter using Owen tube. J. Sea Res. 36 (1-2), 147-152.

Wren, D.G., Barkdoll, B.D., Kuhnle, R.A., Derrow, R.W. 2000. Field techniques for suspended-sediment measurement. J. Hydraulic Eng. 126 (2), 97-104.

Wren, D.G., Kuhnle, R.A. 2002. Surrogate techniques for suspended-sediment measurement. Turbidity and other sediment surrogates Workshop, April 30-May 2, Reno, NV, 3p.

Wüst, R.A.J., 2001. Holocene evolution of the intermontane Tasek Bera peat deposit, Peninsular Malaysia: Controls on composition and accumulation of a tropical

freshwater peat deposit. Ph.D. Thesis, University of British Columbia, Vancouver, B.C., Canada, 478 p.

Xia, X.M.; Li, Y.; Yang, H.; Wu, C.Y.; Sing, T.H., Pong, H.K. 2004. Observations on the size and settling velocity distributions of suspended sediment in the Pearl River Estuary, China. Continental Shelf Research, 24: 1809-1826.

Zaneveld, J. R., Spinrad, R. W., Bartz, R. 1982. An optical settling tube for the determination of particle-size distributions. Mar. Geol. 49, 357-376.

http://www.balances.com.

http://www.cabelas.com

Rubotherm (http://www.rubotherm.de)

Appendix A: Basic concepts about magnetism

Some concepts related to magnetic field measurements and magnetic circuits mentioned on the text are related in the Table 3.1. These descriptions were based on Lorrain and Corson, (1970), Adams (1971) and Smith (1960).

Table A1: Glossary of terms related with magnetic field generation and measurements mentioned in the text.

Magnetic circuit parameter	Symbol	Definition	Explanation
Magnetic field	H	$H = \dfrac{NI}{2\pi r}$	Magnetic field is the region surrounding a magnet or an electric current. A magnetic field is produced when a current (I) passes through a conductor of radius (r) and N turns. It is perpendicular to the current direction.
Magnetic flux density	B	$B = \mu_0 \mu_R H = \mu H$ $\mu = \mu_0 \mu_R$	The magnetic flux passing through a unit area of magnetic field in a direction at right angle to the magnetic force is the magnetic induction or flux density (B). Where μ_0 is the free space permeability and μ_R is the relative permeability.
Magnetomotive force	F_m	$F_m \propto NI$	The magnetomotive force (F_m or m.m.f) is the force by which a magnetic field is produced, either by a current (I) flowing through a coil of wire (with N turns) or by the proximity of a magnetized body.
Permeability	μ	$\mu = l/(\Re A)$	Permeability is the ease with which a magnetic field can be established in a substance of cross sectional area A and length l. Usually referred as how better a given material is than air ($\mu = 1$) as a path for magnetic lines of force.
Reluctance	$\Re$	$\Re = l/\mu A$	Reluctance is the opposition to the establishment of a magnetic field (magnetic resistance). Symbols as above.
Magnetic flux	Φ	$\Phi = F_m/\Re$	It is the flux generated by any closed circuit, such as a coil, and it corresponds to the number of lines of magnetic induction (B) that pass through a surface of cross sectional area, A), i.e. $\Phi = BA$. A magnetic circuit occurs when the lines of magnetic induction (B) are confined to well-defined circuital paths lying mainly within a ferromagnetic material.
Inductance	L	$L = \Phi/I$	Inductance is the ratio of magnetic flux (Φ) divided by the current (I) producing it.
Impedance	Z	$Z = \sqrt{R^2 + X_L^2}$	Impedance is the total opposition that a RL circuit presents to an alternating current, including resistance (R) and inductive reactance (X_L)

Appendix B: Relationship between the raw sensor output in Volts and in a arbitrary unit (data logger/controller output)

Figure B1 shows graphic relating the raw sensor reading (arbitrary units) as download in the data logger/controller and the sensor output directly measured in Volts at identical distances between the target and the sensor head.
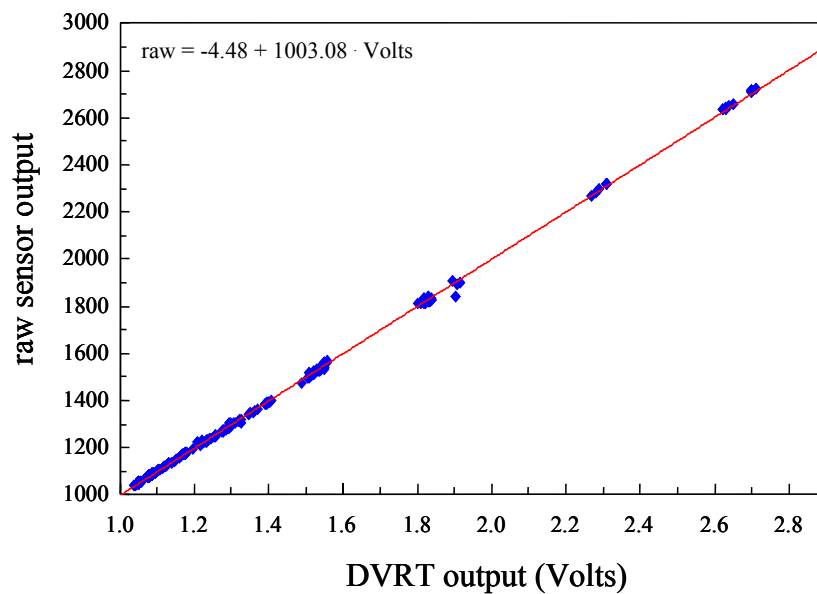

Figure B1: Relationship between the raw sensor output (arbitrary units) produced by the data logger/controller and the DVRT sensor output in Volts.

Appendix C: Circuit diagram of the logical control of the slow rotation motor

Motor technical information

Manufacturer:	TAMIYA	On load speed:	10,500 RPM
Model:	RC-260	Stall torque:	15 gcm
Input voltage:	3.0–4.5 V	Gear ratio used:	8000: 1
Current:	1.0 A		

Circuit diagram for the control of the slow rotation speed motor

The schematic board diagram of the logical circuit that controls the switching on and rotation direction of the motor used to move the big magnet up and down for adjusting the balance zero position is shown in Figure C1. This circuit was designed by Raymond Casey, School of Mathematical and Physical Sciences, James Cook University, Townsville, Australia. The transistors used in this circuit are TIP 122 (NPN, ON Semiconductor).

Figure C1: Schematic diagram of the controlling circuit of the slow-motion motor rotation

Appendix D: Balance plate immersed weight calculation

Table D1: Specifications used in the calculation of the immersed weight (P_I) and the effective immersed mass (M_{EI}) of the aluminium Pan 4, used in the second SEDVEL prototype.

Aluminium Pan 4			dimensions											
Part	Material	Form	Diameter	other	Thickness	Density	Mass	Area	Volume	Quantity	Weight	Bouyancy	P_I	M_{EI}
			m	m	m	kg m^3	kg	m^2	m^3		N	N	N	g
plate	aluminium				0.001	2467.2	0.012	0.007	0.0000048	1	0.115	0.048	0.07	6.87
magnet	neodymium		0.010		0.003	7329.7	0.002	0.000	0.0000002	2	0.034	0.005	0.03	2.95
washer	aluminium		0.010	0.001	0.002	2447.0	0.000	0.000	0.0000001	1	0.002	0.001	0.00	0.14
coating	epoxy	layer				1200.0	0.001		0.0000007	1	0.009	0.007	0.00	0.13
TOTAL							0.02				0.16	0.06	0.10	10.09

Appendix E: Technical specification of the data logger and controller of SEDVEL instrument

Technical specifications of AC Data Logger

| Manufacturer:	James Cook University, Marine Geophysical Laboratory
Designer:	S.J. Smith and P.V. Ridd
Model:	JCU ATOM-LOGGER
Data recovery:	ASCII format to RS 232 interface
Power supply:	6 x 1.5 V D–cell alkaline batteries
Back up battery:	3 V lithium
Power consumption:	2–3 mA h^{-1} in sleep mode, 50–60 mA h^{-1} in recording mode
Logging interval:	minimum of 20 s
Memory:	256 Kbyte RAM, 128000 samples
Deployment time:	5 days at 20 s logging interval, pump on for 60 s
	2 days at 20 s logging interval, pump on for 150 s
Dimensions:	Height: 39 cm
	Diameter: 16 cm
	Weight: 4kg in air/ 0.5 kg in water
Material:	PVC plastic
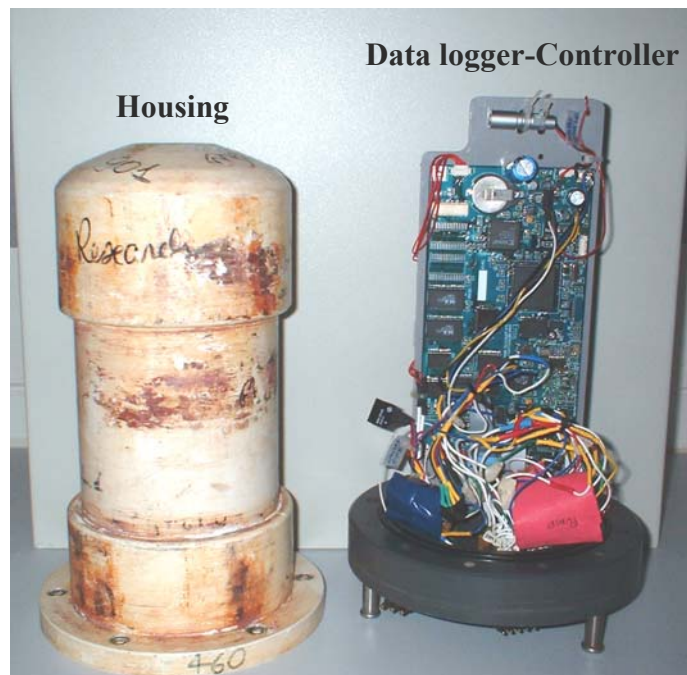
Figure E1: Waterproof housing of data logger (left) and main circuit board plus the additional circuit boards.

Appendix F: Circuit diagram of the control of the pumps

Circuit diagram for the control of the main and auxiliary pumps switching on and off

The schematic board diagram of the logical circuit that controls the switching on and off of the main pump (on the top of the settling tube) and the two auxiliaries pumps (on bottom of the settling tube) is shown in Figure F1. This circuit was designed by Raymond Casey, School of Mathematical and Physical Sciences, James Cook University, Townsville, Australia. Three similar circuits were built for each pump. Relays G6D-1A (12 V, 5A at 250 VAC/30VDC, Omron) were used in these circuits.
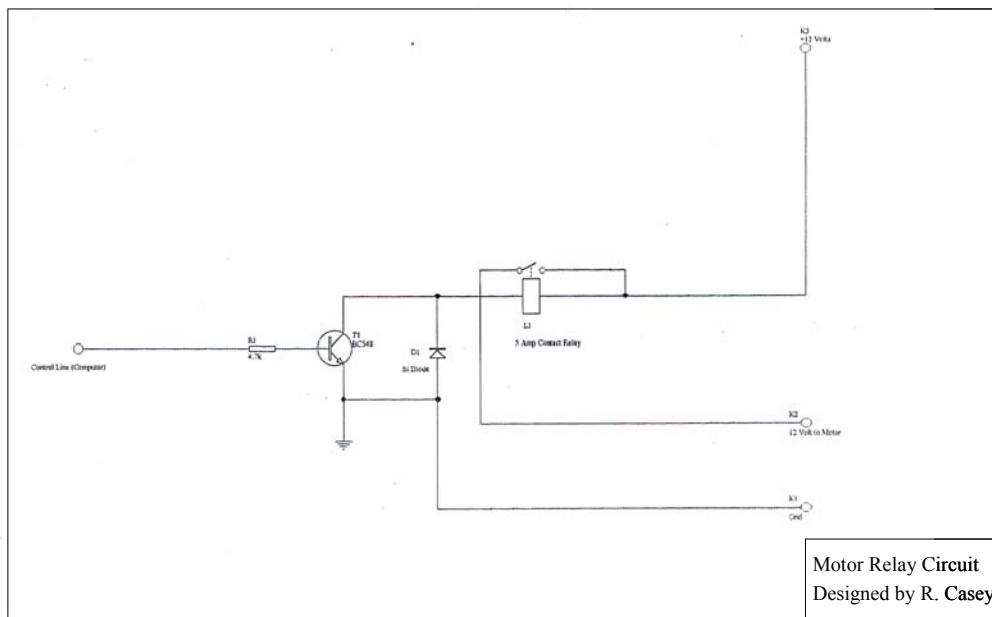

Figure F1: Schematic diagram of the two auxiliaries and main pump on/off switch control.

Appendix G: Calibration curves for the first SEDVEL version

First SEDVEL version set of calibration curves

The first SEDVEL version was used in the field trips realized in October and November 2003. Its balance plate, tube base and water replacement and cleaning systems differed from the second SEDVEL version, and therefore, it presents distinct calibration curves as shown in the Figure G1.
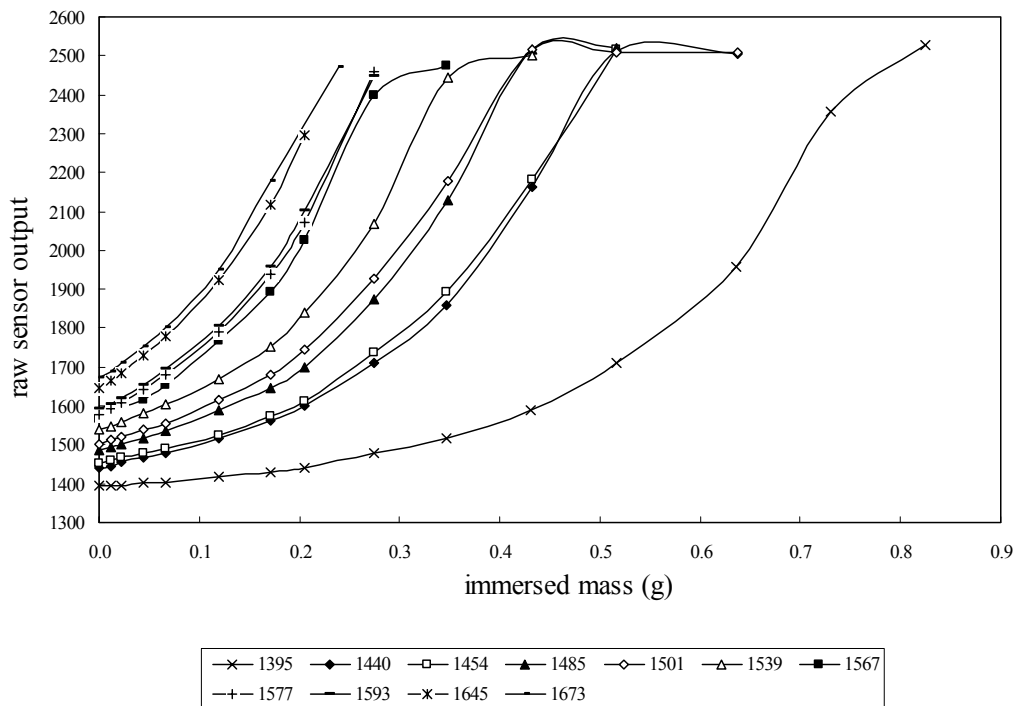

Figure G1: Set of calibration curves for the first SEDVEL version (aluminium Pan 1) relating the effective immersed mass (g) to the raw sensor output.